

**The mineralogy and petrology of layered series nepheline syenite  
within Center II of the Coldwell Complex**

**By: Douglas Nikkila**



**A thesis submitted to the Department of Geology in partial fulfillment of  
requirements for the Degree of Master of Science**

**Lakehead University, Thunder Bay, Ontario**

**December 2017**

## Abstract

The Coldwell Complex is situated within the Archean Schreiber-White River metavolcanic and metasediment of the Superior Province. Spanning over 25km in diameter, it is the largest alkaline intrusion in North America. The  $1108 \pm 1$  Ma age of the Coldwell Complex and its close spatial proximity supports a strong relationship to the magmatism of the Keweenaw Midcontinent Rift. Early studies define three magmatic centers of the Coldwell Complex, which in order of intrusion are Center I, Center II, and Center III. Center I consists of an oldest phase gabbro, which borders a ferroaugite syenite to the east and north. Center II includes a nepheline-bearing biotite-gabbro and several intrusions of nepheline syenite, and Center III is composed of four syenites which in order of intrusion are: magnesiohornblende syenite, contaminated ferroedenite syenite, ferroedenite syenite, and quartz syenite.

This study evaluated the formation of the layered series nepheline syenite in Center II of the Coldwell Complex. Field mapping and sampling were completed along the shoreline of Neys Provincial Park, where extensive exposures of massive, hybrid, and layered syenite; together with xenolith-rich zones, biotite-gabbro, lamprophyre dykes and pegmatitic syenite of diverse composition are preserved. In the layered series, perthitic K-feldspar with secondary plagioclase forms the cumulus phase. Feldspar observed through cathodoluminescence (CL) imaging demonstrated multiple feldspar species within single crystals. K-feldspar ranged in orthoclase component from 87-100%, whereas plagioclase exsolution and alterations were characterized as albite, with anorthite components ranging from 0-3%. Amphibole (classified as ferro-pargasite) and minor apatite represent post-cumulus phases, forming interstitially to feldspar laths or in amphibole-rich laminae at the base of individual layers. Biotite, also a post-cumulus phase, was classified as the iron-rich end member annite. Fluorapatite is the most abundant accessory mineral, hosting light rare earth elements (LREE), along with less abundant britholite, wöhlerite, pyrochlore, titanite and other minor accessory minerals hosting incompatible elements.

Layers commonly display modal grading from amphibole-dominant laminae, to a mixture of amphibole and feldspar, followed by a section of 'normal syenite' (dominantly feldspar with disseminated amphibole). Hydrodynamic processes are favoured for the origin of the layered series, specifically surge-type density currents and separation and reattachment vortex cells, are proposed to have formed the modally graded cumulate layers. In conjunction with graded layers, other magmatic "sedimentary" features including slumping, scour channels, flame structures, load casts, and various stages of hybridization and deformation of mafic xenoliths produced during hydrodynamic processes, indicate a strong convecting current operating during the formation of these rocks. The formation of the layered series was a product of fractional crystallization, varying deposition mechanisms, and reworking through erosion or deformational processes.

## Table of Contents

**Abstract**

**Acknowledgements**

**1. Introduction**

1.1	Scope of Research	1
1.2	Regional Geology	1
1.3	Introduction to the Coldwell Complex	5

**2. Analytical Methods**

2.1	Field Work and Sampling	13
2.2	Petrography	13
2.3	Cathodoluminescence of Feldspar	13
2.4	Back-scattered Electron Petrography and Quantitative Analysis	14

**3. Results**

3.1	Summary of Field Mapping, Neys Provincial Park (Center II)	15
3.2	Mineralogy of Syenite	24

**4. Discussion**

4.1	Mineralogy of the Layered Series	51
4.2	Dynamics of Magma Chamber	61
4.3	Analysis of Rhythmic, Modal Layering	65
4.4	Supporting Evidence of Hydrodynamic Sorting	69

**5. Conclusion** 74

<b>References</b>		76
-------------------	--	----

<b>Appendices</b>	I	Hand Sample and Petrographic Descriptions	80
	II	SEM Results	109
	III	Cathodoluminescence Results	193

## List of Figures

<b>Fig. 1.1</b>	Regional geology map	5
<b>Fig. 1.2</b>	Geological map of the Coldwell Complex	12
<b>Fig. 3.1</b>	Field area map	16
<b>Fig. 3.2</b>	Photo of mottled texture in nepheline syenite	18
<b>Fig. 3.3</b>	Photos of xenoliths and block of gabbro	19
<b>Fig. 3.4</b>	Photos of layered block of nepheline syenite	20
<b>Fig. 3.5</b>	Photos of pegmatite pod and vein	20
<b>Fig. 3.6</b>	Photos displaying modal grading and scour channels	22
<b>Fig. 3.7</b>	Photos of disturbed layered syenite	23
<b>Fig. 3.8</b>	Photos of pegmatite and lamprophyre	24
<b>Fig. 3.9</b>	Photos of cut hand samples of layered and massive syenite	25
<b>Fig. 3.10</b>	Photomicrograph of representative feldspar	26
<b>Fig. 3.11</b>	CL imaging of feldspar	27
<b>Fig. 3.12</b>	Back-scattered image of perthite texture	27
<b>Fig. 3.13</b>	Representative images of amphibole	29
<b>Fig. 3.14</b>	Classification plot of amphibole in nepheline syenite	31
<b>Fig. 3.15</b>	Classification plot of amphibole of core and rim	32
<b>Fig. 3.16</b>	Photomicrograph of representative biotite	33
<b>Fig. 3.17</b>	Classification plot of biotite	34
<b>Fig. 3.18</b>	Photomicrograph of representative zeolites	36
<b>Fig. 3.19</b>	Representative images of pyroxene	37
<b>Fig. 3.20</b>	Classification plot of pyroxene	38
<b>Fig. 3.21</b>	Representative images of apatite	40
<b>Fig. 3.22</b>	Back-scattered image of apatite and britholite	43
<b>Fig. 3.23</b>	Back-scattered image of britholite alteration	43
<b>Fig. 3.24</b>	Substitution plot of apatite	44
<b>Fig. 3.25</b>	Substitution plot of britholite and apatite	44
<b>Fig. 3.26</b>	Classification plot of wöhlerite	45
<b>Fig. 3.27</b>	Back-scattered image of wöhlerite, zircon, and pyrochlore	46
<b>Fig. 3.28</b>	Composition plot of pyrochlore	47
<b>Fig. 3.29</b>	Back-scattered image of zircon and pyrochlore	47
<b>Fig. 3.30</b>	Back-scattered image of fluorite, pyroxene, and magnetite	50
<b>Fig. 3.31</b>	Back-scattered image of pyrite and pyrochlore	50
<b>Fig. 4.1</b>	Photo of layered block of nepheline syenite	52
<b>Fig. 4.2</b>	Photo of well-preserved layered block of nepheline syenite	54
<b>Fig. 4.3</b>	Photos of Pegmatite	56
<b>Fig. 4.4</b>	Classification plots of pyroxene	58
<b>Fig. 4.5</b>	Photos of deformed xenoliths	64
<b>Fig. 4.6</b>	Photos of mottled textured nepheline syenite	65
<b>Fig. 4.7</b>	Diagram of boundary-layer flow separation	67
<b>Fig. 4.8</b>	Photos of layered nepheline syenite	69
<b>Fig. 4.9</b>	Photos of distorted layering	70

## List of Tables

<b>Table 3.1</b>	Representative compositions of amphibole	30
<b>Table 3.2</b>	Representative compositions of zeolite, boehmite, and nepheline	35
<b>Table 3.3</b>	Representative compositions of apatite group minerals	41
<b>Table 3.4</b>	Representative compositions of accessory minerals	49

## **Acknowledgements**

I would like to thank Dr. Shannon Zurevinski and Dr. Roger Mitchell for providing me the opportunity to work on this project, and for their support and guidance throughout the undertaking of my MSc degree. Thanks goes out to Ontario Parks for allowing me to conduct research at Neys Provincial Park, Al MacTavish for his detailed mapping of the Neys shoreline, and Dorothy Campbell for assistance with the making of my field map. Finally, I would like to thank all my family and friends, for their support throughout my entire academic journey.

## **Chapter 1**

### **Introduction**

#### **1.1. Scope of Research**

The objective of this study was to evaluate the formation of the layered series nepheline syenite in Center II of the Coldwell Complex, where limited research has been previously completed. Field mapping and sampling were completed along the shoreline of Neys Provincial Park, where extensive exposures of the layered series are preserved. Field structures and textures present in the rocks provide insight to the evolution of the magma chamber during emplacement and provide information regarding the mechanism of formation of the layering. The mineralogical data is used to characterize and classify the syenite, and identify accessory minerals hosting incompatible elements. This work provides insight to the formation of layered alkaline plutons, as well as further the understanding of potential REE-bearing mineral deposits hosted in these systems.

#### **1.2. Regional Geology**

The Coldwell Complex is the largest alkaline complex in North America. The intrusive rocks of the Complex are directly related to the ~1.1 Ga Midcontinent Rift system, one of the largest known aborted continental rifts (Heaman & Machado 1992). A U-Pb zircon/baddeleyite age study by Heaman and Machado indicates that the Complex was emplaced at  $1108 \pm 1$  Ma, and probably experienced a rapid cooling history. The rift system, initially forming on the Laurentian Supercontinent, can be traced over 2000 km from Kansas, North to the Lake Superior region, and Southeast beneath the Michigan basin to the Grenville Front (Cannon 1994). Seismic

reflection profiles show the rift reaches a depth of up to 30 km along large normal growth faults, containing 20 km of rift-related volcanic rocks and 10 km of overlying sedimentary rocks (Nicholson et al. 1997). Although initially magmatism was thought to have occurred for approximately 22 million years between 1108-1086 Ma, more recent data indicates an early stage of magmatism between 1150 and 1130 Ma (Heaman et al. 2007). Midcontinent Rift magmatism is considered the result of the impingement of a mantle plume on the base of the continental lithosphere (Hollings et al. 2007).

The oldest possible magmatism related to the Midcontinent Rift system includes numerous lamprophyre dykes occurring along the north shore of Lake Superior, with ages between 1147 and 1141 Ma as determined by U-Pb perovskite and  $^{40}\text{Ar}/^{39}\text{Ar}$  phlogopite methods (Heaman et al. 2007). Other evidence of magmatism in this time frame include tholeiitic basalt and associated feeder dykes from the Abitibi dyke swarm and some possible felsic magmas in the U.S. region of the rift. This stage of magmatism from approximately 1150-1130 Ma might be a response to the development of a regional crustal depression and deposition of the oldest clastic sedimentary rocks in the rift (Heaman et al. 2007). The second stage of magmatism between 1115 and 1105 Ma contains the greatest diversity in magma compositions, including: ultramafic intrusions; basaltic sills and flows; rhyolite flows; and alkaline magmatism. Heaman et al. (2007) showed that the abundant mafic, ultramafic, and alkaline intrusions emplaced in the Lake Nipigon region between 1115 and 1110 Ma, must have experienced substantial crustal swelling. In addition, these intrusions precede the voluminous basaltic flows of the 1108 Ma Osler Group along the north shore of Lake Superior. In total, the Midcontinent Rift contains greater than 500 000 km<sup>2</sup> of basaltic sheets, flows, and diabase sills (Klewin & Shirey 1992). Also included in this time period are several alkaline intrusions (including Coldwell), which were emplaced along

a north-east trending failed arm. Based on more than 60 high-precision U-Pb ages for Midcontinent Rift, there is an apparent gap in magmatism between 1105 and 1100 Ma, with the third stage of magmatism occurring between 1100 and 1094 Ma (Heaman et al. 2007). This includes volcanic rocks (e.g. 1096 Ma Mamainse Point), gabbro intrusions (e.g. 1099 Ma Crystal Lake intrusion), and some minor alkaline intrusions (Heaman et al. 2007). Also, included at this time is the emplacement of the Duluth Complex initiated at approximately 1099 Ma. Final magmatism related to the Midcontinent Rift occurred at 1087 Ma, some 7 million years after the final magmatism in stage three. This time is represented by waning volcanism, subsidence, and post-rift sedimentation (Heaman et al. 2007). Following this, a change from extension to compressional forces is proposed to have occurred in the interval of 1080-1040 Ma (Cannon 1994), closing the southwest arm of the rift 30 km, and reactivating listric extensional faults into thrust faults. The rapid evolution in tectonic stresses stopping the crustal separation is hypothesized to be linked to the western Grenville province (Cannon et al. 1994). Compressional tectonics and thrust faulting resumed at ~1080 Ma, when large-scale northwest-directed thrusting was renewed after a period of waned tectonism.

The Coldwell Complex is one of several plutonic alkaline and carbonatite suites lying along strike of the Big Bay-Ashburton fault, a northern extension of the Thiel Fault and northern component of the Trans-Superior Tectonic zone. This plutonic chain extends up to 150 km north of the main rift structure, and includes: the Chipman Lake syenite and carbonatite, the Prairie Lake carbonatite, the Killala Lake alkaline complex, and the Deadhorse Creek volcanoclastic breccia. Chipman Lake consists of a group of carbonatite dikes and fenites emplaced in the Wabigoon subprovince and is the most northerly alkaline complex along the Big-Bay Ashburton fault (Symons 1992). Niobium and rare earth element concentrations are too low to be of

economic interest (Sage 1985). The Prairie Lake Complex consists of carbonatite, biotite pyroxenite, ijolite, malignite, and lamprophyres emplaced into the Wawa subprovince of the Superior Province (Zurevinski & Mitchell 2015). The Killala Lake Alkaline Complex displays a circular pattern with an older gabbro rim, followed by nepheline syenite and a syenite core. The gabbro rim hosts disseminated sulphides, with pyrrhotite being the most abundant, and does not appear to be economic (Sage 1988). The Deadhorse Creek volcanoclastic breccia is ~ 1 km from the western margin of the Coldwell Complex. It was emplaced into Archean metasedimentary and metavolcanic rocks of the Schreiber-White River greenstone belt. The mineralogy is complex, and is described as forming in three separate stages (Potter & Mitchell 2005). First, the emplacement of a granitic melt, considered to be derived from an A-type source and which formed the breccia which contains clasts of Archean rocks. This emplacement was followed by the introduction of fault controlled CO<sub>2</sub>-bearing Cr-Nb-V-Ti-enriched alkaline fluids, mainly depositing in the porous breccia structure. This subsequent fluid reacted with the initial melt to produce an unusual suite of V-, Sc- and Nb-bearing minerals (Potter & Mitchell 2005). A supergene suite of minerals was later produced during post-Pleistocene alteration, exposing the Complex through erosion resulting in oxidation and leaching of minerals. U-Be mineralization at Deadhorse Creek is determined as  $1129 \pm 6$  Ma by U-Pb zircon methods, and thus older than the  $1108 \pm 1$  Ma age of the adjacent Coldwell Complex – the nearest potential source for the granitic melt. Further work is suggested to confirm the age and determine the origin of this melt and the Cr-Nb-V-Ti-bearing fluid (Potter & Mitchell 2005).

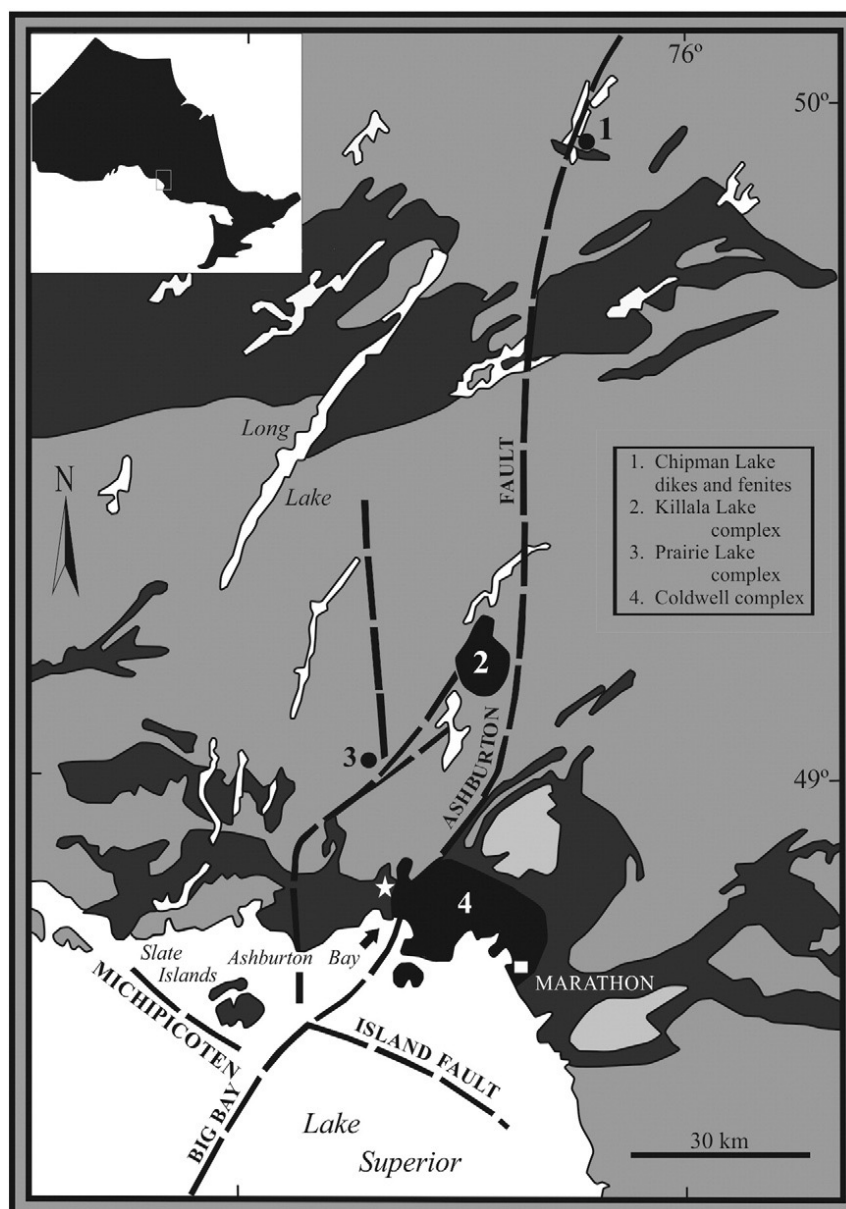


Figure 1.1. Location of Coldwell Complex in relation to the Trans-Superior Tectonic Zone (TSTZ), represented by the Big Bay-Ashburton Fault system (most Northerly extension of the TSTZ) and other alkaline and carbonatite intrusions in area. 1: Chipman Lake carbonatitic dikes and fenites; 2: Killala Lake alkaline complex; 3: Prairie Lake carbonatite complex; 4: Coldwell alkaline complex; Star: Deadhorse Creek volcanoclastic breccia (modified from Smyk et al. 1993 & Zurevinski and Mitchell 2015).

### 1.3. Introduction to the Coldwell Complex

The Coldwell Complex spans over 25 km in diameter. It is located on the north shore of Lake Superior, between the Pic and Little Pic Rivers on the western side of Marathon, Ontario.

Emplaced along the Big Bay-Ashburton fault, a northern component of the Trans-Superior Tectonic zone, it is the southernmost pluton in a group of spatially-related alkaline and carbonatite intrusions along strike of the fault. The Mesoproterozoic complex is situated in the East-West trending Archean Schreiber-White River metavolcanic-metasediment terrain of the Superior Province. Three distinct intrusive magmatic episodes have occurred in the Coldwell Complex, designated (in order of intrusion) as Centers I, II, and III (see Fig. 1.2). Center I consist of a subalkaline gabbro and ferroaugite syenite; Center II is a nepheline-bearing alkali biotite-gabbro and miaskitic nepheline syenite (including the layered series); and Center III is composed of four separate varieties of syenite (Mitchell & Platt 1982). Lamprophyres are present in Center I and II of the complex but absent in Center III. Five varieties have been identified including: ocellar camptonites, camptonites with quartz macrocrysts, amphibole camptonites, monchiquites, and sannites (Mitchell et al. 1991). None of these dikes represent primitive liquids, and are formed by mixing of several batches of magma continuously replenished in an evolving magma chamber. Magmatic activity within the complex was not stationary, and migrated with time in a northwesterly direction. This migration would isolate magma chambers, which would no longer be replenished, and extensive fractionation would occur. These derivative magmas were subsequently emplaced at higher structural levels due to cauldron subsidence and faulting, which had a major structural influence on the complex (Mitchell et al. 1993). Modelling of the complex revealed felsic rocks form a 3-5 km thick layer overlying a differentiated basic intrusion. This intrusion is interpreted to be gabbro (3-5 km thick), which is overlying another 3 km of peridotite and pyroxenite (Mitchell et al. 1993).

Each center is characterized by multiple magmatic events. Heaman & Machado (1992) have shown through U-Pb zircon/baddeleyite age determinations that the complex was emplaced

at  $1108 \pm 1$  Ma, and likely experienced a rapid cooling history. As well, the definitive scatter of Sr-Nd-Pb isotopic compositions of various minerals from the complex indicate the presence of at least two distinct subcontinental mantle isotopic reservoirs in this region (Heaman & Machado 1992). The isotopic data also indicates that crustal contamination was not a significant factor in magma evolution. This is supported by similar  $\epsilon_{Nd}$  ( $+0.5 \pm 0.4$ ) signatures of clinopyroxene and amphibole in Center I gabbro and Center II nepheline syenite respectively; as mixing between a depleted mantle source ( $\epsilon_{Nd} \cong +5$ ) and Archean crust ( $\epsilon_{Nd} = -12$  to  $-17$ ) would have to be extremely reproducible to produce similar Nd isotopic signatures (Heaman & Machado 1992). The structure of the complex is hypothesized to have formed through multiple episodes of magmatism that were emplaced by cauldron subsidence. Many intrusive phases of the complex contain large xenoliths, mostly representing cap rock metabasalt that subsided during emplacement (Mitchell et al. 1993). Although the complex was emplaced in a relatively short time span ( $<3$  Ma), each batch of magma had time to evolve and nearly solidify before the rise of the following magma batch (Heaman & Machado 1992). Evidence for the cauldron subsidence includes the formation of ring dykes and arcuate fault zones, as well as comparable plutonic rocks from the Oslo Rift, which was emplaced by cauldron subsidence (Mitchell & Platt 1982). The mineral deposits located in the Coldwell complex have economic potential, and are located throughout each of the centers. The mineral occurrences include base metals (Cu, Ni), platinum group metals (Pd, Pt) along with associated metals (V, Ti) and rare metals (Nb, Zr, Y, REE), building stone, industrial minerals (nepheline), and semi-gemstones (spectrolite) (Walker 1993).

Center I is the oldest intrusive center and is situated at the eastern end of the complex. The oldest intrusive phase represents a subalkaline gabbro, which borders a ferroaugite syenite unit on the eastern and northern margin of the intrusion. The eastern border gabbro consists of at

least two major intrusive events; characterized by massive and layered intrusions, megaxenoliths, and is considered a multiple-ring dyke (Mitchell & Platt 1978). The first intrusion is termed the Layered Gabbro Series (LGS), and consists of alternating layers of gabbro, olivine gabbro, and troctolite (Stillwater 2012). The most common rock type within the Layered Gabbro Series is a fine-grained gabbro, which may contain massive magnetite layers up to 20 m thick. This was intruded by the Two Duck Intrusion; which is host to the Marathon Cu-PGE deposit. It dominantly occurs as massive and poorly-layered gabbro units approximately 50-250m thick, and generally displays a larger grain size than the Layered Gabbro Series (Stillwater 2012). The border gabbro is crosscut by pegmatites of ferroaugite syenite, suggesting it was emplaced prior to the ferroaugite syenite (Mitchell et al. 1993).

The ferroaugite syenite is the dominant unit found in this center, and is characterized as a series of shallow dipping sheet-like bodies with extreme iron enrichment (Mitchell & Platt 1978). Magma of each of the ferroaugite syenite intrusions crystallized predominantly from the base upwards, along with contemporaneous crystallization at the roof resulting in trapped volatiles and intercumulus liquid, which is peralkaline in the upper section (Mitchell & Platt 1978). Some of the lower level syenites contain small amounts of volatiles and intercumulus liquid, which is not peralkaline, and display well-developed igneous layering with turbulent features such as cross bedding and trough banding common. Mafic layers are defined by cumulus phase olivine, diopside-hedenbergitic pyroxenes, and iron-titanium oxides, while adjacent felsic layers contain cumulus alkali feldspar. Compositions of the pyroxene and amphibole trend towards iron enrichment with a lack of sodium enrichment (Mitchell & Platt 1978). Upper section syenites are dominantly coarse grained cumulates with only rare turbulent layering features; with pyroxenes evolving to a more sodic composition. The change in nature of

the intercumulus liquid between the upper and lower syenites can be attributed to the permeability of the upper cumulates, and free circulation of a water-rich residual magma (Mitchell & Platt 1978). In the lower series, weight of the cumulate crystals, adcumulus growth, and intercumulus liquid crystallization would result in a decrease of porosity and prevent free circulation of an interstitial liquid. Overall the geochemistry and the iron-rich character of the Center I magmas supports the hypothesis that significant crystallization occurred in subcrustal magma chambers prior to emplacement (Heaman & Machado 1992).

Center II is located in the central region of the Coldwell Complex, and is characterized by the presence of nepheline-bearing alkali biotite gabbro which was followed by several intrusions of nepheline syenite. Both Center I and II rocks are intruded by numerous lamprophyre dykes, which are absent from Center III (Mitchell et al. 1991). Hosted within the alkali biotite gabbro are concentrations of platinum-group minerals (PGM), palladium tellurides, and chalcopyrite (Mulja & Mitchell 1991). Located along the extension of the Red sucker fault zone; an arcuate fault zone associated with cauldron subsidence, the main body of the Geordie Lake intrusion is approximately 500 x 2000 m in size and is interpreted to be a rapidly cooled series of tholeiitic basaltic magma (Mulja & Mitchell 1991). The rapid crystallization of olivine and magnetite in the magma is thought to have induced early separation of an immiscible sulfide melt due to oversaturation of the magma with respect to sulfur. Sulfides are most commonly disseminated and include chalcopyrite with minor bornite, pyrite, millerite, cobaltite, siegenite, sphalerite, and galena.

Nepheline syenites of Center II are emplaced during a period of cauldron subsidence as hot, hydrous, relatively unevolved magmas that experienced a rapid cooling history (Mitchell & Platt 1982). Zones of nepheline syenite have undergone post-emplacement, high-temperature

shearing and recrystallization confined to arcuate faults at the margins of the intrusive pluton. The most common texture observed in the syenite involves allotriomorphic granular texture feldspar forming around prismatic amphibole. No obvious layering is present, with all phases recrystallizing together. Throughout the nepheline syenite of Center II, igneous layering is not a common feature. Mitchell & Platt (1982) completed an in-depth study on layered nepheline syenite along Pic Island, which consists of cumulus phase olivine, pyroxene, amphibole, magnetite, and apatite with intercumulus feldspar and amphibole. These layered series grade into zones of normal syenite, and display an array of features indicating the existence of turbulent currents (i.e. crossbedding, scouring of deposited layers, and the absence of planar layering). The cumulus phases would crystallize along the cool chamber walls from an unevolved convecting magma, where unstable masses would slump and produce surge-type density currents which could erode previously deposited layers (Mitchell & Platt 1982). Zoning is commonly present in amphibole crystals due to interaction between a poorly consolidated mush and an increased porosity in the layered series following slumping. During the waning stages of consolidation late stage primary and deuteritic fluids were present throughout; evidenced by the formation of secondary albite and natrolite, sericitization of nepheline, formation of boehmite and other zeolites, and the remobilization of rare earth elements (Mitchell & Platt 1982). Pegmatites are also associated with the syenites, and may represent a final stage of crystallization or an alteration product of the nepheline syenites. All rocks in this center are considered to have formed by fractional crystallization of alkali-basaltic parental magmas (Mitchell et al. 1993).

Center III forms the western portion of the Coldwell Complex and is the youngest intrusive unit. This center contains a variety syenites, which in order of intrusion are: magnesiohornblende syenite, contaminated ferroedenite syenite, ferroedenite syenite, and quartz

syenite. Magnesiohornblende syenites are the least abundant while ferroedenite syenites are the most abundant (Mitchell et al. 1993). Both the contaminated and non-contaminated ferroedenite syenites contain abundant xenoliths of basaltic material in all stages of assimilation. The syenites in Center III have high contents of Nb, Zr, Th, U, Y, and Ga and have the geochemical signature of an A-type granitoid. Most of these elements are not sequestered in the alkali feldspar (the dominant phase), indicating residual liquids present must have been enriched in these elements and were products of extreme fractionation. Accessory minerals enriched in these elements include: zircon, chevkinite, pyrochlore, synchysite, and bastnasite. There is no simple relationship between the various syenites, with their major element compositions determined by crystal accumulation and none represent the original parental magma (Mitchell et al. 1993). Unevolved (SiO<sub>2</sub>-poor) rocks are characterized by light REE enrichment, while later quartz-rich rocks display distribution patterns of light REE depletion and heavy REE enrichment (Mitchell et al. 1993). Unlike Center I, Center III syenite emplacement is not preceded by an intrusion of gabbro and Center I syenites are characterized as being relatively water and fluorine-poor. Initial Sr ratios indicate that continental crust had not been involved in the genesis of the magmas, with the Center III syenites forming from extensive fractionation crystallization of mantle-derived basalt within the plutonic infrastructure of the complex (Mitchell et al. 1992). There has been some interest in Center III syenites for niobium, zirconium, yttrium, and rare earth element occurrences.

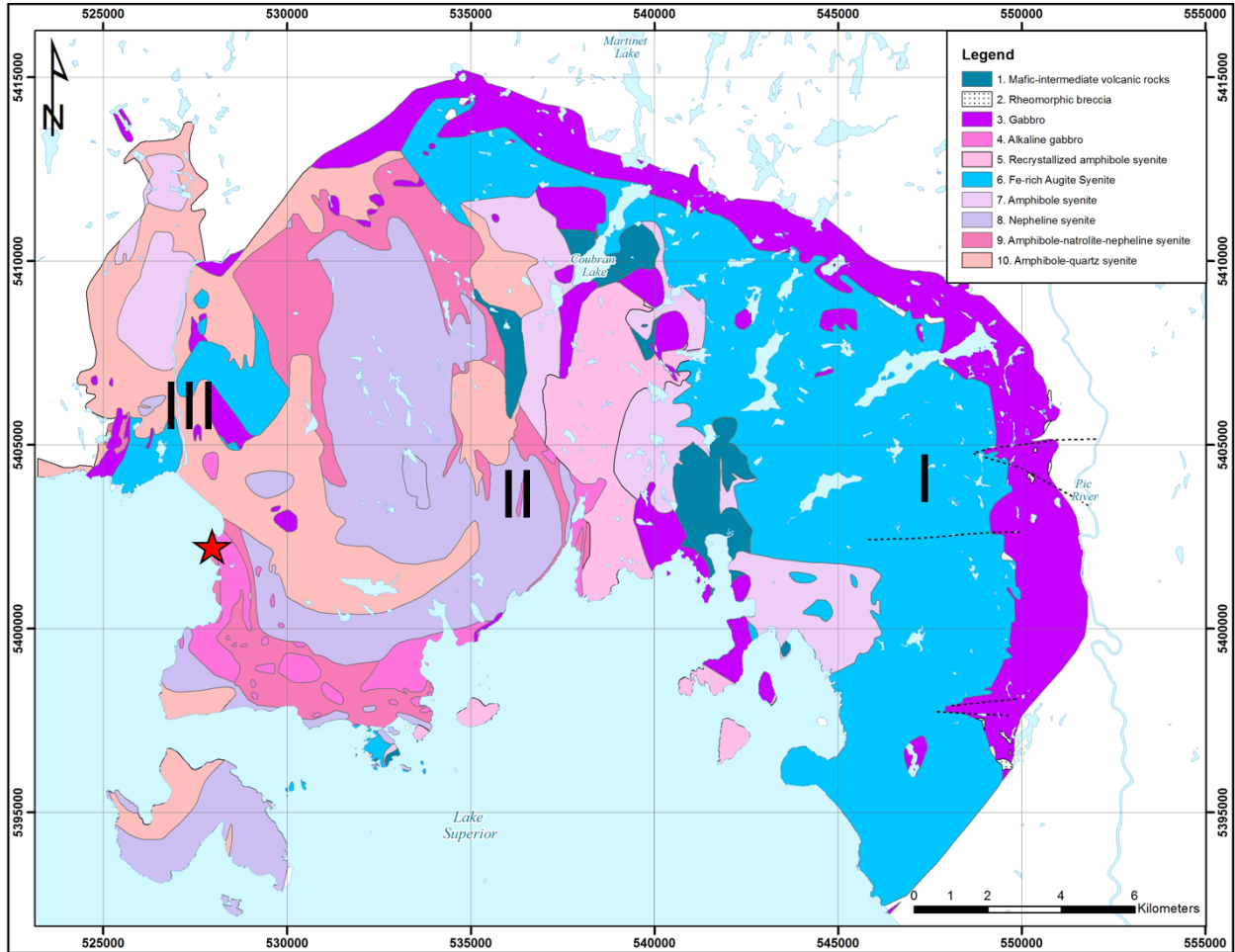


Figure 1.2. Geological map of the Coldwell Complex indicating the locations of Center I, II, and III. Red star denotes field area of this study (Ontario Geological Survey, 2015). Bright purple: gabbro, blue: Fe-rich augite syenite, blue-green: mafic-intermediate volcanic rocks, bright pink: alkaline gabbro, faded purple/pink/peach/tan: various syenite.

## **Chapter 2**

### **Analytical Methods**

#### **2.1. Field Work and Sampling**

Mapping and sampling of the nepheline syenite were completed along the shoreline of Lake Superior in Neys Provincial Park west of Marathon (See Figure 3.1 for map of sample locations). Samples previously collected by Dr. Mitchell within Neys Provincial Park were also examined as part of this study. A letter of authorization to conduct research in the Provincial Park was granted by Ontario Parks. In total, 28 samples were analyzed, with GPS coordinates taken for 11 samples.

#### **2.2. Petrography**

Polished thin sections were prepared at Lakehead University. Thin sections from 29 different sample sites were examined under transmitted and reflected light, to identify the minerals and textures present and classify the syenite(s). Representative photomicrographs of each thin section were taken under plane-polarized light (PPL) and cross-polarized light (XPL) for transmitted light at varying magnifications. Petrographic reports for each sample were completed (see Appendix I).

#### **2.3. Cathodoluminescence of Feldspar**

Seven samples of nepheline syenite including layered, massive, and pegmatite sections were selected for cathodoluminescence (CL) petrography and spectral studies using a Relion Luminoscope with an Oceans Optics spectrometer. The CL spectra were collected at three

separate times when possible, and obtained using both 5x (FOV = 2 mm) and 10x (FOV = 1 mm) objectives. The CL operating conditions were: 1.50-1.68 mA, 4.2-5.1 kV, and 66.5-70.5 mTorr. Photomicrographs were taken using a 5x and 10x objective (see Appendix III).

#### **2.4. Back-scattered electron petrography and quantitative analysis**

Thirty thin sections were selected from layered, massive, hybrid, and pegmatite nepheline syenite for detailed quantitative analysis using the Hitachi SU-70 scanning electron microscope (SEM) in the Lakehead University Instrumentation Laboratory (see Appendix II). The Hitachi SU-70 Schottky Field Emission SEM is equipped with a back-scattered electron (BSE) detector and energy dispersive X-ray spectrometry. Qualitative and quantitative phase analysis of the minerals was completed using a 15 mm working distance, and an accelerating voltage of 20kV and beam current of 300 pA using the Oxford Aztec 80mm/124 eV electron dispersive X-ray spectrometer (EDX). The following well-characterized mineral and synthetic standards were used for calibration: factory elements (Fe, Ti, Cr, Mn, Hf, U), jadeite (Na, Al, Si), periclase (Mg), apatite (P, Ca), orthoclase (K), SrTiO<sub>3</sub> (Sr), yttrium fluoride (Y), zirconium metal (Zr), ThNb<sub>4</sub>O<sub>12</sub> (Nb, Th), FeS<sub>2</sub> (S), CaF<sub>2</sub> (F), BaF<sub>2</sub> (Ba), and synthetic orthophosphates (REE, Sc).

## Chapter 3

### Results

#### 3.1. Summary of Field Mapping, Neys Provincial Park (Center II)

Although there are well-exposed outcrops along the shores of Lake Superior within Neys Provincial Park boundary, the mineralogy and petrology of the nepheline syenite is very complicated due to the complex interrelationships observed between the rock types present. Figure 3.1 represents the shoreline map that has been produced from field work completed in Neys Provincial Park. Normal, hybrid, and layered nepheline syenite; together with xenolith-rich zones, biotite-gabbro, lamprophyre dikes and pegmatitic syenites of diverse composition comprise Center II, and commonly are associated with each other in heterogeneous zones. Textures within the nepheline syenite vary from fine- to coarse-grained, massive, layered, and flow-orientated, and include varying amounts of feldspar, nepheline, natrolite, and amphibole. Layered series display modifications in textures, with well-preserved, rhythmic graded bedding, to disrupted bedding re-worked from its original structure. Hybrid and mottled rock types contain both 'normal' and mafic syenites, with amphibole of mafic syenites displaying flow orientations within the magma. Normal syenite represents the most abundant rock type observed, present in relatively all sections as granular texture feldspar and amphibole. Pegmatites and lamprophyres also cross-cut syenite throughout the field area, further disturbing any primary deposition of magmas.

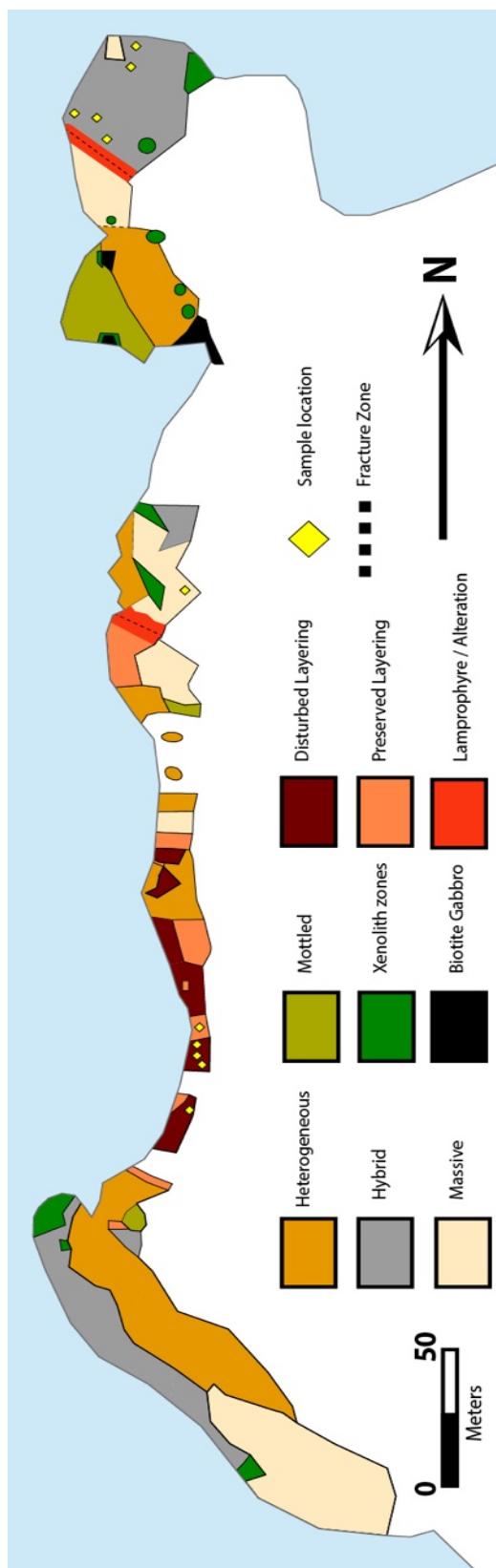


Figure 3.1. Shoreline map of field area displaying variation in syenite textures.

Massive syenite is abundant in Center II of the complex, and is the principal variety of nepheline syenite exposed along the shores of Neys Provincial Park. These nepheline syenites may represent the original magma that intruded the biotite-gabbro (see Fig. 3.3) or unconsolidated crystal mush piles, deposited through slumping and other mechanisms relating to the strong convecting current. Elongated, diffuse zones of massive syenite can be found associated with hybrid and/or layered syenite rocks in heterogeneous zones. As with other sections of syenite, the massive syenite is commonly cross-cut by irregular clots, pods, and veins of pegmatitic syenite.

Hybrid syenites display variable compositions, typically, with a mafic and intermediate or 'normal' syenite component. Amphibole is the dominant phase in the mafic syenite, with crystal alignment displaying the direction of flow around the normal syenite. The orientation of the mafic hybrids themselves also display the direction of flow in the magma chamber. Normal syenites consist of feldspar, nepheline, and zeolites with minor disseminated amphibole. The ratio of these components varies locally along with the relationship between the syenites (textures, contacts, abundance). These hybrid syenites primarily demonstrate a wispy or mottled texture, with mafic syenite flowing around normal syenite in irregular patterns, or completely engulfing the normal syenite forming the mottled appearance (Fig. 3.2). Mottled syenites contain clots of normal syenite ranging from 1-10 cm in diameter, and may represent immiscible syenite blebs in various stages of assimilation within mafic syenites; comparable to sulfide blebs in a basic magma.

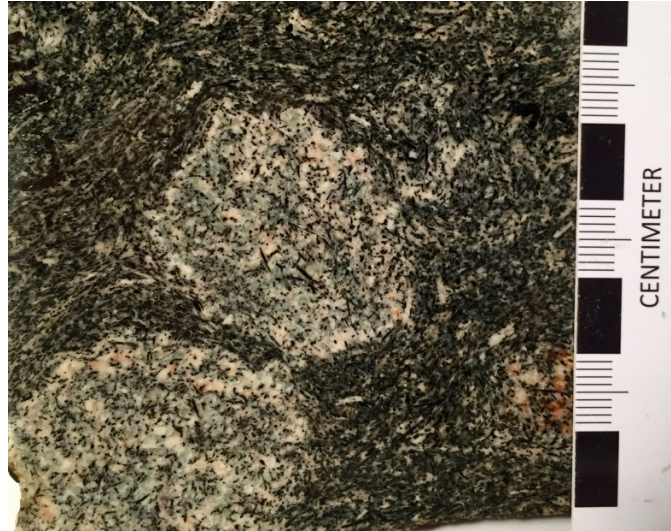


Figure 3.2. Cut slab of sample CC15 showing mottled texture of mafic syenite engulfing normal syenite.

Xenolith zones of basalt and biotite gabbro are present within areas of the nepheline syenite, commonly displaying diffuse contacts with variable shape, size, and assimilation. Basaltic xenoliths are observed in various stages of deformation from disaggregated blebs (see Fig. 3.3) to nearly unobservable basaltic xenolith ghosts present as general concentrations of amphibole. Large blocks of the gabbro up to 7x14m with little assimilation are observed near the upper contact of the biotite-gabbro body. Syenite veins and dykes are observed cross-cutting the biotite-gabbro at varying attitudes (Fig. 3.3). In some cases, amphibole within surrounding syenite may display flow around and between fragments. The volcanic (basaltic) xenoliths are thought to have been foundered during cauldron subsidence along the margins of the pluton by convection currents, while gabbro xenoliths were brought up from deeper levels of the plutonic structure with the rising magma (Mitchell & Platt 1982). Mafic hybrid syenites might form from the almost completely assimilated basalt and/or gabbro, with xenoliths becoming increasingly less mafic and finer-grained as assimilation proceeds.



Figure 3.3. Left: Basaltic xenoliths, Right: Biotite gabbro block cross-cut by syenite.

Heterogeneous zones of syenite were observed throughout the field area, representing the mixing of massive, hybrid and preserved/disturbed layered lithology's. These zones are extremely complex, with significant variation in grain size and modal composition. Primary structures of cumulus feldspar formed graded, parallel beds, which may exhibit extensive remobilization with convoluted bedding, flows of mafic and normal syenite, and cross-cutting coarse-grained to pegmatitic material which may be natrolite-rich (Fig. 3.7). Massive syenite is observed hosting localized, preserved layered blocks, with one block up to 3 m in thickness and 7 m in length (Fig. 3.4). Boundaries of these blocks are typically distorted and hard to recognize. Coarse-grained to pegmatitic syenite occurs as irregular injections, veins, pods, and discontinuous dyke-like masses with little continuity. This rock type is observed to weather readily into ovoid masses up to 4 cm in diameter, consisting of an irregular mix of feldspar, amphibole, natrolite, and nepheline (Fig. 3.5).



Figure 3.4. Left: Rhythmic, modally graded layered block hosted in massive syenite, Right: Weak layering hosted within heterogeneous syenite.



Figure 3.5. Left: Pegmatite pod within heterogeneous zone, Right: Weathered massive syenite with cross-cutting pegmatite vein.

Modal layering within the nepheline syenites of Center II is an uncommon feature, only identified on Pic and Allouez Islands and shoreline of Neys Provincial Park. Layering present on

the islands is well-developed, although individual layers are not extensive, never exceeding 50 m in length (Mitchell & Platt 1982). Layered sections display sharp bases and grade into zones of normal syenite, ending with a gradual decrease in the amount of mafic minerals. The cumulus minerals include: olivine, pyroxene, amphibole, magnetite, and apatite – with felsic minerals and amphibole representing the inter-cumulus phases.

Within the rocks along the Neys shoreline there is a significant variation in the structure and distribution of the layered rocks; from weak to strongly layered and disturbed to well-preserved sections present (Fig. 3.5, 3.6, 3.7). These layered sections are intimately associated with the rest of the syenite lithology's. Disturbed layering can show gradational boundaries into the surrounding syenite, with material mixing into heterogeneous syenite. Layered blocks are also found hosted within massive to heterogeneous syenite. Disturbed layering is characterized by diffuse, disrupted, and contorted layers (see Fig. 3.7). Grain size and modal grading is common, with most layers fining upwards to a top of K-feldspar, amphibole, and interstitial natrolite. Rhythmic layering is also observed, defined by a sharp base of amphibole content on a grain size scale, which grades upwards into a more felsic composition. The bases of these layers may be planar, wispy, or show a general curve along their length. Layered sections are observed up to 4 m in thickness and 9 m in length, with individual layers up to 40 cm in thickness and dipping 70-90° West. The dips of these layers observed are not considered a primary feature, but rather a product of over-steepening through rotation and tilting as a consequence of cauldron subsidence, or represent blocks detached from the walls or roof of the chamber. The cumulus phase is K-feldspar, with post cumulus nepheline and amphibole. Primary nepheline is absent, as it is commonly altered to zeolite (primarily natrolite). Alignment of feldspar laths and amphibole crystals parallel to the layers is common, although preferred orientation may decrease upwards in

layers (Fig. 3.6). In disturbed sections layering is disrupted by pods, clots and veins of a variety of syenitic material, displaying different grain size and mineral composition. Coarse-grained material may force its way through earlier formed layering, and fine-grained material may flow into spaces left by this “disruption”. Scour channels are also observed cross-cutting layering, with sharp contacts and an increased amphibole concentration within (see Fig. 3.6). Slumping and other soft sediment-type deformation features are also variably present throughout. Contorted zones around layered blocks are extremely complex and represent heterogeneous syenite, which has flowed around the layers (Fig. 3.7).

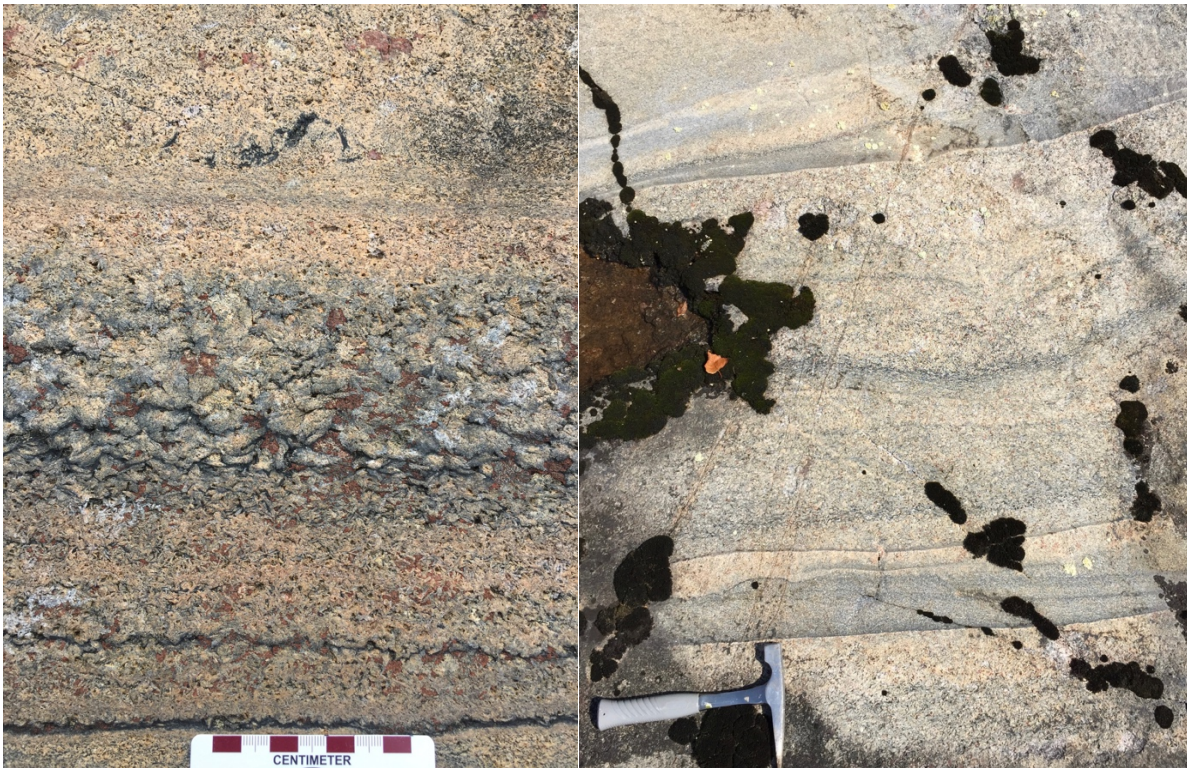


Figure 3.6. Left: Layered syenite displaying mineral alignment and modal grading, Right: Scour channel with increased amphibole concentration (next to hammer).



Figure 3.7. Left: Disrupted layering at edge of layered block, Right: Disrupted layering grading into heterogeneous syenite.

Pegmatite sections can be found throughout the Center II nepheline syenites and are abundant in the mapped section of shoreline in Neys Provincial Park. The mineral compositions of these pegmatites vary with differing amounts of: feldspar, nepheline, natrolite, amphibole, and accessory minerals. Commonly, pegmatite sections cross-cut other rock types as irregular clots, pods and veins with no consistent trend or pattern (see Fig. 3.8). Three lamprophyre dikes are also observed in the mapping area, measuring 50-100 cm in width and commonly surrounded by an altered fracture zone 4-5 m in width. These dikes dip sub-vertically and are enclosed by a brick red alteration halo due to fluid release during emplacement (see Fig. 3.8).



Figure 3.8. Left: Feldspar-Natrolite-rich pegmatite pod, Right: Lamprophyre dyke cross-cutting syenite.

## 3.2. Mineralogy of Syenite

### 3.2.1. Feldspar

Feldspar is observed as colourless, tan, cream, and pink, and may display signs of metasomatic alteration. It is the cumulus phase of the layered syenites, and forms a framework of fine- (<1 mm) to coarse-grained laths (up to 1 cm), which can display grain size grading and moderate- to- strong alignment (Fig. 3.9). In massive syenite sections, alignment and grading is virtually absent, with feldspar more commonly forming aggregates with equant and irregular crystals (Fig. 3.9). For mottled sections, leucocratic clots contain feldspar forming a massive texture; while the mafic syenite enclosing these clots contains feldspar that displays some alignment together with amphibole. Pegmatite veins and pods throughout the field area contain feldspar as primary component with crystals up to 2 cm.

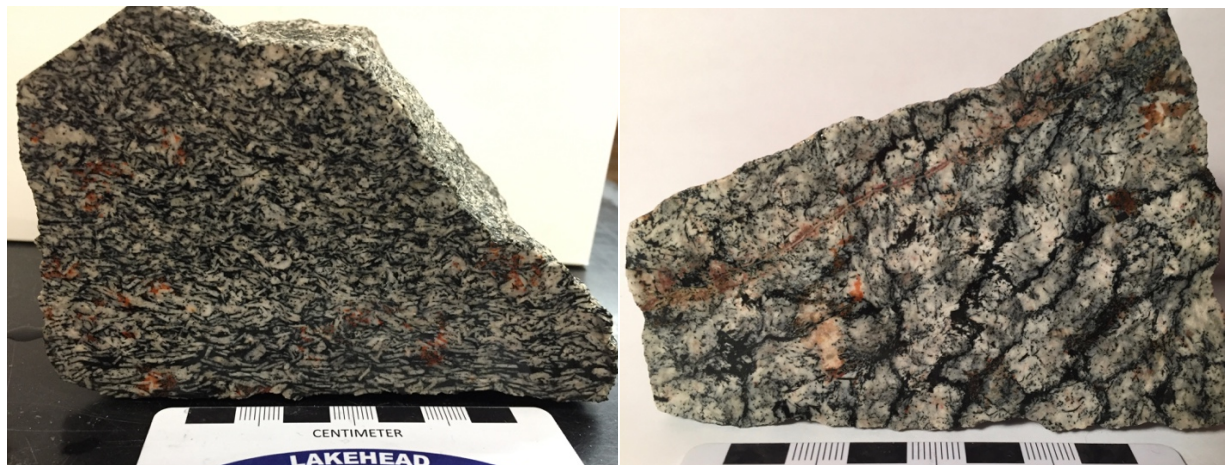


Figure 3.9. Left: Cut sample CC7 displaying feldspar alignment in layered syenite, Right: Cut sample CC13, massive syenite.

In thin section, feldspar appears colourless, cloudy or dusty in plane polarized light, with a perthitic texture in virtually all crystals. These perthites display K-feldspar hosting albite formed as either an exsolution product or by secondary processes. This produces a wide range of perthitic textures including: braided, net-work, stringers, irregular and replacement (Fig. 3.12, 3.13C). Secondary processes also produce iron-staining which can be prominent in some crystals as well as minor- to- moderate sericite alteration. For layered samples, the cumulus texture is evident with fine- to coarse-grained laths (rarely up to 1.5 cm; avg. 3 mm) and minor equant and irregular masses commonly forming aggregates between laths (see Fig. 3.10). Modes range from 45-75 vol. %, and crystals may share irregular to sharp grain boundaries with zeolites and amphibole in the groundmass. Crystals may also host minor to moderate fine-grained (<1 mm) amphibole and apatite inclusions (see Fig. 3.12). In non-layered sections, feldspar is present in similar modes, but forms elongate, equant or irregular crystals that can form pods or individual aggregates separated by amphibole masses (see Fig. 3.10).

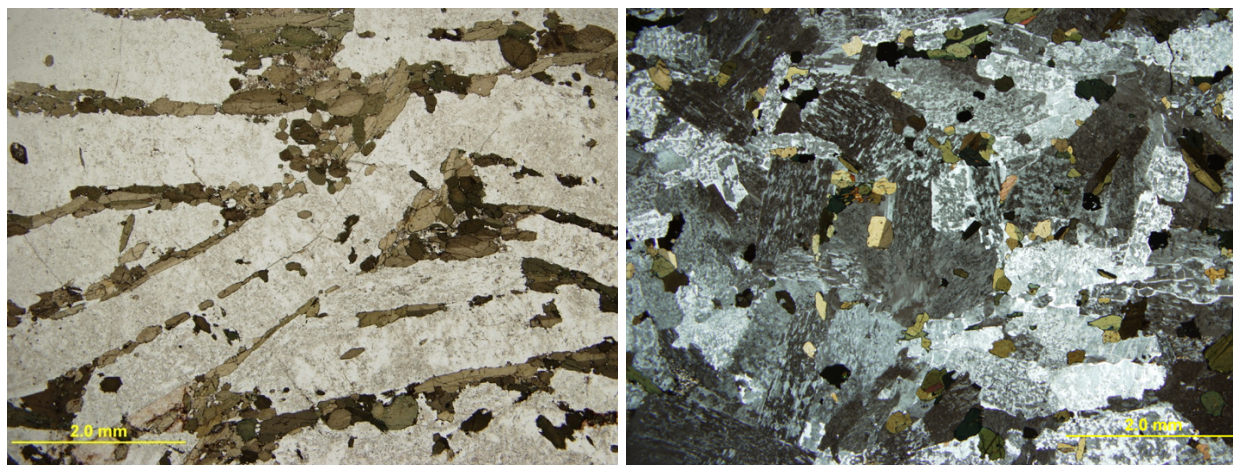


Figure 3.10. Left: Cumulus feldspar of CC7 (Layered; plane-polarized light), Right: Feldspar groundmass of CC3 (Massive; cross-polarized light).

Feldspar analyzed through cathodoluminescence imaging demonstrated detailed multiple feldspar species present within single crystals. In the unaltered (or least altered) parts of the feldspar, representing the primary exsolved phases, both K-feldspar and albite can be identified. K-feldspar displays a dull blue-grey CL, whereas albite shows a vibrant light blue CL appearing as well formed perthite lamellae or irregular patches (see Fig. 3.11). Secondary feldspar displays a violet- to- red CL, commonly forming along grain boundaries or as irregular patches within the crystal depending on the extent of contamination. Violet CL represents secondary (unexsolved) feldspar, with a more vibrant red CL reflecting an increase in iron (Maki et al. 2016). In all the thin sections investigated two CL spectral peaks are always present at circa. 480 nm in the blue region and 700-710 nm in the red region (see Appendix III). The intensities vary both individually and with respect to each other, depending on the content of primary and altered feldspar. Spectra ratios are also dependant on what specific feldspar section was analyzed (i.e. exsolved or secondary albite).

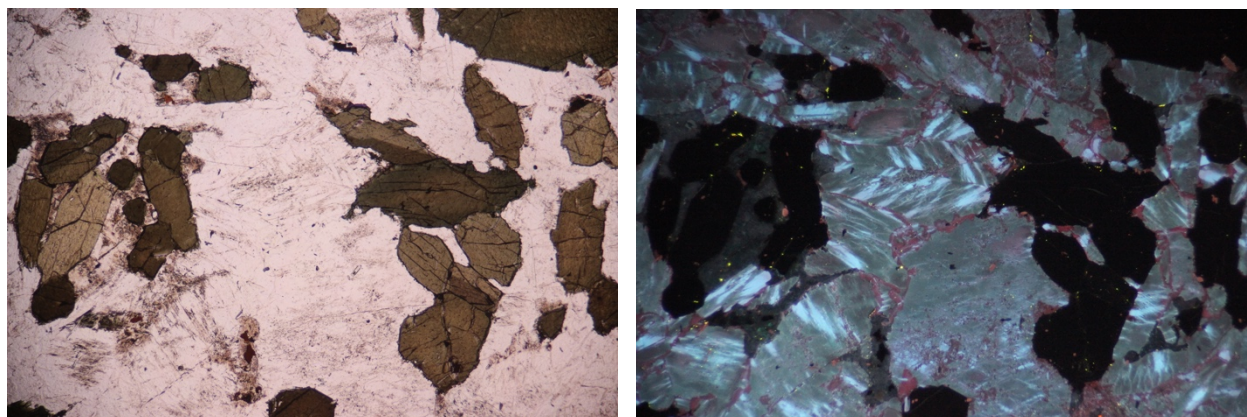


Figure 3.11. Left: Feldspar of CC1A (plane-polarized light), Right: Feldspar displaying albite exsolution and alteration along grain boundaries (CL image; both 5x objective lens).

SEM-EDX analysis of feldspar revealed little change in composition regardless of petrographic type of syenite samples (refer to Appendix II for representative compositions). Albite (both exsolved and secondary) was easily observed, with micropores also a common feature. K-feldspar ranged in orthoclase component [ $100 \cdot K/(K+Na)$  cations per formula unit] from 87.00-100%, whereas plagioclase exsolution and alteration in the K-feldspar were characterized as albite, with the anorthite component [ $100 \cdot Ca/(Na+Ca+K)$  cations per formula unit] ranging from 0-3.03%.

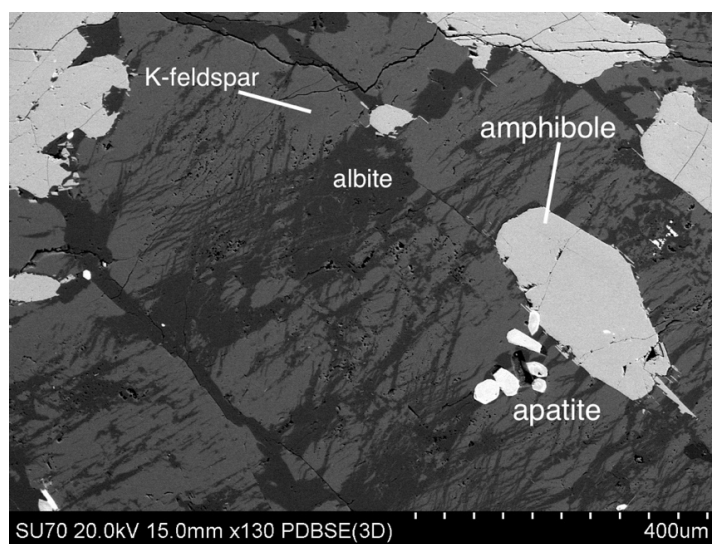


Figure 3.12. Feldspar laths displaying perthite texture of CC1B (layered; SEM image).

### 3.2.2. Amphibole

In hand sample, amphibole crystals range from fine- (<1 mm) to coarse-grained (up to 1 cm), dominantly green- to- black acicular or elongate crystals. In layered sections, crystals typically are aligned in a sub-parallel manner and form minor aggregates between feldspar. They also form grain-scale laminae in the graded beds and appear to infill potential scour channels (Fig. 3.6). In massive and pegmatite samples, amphibole has crystallized throughout the groundmass commonly in larger aggregates than in layered sections (Fig. 3.9). Mafic syenite in both hybrid and mottled sections contains amphibole in a greater abundance, with fine- to medium-grained crystals displaying alignment around normal syenite (Fig. 3.2).

In all thin sections examined, excluding late-stage pegmatites, amphiboles are a primary component with modes ranging from 10-45 vol. %. Crystals display a range of composition and colour zoning from pleochroic brown to green in plane polarized light. Crystal habits vary from fine- to medium-grained (up to 3 mm), anhedral to euhedral, blebby, acicular and elongate form. Irregular grain boundaries are a regular feature. In layered sections, amphiboles represent the post-cumulus phase (interstitial to feldspar laths) and form linear masses sub-parallel to feldspar laths, commonly along the long-axis displaying some alignment (see Fig. 3.13A and C). Crystals typically do not exhibit a euhedral habit and can form an irregular ‘blebby’ texture, space-filling between feldspar (see Fig. 3.13D). Amphibole crystals commonly host inclusions of apatite. In massive sections, amphibole may form larger and more abundant aggregates; with euhedral crystal habit a more prominent feature (see Fig. 3.13B). Amphibole in hybrid and mottled sections tends to form in alignment with the postulated flow direction of the magma. Mafic syenite in mottled sections may contain up to 75 vol. % amphibole. In two pegmatites (DN6 and DN7), amphibole makes up to 5 vol. % of the mode, forming medium- to- coarse-grained (up to

6 mm), disseminated prismatic crystals which are altered to biotite. In all sections, amphibole may share irregular grain boundaries with each primary constituent, and is commonly altered to biotite along grain boundaries and cleavage planes. Aggregates may host inclusions of: biotite, apatite, pyroxene, fluorite, and calcite (in decreasing relative abundance). Fine-grained amphibole inclusions are also hosted in zeolites and feldspar.

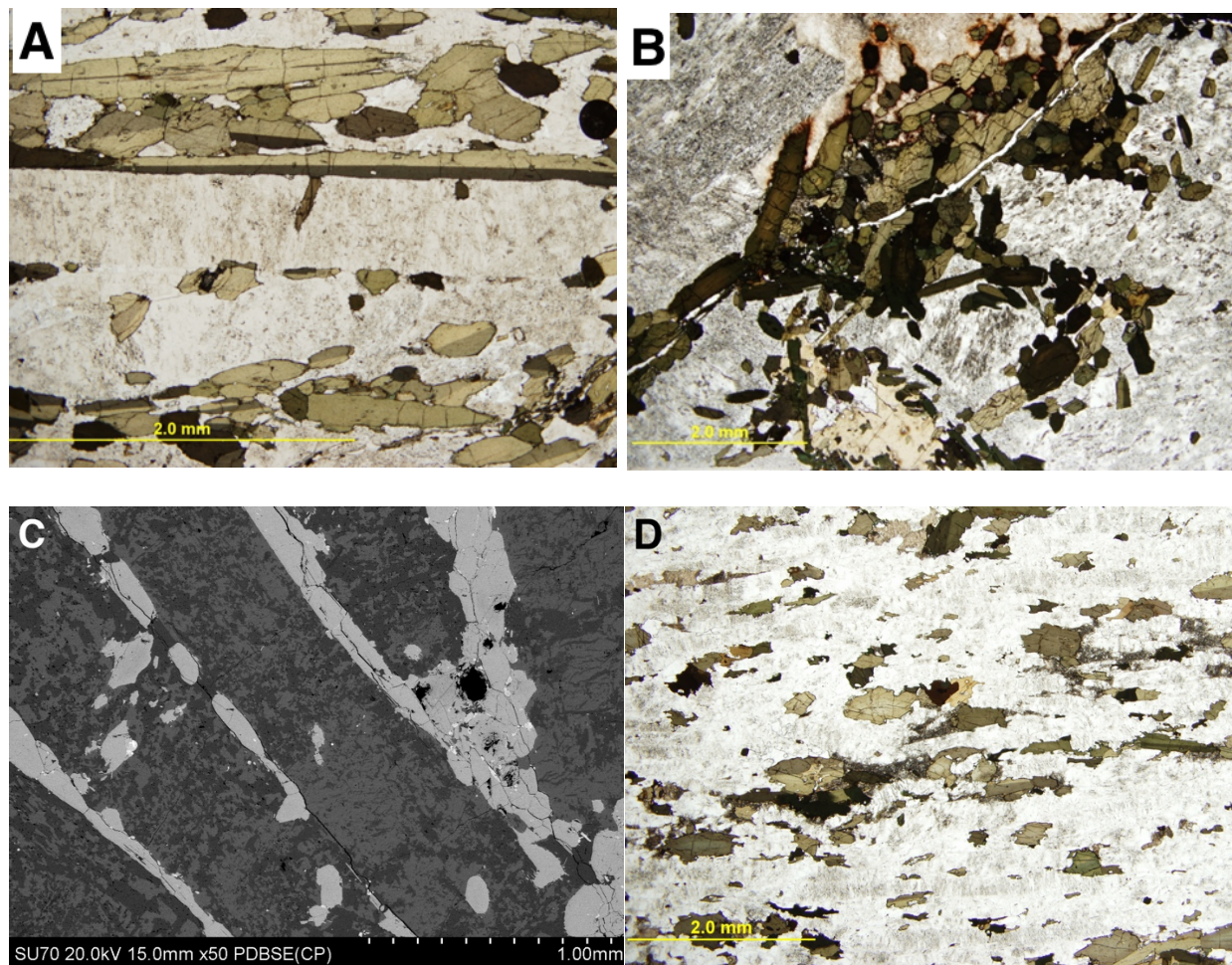


Figure 3.13. A: Amphibole forming along feldspar lath of CC2 (Layered), B: Amphibole aggregate of CC3 (Massive) (both in plane-polarized light), C: Post-cumulus amphibole interstitial to feldspar laths of CC7 (layered; SEM-BSE image), D: Blebby amphibole space-filling between fine-grained (<1mm) feldspar laths (layered; PPL image).

Amphiboles were analyzed by quantitative energy dispersive X-ray spectrometry and classified following the nomenclature of Leake et al. (1997) (with no revisions made in Leake et

al. 2003). The data was input into a classification program made by Locock (2014), which determines valence states for Fe and Mn. The Leake et al. (1997) nomenclature scheme is based on Mg# [Mg atoms per formula unit (hereafter noted as apfu) / Mg + Fe<sup>2+</sup> apfu] v. Si apfu, with amphiboles plotting in the calcic subgroup and classified ferro-pargasite rather than hastingsite because Fe<sup>3+</sup> apfu < Al apfu (Fig. 3.14).

**Table 3.1.** Representative compositions of amphibole.

Rock Type	Layered	Layered		Massive	Massive		Hybrid	Hybrid	
Zone	—	Core	Rim	—	Core	Rim	—	Core	Rim
Sample	CC1	DN2		CC13	CC3		DN3	CC11	
Na <sub>2</sub> O	3.43	3.18	3.5	3.02	3.21	3.16	3.73	3.05	3.02
MgO	3.57	6.28	2.92	2.96	7.81	2.6	3.06	4.9	2.75
Al <sub>2</sub> O <sub>3</sub>	10.1	9.63	7.94	9.93	10.29	10.7	8.16	10.01	9.77
SiO <sub>2</sub>	38.4	40.52	40.51	38.05	39.93	37.28	40.1	38.73	37.92
K <sub>2</sub> O	1.78	1.67	1.75	1.73	1.59	1.72	1.72	1.63	1.71
CaO	10.05	10.22	8.96	9.74	10.86	10.13	8.86	10.11	9.81
TiO <sub>2</sub>	1.81	1.92	1.66	1.89	2.13	2.05	1.6	2.48	2.49
MnO	0.69	0.81	0.92	0.84	0.57	0.77	0.94	0.75	0.91
FeO	21.302	20.517	25.479	23.897	17.04	22.976	24.316	21.956	24.742
Fe <sub>2</sub> O <sub>3</sub>	7.232	4.182	4.802	5.949	5.156	6.584	6.339	3.972	4.776
H <sub>2</sub> O <sup>+</sup>	1.88	1.91	1.87	1.86	1.93	1.86	1.87	1.89	1.86
Total	100.244	100.839	100.311	99.866	100.516	99.83	100.695	99.478	99.758
Cation Assignment - Based on 23 O-equivalents									
Si	6.112	6.298	6.492	6.129	6.155	6.007	6.401	6.165	6.127
Al	1.895	1.764	1.5	1.885	1.869	2.031	1.535	1.877	1.861
Ti	0.217	0.225	0.191	0.229	0.247	0.248	0.128	0.297	0.29
Fe <sup>2+</sup>	2.835	2.665	3.413	3.221	2.195	3.095	3.246	2.923	3.342
Fe <sup>3+</sup>	0.867	0.491	0.58	0.72	0.599	0.799	0.761	0.475	0.582
Mn	0.093	0.103	0.118	0.106	0.074	0.105	0.127	0.1	0.123
Mg	0.847	1.455	0.698	0.711	1.795	0.624	0.728	1.163	0.662
Ca	1.714	1.702	1.538	1.681	1.794	1.749	1.515	1.724	1.698
Na	1.059	0.958	1.087	0.943	0.959	0.987	1.155	0.941	0.946
K	0.361	0.331	0.358	0.356	0.313	0.354	0.35	0.331	0.352
Total	16	15.996	15.991	15.99	16	16	16.01	15.998	15.996
Mg#	0.186	0.315	0.149	0.153	0.391	0.139	0.154	0.254	0.144

For all amphiboles, Si totals varied from 5.997 to 6.593 apfu, while Mg# ranged from 0.098 to 0.492. The differences in totals observed for amphibole are more significant for zoned crystals compared to a change in rock type (see Table 3.1). For massive, hybrid, and mottled

samples, zoned amphiboles displayed a trend of Fe and Mn enrichment with Mg and weak Si depletion from core to rim (Fig. 3.15). For layered samples, some crystal zoning involved an increase in Si from core to rim, while all other element trends remained similar. For all element trends, the difference in weight percent did not exceed one, with the exception for Fe and Mg which ranged from 5-10 wt. % from core to rim.

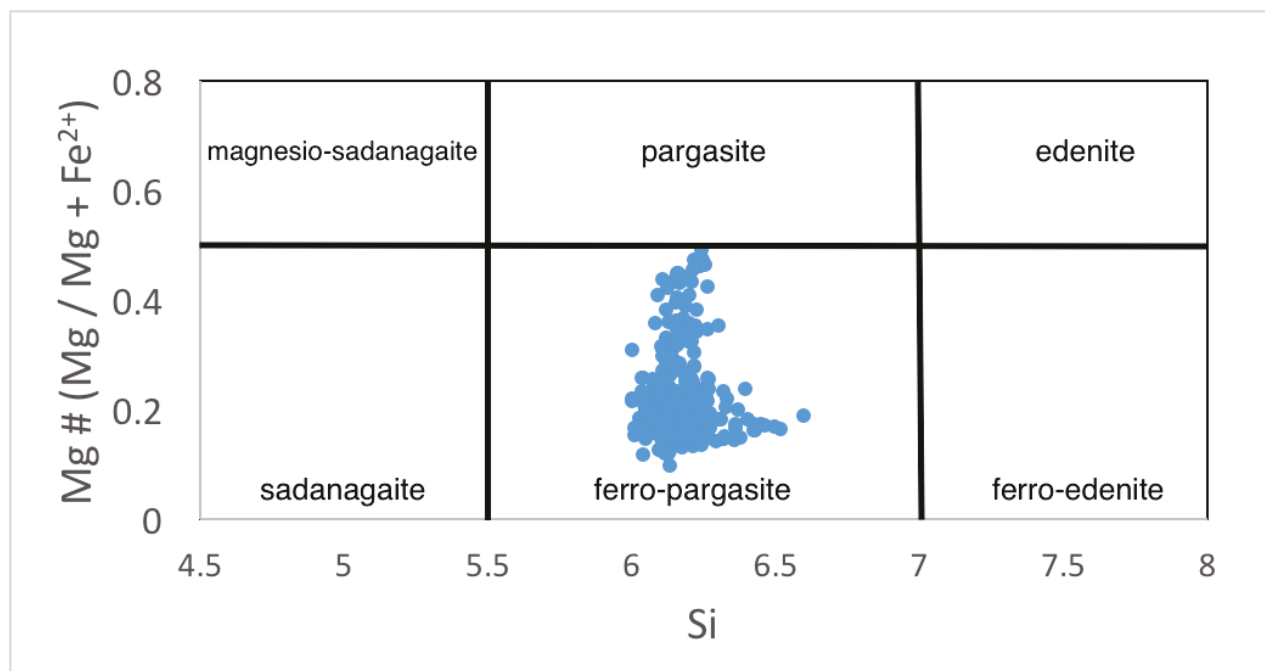


Figure 3.14. Composition variation and classification of amphiboles in nepheline syenite adapted from Leake et al. (1997).

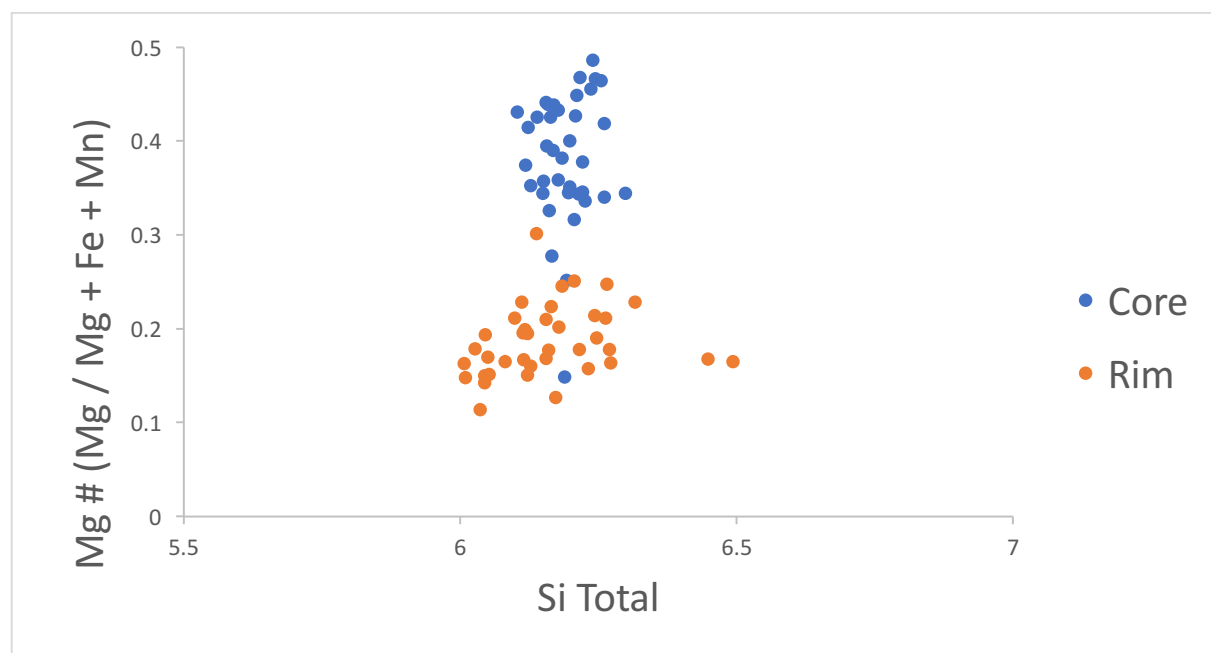


Figure 3.15. Compositional variation from core to rim of amphibole in nepheline syenite.

### 3.2.3. Mica

Biotite is a minor phase in all syenites with modes of 5-10 vol.%. In hand sample, it is observed as a black reflective mineral associated with amphibole aggregates, or as hexagonal crystals disseminated in massive and pegmatite sections. In thin section, it is pleochroic brown in plane polarized light, forming fine- to medium-grained tabular ‘books’ or anhedral masses (see Fig. 3.16). It is almost always associated with amphibole along grain boundaries or cleavage planes (rarely as shredded masses surrounding amphibole) and may be altered to chlorite. Larger crystals can be associated with calcite, fluorite, pyroxene, and magnetite. Rare apatite inclusions are also hosted within biotite.

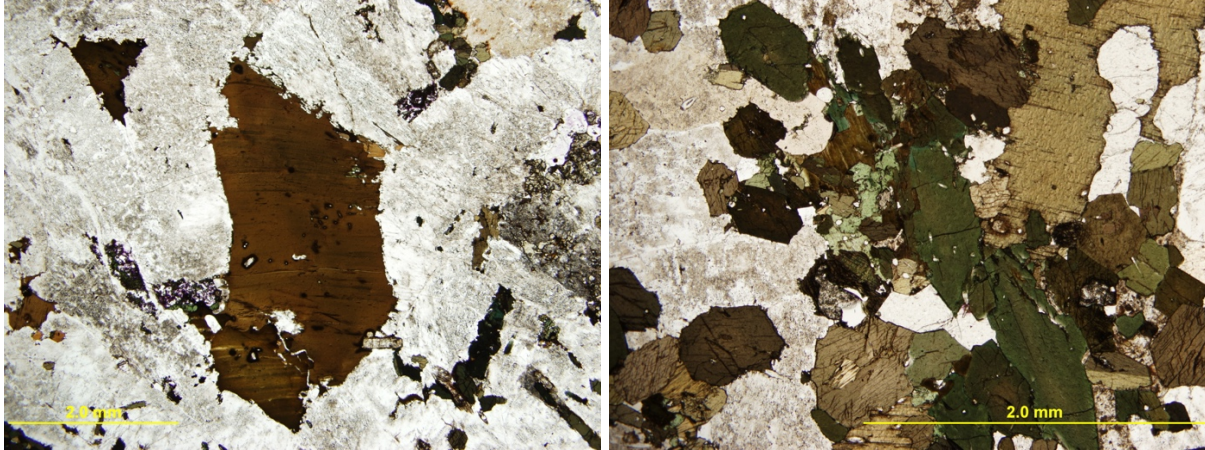


Figure 3.16. Left: Biotite with disseminated fluorite and pyroxene of DN2B (Layered), Right: Aggregate of biotite, amphibole, pyroxene, apatite, and fluorite of CC13B (Massive) (both in plane-polarized light).

Quantitative X-ray EDS analysis of the biotite gave Mg# ranging from 0.103 to 0.394 and Al ranging from 1.991 to 3.460 apfu (refer to Appendix III for representative compositions). Mica composition plot within the annite field in Figure 3.17, with two crystals plotting as siderophyllite. Layered, massive, and hybrid samples displayed little variation in biotite composition; whereas pegmatites displayed the largest variation in both aluminum and magnesium contents.

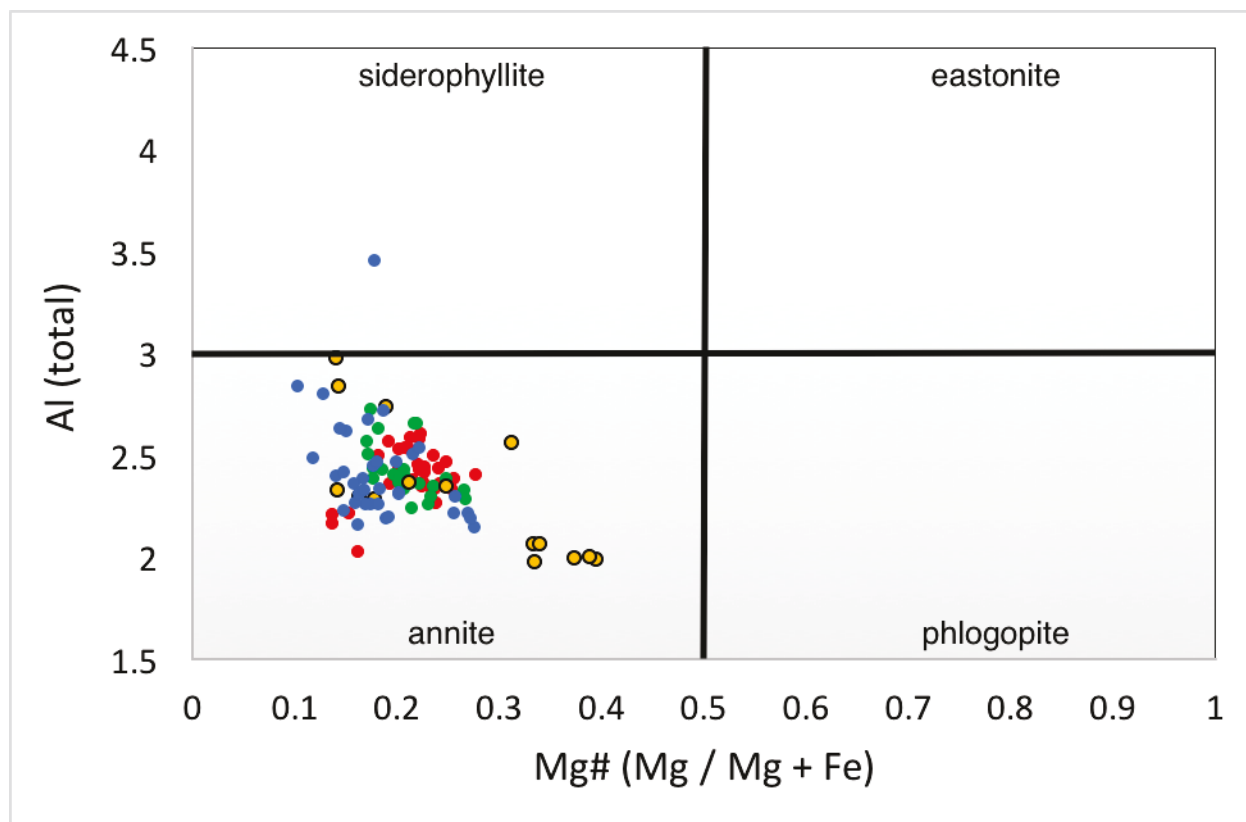


Figure 3.17. Compositional classification of biotite in various nepheline syenite lithology's where layered = red; green = massive; blue = hybrid/mottled; and yellow = pegmatite.

### 3.2.4. Nepheline and associated minerals

Nepheline  $\{Na_3(Na,K)[Al_4Si_4O_{16}]\}$  and zeolites (an alteration product of nepheline and feldspar) are found disseminated throughout the syenites, commonly as grey and red crystals, respectively. Natrolite  $[Na_2(Al_2Si_3O_{10})2H_2O]$ , the most common zeolite present, is observed as white to brick red anhedral masses altering nepheline/feldspar or forming interstitial to feldspar laths. Its red colour is attributed to finely divided hematite, derived from the breakdown of amphiboles and pyroxenes in late stage fluids (Mitchell & Platt 1982, see Fig. 3.18). Other zeolites identified include thomsonite  $[Ca_2Na(Al_5Si_5O_{20})6H_2O]$  and boehmite  $[AlO(OH)]$ . In thin section, nepheline is a minor component, forming up to 5 vol. % commonly as relict grains within zeolites. Zeolites may form up to 45 vol. % in massive sections, occurring as irregular

masses (up to 3 cm), consisting of fine-grained polymineralic aggregates (Fig. 3.18). Cloudy to red in plane-polarized light, the red colouration is more common when sharing grain boundaries with amphibole. Fine-grained inclusions of amphibole, feldspar, and pyroxene are not uncommon. Hydromuscovite  $\{(K,H_3O)(Al,Mg,Fe)_2(Si,Al)_4O_{10}[(OH)_2,(H_2O)]\}$  is also present in the syenites as a very fine-grained alteration product of nepheline. It is associated with the polymineralic zeolite aggregates which form disseminated alteration masses. Representative compositions are given in Table 3.2, with some low totals representing both the fine-grained nature of the minerals and their hydrated structures.

**Table 3.2.** Representative SEM-EDX compositions of zeolite, boehmite, and nepheline.

Wt.%	1 (boehmite)	2 (thomsonite)	3 (natrolite)	4 (hydromuscovite)	5 (nepheline)
Na <sub>2</sub> O	-	3.54	15.26	1.45	15.55
Al <sub>2</sub> O <sub>3</sub>	79.01	29.53	26.49	39.3	32.51
SiO <sub>2</sub>	1.16	35.85	47.42	43.05	44.96
K <sub>2</sub> O	-	-	-	10.73	5
CaO	0.17	13.39	-	-	0.48
FeO	0.54	-	-	-	-
Total	80.88	82.31	89.17	94.53	98.51
<b>Structural formula</b>					
O	2	10	10	22	32
Na	-	0.48	1.89	0.38	5.81
Al	1.31	2.46	2	6.22	7.38
Si	0.02	2.53	3.03	5.78	8.66
K	-	-	-	1.84	1.23
Ca	0.01	1.01	-	-	0.1
Fe	0.01	-	-	-	-
Total	1.34	6.48	6.92	14.22	23.17

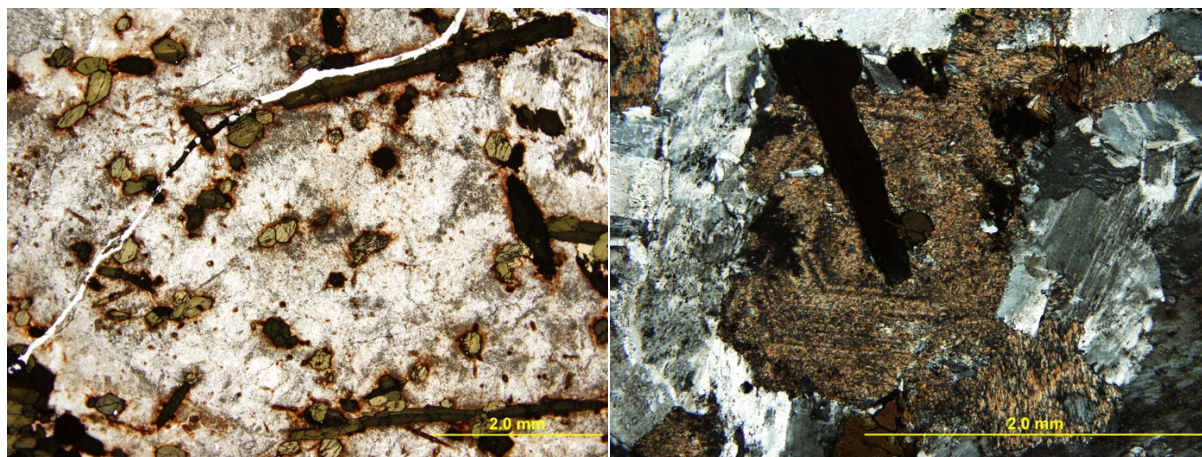


Figure 3.18. Left: Amphibole inclusions in natrolite of CC3 (plane-polarized light), Right: Zoned zeolite aggregate of DN5 (cross-polarized light).

### 3.2.5. Pyroxene

Pyroxene occurs only as a primary mineral in two pegmatite samples (CC4 and CC5), forming elongate, acicular, or prismatic dark green crystals disseminated throughout the zeolite/feldspar matrix. These samples contain no amphibole; with feldspar, brick red natrolite (with relict nepheline), and pyroxene sharing irregular grain boundaries making up the groundmass. In thin section, modes range from 10-45 vol.%, and crystals may be extensively altered containing inclusions or rims of magnetite and biotite (see Fig. 3.19 & 3.30). In the layered, hybrid and massive nepheline syenite, pyroxene forms <5vol % of the groundmass, as fine-grained (<1 mm) crystals disseminated with amphibole/biotite aggregates. It may also be associated with calcite and fluorite.

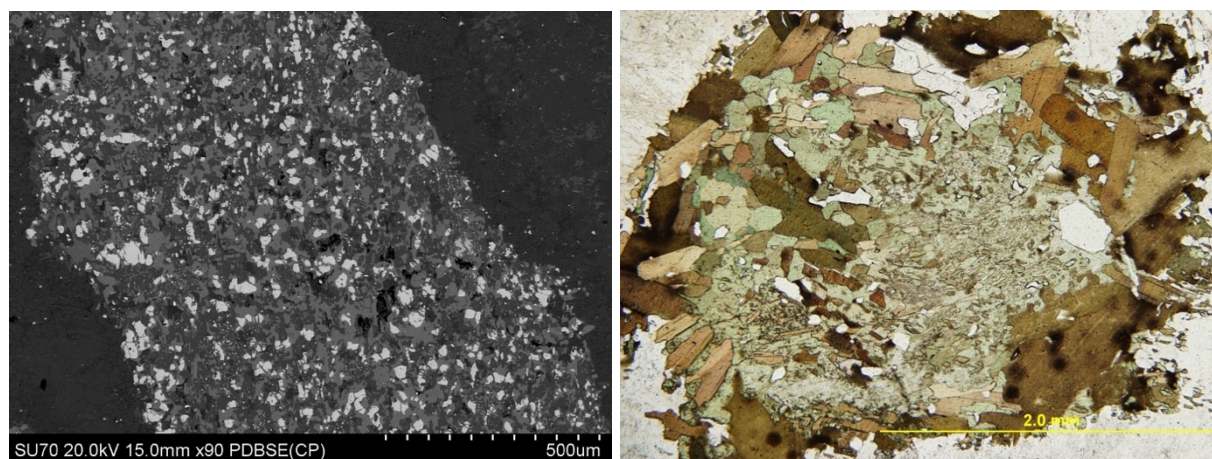


Figure 3.19. Left: Altered pyroxene with abundant magnetite inclusions of CC4 (Pegmatite; SEM-BSE image), Right: Pyroxene with biotite rim of DN4A (Hybrid; plane-polarized light).

Quantitative EDS analysis of the pyroxene indicated compositional variation between this mineral in nepheline syenite and late-stage pegmatites. In the pegmatite, pyroxene contained higher  $\text{Na}_2\text{O}$ ,  $\text{Fe}_2\text{O}_3$ , and lower  $\text{CaO}$  compared to the nepheline syenite. The compositional variation in these pyroxenes is shown in terms of three pyroxene end-members: aegerine, hedenbergite, and diopside in Figure 3.20. The overall general trend shows pegmatite pyroxene plotting closer to the aegerine end-member, while nepheline syenite pyroxene plot closer to the hedenbergite end-member.

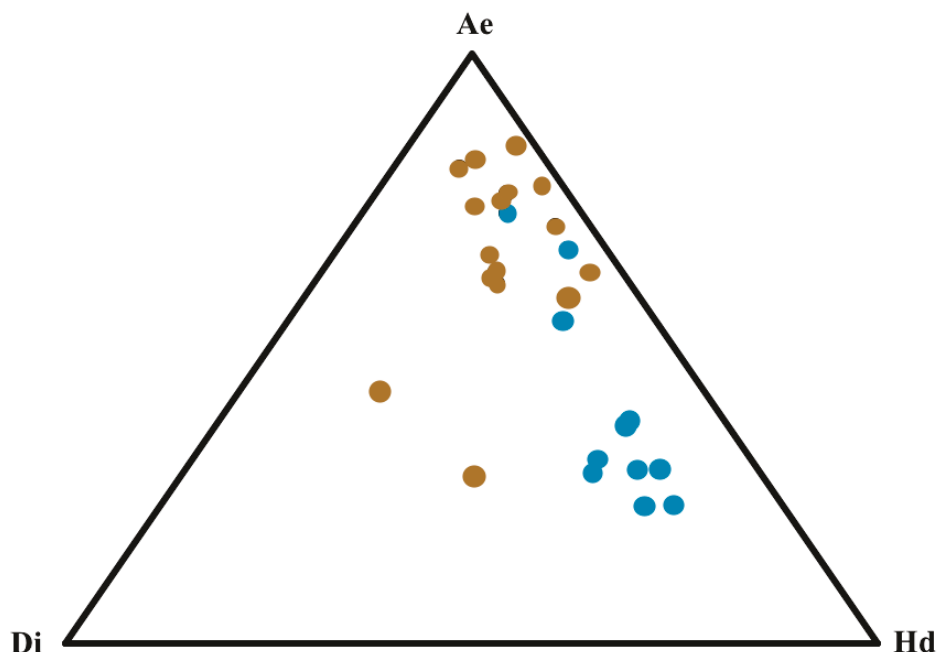


Figure 3.20. Compositional variation of pyroxene between late-stage pegmatites (brown) and nepheline syenites (blue) in Center II of Coldwell complex where Di = diopside; Ae = aegirine; Hd = hedenbergite.

### 3.2.6. Apatite Group Minerals

Fluorapatite  $[\text{Ca}_5(\text{PO}_4)_3\text{F}]$  occurs principally as small ( $<50 \mu\text{m}$ ), anhedral to euhedral elongate, acicular and hexagonal prisms commonly between 50 to 80  $\mu\text{m}$  in length, with a maximum observed length of 300  $\mu\text{m}$ . Apatite is the most abundant accessory mineral present, occurring within amphibole as inclusions or along fractures and grain boundaries, with fewer crystals hosted in feldspar (generally albite), biotite, and natrolite (see Fig. 3.21, 3.23). Zoning in apatite is common throughout all syenites, demonstrating changes in rare earth element (REE) concentrations (Fig. 3.22). Based on SEM-EDX compositions, concentric zoning predominantly displays increasing REE concentrations from core to rim, as Sr was undetectable in any grains analyzed. Irregular zoning is also common, occurring as rims or overgrowths of REE-rich apatite on an earlier generation of apatite, inclusions/patches within apatite displaying a change in REE,

or as increasing REE content from core to rim with an uneven growth pattern. The outer sections of apatite are commonly altered to britholite, which forms irregular masses along grain boundaries of apatite (see Fig. 3.23). The fluorine content of the apatite varies between 1.70 and 4.92 wt.%, with little difference observed between rock types. Apatite grains are enriched in light rare earth elements (La, Ce, Pr, Nd) as well as Y in varying abundance. For unzoned crystals, total REE<sub>2</sub>O<sub>3</sub> varies from 2.27 to 19.79 wt.%, although these end-member totals are rare, with an average of 8.61 wt.%. There are little differences in average REE<sub>2</sub>O<sub>3</sub> wt.% for unzoned crystals between layered, massive, hybrid and pegmatite sections (9.50, 8.23, 8.04, and 10.19 respectively), with larger variations observed between apatite from the same sample. For concentric and irregular zonation, average differences observed between core- to- rim or low- to high REE<sub>2</sub>O<sub>3</sub> varied from 4.88-6.45 wt.% for layered, massive, and hybrid syenites. Apatite cores reached as low as 1.76 REE<sub>2</sub>O<sub>3</sub> wt.% while rims extended up to 17.1 REE<sub>2</sub>O<sub>3</sub> wt.% for concentric zoning, while low to high totals for irregular zoning ranged from 1.78 to 19.79 REE<sub>2</sub>O<sub>3</sub> wt.% respectively. Reverse zoning was documented in eight crystals, with an average core to rim REE<sub>2</sub>O<sub>3</sub> of 13.20 and 7.80 wt.% respectively. Y<sub>2</sub>O<sub>3</sub> content for all apatite rarely exceeded 1 wt.%. The REE, Si, Ca, and P contents of the apatite crystals display a linear trend in Figure 3.23, indicating the well-known coupled substitution of  $\text{Ca}^{2+} + \text{P}^{5+} \leftrightarrow \text{LREE}^{3+} + \text{Si}^{4+}$  (Liferovich & Mitchell 2006).

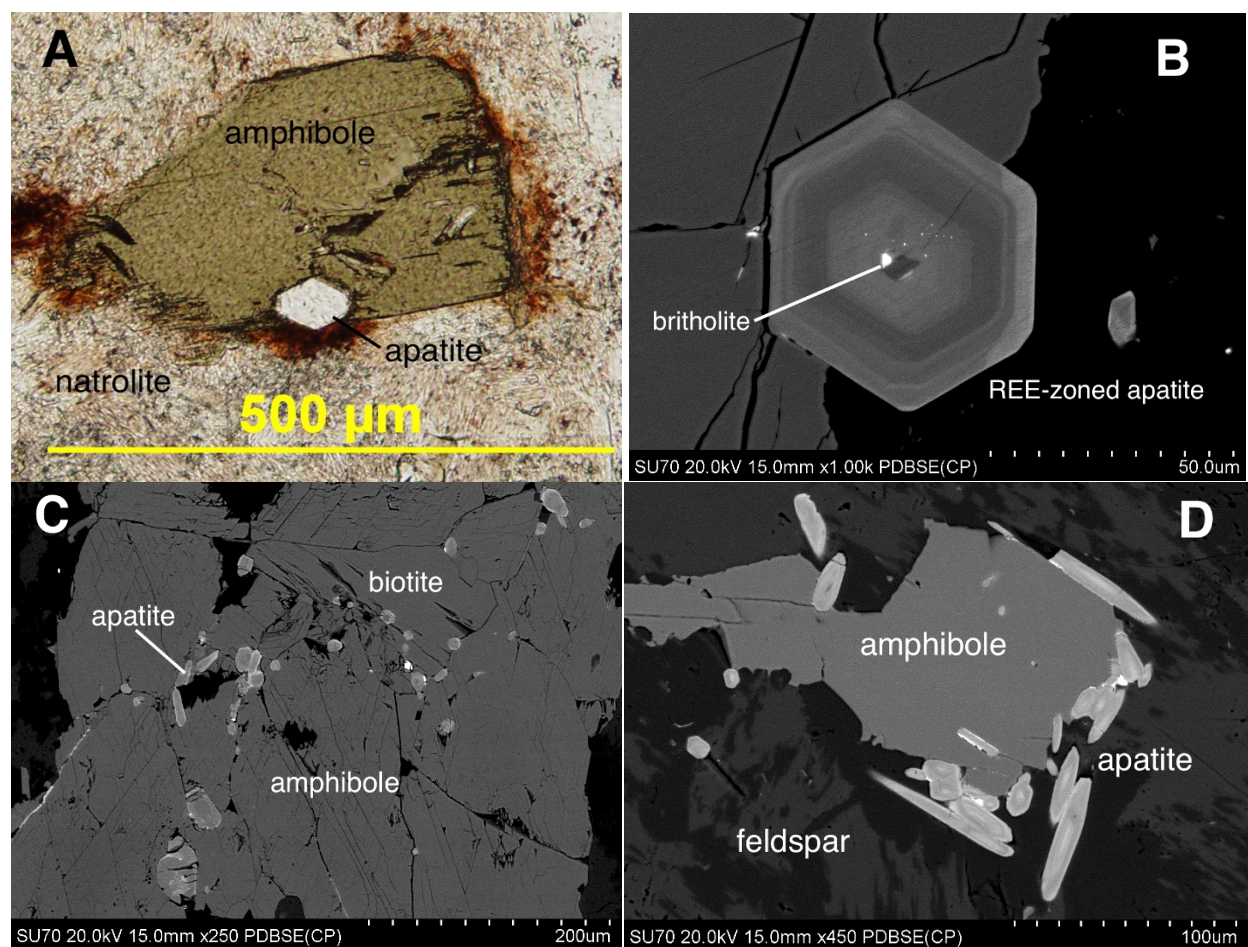


Figure 3.21. A is PPL-image, B-D are SEM-BSE images: (A) euhedral apatite along amphibole (CC14, mottled); (B) concentric apatite with britholite alteration (DN9, layered); (C) apatite along grain boundaries of amphibole and biotite (CC2, layered); (D) apatite cluster along amphibole-feldspar boundary (CC17B, mottled).

**Table 3.3.** Representative compositions of apatite group minerals.

Mineral Lithology Zoning	Britholite			Apatite				
	Layered	Hybrid	Massive	Layered	Massive Concentric		Hybrid Irregular	
	—	—	—	—	Core	Rim	Low	High
SiO <sub>2</sub>	16.06	18.85	21.8	3.29	0.81	3.23	2.65	4.02
P <sub>2</sub> O <sub>5</sub>	7.35	2.51	—	36.94	41.44	37.44	37.23	36.41
CaO	18.4	14.59	12.01	49.38	53.41	49.6	49.34	48.84
Y <sub>2</sub> O <sub>3</sub>	1.59	1.61	—	0.63	—	0.81	1.01	—
La <sub>2</sub> O <sub>3</sub>	13.2	15.83	18.67	2.47	0.55	2.55	1.65	2.76
Ce <sub>2</sub> O <sub>3</sub>	25.16	30.77	33.08	4.54	1.04	4.33	3.53	5.66
Pr <sub>2</sub> O <sub>3</sub>	2.6	2.84	2.81	—	—	—	0.59	0.75
Nd <sub>2</sub> O <sub>3</sub>	6.63	8.23	8.62	1.19	0.41	1.15	1.37	1.62
Sm <sub>2</sub> O <sub>3</sub>	1.23	—	1.15	—	—	—	—	—
Gd <sub>2</sub> O <sub>3</sub>	—	—	0.69	—	—	—	—	—
ThO <sub>2</sub>	5.89	5.18	—	—	—	—	—	—
F	1.31	—	—	2.37	3.31	2.56	3.01	2.32
Total	99.62	100.41	98.83	100.86	100.97	101.68	100.38	102.37
O=F, Cl	0.55	—	—	1	1.39	1.08	1.27	0.98
Total	99.07	100.41	98.83	99.86	99.58	100.6	99.11	101.39
REE <sub>2</sub> O <sub>3</sub>	48.82	57.67	65.02	8.2	2	8.03	7.14	10.79
O	36	—	—	26	—	—	—	—
P	2.18	0.81	—	5.41	5.77	5.42	5.32	5.42
Si	5.62	7.23	8.52	0.57	0.13	0.55	0.69	0.46
Ca	6.9	5.99	5.03	9.15	9.41	9.09	9.03	9.09
Y	0.3	0.33	—	0.06	—	0.07	—	0.09
La	1.7	2.24	2.69	0.16	0.03	0.16	0.18	0.1
Ce	3.22	4.32	4.74	0.29	0.06	0.27	0.36	0.22
Pr	0.33	0.4	0.4	—	—	—	0.05	0.04
Nd	0.83	1.13	1.2	0.07	0.02	0.07	0.1	0.08
Sm	0.15	—	0.15	—	—	—	—	—
Gd	—	—	0.09	—	—	—	—	—
Th	0.47	0.45	—	—	—	—	—	—
Total	21.68	22.9	22.84	15.7	15.43	15.64	15.72	15.51
F	1.45	—	—	1.29	1.72	1.39	1.26	1.64

Britholite [(LREE,Ca,Th,Y)<sub>5</sub>(SiO<sub>4</sub>,PO<sub>4</sub>)<sub>3</sub>(OH,F)] was not observed in hand sample or thin section petrography due to its small grain size (dominantly <50 μm), but was identified under SEM examination and analyzed using EDS. Found in all lithology's, britholite commonly displayed an anhedral crystal habit with micropores, fractures and irregular grain boundaries. It tends to form disseminated crystals, rare aggregates or intergrowths with fluorapatite. Britholite is the main alteration product of fluorapatite, crystallizing as overgrowths or replacement with different textures (see Fig. 3.22 & 3.23). Fluorapatite containing fractures or porosity may display britholite nucleating in these open cavities (see Fig. 3.21B). It is a major REE-sink in the syenite, with REE<sub>2</sub>O<sub>3</sub> ranging from 44.19-69.75 wt.% (avg. 54.36). The britholite contained high Th (up to 8.78 ThO<sub>2</sub> wt.%) contents with rare U concentrations comparable to pyrochlore (up to 0.92 UO<sub>3</sub> wt.%). Low Cl and F concentrations were also observed in some crystals up to 0.3 and 1.31 wt.% respectively, and moderate Y concentrations ranging from 0-3.95 Y<sub>2</sub>O<sub>3</sub> wt.%. In common with apatite, britholite does display significant variation in Ca, Si, LREE, and P contents, demonstrating the substitution scheme: REE<sup>3+</sup> + Si<sup>4+</sup> ↔ Ca<sup>2+</sup> + P<sup>5+</sup>. However, as seen in Figure 3.25, britholite does display some scatter when plotting these elements compared to apatite, which may be due to increased abundances in Th and U in the crystal structure which may require other elemental substitutions. Deviations from this substitution scheme have been described by Liferovich & Mitchell (2006), where britholite exhibiting excess Si and P cations may result from a deficiency in large cations (Ca and REE). However, the presence of actinides or large ion lithophile elements (LILE) may account for Ca- and REE-deficient compositions (Liferovich & Mitchell 2006).

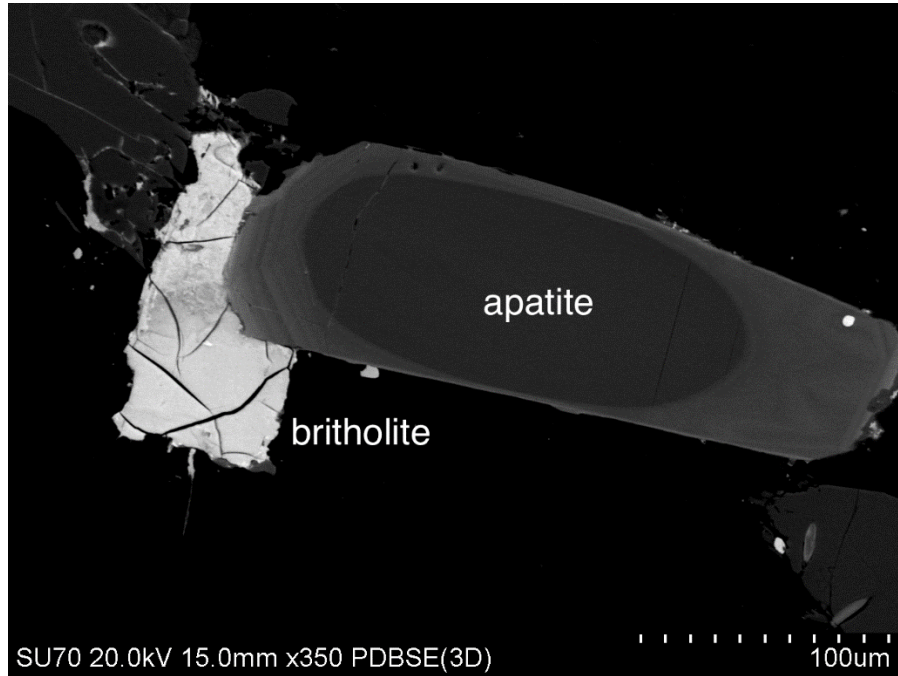


Figure 3.22. Zoned apatite with overgrowth of britholite of DN2 (Layered; SEM image).

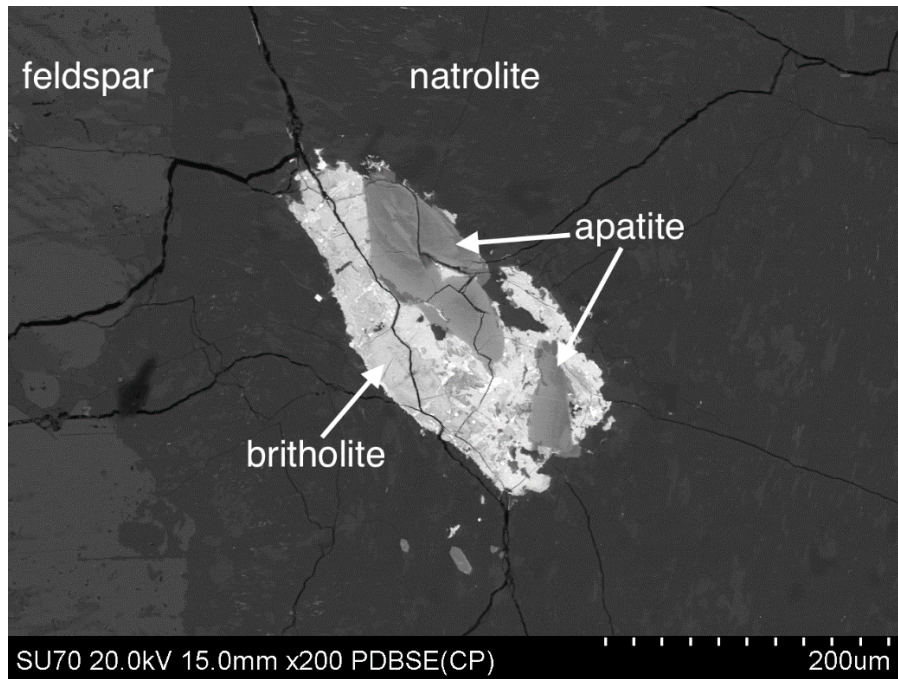


Figure 3.23. Britholite alteration of apatite in CC1A (Layered; SEM image).

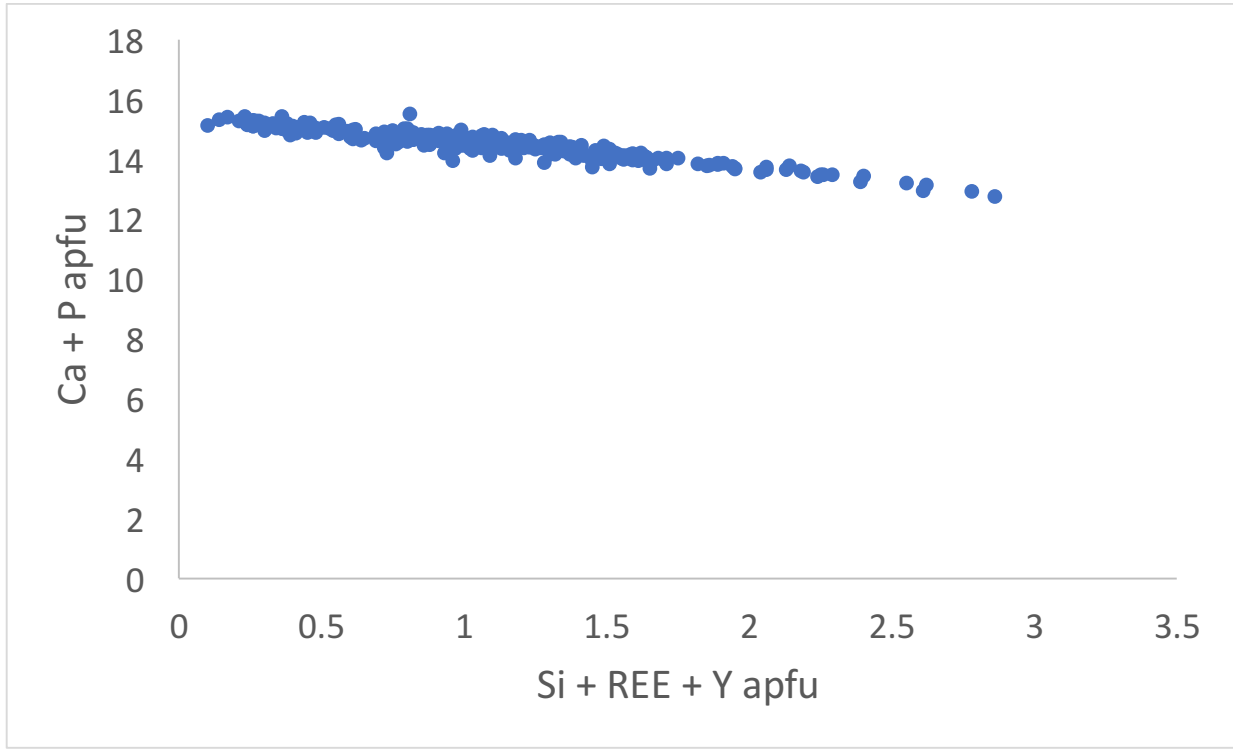


Figure 3.24. Cation substitution and composition of apatite.

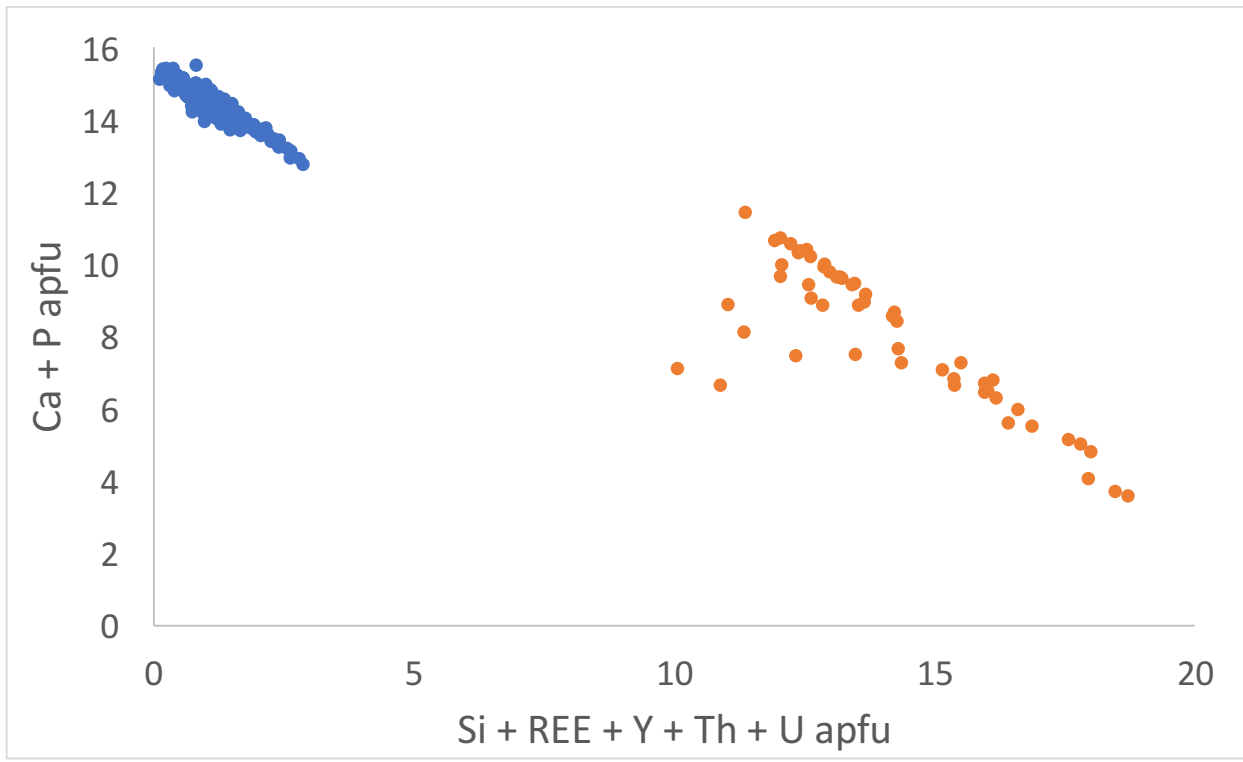


Figure 3.25. Cation substitution and composition variation of britholite and apatite where blue = apatite & orange = britholite.

### 3.2.7. Other accessory phases

After the apatite group minerals, wöhlerite [ideally  $\text{NaCa}_2(\text{Zr,Nb})\text{Si}_2\text{O}_7(\text{O,OH,F})_2$ ] is the next most abundant accessory phase. Forming crystals up to 500  $\mu\text{m}$  in size, wöhlerite occurs as anhedral crystals in all lithology's, and is commonly associated with amphibole and biotite aggregates (see Fig. 3.27). Crystals tend to form in assemblages with a variety of alteration minerals including: zircon, baddeleyite, thorianite, huttonite-thorite, fluorite, pyrochlore and fergusonite. Wöhlerite has significant amounts of  $\text{ZrO}_2$  and  $\text{Nb}_2\text{O}_5$ , varying between 13.49-14.83 wt.% and 8.86-13.22 wt.% respectively, with low concentrations of FeO, MgO,  $\text{TiO}_2$ , and MnO. Compositions are shown in Figure 3.26 with general compositions ranges of wöhlerite group minerals including: cuspidine [ideally  $\text{Ca}_4(\text{Si}_2\text{O}_7)(\text{F,OH})_2$ ], niocalite [ideally  $\text{Ca}_{14}\text{Nb}_2(\text{Si}_2\text{O}_7)_4(\text{O}_6\text{F}_2)$ ], hiordahlite [ideally  $(\text{Ca,Na,Y})_3(\text{Zr,Ti})\text{Si}_2\text{O}_7(\text{F,O,OH})_2$ ], lavenite [ideally  $(\text{Na,Ca})_2(\text{Mn,Fe}^{2+})(\text{Zr,Ti,Nb})\text{Si}_2\text{O}_7(\text{O,OH,F})$ ] and wöhlerite. All crystals plotted within the wöhlerite range.

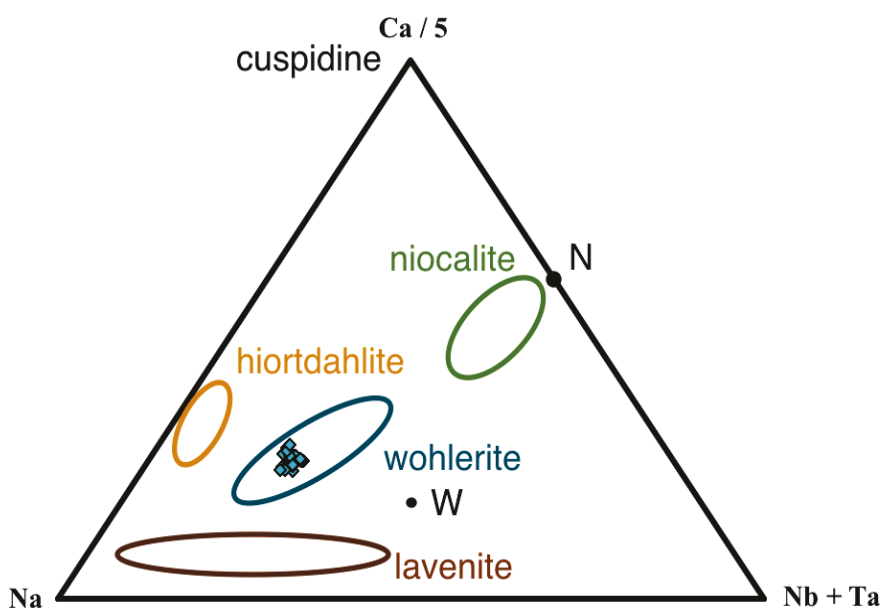


Figure 3.26. Compositions of wöhlerite with mineral ranges adapted from Mitchell & Belton (2004). W and N are the ideal compositions of wöhlerite and niocalite, respectively.

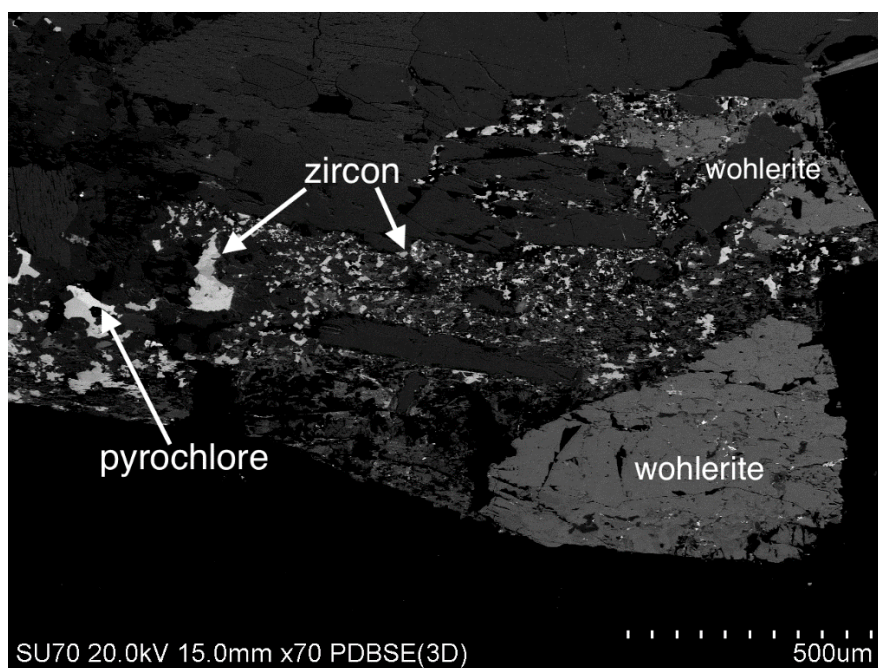


Figure 3.27. Wöhlerite altered to zircon and pyrochlore in DN2 (Layered; SEM image).

Pyrochlore [ideally  $(\text{Na,Ca})_2\text{Nb}_2\text{O}_6(\text{OH,F})$ ] occurs as anhedral crystals with a primarily  $<100 \mu\text{m}$  grain size. They are commonly found in association with other accessory minerals (i.e. zircon and wohlerite) which may form large alteration assemblages (see Fig. 3.27), although rare disseminated magmatic crystals are present. They are most abundant in pegmatite rocks (see Fig. 3.29), and display a wide range in composition with varying oxide wt.% in:  $\text{Nb}_2\text{O}_5$  (32.20-66.16%),  $\text{LREE}_2\text{O}_3$  (0-33.16%),  $\text{TiO}_2$  (2.24-15.57%), and  $\text{ZrO}_2$  (0-5.41%).  $\text{UO}_3$  and F were also present in some crystals with up to .72 and 4.37 wt.% respectively. Compositions of the pyrochlore are shown in Figure 3.28, with all crystals plotting within the pyrochlore field in the Nb-Ti-Ta ternary system (Hogarth 1977).

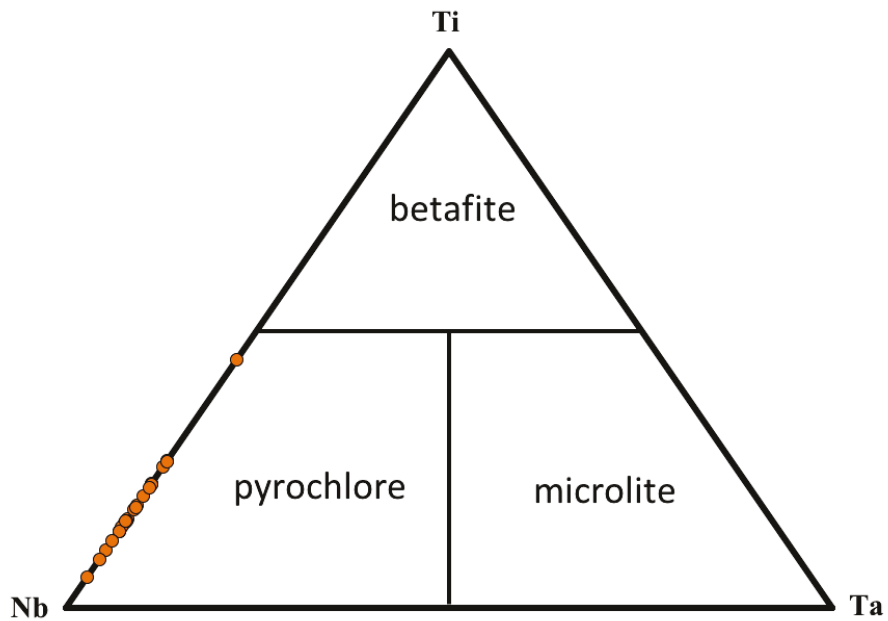


Figure 3.28. Compositions of pyrochlore plotted in the Nb-Ta-Ti system.

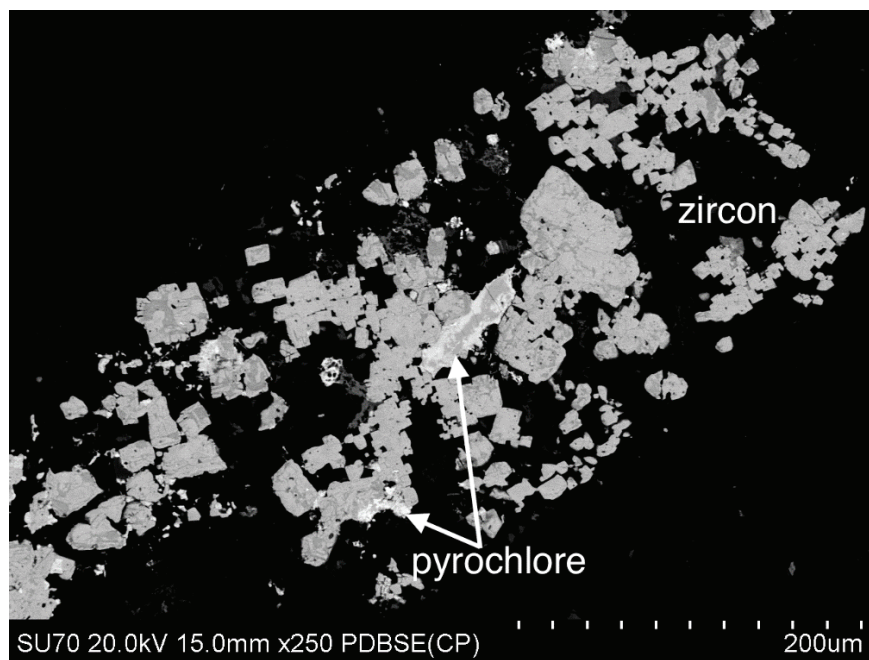


Figure 3.29. Disseminated zircon with pyrochlore of CC5 (Pegmatite; SEM-BSE image).

Together with the previously described minerals, there is also an array of less abundant accessory phases, all of which were only identified through SEM-EDS analysis. Titanite ( $\text{CaTiSiO}_5$ ), typically forming anhedral masses  $<200 \mu\text{m}$ , is present throughout all the rocks and are relatively stoichiometric, with varying amounts of: Na, Mg, Al, Fe, Zr, Nb, and F (all  $<5$  oxide wt.%). Allanite  $[(\text{Ca},\text{REE})_2(\text{Al},\text{Fe},\text{Ti})_3(\text{SiO}_4)(\text{Si}_2\text{O}_7)\text{O}(\text{OH})]$ , a rare phase, forms anhedral crystals with a significant concentration of total  $\text{REE}_2\text{O}_3$ , averaging 27.59 wt.%. Fergusonite ( $\text{YNbO}_4$ ) is another rare phase, typically forming very small ( $<20 \mu\text{m}$ ) crystals in alteration masses up to 2 mm associated with zircon and pyrochlore. It is most common in the pegmatite samples, and is the only mineral phase analyzed which contained heavy rare earth elements (Dy, Ho, Er, Tm, Yb) in detectable amounts. Total HREE $_2\text{O}_3$  for this mineral averaged 11.22 wt.% with  $\Sigma\text{REE}_2\text{O}_3$  averaging 17.83 wt.%. Representative compositions of these phases are listed in Table 3.4. Other phases which were identified, forming as primary minerals or alteration products of primary or accessory minerals include: fluorite, zircon, baddeleyite, thorianite, huttonite, Fe-Ti-Mn oxides (dominantly magnetite and ilmenite), and sulphides (pyrite, chalcopyrite, molybdenite, galena) (Fig. 3.30 & 3.31).

**Table 3.4.** Representative compositions of accessory minerals.

Wt.%	1	2	3	4	5
Na <sub>2</sub> O	7.53	—	—	—	—
Al <sub>2</sub> O <sub>3</sub>	—	2.12	—	—	11.28
SiO <sub>2</sub>	30.91	30.6	2.92	5.9	30.23
CaO	29.99	28.44	15.66	6.72	8.42
TiO <sub>2</sub>	0.99	34.93	8.39	4.67	—
MnO	0.74	—	—	—	—
FeO	1.76	2.84	1.39	3.53	18.15
ZrO <sub>2</sub>	14.15	0.46	—	3.15	—
Nb <sub>2</sub> O <sub>5</sub>	11.32	1.03	63.23	45.92	—
La <sub>2</sub> O <sub>3</sub>	—	—	1.65	3.84	5.74
Ce <sub>2</sub> O <sub>3</sub>	—	—	3.55	17.46	15.48
Pr <sub>2</sub> O <sub>3</sub>	—	—	—	2.06	2.38
Nd <sub>2</sub> O <sub>3</sub>	—	—	1.25	4.71	5.35
Sm <sub>2</sub> O <sub>3</sub>	—	—	—	0.7	0.88
F	4.17	1.07	—	—	—
Total	101.57	101.5	98.04	98.66	97.9
O=F	1.76	0.45	—	—	—
Total	99.81	101.05	98.04	98.66	97.9
REE <sub>2</sub> O <sub>3</sub>	—	—	6.45	28.77	29.83
O	36	20	6	6	13
Si	7.69	3.94	0.15	0.34	3.25
Ti	0.19	3.38	0.33	0.2	—
Al	—	0.32	—	—	1.43
Fe	0.37	0.31	0.05	0.16	1.63
Mn	0.16	—	—	—	—
Ca	8	3.92	0.86	0.42	0.97
Na	3.63	—	—	—	—
Zr	1.72	0.03	—	0.09	—
Nb	1.27	0.06	1.47	1.21	—
La	—	—	0.03	0.08	0.61
Ce	—	—	0.07	0.37	0.09
Pr	—	—	—	0.04	0.21
Nd	—	—	0.02	0.1	0.03
Sm	—	—	—	0.01	0.23
Total	23.03	11.94	2.98	3.02	8.45
F	3.29	0.44	—	—	—

Total Fe expressed as FeO. 1: wohlerite, 2: titanite, 3-4: pyrochlore, 5: allanite

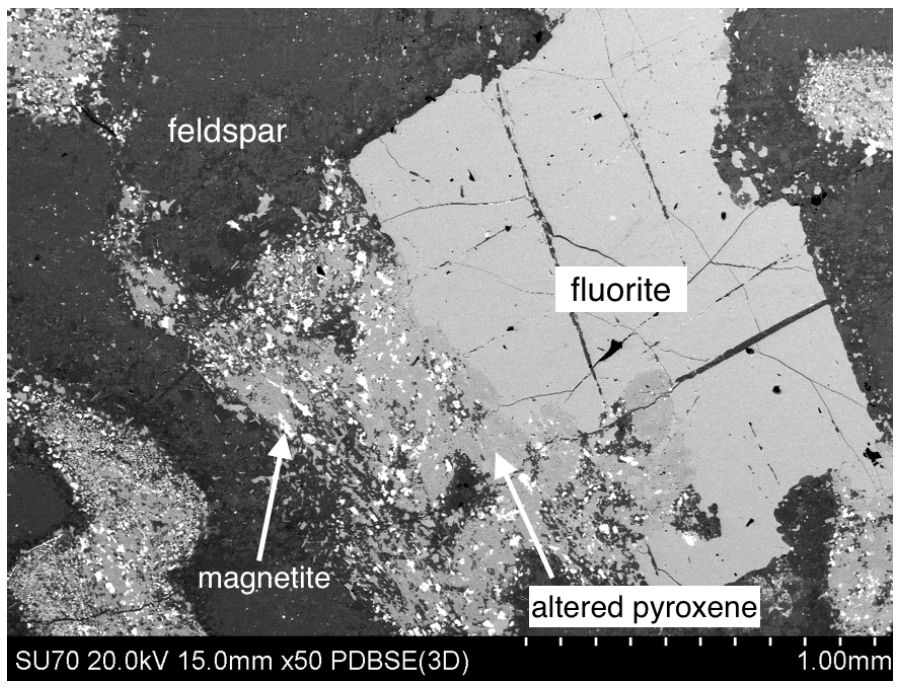


Figure 3.30. Fluorite rimming pyroxene/magnetite assemblage of CC5 (Pegmatite; SEM image).

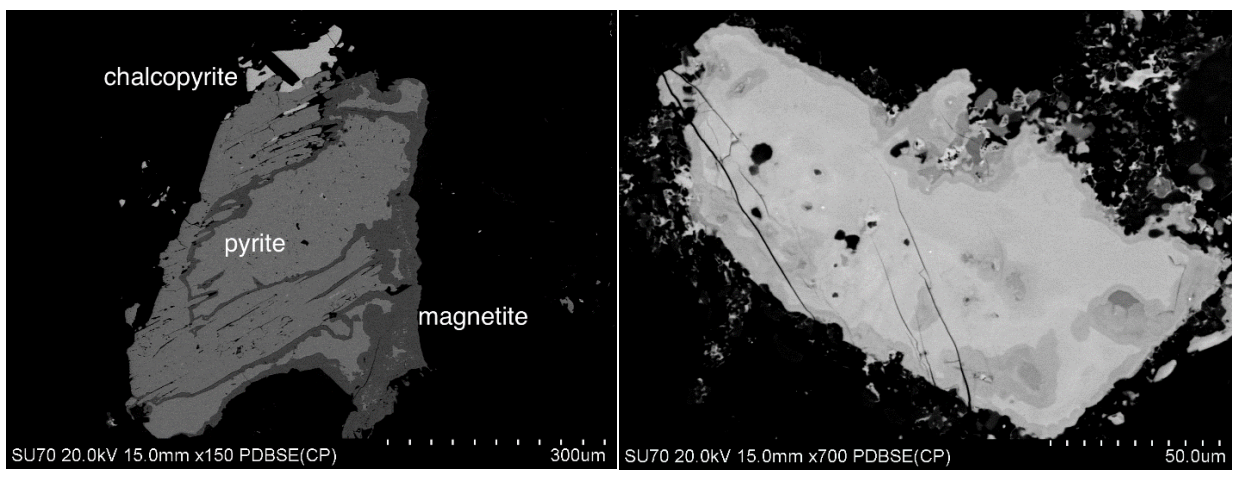


Figure 3.31. Left: Pyrite oxidized to magnetite of DN6 (Pegmatite), Right: Zoned pyrochlore of CC4 (Pegmatite) (both SEM images).

## Chapter 4

### Discussion

#### 4.1. Mineralogy of the Layered Series

Alkali feldspar is the primary mineral of the nepheline syenite in the area investigated. In the layered series, K-feldspar forms the cumulus phase, with amphibole and minor apatite forming interstitially to feldspar laths or in amphibole-rich laminae at the base of individual layers. Layers commonly display modal grading from amphibole laminae, to a mixture of amphibole and feldspar, followed by a section of 'normal syenite' (dominantly feldspar with disseminated amphibole; Fig. 4.1 & 4.2). The mineralogy observed differs from the layered series nepheline syenite described on Pic and Allouez Islands by Mitchell & Platt (1982), where rhythmic layering is defined by varying concentrations of olivine, pyroxene, amphibole, magnetite, and apatite. In the Mitchell & Platt (1982) study, feldspar is the primary intercumulus phase together with amphibole. However, in common with the layered series examined in this study, evidence of hydrodynamic sorting is prevalent with graded beds, cross-bedding, and scouring of previously deposited channels all characteristic, suggestive that strong currents were also in effect (cf. Mitchell & Platt 1982).



Figure 4.1. Modal grading displaying amphibole laminae and sections of dominantly feldspar.

Whereas crystallization in the magma chamber is driven by cooling, the cumulus mineralogy at any time is essentially controlled by composition-dependant parameters (i.e. element concentration, temperature, pressure, water content; Bailey et al. 2006). For the Pic Island layered nepheline syenite, olivine and magnetite were probably the earliest and highest temperature minerals to fractionate from the magma (Mitchell & Platt 1982). Although determining the temperature of crystallization for these cumulate minerals is impractical due to the extensive sub-solidus reactions, Mitchell & Platt (1982) proposed that the nepheline syenite crystallized over a range of 900-700°C, followed by sub-solidus reactions with hydrothermal

fluids. In the Center II normal syenites and cumulate feldspar layering of this study, the cotectic crystallization and H<sub>2</sub>O-rich nature of the magma would inhibit the formation of mafic-rich cumulate phases (Mitchell & Platt 1982). The anhydrous mafic phases must have crystallized in portions of magma where they were the only liquidus phases, and where liquids were not sufficiently evolved to reach a cotectic involving amphiboles and feldspars. The layered syenite investigated in this work probably represented a different magma pulse than that at Pic Island, potentially derived from an evolved source relative to that of Pic Island, but which would allow the formation of cumulus alkali feldspar. Normal syenite associated with the layered series represents un-sorted crystal mush piles, as well as syenite crystallizing towards the central portions of the chamber, where convection might have slowed and an allotriomorphic granular texture is produced, indicating cotectic crystallization of feldspar, nepheline, and amphibole (Mitchell & Platt 1982).

The initial crystallization of olivine and magnetite may have been due to their structural simplicity, low volatile concentrations, or pressure conditions of the magma chamber. These mafic phases would have continued to crystallize until the bulk composition of the magma passed out of their phase stability field and they were no longer liquidus phases. Another controlling factor for mineral nucleation, which has been hypothesized to contribute to the formation of layered syenites in other alkaline complexes (i.e. Illimaussaq Complex), could have been the sequential change in volatile content (Bailey et al. 2006). Initially, low volatile contents allowed the nucleation of olivine and magnetite, until these volatile concentrations increased to an amount which suppressed the nucleation of these minerals. Amphibole would then begin to form the cumulus minerals, which could nucleate and grow in an environment with high contents of volatiles. Crystallization of amphibole and apatite would have proceeded until volatiles were

sufficiently decreased to where the nucleation of cumulus feldspar could occur. The conditions in the magma might have been a response to short-lived events (fracturing, cauldron collapse, local seismicity), which would have reduced pressure and volatile concentrations in the chamber, and potentially initiated a change in the cumulus mineral crystallizing (Bailey et al. 2006).



Figure 4.2. Well-preserved block of layered nepheline syenite displaying alternating mafic- and feldspar-rich layers.

This sequential change in cumulus mineralogy is well documented in the Illimaussaq peralkaline complex of the Gardar Province in South Greenland (Marks & Markl 2015). Although the layered sequences in Illimaussaq lack structures indicative of current processes like in Coldwell, they may provide some insight into the change of cumulus mineralogy observed in the rocks. Macro-layering within the kakortokites (agpaitic nepheline syenite) consists of three

modally graded layers dominated by arfvedsonite (amphibole), eudialyte-group minerals, and alkali feldspar. Hunt et al. (2017) proposed the key control on layering was an oscillating volatile concentration in the magma. An initial high concentration of volatile elements would allow formation of the arfvedsonite layer, when nucleation of other minerals was suppressed (Hunt et al. 2017). This nucleation, along with minor processes of equilibration, and upwards loss of volatiles would have decreased the concentration of halogens, and enabled the sequential development of eudialyte followed by alkali feldspar layers (Hunt et al. 2017). Micro-rhythmic layering in arfvedsonite lujavrite (agpaitic nepheline syenite rich in eudialyte) of the Illimaussaq complex has also been linked to changing volatile concentrations in the magma. Crystallization of the 'dark layers' present, with relatively high contents of sodalite, microcline, and arfvedsonite, would reduce the immediately adjacent layer of these components, and lead to the eventual crystallization of an urtitic layer, with high contents of nepheline, eudialyte and late-stage analcime (Bailey et al. 2006). The nature of the cumulus mineralogy was intimately linked to the oscillating contents of volatiles (specifically NaCl and H<sub>2</sub>O) along the crystallization front. Alternative origins for the layering are given by Bailey et al. (2006), including the initiation of nepheline and eudialyte rich layers by a pressure decrease and/or loss of volatiles from the collapse of the magma chamber roof or earthquakes, which may have been associated with the change in cumulus mineralogy in the layered nepheline syenites of the Coldwell Complex.

Late-stage pegmatites and lamprophyres cross-cut the nepheline syenite throughout the field area (see Fig. 4.3). The lamprophyres represent late-stage, potentially fracture filling units forming after the pluton reached a state where brittle fracturing could be produced. However, this brittle behaviour may develop in crystallized magmas with as much as 30-35% melt (Duke et al. 1988). The magma of these dykes probably represents some of the final residual melts from the

evolution of the parental magma. There may be a variety of origins for the pegmatite material, with different mechanisms operating in different magma batches. Pegmatite units would have been the last to crystallize within the magma chamber and remained mobile until late stages of consolidation. Where the pegmatitic fluid crystallizes may depend upon the local structure setting and stresses during crystallization (Duke et al. 1988). Continued fractionation in the chamber would develop these late-stage rocks, enriching them in volatiles and incompatible elements. The abundance of volatiles would have resulted in the formation of natrolite and zeolites as late-stage primary and deuteric phases, and promoted extensive ion exchange between fluids and feldspar (Mitchell & Platt 1982). This abundance of incompatible elements is demonstrated by the mineralogy of the pegmatites, which contain the most exotic suite of minerals. Accessory minerals in these rocks contain an increased concentration of Nb, Zr, Th, and Ti-bearing minerals including pyrochlore, Nb-Fe-bearing titanite, fergusonite, zircon, baddeleyite, thorianite, and huttonite. In addition, fergusonite analyzed in one sample (DN6) contained up to 12.28 wt.% HREE<sub>2</sub>O<sub>3</sub>, the only mineral analyzed in all samples to contain any detectable HREE, signifying the extreme differentiation of the rocks.

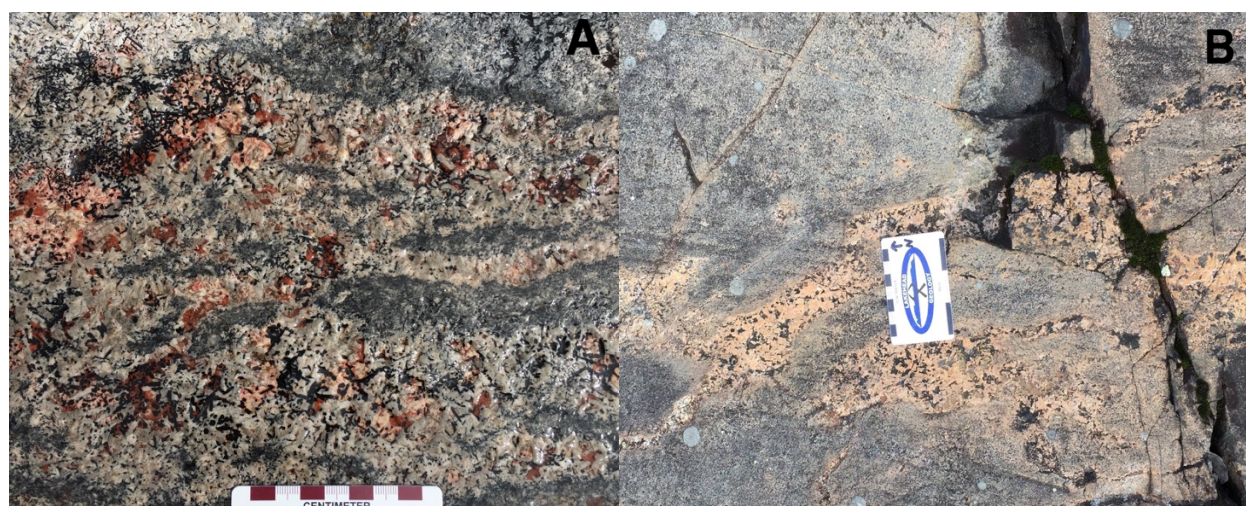


Figure 4.3. A & B: Late-stage pegmatite veins/blebs cross-cutting syenite.

In two pegmatite samples, CC4 and CC5, pyroxene was a primary constituent. Throughout the rest of the nepheline syenite samples, pyroxene is only present as rare, fine-grained crystals associated with amphibole aggregates. Composition of the pyroxenes are shown within Figure 4.4, displaying a trend from hedenbergite ( $\text{CaFe}^{2+}\text{Si}_2\text{O}_6$ ) to aegirine ( $\text{NaFe}^{3+}\text{Si}_2\text{O}_6$ ) composition. The development towards an aegirine composition is dependent upon  $f_{\text{O}_2}$ , temperature, and magma composition (especially  $\text{Na}_2\text{O}$  and  $\text{CaO}$ ), with silica saturation not being a determining factor (Mitchell & Platt 1982). Pyroxene in the nepheline syenite formed as secondary crystals after amphibole when the magma would have evolved to a relatively Fe-rich composition, as shown by the formation of hedenbergite relative to diopside. In the pegmatites, pyroxene plots close to the end-member aegirine, displaying the evolution of the magma to a relative enrichment in  $\text{Fe}_2\text{O}_3$  and  $\text{Na}_2\text{O}$  and depletion in  $\text{MgO}$  and  $\text{CaO}$ . A decreasing temperature and oxygen fugacity, and an increase in alkalinity ( $a_{\text{liq Na}_2\text{O}}$ , which can in turn increase  $a_{\text{liq Fe}^{3+}}$ ) all accompanied an increase in aegirine content for Pic Island syenites (Mitchell & Platt 1982). The compositions observed at Neys are generally also more evolved than those given in the Mitchell & Platt (1982) study, with pyroxenes having compositions between the diopside-hedenbergite end members (Fig. 4.4).

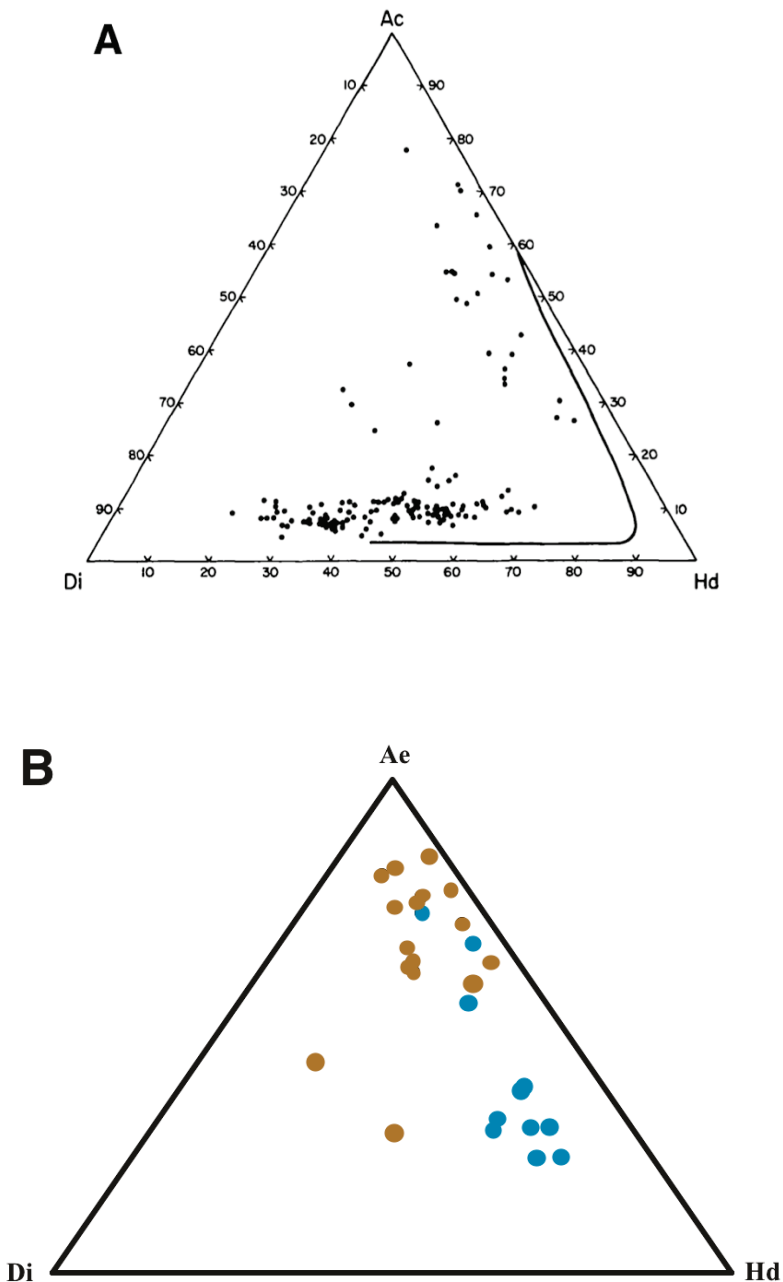


Figure 4.4. A: Compositions of pyroxene in nepheline syenite of Pic Island (Mitchell & Platt 1982), solid line is trend of pyroxene in Center I ferroaugite syenite (Mitchell & Platt 1978), B: Compositions of pyroxene from nepheline syenite (blue) and pegmatite (brown) from this study.

Further examples of the continued fractionation and evolution of the magma chamber are demonstrated by the compositions of amphibole, biotite, and apatite. Zoned amphibole in the

nepheline syenite displays a trend of Fe, Mn, and K enrichment and Mg, Si, Ca, and Ti depletion from core to rim. Initially, amphibole crystallized in a relatively unevolved magma, forming interstitial to cumulus feldspar laths along the chamber walls or at the wall-floor interface where crystals accumulated as unstable crystal mushes. These piles would eventually slump, potentially due to over-steepening or other tectonic events, and form surge-type density currents which could also erode previously deposited layered syenite (Mitchell & Platt 1982). The high degree of porosity in the deformed crystal piles allowed for interaction between the amphibole and evolved magma, forming strongly zoned amphibole crystals present in the layered and massive syenites. Zoning in the hybrid syenites may be accounted for by the amphibole in the normal syenite interacting with emplacement of the mafic syenite magma.

Apatite present in the nepheline syenite would have formed in a similar fashion to amphibole, forming in pockets of magma interstitial to the cumulus feldspar. Most apatite crystals are found along the grain boundaries or fractures in amphibole, with zoned crystals displaying an increase in LREE from core to rim. Apatite is the primary mineral hosting P, REE, and F, and would have initially formed with relatively low to moderate concentrations of LREE. Again, following the slumping or disturbance of initial deposition, apatite crystals would interact with a more evolved magma, presumably with increased concentrations of volatiles and LREE, which would initiate the crystallization of the increased LREE rim. The small crystal size of the apatite crystals would allow them to remain nucleated with the amphibole crystals, however larger crystals (>100  $\mu\text{m}$ ) may have mechanically concentrated with amphibole due to density similarities.

Biotite appears to form after amphibole ceased to crystallize, forming along amphibole grain boundaries or cleavage planes as well as some disseminated crystals. In some aggregates,

biotite may have been an alteration product of amphibole from the interaction of fluids, where it can be intimately associated with calcite, fluorite, pyroxene, and magnetite. It may also alter to chlorite along grain boundaries and cleavage planes displaying alteration from late stage deuteric fluids. All mica crystals analyzed (except one) plot within the Fe-rich annite field (with pure annite not found in nature), demonstrating the evolved nature of the magma from which it formed.

Although feldspar is the primary mineral present within the nepheline syenite, and the cumulus phase, it cannot be used to analyze the evolution of the magma chamber. The general cloudiness of the feldspar crystals observed optically, together with the presence of micropores, and coarse, disordered patch perthite is commonly attributed to partial replacement in a deuteric fluid during the cooling of the rock (Parsons et al. 2013). It is obvious from the perthitic texture present that initially K-feldspar was the primary mineral, which later exsolved Na from its structure to produce the albite lamellae observed with optical SEM, and CL imaging (see Fig. 3.11 & 3.12). However, the interaction of the feldspar with residual fluids at high temperatures has destroyed the original magmatic composition through recrystallization, albitization, and ion-exchange (Mitchell & Platt 1982). The presence of secondary albite (displaying a violet colour in CL images), natrolization of feldspar and nepheline, formation of boehmite and Na-Ca zeolites indicates the abundance of mobile Ca-Na-K fluids present during the final stages of consolidation, and demonstrates the evolved nature of the feldspar from their original magmatic composition (Mitchell & Platt 1982).

## 4.2. Dynamics of Magma Chamber

The style of intrusion, structural/textural observations, and mineralogy of nepheline syenites within Center II of the Coldwell Complex are similar to many other layered alkaline and granitoid plutons. These can be used as analogues to determine aspects of the petrology of nepheline syenites in this study, specifically the layered lithology's. Mechanisms which have been proposed to produce layering in felsic magmas, some of which are applicable to the nepheline syenites of Center II, have been summarized by Gaweda & Szopa (2011):

- 1) Gravitational settling of early- formed dense minerals; concurrent nucleation of minerals in magma chamber separated by density contrasts (e.g. kakortokites in Ilimaussaq complex, Lundhuber et al. 2015).
- 2) Hydrodynamic sorting; density currents, convecting magma redistributes fractionated cumulate minerals producing magmatic sedimentation features (e.g. Nunarssuit syenite, Hodson 1998 and Skaergaard Intrusion, Irvine et al. 1998).
- 3) Growth along a boundary layer; each liquid layer generated through open-system processes at crystallization front, controlled by composition within interface between crystal pile and crystal-free magma (e.g. Iujavrites Ilimaussaq complex, Bailey et al. 2006, and Dobel batholith, Pupier et al. 2008).
- 4) Submagmatic processes; including filter pressing, and grain supported flow in crystal mush (Tarcuocate Laccolith, Pons et al. 2006 & Dobel batholith, Pupier et al. 2008).
- 5) Open system processes based on intrusion of magma batches into syn-plutonic shear zones.

In this study, hydrodynamic processes are favoured for the origin of the layered syenites, producing an array of magmatic sedimentation features (graded layers, slumping, scour channels, flame structures and load casts). Two mechanisms in particular, surge-type density currents and separation and reattachment vortex cells, are proposed to have formed the modally graded cumulate layers.

The layering of nepheline syenite within Center II, in conjunction with other magmatic sedimentary features, indicates a strong convecting current operating during the formation of the rocks. The formation of these layers was a product of fractional crystallization, varying

deposition mechanisms, and reworking through erosion or deformational processes. Previous research done by Clark (1983) and Mitchell & Platt (1982) on layered nepheline syenites within Center II have also concluded that the layered nepheline syenites were a product of strong currents within the magma chamber. Crystallization occurs when a hot, unevolved magma begins to cool along roof and walls of the chamber. Crystals may be frozen along the roof and walls, while others may be carried down and spread across the chamber floor (Irvine 1998). As flow in the magma chamber approaches the change in slope at the floor, it is abruptly slowed and results in hydraulic jumps and associated complex circulation patterns (Irvine 1998). These mechanisms can result in episodes of erosion and deposition, where unstable masses of early phases slump and erode previously deposited layers and mingle with poorly consolidated crystal mush (Mitchell & Platt 1982). Alternatively, tectonic activity may have also contributed to the initiation of density currents, causing the redistribution of cumulus minerals. Faults forming during magmatism or potential cauldron subsidence could have destabilized accumulated crystal piles and stimulated slumping (Gaweda & Szopa 2011). As well, during periods of cauldron subsidence, volcanic xenoliths were brought down forming some of the xenolith-rich zones observed, along with ghost xenoliths (highly assimilated rocks), which may contain relict vesicles.

Center II in the Coldwell Complex would have represented an open system, with continuous but irregular magma injection and recharge, feeding convection currents within batches of nepheline syenite. This is represented by layered syenites of variable cumulus mineralogy, multiple xenolith zones of basalt and biotite-gabbro, and heterogeneous zones of cross-cutting normal, mafic, and pegmatitic syenite. The deposition of the layered series may have been associated with magma replenishments, with the thermal input of magma contributing

to the ability of the magma to effectively convect. In the nepheline syenites on Pic Island, xenoliths of nepheline syenite, sometimes more evolved (iron-enrichment), have been found hosted within nepheline syenite, indicating several batches of magma were present (Mitchell & Platt 1982). These intermittent pulses of magma could have various origins; from periodic pressure build-ups and subsequent release from a deeper magma source, recurrent melt releases from a progressively melting source region, or a continued, steady state influx of magma, with fluctuating conduits as each becomes successively choked off (Duke et al. 1988). It may have also induced protracted magma crystallization, hybridization of magmas, and eventual hydrodynamic sorting of minerals through density currents (Pons et al. 2006). Previously deposited biotite gabbro would be taken upwards through the injection of this nepheline syenite, and be preserved in the xenolith-rich zones observed or potentially completely attenuating to form hybrid mafic syenites (see Fig. 4.5). These xenoliths may have also acted as heat sinks, influencing thermal convection in the magma chamber and the formation of crystallization fronts (Gaweda & Szopa 2011).

Hybridization of the syenite magma occurred at various stages and locations within the field area and Center II of the Complex, with magma mixing controlled by physical parameters (temperature, viscosity, rheology), composition and dynamics associated with the evolving chamber. Evidence of this mixing, with varying homogenization between interacting magmas, is preserved in the hybrid magmas, mafic enclaves displaying a range of assimilation, flow structures, and the mottled texture syenite. Progressive stages of hybridization for both the volcanic and biotite gabbro enclaves are observed, with whole blocks, deformed blebby inclusions, wispy/stretched enclaves, and general concentrations of mafic crystals representing completely attenuated xenoliths (Fig. 4.5). These xenoliths may be linearly stretched by shear

flow of the host syenite or compact due to over-lying crystal mush, with the long axis of these enclaves aligning parallel to the flow in the magma (Renjith et al. 2014).

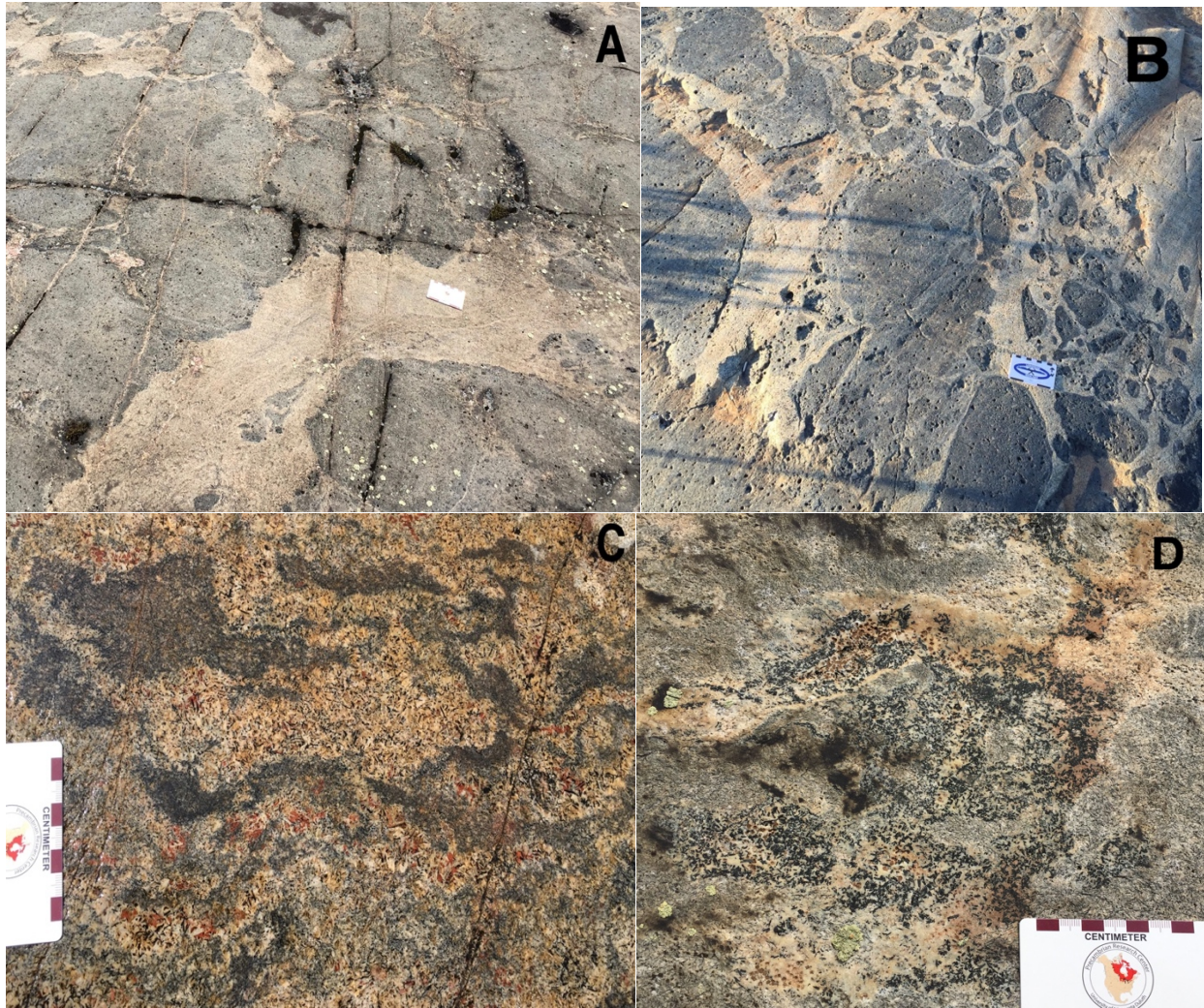


Figure 4.5. Various stages of hybridization and deformation of xenoliths. A. Biotite-gabbro block beginning to round and deform; B. Volcanic xenoliths disaggregating into smaller, rounded clasts; C. A wispy mafic enclave; D. Accumulation of amphibole crystals representing highly assimilated mafic clasts.

The deformation of these xenoliths, flow fabrics and accumulations of acicular amphibole in mafic and hybrid syenite illustrates the dynamic environment and heterogeneity in the nepheline syenite magma. Irregular magma injections into these regions would continue to make the process more complex in the chamber. These recharges are demonstrated by the mottled

texture syenite present, which may represent pulses of ‘normal’ syenitic magma into the mafic syenite. Contrasting temperatures, viscosity, and composition would prevent thorough mixing and mingling, and form syenite blebs within the mafic syenite. Acicular amphibole within the mafic syenite displays the direction and distortion of flow around these blebs (Fig. 4.6). While magma mixing is uncommon in the formation of syenite associated with alkaline complexes, the Yelagari Alkaline Complex in South India also displays similar outcrop-scale features of crystal accumulation and flow fabrics, used as evidence for multiple processes including: convection, shear flow, crystal accumulation, and magma mixing (Renjith et al. 2014).

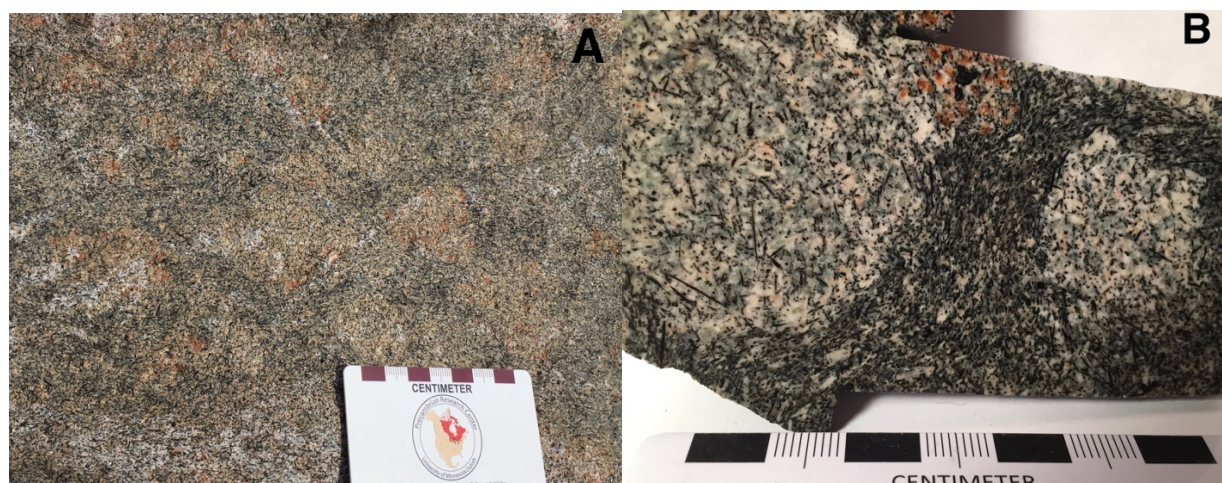


Figure 4.6. A: Weathered mottled texture syenite in field area; B: Cut hand sample displaying mottled syenite and alignment of amphibole crystals around ‘normal’ syenite blebs.

### 4.3. Analysis of Rhythmic, Modal Layering

A common feature in the layered nepheline syenites of the Coldwell Complex is the appearance of an amphibole-rich layer (grain-size scale) grading into a feldspar-rich layer (Fig. 4.8). This modal grading, which may occur rhythmically through a layered unit, has been attributed to density currents and separation and reattachment vortex cells. These have been processes well explained by Irvine et al. (1998) as the mechanisms which formed rhythmically graded layers within the Skaergaard Intrusion (Fig. 4.7). These mechanisms, in general (see

Irvine et al. 1998), form because fluid next to a boundary can advance more rapidly by breaking away and reattaching downstream, producing a vortex cell developing on the wall in between (Irvine et al. 1998). The flow structure of these currents includes a main body, a head vortex (along with other back vortices), and a “tail”. The tail of the current includes material left behind because of joint drag effects of the floor and host liquid, and would represent the cumulate layers deposited by the magmatic current (Irvine et al. 1998). The dense mafic minerals are selectively caught by floor drag to produce the bottom of the graded layer, while feldspar is stripped off by the host fluid drag to form the top layer. Arguments against this formation of layering come from the floatation problem of feldspar (Murase & McBirney 1973, McBirney & Noyes 1979). Possible mechanisms which would prevent the floatation of feldspar include: (1) feldspar being entangled with the dense mafic minerals during current transportation; (2) intercumulus liquid began to crystallize immediately after deposition acting as a cement; and (3) the feldspar-enriched layers were immediately buried beneath a layer of dense mafic minerals (Irvine et al. 1998). All of these mechanisms seem plausible to deter the floatation of feldspar. In the Skaergaard intrusion, the large extent of layering, as well as intervening ‘normal’ syenite layers, was hard to justify by continuous density currents forming along the walls and floor of the chamber. Convective boundary-layer currents exhibiting separation-reattachment cells are proposed, which produce the same graded layers but advance more slowly than the general convective flow (or the fast surge-type density currents). These cells would form in environments where flow along a boundary is choked with crystals, and rapidly deposit a graded layer of the same thickness as a normal syenite layer, representing both the depositional rate of the normal syenite and inverse frequency rate of the S-R cells (Irvine et al. 1998). These

intervening normal syenite layers would be laid down by broader, more gentle, continuous convection currents of the magma chamber.

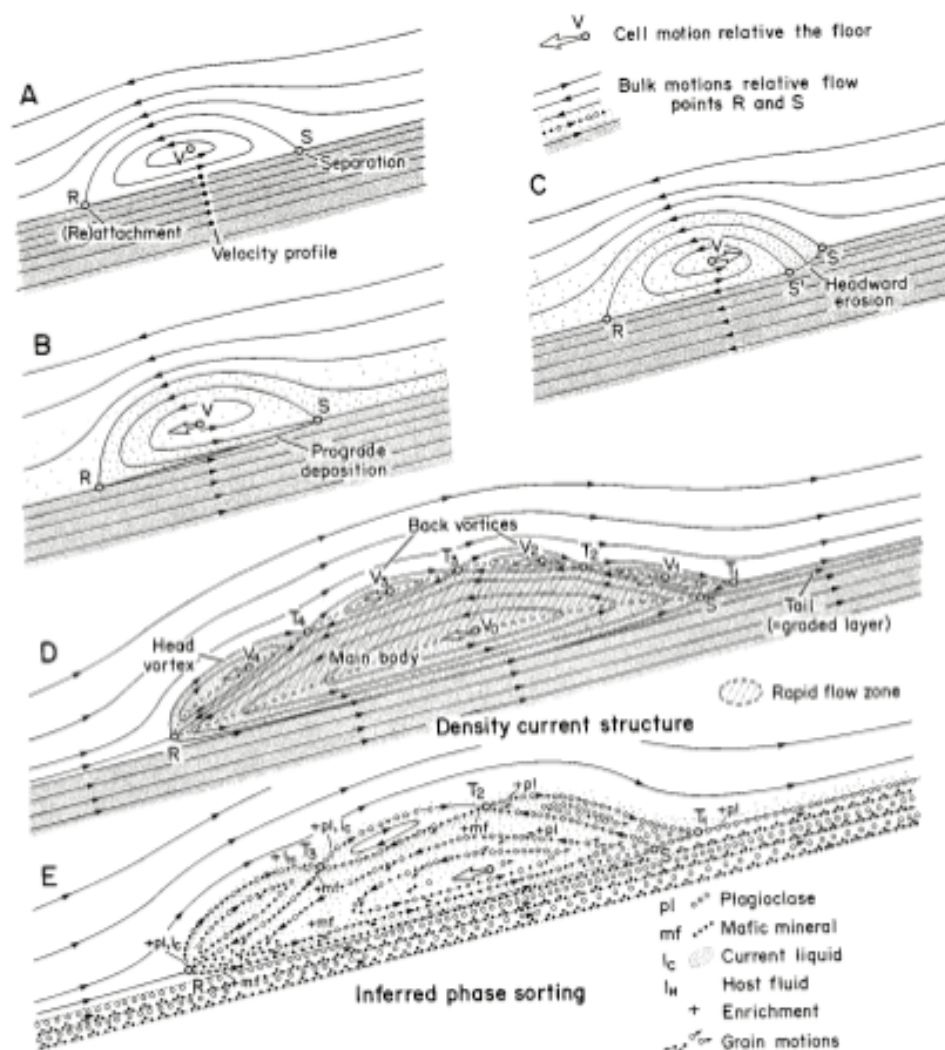


Figure 4.7. Schematic diagrams illustrating modal graded layering through density currents and boundary-layer flow separation (S) and reattachment (R) vortex cells. A: Steady-state S-R vortex cell; B: Prograde sedimentation by flow reattachment; C: Head ward erosion caused by flow separation; D: Structure of density surge current; main body rolls forward, the head and back vortices facilitate advance, the tail at the rear is left behind (the graded layers); E: Inferred sorting of feldspar, mafic minerals, and liquids. Current is decelerated by drag of floor and resistance of host liquid, dense minerals selectively caught by no-slip floor drag to form bottom of graded layer, and feldspar lags behind and is stripped off by host-fluid drag to form layer top (Adapted from Irvine et al. 1998).

In the Nunarssuit complex, part of the Gardar alkaline province in South Greenland, Parsons & Butterfield (1981) and Hodson (1998) also observed rhythmic modal layering from cumulus hedenbergite and fayalite grading into an alkali feldspar unit, with each cycle terminating in a melanocratic zone until progression terminated abruptly by slumping, discordant troughs and erosion channels. Again, this was attributed to density currents, forming when layers of magma, crystallized along the roof of the chamber, sank as crystal-melt plumes to the bottom of the chamber where they sourced density currents from which layers deposited (Hodson 1998). These plumes could collapse unstable piles of crystals accumulating beneath descending currents or wall-parallel boundaries at the edge of the chamber. Differences in layering intensity (sorting efficiency between dense, mafic minerals and less dense, felsic minerals) could also be attributed to density currents. High contrast between the bases and tops of layers would reflect areas close to the source of the density current, while lower contrasts would reflect deposition farther from the its source (Hodson 1998). This could potentially also be attributed to the buildup of volatiles, which would reduce viscosity and the resistance to sorting of the density current. The High Tatra granite intrusion is another example of containing well-developed modally graded beds forming in similar fashion to those observed in the Coldwell Complex. Layering contains a base of biotite, opaque minerals, and apatite with tops enriched in feldspars and quartz. Thickness of the layers are comparable to nepheline syenite at Coldwell, ranging from 1-50 cm, with intervening massive sections 3-6 m thick. Syn-magmatic tectonic activity producing density currents was suggested to destabilise accumulated crystal mush and stimulate slumping (Gaweda & Szopa 2011).



Figure 4.8. A: Top of layered block displaying termination of feldspar layer by mafic-rich laminae grading into another feldspar-rich layer. B: Rhythmic alternation of mafic and feldspar-rich layers grading into chaotic crystal mush.

#### 4.4. Supporting Evidence of Hydrodynamic Sorting

Two main processes, hydrodynamic sorting and crystallization along a thermal boundary layer, are commonly invoked to explain igneous layering (e.g. Irvine et al. 1998, Hodson 1998, Bailey et al. 2006, Pupier et al. 2008). Accompanying evidence is needed to prove hydrodynamic sorting was dominating in the layered nepheline syenite of the Coldwell complex. This can include, but is not limited to, depositional features (i.e. graded layering, cross-bedding, trough structures, mineral alignment), and signs of deformation from flow.

In the layered series nepheline syenite of the Coldwell complex, the depositional and deformation features are documented throughout Center II. These features give supporting evidence of a convecting magma over a stagnant one, and support the idea of surge-type density currents and S-R vortex cells forming the rhythmic layering in the nepheline syenite. Most of the zones surrounding the layered series rocks are highly irregular and represent disrupted layered zones along with a heterogeneous magma (see Fig. 4.9B). Areas where slumping or dislodged

blocks are observed folds and thrusts may form, along with irregular mixing of magmas and crystal mush. The tops of previously deposited layers may be eroded and/or truncated by these slumps and slides, as well as localized scour channels (see Fig. 4.9A). These form as secondary off-shoots produced from the surge-type density currents, and are infilled with mafic syenite concentrations. Other types of deformational features observed in the layered series include load casts and flame structures. These features are commonly produced when a mafic magma is emplaced overtop a syenitic mush, with the density contrasts and lack of mechanical stability allowing the downward movement of dense load casts and the upward movement of less dense flame structures. The structures display that the syenite material was not rigid when the layers came into position.

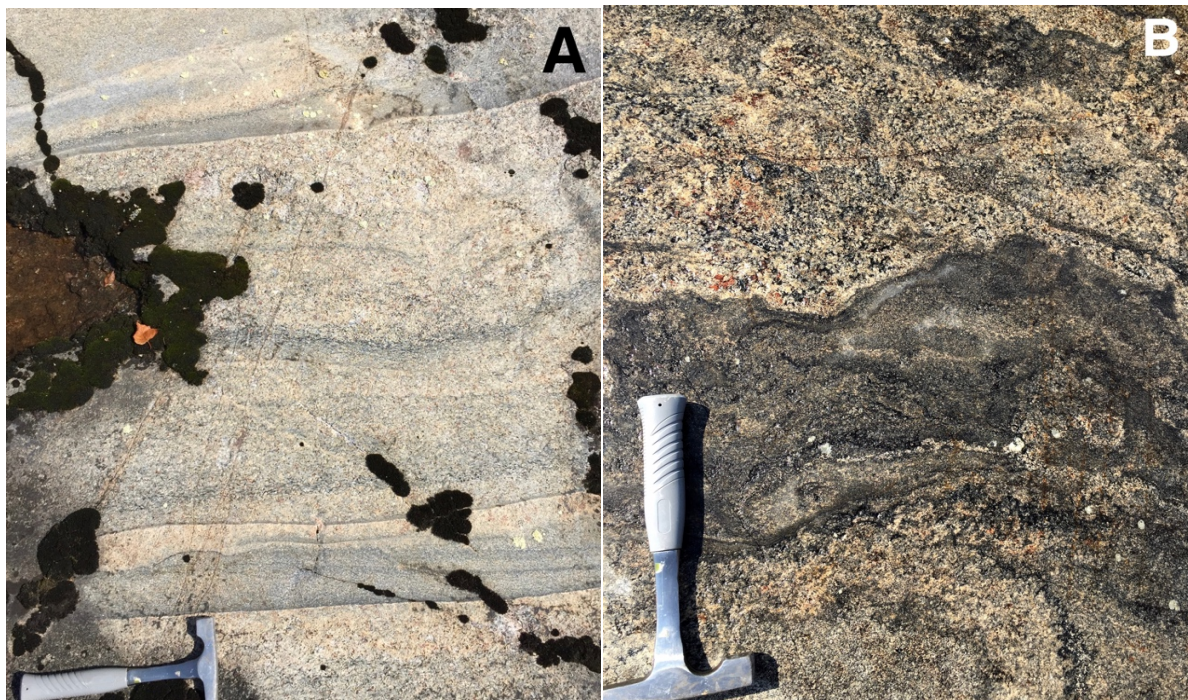


Figure 4.9. A: Scour channel next to hammer with rhythmic layering above. B: Distorted layering/mafic syenite flow next to layered block.

There are many examples of felsic layered plutons which display processes of a convecting magma operating during formation. The High Tatra granite displays an array of

sedimentary features including: graded beds, cross-bedding, scour channels, K-feldspar cumulates, magmatic breccia's, and load/flame structures. The formation of these structures is related to fractional crystallization and the development of a crystal mush through processes of: gravity-controlled separation, magma flow segregation, deposition on the magma-chamber floor, and density currents (Gaweda & Szopa 2011). The Tarcouate Laccolith contains depositional features including cross-bedding and trough structures indicating accumulation from an overlying convecting magma rather than the progression of a crystallization front (Pons et al. 2006). In the Nunarssuit syenite of South Greenland; slumps, slump breccias, troughs, and cross-bedding are observed. All these features support Hodson's (1998) model of a vigorously convecting magma, which would decrease in energy as crystals accumulated on the chamber walls until the collapse of the unstable crystal accumulations result in density currents from which the rhythmic modal layered material is deposited. For Skaergaard, the most enticing evidence of hydrodynamic sorting producing layering is the presence of layered autoliths within the micro-rhythmic, graded layers. These autoliths are observed to produce indents in older layering and covered by younger layers, indicating a sharp interface between the cumulate pile and the magma body as well as the distribution of these layers through magmatic currents (Irvine et al. 1998). Other accompanying evidence of convection currents producing layering includes trough channels and the 'cross-bedded belt', located at the junction of the chamber wall and floor. This area displays cross-bedding of layered cumulates with associated episodes of erosion or slumping of over-steepened crystal piles producing from convection currents descending from the chamber wall.

In comparison, other plutonic suites with rhythmic layering which are concluded to have not formed through hydrodynamic mechanisms, lack such features as: graded layering, magmatic

sedimentation features and/or signs of deformation. This is the case for layering described in the lujavrite and kakortokite (both agpaitic nepheline syenite) of the Ilimaussaq alkaline complex (Bailey et al. 2006, Lindhuber et al. 2015, Hunt et al. 2017). Microlayering of the lujavrite was confined to a stagnant basal layer of the floor of the magma chamber, with each liquid layer generated through open-system processes at the crystallization front (Bailey et al. 2006). Alternation between a dark arfvedsonite-rich layer and a light urtite layer was controlled by variations in volatile content of the immediately adjacent liquid within the stagnant layer. The sharp contacts between these layers, along with the occurrence of vertical layers and lack of grading in layers or signs of deformation also suggests mechanisms of hydrodynamic sorting were not in affect (Bailey et al. 2006). For macrolayering of the kakortokites, Lindhuber et al. (2015) hypothesized the contemporaneous nucleation of the main phases amphibole, eudialyte, and alkali feldspar; which separated by density contrasts throughout the chamber. Amphibole, being the densest mineral, formed crystal mats which acted as barriers inhibiting vertical movement of melt and crystals (primarily the floatation of alkali feldspar). This hypothesis was used to explain the repetitive nature of the layering and required a magma which was not convecting. Hunt et al. (2017) also studied these rocks applying crystal size distributions (CSDs) and eudialyte crystal compositions to determine the processes of development. This study also suggested the presence of a stagnant magma, with pseudo-sedimentary indicators (scour and flow indicators, shearing of crystals, slumping or current bedding) absent in the relatively homogenous layering of the kakortokites. However, CSD data in the study did not correlate with gravitational settling, instead indicating the bulk of crystals formed through in-situ crystallization. A sequential change in volatile content would cause the repetition of layering, with arfvedsonite initially crystallizing in high concentrations of halogens followed by eudialyte

and alkali feldspar with decreasing halogen concentrations in the basal magma layer (Hunt et al. 2017). In the Klokken Complex of South Greenland, the formation of laminated syenite may have been initiated through a viscosity decrease resulting from a build-up of dissolved water (Parsons & Becker 1987). Macrorhythmic layering from feldspathic 'normal' rock to pyroxenite (+- fayalite) developed due to variable crystal supply in a eutectic liquid with no equilibrium crystallization interval, caused by changes in relative growth and nucleation rates as magma undercooling varied. The cumulus crystals grew in a stagnant boundary layer within a few meters crystal pile surface, and moved to their deposition site once they had grown to a critical dimension where they could overcome the yield-strength of the surrounding magma (Parsons & Becker 1987). Rhythmic igneous layering in the Dobel batholith in SW Niger is also understood to have been formed through processes other than hydrodynamic sorting. The formation of the layered series is principally formed through in situ differentiation from successive magma batches, with each unit ending and compacting with a new injection of magma into the chamber (Pupier et al. 2008). Crystal settling related to density currents is ruled out, in favour of fractional crystallization in thermal boundary layers at the margin of the magma chamber due to: vertical geometry of layering, absence of mineral grading, cross-stratification, trough layering, and schlieren (Pupier et al. 2008). These layered complexes are all favoured to have formed through in-situ crystallization rather than hydrodynamic sorting, primarily due to the absence of depositional features and flow indicators in the magma, which are present within the layered nepheline syenites of the Coldwell Complex.

## Chapter 5

### Conclusion

This study evaluated the formation of the layered series nepheline syenite in Center II of the Coldwell Complex. Field mapping and sampling was completed along the shoreline of Neys Provincial Park, where great exposures of massive, hybrid, and layered syenite; together with xenolith-rich zones, biotite-gabbro, lamprophyre dikes and pegmatitic syenite of diverse composition are preserved. Heterogeneous zones hosting a variety of syenite lithology's demonstrate the dynamic and chaotic nature of the magma chamber during consolidation. Layered syenite displays rhythmic beds of amphibole laminae grading into a feldspar-rich syenite, commonly with associated slump and distortion features surrounding the preserved layers. Hybrid and mottled rock types contain both normal and mafic syenites, with amphibole of mafic syenites displaying flow orientations within the magma, and engulfing normal syenite blebs in mottled textures.

Feldspar laths display a perthitic texture of primary K-feldspar and exsolved/secondary plagioclase, and form the cumulus framework of the layered syenite. Feldspar analyzed through cathodoluminescence (CL) imaging demonstrated multiple feldspar species within single crystals. K-feldspar ranged in orthoclase component from 87-100%, whereas plagioclase exsolution and alterations were characterized as albite, with anorthite components ranging from 0-3%. Amphibole was a primary mineral throughout the syenite (excluding some late-stage pegmatites), as well as the dominant post-cumulus phase in the layered series, forming interstitial to feldspar cumulates. Amphibole within all samples were classified as ferro-pargasite, displaying a trend of Fe and Mn enrichment coupled with Mg depletion from core to rim.

Fluorapatite was the most abundant accessory mineral present, and was the dominant host of REE (La, Ce, Pr, Nd) and Y (avg. 8.61 REE<sub>2</sub>O<sub>3</sub> wt.% for unzoned crystals). Zoning of REE was common, displaying an increase in REE concentrations from core to rim. Britholite was the main alteration phase of apatite, and a major REE-sink, with REE<sub>2</sub>O<sub>3</sub> ranging from 44.19-69.75 wt.%. Both minerals demonstrate the substitution scheme:  $REE^{3+} + Si^{4+} \leftrightarrow Ca^{2+} + P^{5+}$ . Other, less abundant, accessory phases present hosting incompatible elements include: wöhlerite, pyrochlore, titanite, allanite, and fergusonite, and represent the final phases to form in residual magmas or alteration products from deuteritic fluids.

Hydrodynamic processes are favoured for the origin of the layered series, specifically surge-type density currents and separation and reattachment vortex cells, which formed the modally graded cumulate layers. Other magmatic sedimentary features including slumping, scour channels, and various stages of hybridization/deformation of xenoliths provide further evidence for a dynamic environment, strong convecting current, and heterogeneity in the nepheline syenite magma during the formation of these rocks. Thermal input from irregular magma injection and recharge contributed to the magmas ability to effectively convect. Varying homogenization between interacting magmas is preserved in the hybrid magmas, with mafic enclaves displaying a range of assimilation and flow structures. The layered series was a product of fractional crystallization, varying deposition mechanisms, and reworking through erosion or deformational processes.

## References

- Bailey, J.C., Sorensen, H., Anderson, T., Kogarko, L.N., and Rose-Hansen, J. 2006. On the origin of microrhythmic layering in arfvedsonite-lujarvite from the Ilimaussaq alkaline complex, South Greenland; *Lithos*, v. 91, p. 301-318.
- Duke, E.F., Redden, J.A., and Papike, J.J. 1988. Calamity Peak layered granite-pegmatite complex, Black Hills, South Dakota: Part I. Structure and emplacement; *Geological Society of America Bulletin*, v. 100, p. 825-840.
- Cannon, W.F. 1994. Closing of the Midcontinent rift- A far-field effect of Grenvillian compression; *Geology*, v. 22, p. 155-158.
- Gaweda, A., and Szopa, K. 2011. The origin of magmatic layering in the High Tatra granite, Central Western Carpathians – implications for the formation of granitoid plutons; *Earth and Environmental Science Transactions of the Royal Society of Edinburgh*, v. 102, p. 129-144.
- Heaman, L.M. and Machado, N. 1992. Timing and origin of midcontinent rift alkaline magmatism, North America: evidence from the Coldwell Complex; *Contributions to Mineralogy and Petrology*, v. 110, p. 289-303.
- Heaman, L.M., Easton, R.M., Hart, T.R., Hollings, P., MacDonald, C.A., and Smyk, M. 2007. Further refinement to the timing of Mesoproterozoic magmatism, Lake Nipigon region, Ontario; *Canadian Journal of Earth Sciences*, v. 44, p. 1055-1086.
- Hodson, M.E. 1998. The origin of igneous layering in the Nunarssuit syenite, South Greenland; *Mineralogical Magazine*, v. 62 (1), p. 9-27.
- Hogarth, D.D. 1977. Classification and nomenclature of the pyrochlore group; *American Mineralogist*, v. 62, p. 403-410.
- Hollings, P., Richardson, A., Creaser R.A., and Franklin, J.M. 2007. Radiogenic isotope characteristics of the Mesoproterozoic intrusive rocks of the Nipigon Embayment, northwestern Ontario; *Canadian Journal of Earth Sciences*, v. 44, p. 1111-1129.
- Hunt E.J., Finch, A.A., and Donaldson, C.H. 2017. Layering in peralkaline magmas, Ilimaussaq Complex, S Greenland; *Lithos*, v. 268-271, p. 1-15.
- Irvine, T.N. Andersen, J.C.O., and Brooks, C.K. 1998. Included blocks (and blocks within blocks) in the Skaergaard intrusion: Geological relations and the origins of rhythmic modally graded layers; *GSA Bulletin*, v. 110, p. 1398-1447.
- Klewin, K.W., and Shirey, S.B. 1992. The igneous petrology and magmatic evolution of the Midcontinent Rift system; *Tectonophysics*, v. 213, p. 33-40.

- Liferovich, R.P., and Mitchell, R.H. 2006. Apatite-group minerals from nepheline syenite, Pilansberg alkaline complex, South Africa; *Mineralogical Magazine*, v. 70 (5), p. 463-484.
- Lindhuber, M.J., Marks, M.A.W., Bons, P.D., Wenzel, T., and Markl, G. 2015. Crystal maturation as an igneous layering-forming process: Textural and geochemical evidence from the 'lower layered' nepheline syenite sequence of the Ilimaussaq complex, South Greenland; *Lithos*, v. 224-225, p. 295-309.
- Locock, A.J. 2014. An excel spreadsheet to classify chemical analyses of amphiboles following the IMA 2012 recommendations; *Computers & Geosciences*, v. 62, p. 1-11.
- Maki, S., Ohgo, S., and Nishido, H. 2016. Cathodoluminescence characterization of feldspar minerals from granite-syenite rocks in Iwagijima Island, Ehime prefecture, Japan; *Naturalistae*, v. 20, p. 13-18.
- Marks, M.A.W., and Markl, G. 2015. The Ilimaussaq alkaline complex, South Greenland; *Springer Geology*, Chapter 14, p. 649-691.
- McBirney, A.R., and Noyes, R.M. 1979. Crystallization and layering in the Skaergaard intrusion; *Journal of Petrology*, v. 20, p. 487-554.
- Mitchell, R.H., Platt, R.G., Downey, M. and Laderoute, D.G. 1991. Petrology of alkaline lamprophyres from the Coldwell alkaline complex, northwestern Ontario; *Canadian Journal of Earth Sciences*, v. 28, p. 1653-1663.
- Mitchell, R.H., Platt, R.G., Lukosius-Sanders, J., Artist-Downey, M. and Moogk-Pickard, S. 1993. Petrology of syenites from centre III of the Coldwell alkaline complex, northwestern Ontario, Canada; *Canadian Journal of Earth Sciences*, v. 30, p. 145-158.
- Mitchell, R.H. and Platt, R.G. 1982. Mineralogy and Petrology of Nepheline Syenites from the Coldwell Alkaline Complex, Ontario, Canada; *Journal of Petrology*, v. 23, p. 186-214.
- Mitchell, R.H. and Platt, R.G. 1978. Mafic Mineralogy of Ferroaugite Syenite from the Coldwell Alkaline Complex, Ontario, Canada; *Journal of Petrology*, v. 19, p. 627-651.
- Mulja, T., and Mitchell, R.H. 1991. The Geordie Lake Intrusion, Coldwell Complex, Ontario: A Palladium- and Tellurium-Rich Disseminated Sulfide Occurrence Derived from an Evolved Tholeiitic Magma; *Economic Geology*, v. 86, p. 1050-1069.
- Murase, T., and McBirney, A.R. 1973. Properties of some common igneous rocks and their melts at high temperatures; *Geological Society of American Bulletin*, v. 84, p. 3563-3592.
- Nicholson, S.W., Shirey, S.B., Schulz, K.J. and Green, J.C. 1997. Rift-wide correlation of 1.1 Ga Midcontinent rift system basalts: implications for multiple mantle sources during rift development; *Canadian Journal of Earth Sciences*, v. 34, p. 504-520.

Ontario Geological Survey, 2015. Geological map of the Coldwell Complex.

Parsons, I., and Becker S.M. 1987. Origins of igneous layering, NATO Advanced Study Institutes Series, Series C: Mathematical and Physical Sciences, v. 196, p. 29-92.

Parsons, I., Gerald, J.D.F., Heizler, M.T., Heizler, L.T., Ivanic, T., Lee, M.R. 2013. Eight-phase alkali feldspars: low-temperature cryptoperthite peristerite and multiple replacement reactions in the Klokken intrusion; *Contributions to Mineralogy and Petrology*, v. 165, p. 931-960.

Pons, J., Barbey, P., Nachit, H., and Burg, J.P. 2006. Development of igneous layering during growth of pluton: The Tarcouate Laccolith (Morocco); *Tectonophysics*, v. 413, p. 271-286.

Potter, E.G. and Mitchell, R.H. 2005. Mineralogy of the deadhorse creek volcanoclastic breccia complex, northwestern Ontario, Canada; *Contributions to Mineralogy and Petrology*, v. 150, p. 212-229.

Pupier, E., Barbey, P., Toplis, M.J., and Bussy, F. 2008. Igneous Layering, Fractional Crystallization and Growth of Granitic Plutons: the Dolbel Batholith in SW Niger; *Journal of Petrology*, v. 49, n. 6, p. 1043-1068.

Renjith, M.L., Charan, S.N., Subbarao, D.V., Babu, E.V.S.S.K., and Rajashekhar, V.B. 2014. Grain to outcrop-scale frozen moments of dynamic magma mixing in the syenite magma chamber, Yelagiri Alkaline Complex, South India; *Geoscience Frontiers*, v. 5, p. 801-820.

Sage, R.P. 1985. Geology of Carbonatite – Alkalic Rock Complexes of Ontario: Chipman Lake Area, Districts of Thunder Bay and Cochrane; Ontario Geological Survey, Study 44, 40 p. ISBN 0-7729-0579-7.

Sage, R.P. 1988. Geology of Carbonatite – Alkalic Rock Complexes in Ontario: Killala Lake Alkalic Rock Complex, District of Thunder Bay; Ontario Geological Survey, Study 45, 120 p. ISBN 0-7729-0580-0.

Stillwater Canada Inc. 2012. Assessment Report of Diamond Core Drilling and Downhole Surveying; Stillwater Canada Inc. Marathon Property, p. 1-32.

Stillwater Canada Inc. 2012. Geological Conditions at the Marathon PGM-Cu Project Site; prepared by Ecometrix Incorporated.

Symons, D.T.A. 1992. Paleomagnetism of the Keweenawan Chipman Lake and Seabrook Lake carbonatite complexes, Ontario; *Canadian Journal of Earth Sciences*, v. 29, p. 1215-1223.

Walker, E.C, Sutcliffe, R.H., Shaw, C.S.J., Shore, G.T., and Penczak, R.S. 1993. Precambrian Geology of the Coldwell Alkalic Complex; Ontario Geological Survey, Open File Report 5868, p. 1-30.

Zurevinski, S.E. and Mitchell, R.H. 2015. Petrogenesis of orbicular ijolites from the Prairie Lake complex, Marathon, Ontario: Textural evidence from rare processes of carbonatitic magmatism; *Lithos*, v. 239, p. 234-244.

## **Appendix I**

### Hand Sample and Petrographic Descriptions

**CC1:** On surface, rock displays modal and grain size grading along with a cumulus texture with a framework of feldspar crystals. Rock sample can be divided into three sections.

The bottom or first layer (CC1-B); contains a framework of m.g-c.g, sub-euhedral elongate feldspar laths (3-10mm) observed as a cream to tan colour. F.g-c.g (up to 10mm) black amphibole are also present; forming a trachytoid texture of subhedral acicular crystals which align sub-parallel and form minor aggregates which appear to form between feldspar crystals. This portion of the rock displays a sharp contact with the middle portion (CC1-A). CC1-A contains a slightly more massive composition; with f.g-c.g (up to 5mm) of sub-euhedral acicular amphibole in groundmass of anhedral feldspar. On the cut surface of the section, acicular amphibole (up to 5mm) may show sub-parallel alignment. The top portion is marked by a sharp contact with a thin laminae of mafic minerals (f.g-m.g up to 4mm) overlain by a laminae (~2-3mm wide) of dominantly f.g-m.g feldspar. This gradually grades into a relatively equal mix of f.g-m.g (up to 4mm) an-subhedral acicular amphibole and tabular feldspar. Throughout the sample, red natrolite is found as f.g-m.g disseminated anhedral patches and may contain f.g inclusions of amphibole. Minor visible nepheline is also visible as f.g-m.g (up to 3mm) grey patches.

Sample: CC1-A			
Mineral	Modal Percent (%)	Size & Form	Overall Description
Feldspar	65	f.g-m.g (rarely up to 3.5mm), an-subhedral elongate-laths with minor irregular masses	Colourless to cloudy PPL, forming cumulate framework with other feldspar crystals. Irregular/braided/net-work perthitic texture with albite intergrowths dominant throughout. Disseminated f.g sericite alteration present. Sharp grain boundaries with amphibole.
Amphibole	25	f.g-m.g (rarely up to 3mm), an-euhedral imperfect diamond-shape/elongate laths	Faint colour zoning present with dark green margins to brown cores PPL. Minor alteration to biotite along grain boundaries and cleavage planes. Crystals tend to form along long-axis of feldspar as interstitial disseminated or small aggregates of post-cumulus material. F.g opaques and rutile found as inclusions or along grain boundaries. Rarely found as inclusions in feldspar.
Biotite	<5	f.g-m.g (rarely 1mm), an-subhedral tabular laths	Pleochroic brown PPL. Always found associated with amphibole along grain boundaries or cleavage planes.
Zeolite	<5	Irregular masses up to 2mm, consisting of f.g polymineralic aggregate	Cloudy to dark red at margins in PPL. Commonly associated with amphibole aggregates; red colour observed more frequently when sharing grain boundary (Fe-source for Hematite). May host some f.g inclusions of amphibole.
Apatite	<5	f.g, an-euhedral hexagonal to elongate	Disseminated throughout with majority hosted in feldspar groundmass.

Opakes	<5	f.g, anhedral	Disseminated throughout, with crystals displaying minor exsolutions/intergrowths of magnetite and ilmenite. Minor Pyrite also present (determined through SEM analysis).
--------	----	---------------	--

Sample: CC1-B			
Mineral	Modal Percent (%)	Size and Form	Overall Description
Feldspar	45	f.g-c.g (up to 5mm), an-subhedral laths/equant form	Colourless to cloudy PPL; irregular/braided/network perthitic texture with albite intergrowths dominant throughout. Crystals form cumulus texture with framework of touching minerals. Shares irregular grain boundaries with zeolites and amphibole in groundmass. Minor sericite alteration as f.g disseminated crystals.
Amphibole	40-45	f.g-m.g (up to 2mm), an-subhedral elongate/imperfect diamond form	Minor colour zoning with darker green margins and lighter green to brown cores PPL. Interstitial crystals, forming post-cumulus phase between feldspar laths (uncommonly sub-parallel linear masses along feldspar laths). Also forms irregular masses with f.g-m.g feldspar crystals (not usually laths) between feldspar laths. Commonly found associated with biotite forming along grain boundaries, in cores of aggregates or along cleavage planes. Found as minor f.g inclusions in feldspar and zeolites.
Biotite	5	f.g-m.g (rarely up to 1.5mm), an-subhedral flakes or 'books'	Pleochroic brown PPL. Larger crystals associated with minor calcite veinlets and some along grain boundaries of amphibole. Forms along cleavage planes and in spaces between amphibole in aggregates. Also observed as forming f.g shredded masses around amphibole crystals.
Zeolite	5	Irregular masses up to 3.5mm, consisting of f.g polymineralic aggregate	Cloudy to brick red colour PPL. Shares irregular grain boundaries with amphibole and feldspar in groundmass. Almost always displays red colour along margins when hosting amphibole inclusions.
Calcite	<5	f.g, anhedral	Colourless PPL with variable relief. Forms minor veinlets cross-cutting sample and irregular masses associated with amphibole and biotite (excess Ca <sup>2+</sup> from amphibole alteration to biotite).
Opakes	<5	f.g, anhedral	Disseminated throughout with minor irregular masses associated with amphibole and biotite.

			Identified as magnetite and pyrite in reflected light.
--	--	--	--

**CC2:** A phaneritic rock, displaying a cumulus texture of white feldspar crystals. The base of the sample contains an increase in amphibole crystals, forming f.g-m.g (up to 3mm) an-subhedral elongate to acicular planar aggregates on fractures and radiating/clumps of aggregates on surface. These crystals form a granular, post-cumulus texture around m.g-c.g (up to 10mm) elongate feldspar aligned in parallel manner (trachytoid texture). Mafic content decreases upwards, with feldspar forming in sub-parallel manner and may clump in minor aggregates. Disseminated crystals/clusters of natrolite (up to 3mm) observed throughout; may contain f.g inclusions of amphibole forming poikilitic texture. Minor f.g, anhedral grey nepheline is also disseminated throughout.

Sample: CC2			
Mineral	Modal Percent (%)	Size and Form	Overall Description
Feldspar	70-75	f.g-c.g (up to 6mm) an-subhedral laths to equant/irregular form	Colourless to cloudy PPL with minor sericite alteration. Crystals dominantly display perthitic texture (irregular/network); with c.g laths forming sub-parallel framework of touching minerals (cumulus phase). F.g crystals tend to form irregular aggregates non-parallel to laths.
Amphibole	10-15	f.g-m.g (up to 2mm; avg. <1mm), an-subhedral elongate/diamond form	Minor colour zoning with darker green margins and lighter green to brown cores PPL. Crystals tend to form linear masses sub-parallel to feldspar laths; interstitial post-cumulus material. Also forms irregular masses between aligned crystals. Shares irregular grain boundaries with biotite and zeolites, along with minor calcite and pyroxene.
Biotite	5	f.g, an-subhedral elongate laths, shredded masses or 'books'	Pleochroic brown PPL, always found in association with amphibole. Observed forming along edges or cores of amphibole aggregates. Minor association with calcite.
Zeolite	5	Irregular masses up to 2mm, consisting of f.g polymineralic aggregates	Colourless to cloudy with red tint along margins PPL. Shares irregular grain boundaries with amphibole and feldspar. Can host numerous inclusions of f.g amphibole with an increase in red colour (Hematite). Masses disseminated throughout.
Apatite	<5	f.g, an-euhedral elongate to hexagonal form	Colourless PPL associated with amphibole/biotite aggregates along grain boundaries or as inclusions.
Pyroxene	Trace	f.g, an-subhedral	Green PPL; disseminated in amphibole aggregates.

Fluorite	Trace	f.g, anhedral	Colourless w slight purple tint PPL; found sharing grain boundaries with amphibole.
Calcite	Trace	f.g, anhedral	Colourless PPL; associated with biotite

**CC3:** Sample displays a massive texture; with feldspar aggregates (f.g-c.g up to 5mm) of round-ovoid shape; rimmed by amphibole. Amphibole masses contain f.g-m.g (up to 3mm) an-subhedral acicular amphibole, which wraps around in wispy pattern forming aggregates which apparently fill/cement space between feldspar aggregates. The fractured surface of the rock displays larger accumulations of mafic minerals (up to 3cm in diameter) disseminated and partially connected. Natrolite forms disseminated aggregates throughout, with masses up to 5mm; and may enclose inclusions of disseminated acicular amphibole (up to 3mm) giving it a poikilitic texture.

Sample: CC3			
Mineral	Modal Percent (%)	Size and Form	Overall Description
Feldspar	35-40	f.g-m.g (up to 3mm), an-subhedral irregular to elongate laths	Highly altered sample with very dusty appearance PPL; extensive sericite/zeolite alteration visible XPL. Irregular to patchy perthitic texture observed throughout. Shares irregular grain boundaries with zeolites/amphibole/biotite in matrix. Rare f.g microcline disseminated.
Zeolite	30-35	Irregular masses up to 1cm, consisting of f.g polymineralic aggregates	Dusty to deep red colour PPL; with red more prominent around amphibole inclusions and grain boundaries of crystal. Masses disseminated throughout groundmass; sharing irregular grain boundaries with all constituents.
Amphibole	15-20	f.g-m.g (up to 3mm), an-euhedral imperfect diamond to elongate	Varying colour PPL including: brown, deep green, faded green-yellow and rare blue-green; often displaying colour zoning. May form f.g disseminated crystals in feldspar groundmass (commonly anhedral) or large aggregates. Associated with biotite and fluorite; as well as forming f.g inclusions in zeolites.
Nepheline	5	f.g-m.g (up to 3mm), anhedral	Colourless to cloudy PPL with extensive alteration; commonly associated with feldspar and zeolites. XPL Nepheline appears as relict fragments with interstitial f.g aggregates of alteration minerals (zeolites, muscovite).
Biotite	<5	f.g-m.g (up to 2mm), an-subhedral elongate or 'book' form	Pleochroic brown PPL; and always associated with amphibole and commonly fluorite. M.g crystals commonly host f.g apatite and amphibole.
Muscovite	<5	f.g-m.g (up to 2mm), an-subhedral	Colourless PPL; associated with zeolites and nepheline. Alteration product of nepheline.

		laths or radiating sheaths	
Fluorite	<5	f.g-m.g (up to 1.5mm), anhedral	Colourless with tint of purple PPL; associated with amphibole and biotite.
Apatite	<5	f.g, an-euhedral elongate to hexagonal form	Colourless PPL; disseminated throughout as inclusions in amphibole, biotite, and feldspar groundmass.

**CC4:** A c.g, pegmatitic sample with crystals up to 3cm. Many crystals display a smooth fracture face and reflect in light. Rock is mixture of c.g, an-subhedral: nepheline (grey), alkali-feldspar (pinkish to off white), pyroxene (dark green to black with granular appearance in some spots; appearing much different than other amphibole observed), natrolite (red), and fluorite (purple). Natrolite forms anhedral patches with granular texture; while nepheline, feldspar, and amphibole can form elongate/tabular laths; with some laths displaying more than one constituent. Fluorite is present as purple, vitreous, anhedral, f.g-m.g (up to 3mm) disseminated crystals and aggregates which may form as inclusions; dominantly found along fracture planes where they make up 50-75% of surface minerals observed. Fluorite also observed with unknown, anhedral yellowish-green species. This fluorite forms unique pattern on single surface, observed as very thin parallel lines, also forming at 45° angle to these lines.

Sample: CC4			
Mineral	Modal Percent (%)	Size and Form	Overall Description
Feldspar	40-50	f.g-c.g (up to 1cm), an-subhedral equant to elongate	Colourless to cloudy PPL; dominant phase in groundmass with perthitic texture present throughout (irregular to replacement form). Albite replacement can make up to 75% of crystal. Minor to moderate alteration of sericite present, as well as uncommon inclusions of pyroxene, zeolite, and fluorite.
Zeolite	30-40	Irregular masses up to 3cm, consisting of f.g polymineralic aggregates	Dusty to red PPL; with red tint more common along grain boundaries or with pyroxene inclusions. Displayed sharp contacts with feldspar forming dominant phase in groundmass. Hosts f.g-m.g inclusions of pyroxene, feldspar, fluorite, and relict nepheline.
Pyroxene	10	f.g-m.g (up to 3mm), anhedral prismatic with corroded grain boundaries	Pleochroic green-yellow PPL; present as relict crystals with extensive alteration and inclusions of opaques, biotite, or zeolites. Disseminated or form aggregates; commonly sharing grain boundaries with natrolite.
Fluorite	5	f.g-m.g (up to 2mm), anhedral	Colourless to purple PPL; disseminated or forms interconnected texture in feldspar/natrolite. Associated with all constituents; and

			uncommonly hosts inclusions of pyroxene or zeolites.
Biotite	<5	f.g, anhedral	Pleochroic brown PPL; always associated with pyroxene forming recrystallized masses or disseminated crystals along grain boundaries (alteration product of pyroxene).
Opaques	<5	f.g, anhedral	Associated with pyroxene as alteration product (can form up to 75% of relict pyroxene as disseminated crystals or aggregates).

**CC5:** A pegmatitic sample, containing a caotic mixture of phaneritic dark green to black pyroxene (f.g-c.g up to 1.5cm, an-euhedral elongate/tabular/acicular/prismatic form), red natrolite (aggregeates up to 2cm), grey zeolites (aggregates up to 2cm), and pinkish to off-white feldspar (f.g-c.g up to 1cm, anhedral granular texture). All constituents share grain boundaries, with pyroxene and zeolite forming dominant phases in groundmass. Pyroxene appears to have crystallized first, with anhedral zeolite and feldspar forming groundmass between crystals. Natrolite is disseminated throughout and commonly hosts inclusions/shares grain boundaries with f.g-c.g elongate pyroxene.

Sample: CC5			
Mineral	Modal Percent (%)	Size and Form	Overall Description
Pyroxene	45	f.g-m.g (up to 3.5mm), anhedral elongate to short prismatic (4-8 sided)	Pleochroic green PPL; forming disseminated or large aggregates commonly sharing irregular grain boundaries. Crystals dominantly observed as relict of previous form; with intensely eroded structure with pervasive f.g opaque and biotite alteration products. Opaque inclusions most common, and may form up to 90% of crystal or rim entire crystal. When no alteration present crystals still heavily fractured.
Zeolite	25	Irregular masses up to 5mm, consisting of f.g polymineralic aggregates	Dusty to red PPL; with increased red content along grain margins. Forms irregular masses; and hosts inclusions of f.g-m.g pyroxene and fluorite as disseminated crystals or aggregates with extensive opaque inclusions.
Feldspar	15	f.g-c.g (up to 1cm), an-subhedral elongate laths	Cloudy to colourless PPL with minor sericite alteration. Shares highly irregular grain boundaries with pyroxene and zeolites, dominantly displaying irregular to network-like perthitic texture with a large content of albite. Uncommonly hosts f.g-m.g pyroxene inclusions.
Biotite	5	f.g, anhedral elongate	Pleochroic brown PPL, forming f.g shredded or minor aggregates in pyroxene crystals. Commonly associated with opaques. Dominant phase in recrystallized pyroxene.

Opakes	5	f.g, an-subhedral cubic	Observed as pervasive inclusions within pyroxene, leaving shredded relict crystals with biotite. Also found completely rimming pyroxene crystals (alteration product).
Fluorite	5	f.g-m.g (up to 2mm), an-euhedral rectangular to diamond-shape	Colourless to purple PPL; commonly found as anhedral space-filling constituent. Also observed as inclusions in zeolite sharing grain boundaries with pyroxene; nearly always sharing grain boundaries with pyroxene.

**CC6:** A massive phaneritic sample with dominantly black f.g-m.g (up to 3mm) amphibole, an-subhedral acicular/elongate in form. These crystals occur disseminated throughout the groundmass forming minor aggregates. Feldspar forms a granular texture composing the groundmass, as pinkish/tan/off-white f.g-c.g (up to 6mm) an-subhedral elongate laths. Natrolite forms disseminated brick red patches or aggregates throughout groundmass (up to 4mm) with only minor inclusions of amphibole. Sample also contains f.g biotite laths/plates disseminated throughout, associated with amphibole assemblages. Appearing as dark brown to black reflective crystals, they may form sheets or books between feldspar crystals. Under magnification; minor disseminated pyrite and chalcopyrite are present.

Sample: CC6			
Mineral	Modal Percent (%)	Size and Form	Overall Description
Feldspar	40-45	f.g-m.g (up to 3mm), an-subhedral laths/equant form	Colourless to cloudy PPL with minor sericite alteration. Forms irregular groundmass with zeolite and amphibole, with no preferred orientation. Network to irregular perthitic texture present throughout; with rare tartan twinning observed in some f.g crystals. Crystals may host f.g inclusions of amphibole.
Zeolite	40-45	Irregular masses up to 6mm, consisting of f.g polymineralic aggregates	Cloudy commonly with red tint PPL. Anhedral masses may display sharp grain boundaries with groundmass, and host f.g inclusions of amphibole and feldspar.
Amphibole	10-15	f.g-m.g (up to 2mm), an-subhedral elongate to imperfect diamond form	Pleochroic green-brown PPL; disseminated or forming small aggregates. Commonly found with biotite along grain boundaries/cleavage planes/interior of crystal; where fluorite may also be associated.
Biotite	<5	f.g, an-subhedral laths, 'books', or shredded masses	Pleochroic brown PPL; always associated with amphibole as alteration product. Minor association with chlorite and fluorite.
Chlorite	Trace	f.g, anhedral	Pleochroic green PPL; alteration product of amphibole/biotite forming along cleavage planes or interior of crystal

Fluorite	Trace	f.g, anhedral	Colourless to purple PPL; forming irregular masses commonly associated with biotite and amphibole.
----------	-------	---------------	--

**CC7:** Sample displays a cumulus texture with a framework of feldspar laths; with grain size and modal grading present. At the base of the sample, there is an increase in amphibole content, forming the intercumulus material (1-2mm wide) between and parallel to feldspar laths. These crystals appear to be f.g-m.g, an-subhedral acicular in form although are compacted into aggregates. Feldspar forms sub-euhedral, m.g-c.g laths (up to 10mm) and are off-white in colour; displaying a trachytoid texture. This layer has gradual contact with a more felsic component overlaying it. Amphibole aggregates decrease in content, with an-subhedral, f.g-m.g (up to 3mm) acicular amphibole disseminated or in small clusters in feldspar matrix. Feldspar still forms an-subhedral, m.g-c.g laths, although now sharing over-lapping grain boundaries which makes individual crystal form difficult to identify. In the top layer of the sample grain size is f.g-m.g (up to 3mm) with an-subhedral crystals. There are varying sections with increased amphibole and feldspar components. Sub-parallel to parallel alignment of all minerals is found throughout the entire sample. Anhedral natrolite (up to 1.5mm) is disseminated throughout the sample in aggregates, commonly found enclosing amphibole crystals.

Sample: CC7			
Mineral	Modal Percent (%)	Size and Form	Overall Description
Feldspar	60-70	f.g-c.g (up to 5mm), an-subhedral laths/equant form	Colourless to cloudy PPL with minor sericite alteration. Laths form a connected framework and are aligned in a sub-parallel manner; displaying a cumulus, trachytoid texture. Crystals share irregular grain boundaries with zeolite and amphibole which tend to form along long axis of crystals. Network to irregular perthitic texture is present throughout, with minor f.g crystals completely altered to albite.
Amphibole	15-20	f.g-m.g (up to 2mm), elongate laths to imperfect diamond shape	Pleochroic green-brown PPL with minor colour zoning (green margins to brown core). Crystals form post-cumulus material between feldspar laths as linear masses, disseminated crystals, or irregular masses. Associated with zeolite, fluorite, biotite, and apatite in matrix; with f.g crystals commonly found as inclusions in zeolite. Aggregates can host numerous inclusions of biotite, pyroxene, apatite, and fluorite.
Zeolite	5-10	Irregular masses up to 5mm, consisting of f.g polymineralic aggregates	Dusty with red tint PPL; red more commonly observed along grain boundaries or when amphibole inclusions present. Shares irregular grain boundaries with amphibole and feldspar; commonly associated with amphibole aggregates.

Biotite	5	f.g, an-subhedral laths or shredded form	Pleochroic brown PPL; associated with amphibole aggregates. Shredded masses may form around amphibole while laths form along grain boundaries/cleavage planes/in cores of amphibole.
Apatite	<5	f.g, an-euhedral hexagonal to elongate	Colourless PPL; found as inclusions or along grain boundaries of amphibole, zeolites, and feldspar.
Fluorite	Trace	f.g, anhedral	Colourless to purple PPL; rare disseminated crystals associated with amphibole aggregates and biotite.

**CC8:** A phaneritic, massive sample with f.g-m.g crystals up to 3mm. Rock is mixture of amphibole (black), feldspar (cream to white), and natrolite (red). Amphibole forms sub-euhedral elongate crystals that display sub-parallel alignment (trachytoid texture) and is the dominant constituent present (>50%). Rest of crystals display anhedral form.

Sample: CC8			
Mineral	Modal Percent (%)	Size and Form	Overall Description
Feldspar	65	f.g-m.g (up to 3mm), an-subhedral elongate to irregular	Cumulus phase - dusty PPL with minor sericite alteration. Perthitic texture throughout (irregular to replacement) with some completely albitized. Massive sample with minor crystal alignment.
Amphibole	25	f.g-m.g (up to 1.5mm), anhedral blebs with minor subhedral diamond shape	Pleochroic green-brown PPL; post-cumulus phase interstitial to feldspar (space-filling with lack of structure). Crystals altered to biotite along grain boundary.
Biotite	5	f.g-m.g (up to 3mm), an-subhedral elongate to 'book' form	Pleochroic brown PPL; minor alteration of amphibole. Disseminated as m.g 'books' associated with f.g crystals.
Zeolite	5	Irregular masses up to 2mm, consisting of f.g polymineralic aggregates	Cloudy PPL; common as interstitial phase associated with amphibole between feldspar.
Apatite	Trace	f.g, anhedral	Colourless PPL; associated with amphibole & biotite along grain boundary/cleavage

**CC9:** A phaneritic, f.g-c.g sample (crystals up to 5mm). Rock grades from massive texture with an increased mafic component; with a gradual contact to massive with dominantly feldspar; to a sharp contact to banded layer of dominantly amphibole (layer ~1cm). Overall mineralogy: amphibole (black, sub-euhedral elongate up to 5mm), feldspar (cream to pinkish hue, an-

subhedral, equant to lath form up to 4mm), natrolite (brick red, irregular patches up to 1cm disseminated throughout), and potential minor relict nepheline.

Sample: CC9			
Mineral	Modal Percent (%)	Size and Form	Overall Description
Feldspar	50	f.g-m.g (up to 3mm), an-subhedral elongate	Cloudy PPL, massive texture with lack of alignment/layering. Perthitic texture throughout (irregular/replacement). Cumulus phase.
Zeolite	30	Irregular masses up to 5mm, consisting of f.g polymineralic aggregates	Dusty to red PPL (prominent along grain boundary & associated with amphibole). Masses disseminated commonly hosting amphibole and associated with radiating/sheath mica.
Amphibole	15-20	f.g-m.g (up to 2mm), an-subhedral elongate/imperfect diamond	Pleochroic green-brown PPL, dominantly 'space-filling' structure between feldspar (post-cumulus phase). Found as inclusion in Natrolite. Minor alteration to biotite, hosts f.g apatite.
Apatite	<5	f.g, an-euhedral hexagonal to elongate	Colourless PPL, found as inclusions in amphibole.
Biotite	<5	f.g-m.g (up to 1.5mm), an-subhedral elongate	Pleochroic brown-green PPL; associated with amphibole as alteration product
Fluorite	Trace	f.g, anhedral	Colourless PPL associated with amphibole.

**CC10:** A phaneritic sample (crystals up to 1cm) displaying a massive to weakly layered texture. Feldspar (white, sub-euhedral laths) display cumulus texture as c.g laths forming network of connecting crystals but with no alignment. Post-cumulus, f.g-m.g, an-subhedral amphibole fills space between laths and may be f.g interstitial aggregates. Natrolite patches are disseminated throughout commonly forming along grain boundaries of feldspar.

Sample: CC10			
Mineral	Modal Percent (%)	Size and Form	Overall Description
Feldspar	65	f.g-c.g (up to 1.5cm), sub-euhedral laths	Cloudy PPL; cumulus phase with massive texture with individual pods appearing to settle together (laths in pod show alignment). Irregular perthitic texture with minor amphibole inclusions.
Amphibole	30	f.g-m.g (up to 3mm), an-euhedral elongate to imperfect-diamond	Pleochroic green-brown PPL, majority of crystals show some crystal habit unless altered to biotite. Form as disseminated crystals or aggregates along feldspar laths. Aggregates commonly in space between misaligned feldspar pods. Hosts f.g apatite.

Zeolite	<5	Irregular masses up to 1.5mm, consisting of f.g polymineralic aggregates	Cloudy to red PPL; minor constituent in comparison to other samples. Associated with amphibole commonly with larger aggregates.
Biotite	<5	f.g-m.g (up to 2mm), an-subhedral elongate to 'book' form	Pleochroic brown PPL, commonly fractured into flakes, associated with amphibole forming along grain boundary and may host f.g amphibole inclusions
Apatite	<5	f.g, an-euhedral hexagonal/elongate	Colourless PPL; associated with amphibole and biotite.

**CC11:** A phaneritic, hybrid sample; contains ~80% volume amphibole with f.g-m.g aggregates of feldspar disseminated. Amphibole crystals in this section align in a sub-parallel manner and appear to form around feldspar blebs (may represent secondary magma input).

Sample: CC11A			
Mineral	Modal Percent (%)	Size and Form	Overall Description
Feldspar	45-50	f.g-c.g (up to 5mm; avg. 2mm), an-euhedral elongate laths (some very slender)	Colourless to cloudy PPL, weak to moderate layering with weak alignment. Perthitic texture (irregular/replacement) dominantly throughout with minor tartan twinning. Very minor amphibole inclusions.
Amphibole	40	f.g-m.g (up to 2mm), an-subhedral elongate to diamond shaped	Pleochroic green-brown PPL with minor colour zoning. Irregular to blebby habit common. Majority are disseminated anhedral rounded along lath boundary with minor aggregates. Commonly alters to biotite and associated with fluorite & apatite.
Biotite	10	f.g-m.g (up to 2mm), an-subhedral elongate to 'book' form	Pleochroic brown PPL; associated with amphibole commonly as anhedral masses; minor association with fluorite.
Fluorite	<5	f.g-m.g (up to 1.5mm), anhedral	Colourless PPL; associated with amphibole/biotite masses.
Apatite	<5	f.g, an-subhedral rounded/elongate	Colourless PPL; inclusions/along grain boundary of biotite/amphibole
Zeolite	<5	Irregular masses up to 2mm, consisting of f.g polymineralic aggregates	Cloudy PPL; very minor constituent.
Calcite	Trace	f.g, anhedral	Colourless PPL; associated with amphibole/biotite.

**CC12:** A phaneritic, massive sample with f.g-c.g crystals (up to 6mm). Minerals present include: amphibole (black, sub-euhedral elongate to acicular), feldspar (cream to pinkish with equant to lath form), natrolite (red, irregular patches), and potential grey minor nepheline. Majority of crystals randomly oriented though some amphibole appears to form sub-parallel texture (minor feature).

Sample: CC12			
Mineral	Modal Percent (%)	Size and Form	Overall Description
Feldspar	70	f.g-m.g (up to 3mm), an-subhedral laths with irregular boundaries	Colourless to cloudy PPL with minor sericite alteration. Some sections display crystal alignment with perthitic texture throughout. Minor crystals completely albitized (secondary) and some display tartan twinning.
Biotite	10	f.g-m.g (up to 2.5mm), an-subhedral 'books' or tabular form	Pleochroic green-brown PPL; many display highly irregular structure. Associated with amphibole as alteration product but commonly disseminated or in minor aggregates with no amphibole. Commonly hosts apatite.
Amphibole	10	f.g-m.g (up to 2mm), an-subhedral elongate/hexagonal	Pleochroic green-brown PPL; irregular crystals forming minor aggregates interstitial to feldspar. Can be associated with biotite/fluorite/natrolite. In decreased abundance compared to all other thin sections.
Zeolite	5	Irregular masses up to 1.5mm, consisting of f.g polymineralic aggregates	Dusty to red PPL more prominent around amphibole. Sharp to irregular grain boundaries; alteration of feldspar/nepheline?
Fluorite	<5	f.g-m.g (up to 1mm), anhedral	Colourless to purple PPL associated with biotite and amphibole.
Apatite	<5	Very f.g, an-euhedral hexagonal/elongate	Colourless PPL; disseminated or in minor clusters commonly in biotite as well as amphibole.
Titanite	<5	f.g, an-subhedral diamond-shaped	Colourless to brown PPL; disseminated or associated with amphibole.

**CC13:** A phaneritic, massive sample with f.g-m.g (up to 3mm) feldspar, amphibole, and irregular masses of natrolite. Feldspar is dominant phase of groundmass forming aggregates up to 4cm which are rimmed by elongate to acicular amphibole crystals as interstitial aggregates. Feldspar and natrolite may host f.g amphibole inclusions. Single veinlet cross-cuts sample (natrolite?) displaying red halo around it.

Sample: CC13			
Mineral	Modal Percent (%)	Size and Form	Overall Description

Feldspar	50-60	f.g-c.g (up to 7mm), an-subhedral laths	Cloudy PPL; with moderate to heavy alteration common. May host patches of calcite, muscovite, and zeolite. Appears to have settled in individual pods, with laths inside the pods displaying some alignment (5-10 crystals). Cumulus phase with an overall massive/perthitic texture. Commonly hosts f.g amphibole inclusions.
Amphibole	25-35	f.g-m.g (up to 2mm; dominantly <1mm), an-euhedral elongate to hexagonal	Pleochroic green-brown PPL; an abundant phase but forms very f.g prismatic disseminated crystals (not interstitial to feldspar laths). May form large aggregates with biotite, pyroxene, and fluorite. Commonly clustered together with no touching grain boundaries.
Biotite	5-10	f.g-m.g (up to 1.5mm), an-subhedral elongate to 'book' form	Pleochroic brown PPL; alteration product of amphibole commonly found in large aggregates. Is found hosting numerous apatite inclusions.
Zeolite	25	Irregular masses up to 6mm, consisting of f.g polymineralic aggregates	Dusty to red PPL; with some alteration minerals reaching 1mm. Commonly hosting amphibole inclusions and relict feldspar/nepheline patches.
Apatite	Trace	f.g, an-subhedral hexagonal to elongate	Colourless PPL; hosted in amphibole/biotite. May cluster together in host crystal.
Pyroxene	Trace	f.g, anhedral	Green PPL; associated with amphibole, biotite, and fluorite in large aggregates.
Fluorite	Trace	f.g, anhedral	Colourless to purple PPL; associated with mafic minerals in large aggregates.

**CC14:** A phaneritic, layered sample. Feldspar forms m.g-c.g (up to 8mm) laths displaying a cumulus texture. Amphibole forms f.g-m.g (up to 2mm) post-cumulus/interstitial material. Laths are aligned in a sub-parallel manner (trachytic texture). Natrolite forms irregular masses (up to 5mm) throughout commonly hosting amphibole inclusions.

Sample: CC14			
Mineral	Modal Percent (%)	Size and Form	Overall Description
Feldspar	40-50	f.g-c.g (up to 6mm), an-euhedral laths	Colourless to cloudy PPL; cumulus phase with a trachytoid texture. Perthitic texture (irregular/replacement) throughout with some crystals completely albitized. Minor sericite alteration; f.g crystals are found in junctions between laths.

Amphibole	25-30	f.g-m.g (up to 3mm), an-subhedral elongate/hexagonal	Pleochroic green-brown PPL; dominantly forming large tightly packed aggregates interstitial to laths. Post-cumulus phase commonly forming along long-axis of feldspar. Minor colour zoning and commonly hosted in natrolite. Alteration to biotite common in aggregates. Hosts f.g apatite inclusions.
Zeolite	20	Irregular masses up to 5mm, consisting of f.g polymineralic aggregates	Dusty to red PPL (red hue more common when abundant amphibole inclusions present). Alteration product of feldspar/nepheline. Masses appear to form in junctions between feldspar laths.
Biotite	5	f.g-m.g (rarely up to 2mm), an-subhedral elongate	Pleochroic brown PPL; alteration product of amphibole in aggregates along cleavage/grain boundaries. Minor association with fluorite.
Apatite	Trace	f.g, an-subhedral hexagonal to elongate	Colourless PPL; found as inclusions in amphibole, biotite, and minor feldspar.
Fluorite	Trace	f.g, anhedral	Colourless PPL associated with biotite.

**CC15:** A phaneritic sample displaying a mottled appearance; with leucocratic clots surrounded by a matrix dominantly composed of amphibole and minor feldspar masses. Clots are up to 4mm in diameter and are composed of f.g-m.g feldspar/zeolite/natrolite with minor disseminated amphibole. Amphibole in surrounding groundmass preserves flow direction; flowing around clots with planar and wispy foliation. (f.g-m.g acicular to elongate crystals). Sample potentially represents a combination of separate magmas; with clots of immiscible fluids in magma with increased mafic content.

Sample: CC15			
Mineral	Modal Percent (%)	Size and Form	Overall Description
Mafic Syenite			
Amphibole	60-70	f.g-m.g (up to 1.5mm), an-subhedral hexagonal to acicular	Pleochroic green-brown PPL with minor colour zoning. Definite trachytoid texture displaying flow alignment around syenite blebs. Minor aggregates but dominantly disseminated between feldspar.
Feldspar	30-40	f.g-m.g (up to 2mm), an-subhedral elongate laths	Colourless to cloudy PPL; some alignment evident with perthitic texture throughout.
Biotite	<5	f.g-m.g (up to 1mm), an-subhedral tabular or 'book'	Pleochroic brown PPL; disseminated with minor crystals altering amphibole along grain boundaries.
Normal Syenite			
Zeolite	50-60	Irregular masses up to 3mm, consisting	Cloudy/dusty PPL; abundant throughout altering feldspar & nepheline? Dominant phase

		of f.g polymineralic aggregates	commonly hosting f.g-m.g amphibole and feldspar.
Feldspar	20-30	f.g-m.g (up to 4mm), an-subhedral lath to equant form	Cloudy PPL; perthitic texture throughout (highly irregular, some crystals display only minor features, others completely albitized, varying textures present). Massive and extensively altered to zeolites.
Amphibole	10-20	f.g-m.g (up to 1mm), an-subhedral elongate/hexagonal	Pleochroic green-brown PPL with minor colour zoning. A decreased grain size compared to mafic syenite. No preferred orientation, hosts minor apatite.
Biotite	<5	f.g, anhedral	Pleochroic brown PPL; alters amphibole along grain boundaries.
Apatite	Trace	f.g, anhedral	Colourless PPL; found as inclusions in amphibole.

**CC16:** A phaneritic, layered sample with separate magma compositions. Rock contains massive section typical of other normal syenites observed, with f.g-m.g aggregates of feldspar, natrolite, zeolite, and amphibole lacking orientation. These sections appear cut by magma similar to matrix of CC15; with dominantly amphibole forming f.g-m.g elongate to acicular crystals with sub-parallel alignment (displaying flow direction). Foliation in this section varies from planar to wispy; with minor distortion around other magma blebs. This section also hosts f.g-m.g crystals of feldspar (<5% volume).

Sample: CC16A			
Mineral	Modal Percent (%)	Size and Form	Overall Description
Mafic Syenite			
Amphibole	55	f.g-m.g (up to 3mm), an-subhedral elongate to prismatic.	Pleochroic green-brown PPL; an obvious flow orientation is present especially with elongate crystals. These elongate crystals may form aggregates that remain aligned with f.g prismatic crystals disseminated throughout. Hosts f.g apatite.
Feldspar	40	f.g-m.g (up to 2mm), an-subhedral elongate	Dusty PPL with iron staining throughout (especially obvious along grain boundaries). Relatively massive with irregular perthitic texture.
Biotite	5	f.g-m.g (up to 2mm), an-subhedral tabular	Pleochroic brown PPL; m.g crystals and aggregates disseminated (complete alteration of amphibole?) Only minor alteration along amphibole grain boundaries.
Normal Syenite (5mm width)			
Feldspar	90-95	f.g-c.g (up to 5mm), an-euhedral laths	Dusty PPL with iron staining. Perthitic texture highly irregular and patchy. Minor sericite alteration and minor crystal alignment.

Amphibole	5	f.g-m.g (up to 1mm), an-subhedral prismatic	Pleochroic green-brown PPL; disseminated prismatic crystals.
Biotite	Trace	f.g, anhedral	Pleochroic brown PPL; alters amphibole.
Pegmatite (1.5cm width)			
Feldspar	60	f.g-c.g (up to 1cm), an-subhedral laths	Dusty PPL with rare iron staining. Minor sericite alteration and heavy alteration to zeolite along grain boundaries/in massive sections. No alignment; perthitic texture (irregular/replacement) throughout.
Zeolite	20	Irregular masses up to 2cm, consisting of f.g polymineralic aggregates	Dusty to red PPL; commonly hosts numerous inclusions (up to 3mm) of feldspar and amphibole. Also found in junctions between multiple laths.
Amphibole	10-15	f.g-m.g (up to 2.5mm), an-subhedral prismatic/elongate	Pleochroic light green-brown PPL; disseminated with no aggregates. Some crystals extensively altered/pocketed with magnetite forming rim along grain boundary. Hosts minor apatite.
Biotite	Trace	f.g, anhedral	Pleochroic brown PPL; associated with altered amphibole crystals.
Magnetite	Trace	f.g, anhedral	Opaque; an alteration product of amphibole commonly forming along grain boundary.

**CC16B:**

Mafic syenite: Feldspar/amphibole/biotite display same texture as 16A; slight increase in biotite, flow alignment still present.

Normal syenite: Feldspar has smaller grain size (up to 5mm; avg. 2mm), iron staining and perthitic texture highly irregular, minor zeolite (<5%) present.

Pegmatite: Large natrolite patches present (up to 6mm) displaying a faint red hue PPL; some relict feldspar/nephline observed in patches. Amphibole highly altered with magnetite present and minor pyroxene/fluorite also associated in aggregates.

**CC17:** A diverse, phaneritic sample consisting of 3 different magma compositions. On left; a normal (massive) syenite is present with a chaotic aggregate of f.g-m.g (up to 4mm) feldspar, amphibole, and natrolite. This section of magma is cross-cut by a secondary magma pulse; dominantly composed of f.g-m.g (up to 3mm) elongate to acicular amphibole with minor f.g feldspar and zeolite (<5% volume). Amphibole here forms sub-parallel, planar to wispy foliation displaying flow direction; and hosts irregular blebs of massive syenite which may distort flow banding (producing wispy texture). On right appears a pegmatite with a massive texture, consisting of feldspar and amphibole (up to 1cm) forming lath and imperfect diamond shape respectively. Natrolite forms dominant phase of the groundmass along with feldspar, with irregular masses up to 2cm chaotically observed throughout. This section appears to form a top the amphibole-dominated magma and is not cross-cut by separate magma.

Sample: CC17A			
Mineral	Modal Percent (%)	Size and Form	Overall Description
Pegmatite			
Zeolite	50	Irregular masses up to 1cm, consisting of f.g polymineralic aggregates	Cloudy to reddish PPL throughout; may host f.g magnetite and extensively altered amphibole crystals. Shares irregular grain boundaries throughout.
Feldspar	30	f.g-c.g (up to 7mm), an-subhedral elongate	Dusty PPL with iron staining. Highly irregular perthitic texture with some crystals completely albitized. Heavily pocketed, minor sericite alteration. Associated with natrolite in groundmass which may be main alteration product. Far from primary chemical structure/composition.
Amphibole	15	f.g-m.g (up to 4mm), an-subhedral prismatic/elongate	Pleochroic green-brown PPL; highly fractured/altered crystals disseminated. Associated with biotite/fluorite/pyroxene as alteration by-products. Some crystals extensively fractured with abundant alteration products rimming entire crystal; others with only minor alteration to biotite. Hosts minor apatite inclusions.
Biotite	5	f.g-m.g (up to 1.5mm), an-subhedral tabular or 'book' form	Pleochroic brown PPL; always associated with amphibole as an alteration product. F.g shredded masses may rim amphibole; associated with fluorite when present.
Pyroxene	Trace	f.g, anhedral	Green PPL; associated with altered amphibole.
Fluorite	Trace	f.g, anhedral	Colourless PPL; associated with alteration aggregates.
Apatite	Trace	f.g, an-euhedral hexagonal to elongate	Colourless PPL; disseminated in amphibole.
Mafic Syenite			
Amphibole	50-60	f.g-m.g (up to 3mm), an-subhedral elongate to prismatic.	Pleochroic green-brown PPL; an obvious flow orientation is present especially with elongate crystals. These elongate crystals may form aggregates that remain aligned with f.g prismatic crystals disseminated throughout.
Feldspar	35-40	f.g-m.g (up to 2mm), an-subhedral elongate	Dusty PPL with iron staining throughout (especially obvious along grain boundaries). Relatively massive with irregular perthitic texture.

Biotite	5	f.g-m.g (up to 2mm), an-subhedral tabular	Pleochroic brown PPL; m.g crystals and aggregates disseminated. Only minor alteration along amphibole grain boundaries.
---------	---	---	---

**CC17B:**

Mafic Syenite: Similar to CC17A with some minor sections that grade into a larger grain size feldspar (avg. 3mm). Amphibole elongate aggregates with flow orientation. Perthite displays irregular, lamellar, and replacement texture. No zeolites.

Pegmatite: Amphibole more abundant and less altered than in CC17A. Minor crystals do show magnetite forming along grain boundaries (commonly hosted in zeolite). F.g-m.g biotite books also disseminated sometimes associated with amphibole. Zeolites abundant but with sharp grain boundaries and dominantly lacking natrolite. Zeolites commonly host f.g-m.g feldspar and amphibole. Feldspar relatively similar with minor sericite alteration but with no obvious iron staining.

**DN1: Waypoint: 0527994, 5402583**

A hybrid sample displaying grading of f.g-c.g amphibole and feldspar displaying trachytoid texture (sub-parallel alignment). Sample grades from c.g to f.g crystals with increase in amphibole present in finer section. Amphibole (an-subhedral) up to 5mm in massive section while in banded section f.g-m.g acicular to elongate dominantly disseminated but can form linear aggregate and minor masses. Feldspar up to 5mm in massive section displaying sub-euhedral lath form, while in banded section f.g-m.g an-subhedral elongate laths present. Minor nepheline potentially disseminated throughout (grey colour); along with irregular masses of red natrolite (very rare in banded section, but disseminated throughout massive section up to 1cm in size).

Sample: DN1			
Mineral	Modal Percent (%)	Size and Form	Overall Description
Feldspar	45-50	f.g-c.g (up to 6mm), an-subhedral laths/equant form	Colourless to cloudy PPL with minor sericite alteration; displaying irregular perthitic texture throughout. Cumulus phase with minor alignment of c.g minerals, and may host f.g inclusions of amphibole and biotite.
Amphibole	25	f.g-m.g (up to 2mm), an-subhedral elongate to diamond shaped	Pleochroic dark brown-green PPL, forming interstitial between feldspar laths as post-cumulus phase. Minor aggregates can be observed but dominantly disseminated throughout or in small groupings (up to 5 crystals). Altered to biotite along grain boundaries; and more abundant in finer sections as irregular blebs.
Zeolite	15-20	Irregular masses up to 3mm, consisting of f.g polymineralic aggregate	Dominantly observed as natrolite (reddish hue PPL); secondary product from alteration of feldspar and nepheline. Can form large masses associated with all phases and can host a variety of f.g inclusions.

Biotite	5	f.g-m.g (dominantly <1mm) an-subhedral lath or 'book' form	Pleochroic brown PPL, forming along grain boundaries of amphibole but also disseminated throughout with minor alteration to chlorite. Observed interstitial to feldspar laths; associated with minor fluorite and pyroxene.
Pyroxene	<5	f.g, anhedral	Bright green PPL; associated with biotite, amphibole, and fluorite.
Fluorite	<5	f.g, anhedral	Colourless to purple PPL; associated with mafic constituents.

**DN2: Waypoint: 0527994, 5402583**

A) A phaneritic sample; cumulus texture present with banding and grading of grain size and modal composition. Banding obvious on one surface but appears massive on other. At base of sample; feldspar forms cumulus phase of c.g sub-euhedral laths (up to 1cm) with variable alignment. Amphibole forms f.g-m.g black anhedral masses between laths. Red natrolite masses disseminated throughout as irregular patches (up to 1cm) [SECTION is 1-4cm wide]. In next section (gradual contact), feldspar content decreases significantly, with mafic components (amphibole and biotite) dominating (80-90%). Grain size also f.g-m.g with mafic minerals forming an-subhedral acicular to elongate crystals. Planar lamination apparent with crystals aligned in (sub)-parallel manner. Natrolite also decreases in content; with small (1-4mm) masses disseminated throughout. On separate fractures surface; biotite visibly common throughout forming m.g-c.g (up to 5mm) an-euhedral books; apparent c.g nepheline anhedral masses also disseminated throughout.

Sample: DN2			
Mineral	Modal Percent (%)	Size and Form	Overall Description
Feldspar	50	f.g-c.g up to 1cm (with obvious grading), an-euhedral laths	Colourless to cloudy PPL with minor sericite alteration; cumulus phase with irregular perthitic and trachytoid texture present throughout. Commonly hosts f.g amphibole inclusions and can display minor alteration/irregular grain boundaries with zeolite.
Amphibole	25-30	f.g-m.g, an-subhedral elongate to diamond form	Pleochroic brown-green PPL; post-cumulus phase forming interstitial to feldspar laths (space-filling). Disseminated and aggregates present. Associated with biotite and minor pyroxene/apatite. In f.g section can form highly irregular blebs in feldspar groundmass.
Zeolite	15-20	Irregular masses up to 5mm, consisting of f.g polymineralic aggregate	Dusty with red patches commonly along grain boundaries/surrounding inclusions. Alteration product of nepheline and feldspar and commonly hosts amphibole inclusions. Appears to disrupt feldspar alignment.

Biotite	<5	f.g-m.g, an-subhedral lath-tabular form	Pleochroic brown PPL; commonly found along grain boundaries/cleavage planes/cores of amphibole as alteration product.
Pyroxene	Minor	f.g-m.g (up to 1.5mm), anhedral	Green PPL. Disseminated throughout always rimming/sharing grain boundaries with amphibole.
Apatite	Minor	f.g, sub-euhedral hexagonal to elongate	Colourless PPL; found as inclusions/along grain boundaries of amphibole.
Fluorite	Minor	f.g, an-subhedral tabular form	Colourless PPL; disseminated throughout.

**DN3: Waypoint: 0527987, 5402546**

A banded sample with cumulus feldspar displaying minor alignment at the base and post-cumulus amphibole interstitial. Feldspar laths also display grading from f.g-m.g (up to 3mm) to c.g (up to 1cm). Minerals present includes: feldspar (white, sub-euhedral), amphibole (f.g-m.g, an-subhedral acicular to elongate crystals and aggregates), and natrolite (irregular masses up to 1.5cm disseminated throughout). Natrolite can be intergrown with anhedral feldspar, and also form interstitial masses with amphibole between lath framework.

Sample: DN3			
Mineral	Modal Percent (%)	Size and Form	Overall Description
Amphibole	45-50	f.g-m.g, an-subhedral elongate to imperfect diamond-shaped	Pleochroic dark brown-green PPL; forming post-cumulus - interstitial phase between feldspar laths with no grading present. Observed as aggregates sharing grain boundaries, disseminated in close proximity, or disseminated along grain boundaries/as inclusions (commonly as anhedral blebs). Associated with minor pyroxene and biotite in aggregates; and can make up large volumes (up to 75%) inside zeolite masses.
Feldspar	35-40	f.g-c.g (up to 1cm), an-subhedral laths	Colourless to cloudy PPL; with cumulus/trachtyoid texture and grain size grading present. Irregular perthitic texture present throughout with diffuse/corroded grain boundaries. Minor alteration to sericite/zeolite.
Zeolite	10	Irregular masses up to 7mm, consisting of f.g polymineralic aggregate	Dusty with red patches PPL (more intense along grain boundaries or surrounding inclusions). Alteration aggregate with relict nepheline patches visible throughout masses. Commonly hosts numerous f.g amphibole inclusions. Minor association with biotite/pyroxene and may disrupt alignment of feldspar laths.

Pyroxene	<5	f.g, anhedral	Green PPL; disseminated throughout nearly always associated with amphibole/biotite aggregates. More common in c.g section.
Biotite	<5	f.g, anhedral tabular form	Pleochroic brown PPL; disseminated or in amphibole aggregates. More common in f.g section.
Fluorite	Minor	f.g, anhedral	Colourless to purple PPL; disseminated in groundmass or as inclusions in amphibole.
Apatite	Minor	f.g, an-subhedral elongate to hexagonal	Colourless PPL disseminated or as inclusions in amphibole aggregates.
Titanite	Minor	f.g, anhedral	Colourless to tan PPL; disseminated in amphibole aggregate.

**DN4: Waypoint: 0527979, 5402546**

Phaneritic, banded sample. Rock is weakly layered to massive (feldspar laths not as obvious as other layered examples). F.g-m.g (up to 3mm) an-subhedral crystals forming in sub-parallel alignment including: amphibole (black, an-subhedral acicular to elongate), feldspar (white, elongate laths and equant form), and minor natrolite disseminated throughout.

Sample: DN4			
Mineral	Modal Percent (%)	Size and Form	Overall Description
Feldspar	60	f.g-m.g, an-subhedral lath/equant form	Colourless to dusty PPL with minor alteration to sericite but zeolite alteration observed throughout. Irregular/patchy/wormy perthitic texture dominant.
Amphibole	10-15	f.g-m.g (rarely up to 1mm), an-subhedral elongate to blebby	Pleochroic green-brown PPL; dominantly forming irregular blebs between feldspar. High degree of biotization present along grain boundaries and cleavage planes. Also associated with pyroxene in aggregates.
Zeolite	10-15	Irregular masses up to 5mm, consisting of f.g polymineralic aggregate	Cloudy PPL lacking common red tint from other T.S and appears to dominantly alter feldspar laths. Disseminated throughout in orientation with rest of feldspar framework.
Biotite	5	f.g, an-subhedral 'books', laths, and shards	Pleochroic brown PPL; dominantly present as alteration product of amphibole/pyroxene as anhedral patches along grain boundaries or cleavage planes. Minor association with fluorite.
Pyroxene	5	f.g-mg (up to 1mm), anhedral	Pleochroic green-yellow PPL with highly corroded/altered grain boundaries. Associated in aggregates with amphibole and biotite. Large concentration along one crack in T.S.

Fluorite	Minor	f.g, anhedral	Colourless to purple PPL; associated with pyroxene and biotite.
Apatite	Minor	f.g, an-subhedral elongate to hexagonal	Colourless PPL disseminated throughout amphibole/biotite aggregates.

**DN5: Waypoint: 0527969, 5402543**

A phaneritic; dominantly massive sample which can be divided into two sections separated by a wavy aggregate of natrolite. The first section contains massive to very minor aligned f.g-c.g (up to 5mm) amphibole along with disseminated feldspar and natrolite forming irregular masses up to 3mm. The second section contains a massive feldspar groundmass (f.g-m.g up to 3mm) with disseminated m.g amphibole and natrolite which is the dominant component; forming irregular masses throughout.

Sample: DN5			
Mineral	Modal Percent (%)	Size and Form	Overall Description
Zeolite	50	Irregular masses up to 4mm, consisting of f.g polymineralic aggregate	Two distinct types present – both form large alteration patches. 1) Colourless to red PPL forming irregular patches, containing larger grain size than second variety (though still f.g) forming equant/patchy aggregate with lack of zoning. 2) Cloudy to brown PPL with sharper grain boundaries and potential cores of relict minerals (feldspar/nepheline). Forms very f.g shredded aggregates with concentric zoning patterns observed (mineralogy doesn't appear to change other than fine lines separating zones.)
Feldspar	35	f.g-m.g (up to 2mm), an-subhedral lath-equant form	Cloudy PPL with minor sericite alteration and staining. Displays massive texture with lack of layering and orientation (crystal mush). Moderate alteration to zeolite present; which shares irregular grain boundaries with primary feldspar. Perthitic texture present but some crystals may be entirely altered to albite (polysynthetic twinning; complete ion exchange).
Amphibole	10	f.g-m.g (up to 2mm), anhedral elongate to imperfect diamond-shape	Pleochroic dark brown-green PPL; forming allotriomorphic granular texture around feldspar. Disseminated or forms minor aggregates. Crystals may be corroded with hollow cores and alteration to biotite along cleavage planes and grain boundaries.
Biotite	<5	f.g, an-subhedral 'books' to elongate flakes	Pleochroic brown PPL; alteration product nearly always in association with amphibole along cleavage planes or grain boundaries.

Muscovite	<5	f.g, an-subhedral flaky aggregates	Colourless PPL; disseminated throughout commonly found as radiating sheaths, alteration product of nepheline?
Pyroxene	Minor	f.g, anhedral	Pleochroic green PPL; disseminated crystals associated with amphibole/biotite aggregates.
Fluorite	Minor	f.g, anhedral	Colourless with purple tint PPL; associated with mafic aggregates.

**DN6: Waypoint: 0528031, 5401999**

A massive pegmatite sample (crystals up to 2cm) consisting of: amphibole (black, sub-euhedral hexagonal-elongate-lath form), natrolite (red, anhedral prismatic crystals with straight contacts), feldspar (cream to pink, equant and lath form with some large sections intergrown with nepheline), nepheline (grey anhedral masses), and biotite (anhedral f.g-m.g observed in c.g amphibole). Disseminated amphibole appears to group together separate from large natrolite patches.

Sample: DN6			
Mineral	Modal Percent (%)	Size and Form	Overall Description
Zeolite	50	Irregular masses up to 2cm, consisting of f.g polymineralic aggregate	Dusty to red PPL; commonly associated with amphibole and may contain relict cores of nepheline.
Feldspar	40	f.g-c.g (up to 1cm), an-subhedral elongate lath to equant form	Colourless to cloudy PPL with irregular/patchy perthitic texture. F.g crystals found interstitial to c.g laths. Secondary albite found dominantly along grain boundaries. Associated with nepheline/zeolite in groundmass.
Amphibole	5	m.g-c.g (up to 6mm), an-subhedral imperfect diamond form	Pleochroic green PPL; disseminated crystals with minor (2-3 crystal) aggregates. Associated with biotite commonly forming along cleavage planes.
Biotite	<5	f.g, an-subhedral flakes to 'books'	Pleochroic brown PPL; always associated with amphibole dominantly along cleavage planes.
Nepheline	<5	f.g-m.g, irregular mosaic of anhedral crystals	Colourless PPL; relict patches may be up to 1cm wide and associated with alteration minerals.

**DN7: Waypoint: 0528028, 5401972**

A massive pegmatite sample (crystals up to 2cm) consisting of: amphibole (black, sub-euhedral hexagonal-elongate-lath form), natrolite (red, anhedral masses that may be intergrown with feldspar and nepheline), feldspar (cream to pink, equant and lath form with some large sections inter grown with natrolite), and nepheline (grey, anhedral masses).

Sample: DN7			
Mineral	Modal Percent (%)	Size and Form	Overall Description
Feldspar	40-50	m.g-c.g (up to 2cm), an-subhedral lath/equant	Cloudy PPL with minor sericite alteration and Fe-oxide staining. Irregular to patchy perthitic texture dominant throughout; and shares irregular grain boundaries with zeolite forming dominant groundmass phases.
Zeolite	40-50	Irregular masses up to 2cm, consisting of f.g polymineralic aggregate	Dusty with reddish hue PPL (more common along grain boundaries). Alteration patches disseminated throughout; with minor relict inclusions of feldspar or nepheline observed.
Amphibole	5	m.g-c.g (up to 6mm) an-subhedral imperfect diamond	Pleochroic green PPL; crystals disseminated and all highly fractured/altered to biotite along cleavage planes and grain boundaries. Minor association with fluorite.
Biotite	<5	f.g-m.g (up to 1.5mm), an-subhedral 'books' or shredded aggregates	Pleochroic brown PPL; always associated with amphibole as secondary alteration product. Minor association to chlorite patches and muscovite.
Muscovite	<5	f.g (up to 1mm), an-euhedral acicular/flaky radiating aggregates	Colourless PPL; disseminated throughout as aggregates associated with relict patches in zeolite, biotite alteration, and dusty colourless zeolite.
Chlorite	Minor	f.g, anhedral shredded/patchy aggregates	Green PPL; with aggregates up to 3mm. An alteration product of biotite leaving relict biotite with highly irregular form.
Fluorite	Minor	f.g, an-subhedral	Colourless to purple PPL; disseminated in association with amphibole and biotite.

**DN8: Waypoint: 0528027, 5402024**

A phaneritic, banded sample; with feldspar forming cumulus texture. No obvious grading present, with some sub-parallel alignment of feldspar laths and amphibole aggregates. Feldspar form sub-euhedral f.g-c.g (up to 1cm) laths which may stack atop each other; amphibole f.g-m.g an-subhedral aggregates between feldspar laths (post cumulus material). Minor natrolite disseminated throughout as irregular masses which may show f.g amphibole inclusions throughout. Minor f.g-m.g biotite also disseminated throughout associated with amphibole.

Sample: DN8			
Mineral	Modal Percent (%)	Size and Form	Overall Description

Feldspar	55-60	f.g-c.g (up to 6mm), an-subhedral lath to equant form	Colourless to cloudy PPL with minor to moderate sericite/zeolite alteration. F.g crystals dominantly found between m.g-c.g laths. Cumulus phase with a weak alignment of minerals and irregular perthitic texture dominant throughout.
Zeolite	20	Irregular masses up to 5mm, consisting of f.g polymineralic aggregate	Dusty to red PPL (red more prominent around inclusions); secondary alteration product displaying minor relict cores of nepheline. May also display 'wavy' radiating mica sheaths which form flaky crystals up to 2mm.
Amphibole	10-15	f.g-m.g (up to 2mm), an-subhedral elongate to imperfect diamond form	Pleochroic green-brown PPL; disseminated or aggregates forming post-cumulus phase interstitial to feldspar. Moderate alteration to biotite along grain boundaries and cleavage with rare crystals forming cores in biotite. Also associated with fluorite in aggregates and as f.g inclusions in natrolite.
Fluorite	<5	f.g-m.g, an-subhedral elongate	Colourless with purple tint PPL; associated in aggregates with biotite and amphibole.
Apatite	Minor	f.g, an-euhedral elongate to hexagonal	Colourless PPL; associated with biotite/amphibole aggregates as inclusions or along grain boundaries.
Zircon	Minor	f.g, anhedral	Colourless PPL; associated with biotite.

**DN9: Waypoint: 0528031, 5402020**

A phaneritic sample with cumulus feldspar. Feldspar forms m.g-c.g elongate laths up to 5mm with sub-parallel alignment and planar lamination of feldspar layers. No grading present; but amount of amphibole (f.g-m.g) varies throughout; with some sections displaying little post cumulus material while other sections contain >50% mafic component. Natrolite disseminated throughout as irregular masses, some with a lot of f.g mafic inclusions (acicular). Minor disseminated nepheline and biotite observed throughout.

Sample: DN9			
Mineral	Modal Percent (%)	Size and Form	Overall Description
Feldspar	45	f.g-c.g (up to 6mm), anhedral laths	Dusty PPL with moderate to heavy sericite/zeolite alteration and staining. Cumulus phase; with laths display corroded grain boundaries throughout with a lack of alignment and an irregular perthitic texture. Disseminated f.g amphibole commonly found as inclusions.
Zeolite	35	Irregular masses up to 1cm, consisting of	Dusty to red PPL with sharp and irregular grain boundaries; amphibole inclusions found throughout.

		f.g polymineralic aggregate	
Amphibole	15	f.g-m.g (up to 2mm), an-euhedral elongate/imperfect diamond/hexagonal	Pleochroic brown-green PPL; minor aggregates but dominantly disseminated. Observed as inclusions in all constituents; with greater crystal form than observed in other T.S. Minor alteration to biotite.
Biotite	5	f.g-m.g (up to 3mm), an-subhedral elongate to 'book' form	Pleochroic dark brown PPL (much darker than other T.S); observed intergrown with blebby fluorite inclusions. Minor association with amphibole along grain boundaries but f.g amphibole is found as inclusions in m.g biotite.
Fluorite	<5	f.g-m.g (up to 1.5mm), anhedral	Colourless to purple PPL; found intergrown/as blebby inclusions in biotite.
Pyroxene	Minor	f.g, anhedral	Disseminated crystals found with biotite/amphibole.
Calcite	Minor	f.g, anhedral	Colourless PPL; found with biotite/fluorite.

**DN10: Waypoint:** 0528027, 5402014

Phaneritic sample with a massive texture. Feldspar crystals are observed up to 1.5cm and lack banding, but do form framework of connecting an-subhedral, m.g-c.g laths with no alignment. Feldspar display different colour than rest of samples (dominantly grey with some cream coloured crystals). Amphibole forms irregular masses between feldspar (post-cumulus material), dominantly as acicular to elongate crystals. Irregular natrolite masses (up to 1.5cm) are disseminated throughout sometimes with extensive f.g amphibole inclusions.

Sample: DN10			
Mineral	Modal Percent (%)	Size and Form	Overall Description
Feldspar	45-55	f.g-c.g (up to 6mm), an-subhedral lath to equant form	Dusty PPL with moderate staining; cumulus phase with lack of alignment. Irregular perthitic texture throughout with some crystals completely altered to albite. Highly irregular/diffuse boundaries and can host abundant amphibole inclusions in core or along grain boundary.
Zeolite	35-40	Irregular masses up to 1cm, consisting of f.g polymineralic aggregate	Dusty to red PPL; with sharp to irregular grain boundaries with groundmass. Observed containing relict nepheline/feldspar patches and abundant amphibole inclusions.
Amphibole	10-15	f.g-m.g (up to 1.5mm), an-subhedral elongate, hexagonal, diamond	Pleochroic green-brown PPL; post-cumulus phase interstitial to feldspar as: disseminated crystals along grain boundary or compact aggregates of f.g crystals with moderate grain

			boundary overlap. Aggregates can be up to 6mm
Biotite	Minor	f.g, an-subhedral elongate to 'book'	Pleochroic brown PPL; associated with amphibole/disseminated throughout.
Pyroxene	Minor	f.g, anhedral	Green PPL; disseminated within amphibole.
Apatite	Minor	f.g, an-subhedral elongate/ hexagonal	Colourless PPL; disseminated in amphibole aggregates.

**DN11: Waypoint:** 0528020, 5402273

A massive to weakly layered sample; displaying an overall pinkish hue (K-feldspar metasomatism?) and a sharp boundary between f.g and m.g-c.g (up to 1cm) syenite. Both sections display some alignment of minerals. In f.g section amphibole is the dominant component with the rest alkali feldspar. This section may have cut the m.g-c.g section as perhaps a mafic hybrid magma. The m.g-c.g section displays an increase in alkali feldspar with amphibole forming interstitial to the feldspar laths. Minor relict nepheline may be present.

Sample: DN11			
Note: Section divided in two. Top: f.g-c.g (avg. 3mm) with increase in amphibole content. Bottom: f.g-m.g (avg. 1mm) with decrease in amphibole content.			
Mineral	Modal Percent (%)	Size and Form	Overall Description
Feldspar	70-75	f.g-c.g (up to 5mm), an-subhedral elongate laths	A prominent dusty appearance PPL with pervasive Fe-staining and minor sericite alteration. Cumulus phase - displaying minor alignment with a highly irregular/ replacement perthitic texture. Grain boundaries serrated with no sharp contacts. In f.g section feldspar display a decrease in width (very narrow) and can form large aggregates piled atop eachother (compaction?)
Amphibole	20-25	f.g-m.g (up to 4mm), anhedral elongate to prismatic	Pleochroic green-brown PPL with minor colour zoning. In c.g section all crystals pervasively altered and eroded with no sharp grain boundaries (source Fe-staining?); and may host f,g apatite. In f.g section amphibole present as very f.g blebs (<1mm) between feldspar laths with a decrease in fracturing.
Nepheline	<5	f.g, anhedral	Colourless PPL; associated with feldspar in groundmass. No obvious zeolite alteration.
Biotite	<5	f.g, an-subhedral elongate	Pleochroic brown PPL; associated with amphibole as alteration product along grain boundary or cleavage plane.
Apatite	Minor	f.g, an-euhedral hexagonal to elongate	Colourless PPL associated as inclusions with amphibole.

<b>Key</b>	
f.g	Fine grained (<1mm)
m.g	Medium grained (1-5mm)
c.g	Coarse grained (>5mm)
v. f.g	Very fine grained (<<1mm)
PPL	Plane polarized light
XPL	Cross polarized light

**Appendix II**

SEM Results

## Representative analyses of amphibole from nepheline syenites, Center II, Coldwell Complex

Zoning Sample	CC1-1	2	3	4	5	6	7	8	9	10	11	12	13	14	15
Na2O	3.07	3.18	3.19	2.98	3.43	3.01	3.17	2.99	3.1	3.18	3.24	3.29	3.22	3.18	3.04
MgO	6.04	5.6	4.09	3.96	3.57	3.37	5	4.15	5.03	3.38	4.03	3.52	4.1	6.93	5.71
Al2O3	10.53	10.83	10.68	10.12	10.1	10.27	11.22	10.75	10.42	10.26	10.61	10.71	10.67	10.67	10.51
SiO2	39.2	39.29	38.83	38.85	38.4	36.73	38.62	38.9	38.96	37.86	38.28	38.48	38.49	39.62	39.47
K2O	1.8	1.73	1.73	1.76	1.78	1.73	1.82	1.8	1.73	1.69	1.84	1.87	1.85	1.74	1.66
CaO	10.88	10.76	10.52	10.56	10.05	10.13	10.64	10.92	10.62	10.47	10.55	10.45	10.68	10.89	10.87
TiO2	2.22	2.41	1.92	2.03	1.81	1.92	1.84	1.9	2.38	1.99	1.92	1.94	2.04	2.06	2.28
MnO	0.65	0.55	0.65	0.78	0.69	0.85	0.63	0.65	0.56	0.77	0.77	0.77	0.61	0.59	0.56
FeO	19.201	20.174	21.889	22.911	21.302	21.19	19.8	22.081	21.194	21.847	20.542	21.567	20.92	17.832	20.751
Fe2O3	5.844	4.43	5.78	5.589	7.232	7.034	7.179	5.533	4.996	6.338	7.288	7.038	7.023	6.088	4.134
H2O+	1.91	1.91	1.89	1.88	1.88	1.87	1.9	1.88	1.9	1.88	1.88	1.88	1.88	1.92	1.91
Total	101.345	100.864	101.169	101.42	100.244	98.104	101.819	101.554	100.89	99.665	100.95	101.515	101.483	101.52	100.895
Cation Assignment - Based on 23 O-equivalents															
Si	6.078	6.116	6.101	6.12	6.112	6.001	5.997	6.092	6.106	6.075	6.035	6.051	6.034	6.088	6.15
Al	6.078	6.116	6.101	6.12	6.112	6.001	5.997	6.092	6.106	6.075	6.035	6.051	6.034	6.088	6.15
Ti	12.156	12.232	12.202	12.24	12.224	12.002	11.994	12.184	12.212	12.15	12.07	12.102	12.068	12.176	12.3
Fe <sup>2+</sup>	2.49	2.625	2.875	3.016	2.835	2.897	2.571	2.893	2.778	2.931	2.71	2.836	2.744	2.292	2.706
Fe <sup>3+</sup>	0.682	0.52	0.684	0.664	0.867	0.863	0.839	0.651	0.589	0.765	0.863	0.833	0.827	0.704	0.483
Mn	0.085	0.073	0.087	0.104	0.093	0.118	0.083	0.086	0.074	0.105	0.103	0.103	0.081	0.077	0.074
Mg	1.396	1.299	0.958	0.93	0.847	0.821	1.157	0.969	1.175	0.808	0.947	0.825	0.958	1.587	1.326
Ca	1.807	1.795	1.771	1.782	1.714	1.773	1.77	1.832	1.783	1.8	1.782	1.761	1.794	1.793	1.815
Na	0.193	0.205	0.229	0.218	0.286	0.227	0.23	0.168	0.217	0.2	0.218	0.239	0.206	0.207	0.185
K	0.356	0.344	0.347	0.354	0.361	0.361	0.361	0.36	0.346	0.346	0.37	0.375	0.37	0.341	0.33
Mg#	0.306	0.292	0.212	0.202	0.186	0.179	0.253	0.215	0.259	0.18	0.21	0.184	0.212	0.347	0.293

CC18-1	2	3	4	5	6	7	8	9	10	CC2-1	2	3	4	5
3.01	2.86	2.83	2.99	2.91	2.85	2.88	2.76	3.12	3.22	2.81	2.96	2.96	2.92	2.93
4.84	5.4	4.56	4.01	3.43	4.01	4.88	3.86	4.01	3.6	6.17	3.4	3.17	3.06	3.55
10	10.41	9.98	10.1	10.22	10.05	10.23	10.43	10.24	9.88	9.61	9.68	9.48	9.48	9.69
38.71	38.8	38.14	38.57	38.22	38.41	38.81	38.26	38.36	38.02	39.47	38.69	37.83	38.28	37.99
1.67	1.72	1.77	1.9	1.77	1.85	1.79	1.83	1.73	1.82	1.76	1.86	1.83	1.77	1.79
10.63	10.71	10.43	10.24	10.27	10.81	10.69	10.53	10.44	10.53	10.78	10.13	10.25	10.31	10.03
2.15	2.17	2.08	2.19	1.8	2.02	2.15	1.91	2.05	1.74	2.08	1.83	2.03	1.92	2.22
0.72	0.62	0.67	0.62	0.75	0.74	0.6	0.67	0.72	0.72	0.64	0.65	0.82	0.8	0.59
21.256	21.353	21.724	22.566	23.319	22.252	21.685	23.049	21.804	20.98	20.451	23.744	22.947	23.877	23.685
4.873	4.554	5.408	5.283	5.535	6.221	5.006	5.135	6.364	8.624	4.589	5.252	6.415	5.282	4.939
1.89	1.9	1.88	1.88	1.87	1.87	1.89	1.88	1.88	1.87	1.9	1.87	1.86	1.86	1.87
99.749	100.497	99.472	100.349	100.094	101.083	100.611	100.314	100.718	101.004	100.26	100.066	99.592	99.559	99.284
6.148	6.105	6.103	6.13	6.119	6.076	6.118	6.096	6.075	6.033	6.197	6.198	6.112	6.184	6.138
6.148	6.105	6.103	6.13	6.119	6.076	6.118	6.096	6.075	6.033	6.197	6.198	6.112	6.184	6.138
12.296	12.21	12.206	12.26	12.238	12.152	12.236	12.192	12.15	12.066	12.394	12.396	12.224	12.368	12.276
2.823	2.81	2.908	3.001	3.124	2.945	2.86	3.071	2.889	2.784	2.684	3.181	3.1	3.228	3.2
0.583	0.539	0.65	0.63	0.665	0.74	0.593	0.616	0.757	1.03	0.543	0.634	0.781	0.64	0.601
0.097	0.083	0.091	0.083	0.102	0.099	0.08	0.09	0.097	0.097	0.085	0.088	0.112	0.109	0.081
1.146	1.267	1.088	0.95	0.819	0.946	1.147	0.917	0.947	0.852	1.444	0.812	0.764	0.737	0.855
1.809	1.805	1.788	1.744	1.762	1.832	1.806	1.798	1.772	1.79	1.814	1.739	1.774	1.784	1.736
0.191	0.195	0.212	0.256	0.238	0.168	0.194	0.202	0.228	0.21	0.186	0.261	0.226	0.216	0.264
0.338	0.345	0.361	0.385	0.362	0.373	0.36	0.372	0.35	0.368	0.353	0.38	0.377	0.365	0.369
0.252	0.274	0.234	0.207	0.178	0.204	0.249	0.199	0.206	0.182	0.309	0.175	0.165	0.161	0.184

	6	7	8	9	10	11	12	13	14	15	Core CC3-1	Rim 2	Core 3	Rim 4	Core 5
2.99	3.03	2.71	3.09	3.05	3.1	2.97	3.02	3.04	3.03	2.95	3	3.27	3	3.04	
3.37	3.58	4.28	3.29	3.48	3.65	3.46	3.59	3.4	3.26	6.16	2.34	7.34	2.69	7.5	
9.91	9.6	9.91	9.8	9.77	9.54	10.02	9.53	9.93	9.78	9.74	10.45	10.15	10.09	10	
38.54	38.57	38.78	38.62	38.13	38.95	38.83	38.73	37.84	38.62	39.4	36.55	39.54	37.12	39.74	
1.87	1.72	1.78	1.83	1.7	1.83	1.79	1.82	1.71	1.75	1.7	1.7	1.61	1.86	1.72	
9.9	10.08	10.53	10.39	10.2	10.16	10.29	9.89	10.36	10.34	10.65	9.91	10.7	10.01	11.11	
1.84	1.99	2.19	1.88	2.18	1.96	2.21	2	2.12	2.07	2.24	1.78	2.02	1.7	2.29	
0.58	0.68	0.67	0.68	0.75	0.67	0.85	0.79	0.71	0.77	0.55	0.75	0.48	0.8	0.45	
23.857	23.557	23.549	23.133	23.1	23.135	24.325	23.556	22.735	23.802	20.28	23.132	17.145	22.564	17.598	
5.86	5.249	3.535	6.387	5.712	5.118	4.696	6.061	6.596	5.265	4.357	6.711	5.984	7.197	4.859	
1.87	1.87	1.88	1.87	1.87	1.88	1.87	1.87	1.87	1.87	1.91	1.86	1.93	1.86	1.93	
100.587	99.926	99.814	100.97	99.942	99.993	101.311	100.857	100.311	100.557	99.937	98.183	100.169	98.891	100.237	
6.149	6.183	6.192	6.138	6.117	6.225	6.148	6.162	6.057	6.163	6.195	6.009	6.138	6.049	6.163	
6.149	6.183	6.192	6.138	6.117	6.225	6.148	6.162	6.057	6.163	6.195	6.009	6.138	6.049	6.163	
12.298	12.366	12.384	12.276	12.234	12.45	12.296	12.324	12.114	12.326	12.39	12.018	12.276	12.098	12.326	
3.183	3.157	3.146	3.076	3.099	3.093	3.219	3.134	3.043	3.176	2.668	3.18	2.226	3.077	2.282	
0.704	0.634	0.423	0.763	0.689	0.615	0.561	0.726	0.795	0.632	0.514	0.831	0.699	0.881	0.567	
0.078	0.092	0.091	0.092	0.102	0.091	0.114	0.101	0.096	0.104	0.073	0.104	0.063	0.11	0.059	
0.802	0.855	1.019	0.779	0.832	0.87	0.817	0.851	0.811	0.775	1.444	0.573	1.699	0.654	1.734	
1.692	1.731	1.801	1.769	1.753	1.74	1.746	1.686	1.777	1.768	1.794	1.746	1.78	1.748	1.846	
0.307	0.269	0.199	0.231	0.247	0.26	0.254	0.308	0.223	0.232	0.206	0.254	0.22	0.252	0.154	
0.381	0.352	0.363	0.371	0.348	0.373	0.362	0.369	0.349	0.356	0.341	0.357	0.319	0.387	0.34	
0.17	0.185	0.222	0.168	0.181	0.19	0.178	0.18	0.175	0.17	0.312	0.124	0.368	0.142	0.378	

Rim	6	Core	7	Rim	8	Core	9	Rim	10	Core	11	Rim	12	Core	13	Rim	14	Core	15	Rim	16	Core	17	Rim	18	Core	19	Rim	20
3.01	3.25	2.99	3.05	3.15	3.21	3.16	3.32	3.29	2.95	3.32	3.25	3.16	3.15	3.09	2.85	7.46	2.35	7.36	2.45	7.81	2.6	7.57	2.62	7.88	5.06	3.37	3.35	2.76	7.02
10.13	10.47	10.5	10.12	10.4	10.29	10.7	9.96	10	10.03	9.68	10.7	10.03	9.68	10.15	36.92	39.54	37.21	39.79	37.71	39.93	37.28	40.02	38.17	40.13	39.08	37.91	38.18	38.21	39.82
1.78	1.64	1.75	1.68	1.8	1.59	1.72	1.81	1.89	1.71	1.72	1.89	1.71	1.72	1.61	9.84	10.9	9.88	11.17	9.8	10.86	10.13	10.82	10.12	11.16	10.48	10.34	10.41	10.15	10.79
1.73	2.34	1.87	2.31	1.68	2.13	2.05	2.43	1.72	2.32	2.22	2.08	2.06	1.68	2.29	0.74	0.47	0.93	0.59	0.78	0.57	0.77	0.43	0.75	0.55	0.72	0.72	0.74	0.52	
22.531	17.073	24.206	17.897	23.699	17.04	22.976	16.836	22.777	17.821	20.145	21.933	22.477	23.437	19.063	7.311	5.509	5.905	5.415	7.214	5.156	6.584	5.495	7.95	4.377	6.463	7.199	6.761	7.261	4.809
1.86	1.93	1.86	1.92	1.86	1.93	1.86	1.93	1.86	1.93	1.89	1.87	1.87	1.86	1.92	98.702	100.582	99.451	101.302	100.543	100.516	99.83	100.621	101.147	100.858	100.778	101.142	101.268	101.088	101.082
6.026	6.103	6.044	6.122	6.052	6.155	6.007	6.169	6.08	6.176	6.137	6	6.04	6.09	6.151	6.026	6.103	6.044	6.122	6.052	6.155	6.007	6.169	6.08	6.176	6.137	6	6.04	6.09	6.151
12.052	12.206	12.088	12.244	12.104	12.31	12.014	12.338	12.16	12.352	12.274	12	12.08	12.18	12.302	3.075	2.203	3.287	2.304	3.18	2.195	3.095	2.172	3.035	2.293	2.645	2.904	2.973	3.124	2.461
0.898	0.641	0.723	0.626	0.872	0.599	0.799	0.636	0.952	0.508	0.765	0.856	0.806	0.871	0.56	0.898	0.641	0.723	0.626	0.872	0.599	0.799	0.636	0.952	0.508	0.765	0.856	0.806	0.871	0.56
0.693	0.102	0.061	0.128	0.077	0.074	0.105	0.056	0.101	0.072	0.096	0.102	0.1	0.068	0.1068	0.693	0.102	0.061	0.128	0.077	0.074	0.105	0.056	0.101	0.072	0.096	0.102	0.1	0.068	0.1068
1.721	1.803	1.719	1.688	1.685	1.794	1.749	1.787	1.727	1.84	1.763	1.753	1.765	1.733	1.786	0.279	0.197	0.281	0.159	0.315	0.206	0.251	0.213	0.273	0.16	0.237	0.247	0.235	0.267	0.214
0.371	0.323	0.363	0.33	0.369	0.313	0.354	0.356	0.384	0.336	0.345	0.349	0.359	0.366	0.317	0.149	0.377	0.125	0.365	0.127	0.391	0.139	0.382	0.134	0.393	0.239	0.175	0.172	0.141	0.349

CC6-1		2	3	4	5	6	7	8	9	10	CC7-1	
											2	3
3.21	3.11	3.05	3.16	3	3.17	3.26	3.15	3.07	3.05	3.05	3.05	3.14
3.54	4.73	4.5	3.19	3.83	3.91	2.65	3.54	2.89	2.93	3.85	3.47	3.31
10.52	10.36	10.5	10.54	10.82	10.12	10.09	10.13	10.58	10.02	10.04	10.04	10.18
38.71	38.81	39.36	38.81	38.87	38.92	38.51	38.85	38.37	38.54	39.09	38.81	38.71
1.73	1.65	1.69	1.82	1.76	1.81	1.83	1.65	1.79	1.8	1.82	1.67	1.81
10.15	10.25	10.47	10.2	10.26	10.04	9.85	10.51	9.78	10.02	10.42	10.12	9.99
1.86	2.06	2.13	2.01	2.05	2.07	2.06	2.06	1.99	1.7	1.97	1.86	1.96
0.68	0.57	0.65	0.7	0.84	0.64	0.82	0.72	0.82	0.76	0.67	0.73	0.79
22.891	21.747	22.803	23.64	23.488	22.764	23.939	23.186	24.339	24.387	22.948	24.151	23.469
5.622	4.638	3.787	5.079	3.97	4.963	5.257	4.583	4.736	6.071	4.325	4.333	5.079
1.88	1.89	1.89	1.87	1.88	1.88	1.87	1.88	1.87	1.86	1.88	1.87	1.87
100.793	99.815	100.83	101.019	100.768	100.287	100.136	100.259	100.235	101.138	100.063	100.104	100.308
6.13	6.154	6.186	6.144	6.144	6.18	6.175	6.183	6.14	6.136	6.22	6.202	6.173
6.13	6.154	6.186	6.144	6.144	6.18	6.175	6.183	6.14	6.136	6.22	6.202	6.173
12.26	12.308	12.372	12.288	12.288	12.36	12.35	12.366	12.28	12.272	12.44	12.404	12.346
3.032	2.884	2.997	3.132	3.106	3.022	3.211	3.086	3.257	3.246	3.055	3.227	3.129
0.669	0.554	0.448	0.603	0.471	0.594	0.634	0.548	0.57	0.729	0.517	0.522	0.61
0.091	0.077	0.087	0.094	0.112	0.086	0.111	0.097	0.109	0.102	0.09	0.099	0.107
0.836	1.118	1.054	0.753	0.902	0.926	0.633	0.84	0.689	0.695	0.913	0.827	0.787
1.722	1.742	1.763	1.73	1.738	1.708	1.692	1.792	1.677	1.709	1.776	1.733	1.707
0.278	0.258	0.237	0.27	0.262	0.292	0.308	0.208	0.321	0.291	0.224	0.267	0.293
0.349	0.334	0.339	0.368	0.355	0.367	0.374	0.335	0.365	0.366	0.369	0.34	0.368
0.184	0.245	0.235	0.172	0.201	0.204	0.141	0.188	0.153	0.149	0.203	0.181	0.175

	4	5	6	7	8	9	10	11	12	13	14	15	16	17	CC8-1
						Core	Rim	Core	Rim	Core	Rim	Core	Mid Rim	Outer Rim	
2.67	2.96	3.21	3.15	2.99	2.98	3.03	3.23	3.19	3.07	2.87	3.21	2.86	3.11	2.89	
3.1	5.24	3.44	3.24	3.96	5.97	4.42	5.81	3.35	5.52	3.34	7.72	5.72	3.48	2.71	
10.16	9.88	9.6	9.78	10.46	10.03	10.25	10.5	9.84	10.26	9.57	9.57	10.33	9.93	9.62	
38.28	39.09	38.97	38.8	38.78	39.65	39.22	39.38	38.39	39.4	38.79	39.78	39.34	38.6	37.72	
2.15	1.74	1.82	1.92	1.65	1.86	1.73	1.84	1.75	1.73	1.8	1.62	1.76	1.78	1.74	
10.38	10.4	10.22	10.08	10.63	10.51	10.14	10.41	9.94	10.55	10.08	10.67	10.47	10.54	10.19	
0.98	2.16	1.89	2.03	1.89	2.14	1.91	1.76	1.89	2.02	1.93	3.15	2.08	1.93	1.91	
0.78	0.74	0.71	0.69	0.7	0.53	0.69	0.64	0.76	0.73	0.88	0.53	0.65	0.67	0.88	
22.994	21.279	22.963	23.343	22.958	20.424	22.813	19.048	22.853	20.499	24.404	17.935	21.115	22.657	24.045	
6.752	3.946	5.909	5.465	5.226	3.974	4.231	5.971	5.575	4.147	4.053	3.218	3.662	5.716	5.629	
1.86	1.9	1.87	1.87	1.88	1.91	1.89	1.91	1.87	1.91	1.87	1.93	1.91	1.88	1.86	
100.106	99.335	100.602	100.368	101.124	99.978	100.324	100.499	99.408	99.836	99.587	99.333	99.897	100.293	99.194	
6.148	6.213	6.199	6.192	6.116	6.225	6.205	6.149	6.178	6.206	6.246	6.208	6.195	6.154	6.135	
6.148	6.213	6.199	6.192	6.116	6.225	6.205	6.149	6.178	6.206	6.246	6.208	6.195	6.154	6.135	
12.296	12.426	12.398	12.384	12.232	12.45	12.41	12.298	12.356	12.412	12.492	12.416	12.39	12.308	12.27	
3.088	2.829	3.053	3.117	3.027	2.683	3.017	2.488	3.076	2.701	3.287	2.34	2.781	3.021	3.27	
0.816	0.472	0.709	0.655	0.621	0.468	0.505	0.701	0.675	0.491	0.49	0.378	0.434	0.686	0.69	
0.106	0.1	0.096	0.093	0.094	0.07	0.091	0.085	0.104	0.097	0.12	0.07	0.084	0.09	0.121	
0.742	1.242	0.816	0.771	0.931	1.397	1.043	1.352	0.804	1.296	0.802	1.796	1.343	0.827	0.657	
1.786	1.771	1.742	1.724	1.796	1.768	1.719	1.742	1.714	1.78	1.739	1.784	1.767	1.801	1.776	
0.214	0.229	0.258	0.276	0.204	0.232	0.28	0.258	0.286	0.22	0.261	0.216	0.23	0.199	0.224	
0.44	0.353	0.369	0.391	0.332	0.373	0.349	0.367	0.359	0.348	0.37	0.323	0.354	0.362	0.361	
0.16	0.273	0.178	0.169	0.203	0.307	0.228	0.297	0.175	0.289	0.175	0.398	0.295	0.183	0.143	

2	3	4	5	6	7	8	CC9-1	2	3	4	5	6	7	8
3.13	2.91	2.83	3	2.91	3.01	3.1	3.31	3.25	3.36	3.07	2.96	3.09	3.07	3.01
2.83	2.95	2.75	3.02	2.61	4	3.14	3.18	3.08	3.1	3.07	3.17	2.93	3.03	3.16
9.39	9.73	10.09	9.96	10.18	9.85	9.94	10.17	9.43	9.89	9.77	9.69	10	9.73	10.31
39.07	38.05	37.97	37.99	37.62	38.56	37.5	38.72	39.35	38.93	39.04	38.76	38.37	37.91	37.97
1.72	1.73	1.78	1.65	1.74	1.51	1.72	1.63	1.82	1.73	1.7	1.76	1.68	1.74	1.78
10.16	10.34	10.45	10.45	10.45	10.35	10.17	9.71	9.98	9.85	9.97	10	10.16	10.29	10.09
1.91	1.99	2.09	2.38	2.06	2.51	2.21	1.89	1.77	1.95	1.74	1.63	2.15	2.02	2
0.85	0.9	0.95	0.9	0.75	0.76	0.83	0.8	0.83	0.83	0.71	0.96	0.9	0.81	0.78
24.762	23.984	24.434	23.937	24.413	23.798	22.559	23.594	23.92	23.468	24.653	24.107	24.182	23.033	23.383
5.399	5.93	5.641	5.761	5.676	3.437	6.425	4.163	5.368	5.571	3.386	5.683	5.388	6.32	5.821
1.86	1.86	1.86	1.86	1.86	1.88	1.87	1.88	1.87	1.87	1.87	1.87	1.86	1.86	1.87
101.081	100.374	100.845	100.908	99.989	99.665	99.464	99.047	100.668	100.549	98.979	100.59	100.71	99.813	100.174
6.224	6.111	6.077	6.063	6.071	6.173	6.057	6.238	6.268	6.2	6.309	6.194	6.127	6.107	6.084
6.224	6.111	6.077	6.063	6.071	6.173	6.057	6.238	6.268	6.2	6.309	6.194	6.127	6.107	6.084
12.448	12.222	12.154	12.126	12.142	12.346	12.114	12.476	12.536	12.4	12.618	12.388	12.254	12.214	12.168
3.299	3.222	3.268	3.193	3.295	3.187	3.045	3.18	3.186	3.127	3.333	3.221	3.23	3.105	3.134
0.647	0.716	0.681	0.693	0.689	0.413	0.783	0.503	0.644	0.666	0.411	0.684	0.647	0.765	0.701
0.115	0.122	0.129	0.122	0.103	0.103	0.114	0.109	0.112	0.112	0.097	0.125	0.122	0.111	0.106
0.672	0.706	0.656	0.719	0.628	0.955	0.756	0.764	0.731	0.736	0.74	0.755	0.697	0.728	0.755
1.734	1.779	1.792	1.787	1.759	1.775	1.76	1.676	1.703	1.681	1.726	1.712	1.738	1.776	1.732
0.266	0.221	0.208	0.213	0.241	0.225	0.24	0.324	0.297	0.319	0.274	0.282	0.262	0.224	0.268
0.35	0.354	0.363	0.336	0.358	0.308	0.354	0.335	0.37	0.351	0.35	0.359	0.342	0.358	0.364
0.145	0.153	0.143	0.156	0.136	0.209	0.165	0.171	0.16	0.163	0.166	0.163	0.153	0.158	0.165

	CC10-1								CC11-1					Core
	2	3	4	5	6	7	8		2	3	4	5	6	
3.04	2.64	2.97	2.8	2.81	2.82	2.8	2.91	2.9	3.11	3.04	3.02	3.1	3.17	
3.57	3.68	3.32	3.39	4.61	4.64	3.59	4.07	2.65	2.24	2.39	2.5	2.36	4.43	
10.14	10.33	10.12	10.35	10.12	9.83	10.14	10.12	10.27	9.59	8.89	9.24	9.51	9.86	
37.93	37.6	37.94	38.16	38.91	38.66	38.09	38.76	37.71	37.67	38.79	38.61	38.16	38.92	
1.72	1.65	1.69	1.77	1.66	1.81	1.65	1.73	1.74	1.7	1.73	1.63	1.65	1.59	
10.47	10.8	10.46	10.47	10.72	10.56	10.55	10.61	9.85	9.9	9.51	9.8	9.88	10.27	
2.27	2.46	2.27	1.97	2.2	2.31	2.28	2.13	2.28	2.44	1.68	2.07	2.51	2.78	
0.83	0.79	0.76	0.86	0.6	0.73	0.87	0.67	0.69	0.82	0.85	0.86	0.74	0.65	
22.447	23.563	23.323	23.914	23.047	22.204	23.921	23.098	24.942	24.792	25.553	25.769	25.561	22.808	
6.393	4.087	5.498	4.875	4.449	4.63	4.4	4.926	4.032	4.977	5.409	4.279	3.91	3.359	
1.87	1.87	1.87	1.87	1.88	1.88	1.87	1.88	1.86	1.86	1.85	1.86	1.86	1.89	
100.68	99.47	100.221	100.429	101.006	100.074	100.161	100.904	98.924	99.099	99.692	99.638	99.241	99.727	
6.038	6.055	6.075	6.098	6.131	6.145	6.098	6.13	6.133	6.142	6.291	6.255	6.203	6.192	
6.038	6.055	6.075	6.098	6.131	6.145	6.098	6.13	6.133	6.142	6.291	6.255	6.203	6.192	
12.076	12.11	12.15	12.196	12.262	12.29	12.196	12.26	12.266	12.284	12.582	12.51	12.406	12.384	
2.99	3.172	3.124	3.196	3.038	2.953	3.202	3.054	3.393	3.381	3.465	3.491	3.477	3.035	
0.765	0.497	0.662	0.586	0.526	0.553	0.531	0.588	0.492	0.611	0.661	0.522	0.476	0.402	
0.112	0.108	0.103	0.116	0.08	0.098	0.118	0.09	0.091	0.113	0.102	0.112	0.102	0.088	
0.847	0.883	0.792	0.808	1.083	1.099	0.857	0.96	0.642	0.544	0.578	0.604	0.572	1.051	
1.786	1.863	1.794	1.793	1.81	1.798	1.81	1.798	1.716	1.73	1.652	1.701	1.721	1.751	
0.214	0.137	0.206	0.207	0.19	0.202	0.19	0.202	0.28	0.27	0.332	0.293	0.279	0.249	
0.349	0.339	0.345	0.361	0.334	0.367	0.337	0.349	0.361	0.354	0.358	0.337	0.342	0.323	
0.184	0.193	0.172	0.176	0.232	0.238	0.187	0.208	0.142	0.12	0.123	0.131	0.127	0.234	

Rim	7	Core	8	Rim	9	Core	10	Rim	11	CC12-1	2	3	4	5	6	7	Core	8	Rim	9	Core	10
3.13	3.05	3.02	2.75	3.02	3	2.94	2.19	3.05	3.02	3.02	2.95	2.95	2.91	2.8	2.97	3.06	3.02	3.02	3.03	2.85		
2.68	4.9	2.75	7.12	2.75	7.12	2.19	3.21	3.21	2.95	2.95	2.95	3	3.06	3.36	2.87	2.87	8.06	3.11	8.65			
9.07	10.01	9.77	9.94	9.77	9.94	10.27	9.81	9.62	9.62	9.64	9.64	9.88	9.31	9.24	9.24	9.85	9.53	9.53	9.58			
38.76	38.73	37.92	40.22	38.55	38.55	39.12	38.99	38.99	38.7	38.7	38.88	38.56	38.55	38.1	38.1	40.7	38.75	39.88				
1.81	1.63	1.71	1.63	1.75	1.75	1.78	1.76	1.78	1.76	1.77	1.73	1.73	1.73	1.71	1.66	1.75	1.6	1.75	1.63			
9.96	10.11	9.81	10.62	10.22	10.22	10.09	10.1	10.09	10.1	10.12	10.13	10.13	10.25	10	9.98	10.7	10.06	11.05				
1.98	2.48	2.49	3.11	1.93	1.93	2.21	2.52	2.21	2.52	2.59	2.79	2.44	2.44	2.7	2.44	3.35	2.43	2.86				
0.82	0.75	0.91	0.5	0.88	0.7	0.67	0.72	0.81	0.63	0.8	0.74	0.45	0.78	0								
24.608	21.956	24.742	20.425	25.914	24.868	25.586	25.574	25.917	25.613	25.058	24.31	19.526	24.83	17.741								
5.681	3.972	4.776	2.272	4.341	3.948	3.372	3.73	2.849	3.198	2.225	4.768	1.361	3.978	2.022								
1.86	1.89	1.86	1.92	1.86	1.87	1.87	1.86	1.87	1.87	1.87	1.86	1.94	1.87	1.95								
100.359	99.478	99.758	100.757	100.845	100.656	100.458	100.904	100.526	100.011	98.503	99.118	100.557	100.118	98.213								
6.231	6.165	6.127	6.221	6.172	6.229	6.236	6.168	6.218	6.194	6.269	6.188	6.26	6.215	6.254								
6.231	6.165	6.127	6.221	6.172	6.229	6.236	6.168	6.218	6.194	6.269	6.188	6.26	6.215	6.254								
12.462	12.33	12.254	12.442	12.344	12.458	12.472	12.336	12.436	12.388	12.538	12.376	12.52	12.43	12.508								
3.307	2.923	3.342	2.642	3.469	3.31	3.423	3.409	3.467	3.44	3.409	3.3	2.512	3.329	2.327								
0.688	0.475	0.582	0.265	0.524	0.475	0.405	0.447	0.342	0.388	0.271	0.585	0.157	0.482	0.238								
0.112	0.1	0.123	0.057	0.119	0.094	0.091	0.097	0.106	0.08	0.11	0.102	0.049	0.106	0.238								
0.642	1.163	0.662	1.642	0.523	0.762	0.703	0.701	0.715	0.733	0.815	0.695	1.848	0.744	2.022								
1.715	1.724	1.698	1.76	1.753	1.721	1.731	1.728	1.736	1.764	1.743	1.737	1.763	1.729	1.857								
0.285	0.274	0.3	0.232	0.247	0.279	0.269	0.272	0.26	0.23	0.257	0.263	0.227	0.271	0.143								
0.371	0.331	0.352	0.322	0.357	0.362	0.359	0.36	0.353	0.35	0.344	0.363	0.314	0.358	0.326								
0.159	0.254	0.144	0.361	0.116	0.168	0.155	0.154	0.158	0.161	0.181	0.151	0.408	0.163	0.44								

Rim	CC13 - 1				Core	Rim	Core	Rim	Core	Rim	Core	Rim	Core	Rim	Core	Rim	CC14 - 1	2
11	2	3	4	5	6	7	8	9	10	11	12	CC14 - 1	2					
2.79	3.21	3.09	3.21	3.02	3.2	3.12	3.15	3.11	3.2	3.12	3.26	3.12	3.1	2.96				
2.93	3.46	3.47	3.46	2.96	6.37	3.3	7.24	3.6	6.64	3.35	5.69	3.14	3.47	3.09				
9.63	10.06	9.43	8.51	9.93	10.08	9.76	10.15	10.17	10.38	10.39	10.08	9.73	9.52	9.87				
37.71	38.44	38.85	39.85	38.05	39.53	38.19	39.89	38.28	39.43	38.35	39.12	37.44	38.77	37.66				
1.7	1.78	1.79	1.71	1.73	1.65	1.7	1.65	1.63	1.65	1.78	1.56	1.78	1.68	1.7				
10.08	9.88	9.95	9.6	9.74	10.41	9.74	10.4	9.91	10.17	9.99	10.23	9.92	10.01	10.25				
2.45	2.11	1.5	1.85	1.89	2.52	2	2.21	2.08	2.53	1.97	2.32	2.11	2.05	1.94				
0.69	0.9	0.84	1.01	0.84	0.61	0.94	0.7	0.84	0.71	0.73	0.69	0.81	0.77	0.92				
24.979	22.877	23.448	24.526	23.897	19.651	23.259	18.594	23.081	19.133	23.213	20.221	22.448	24.072	23.099				
3.857	6.237	6.637	4.772	5.949	4.222	6.503	4.263	5.9	5.02	5.586	4.8	7.326	5.21	6.258				
1.86	1.87	1.87	1.87	1.86	1.92	1.87	1.93	1.87	1.92	1.87	1.91	1.86	1.87	1.86				
98.676	100.824	100.875	100.368	99.866	100.163	100.382	100.177	100.471	100.783	100.349	99.881	99.684	100.522	99.607				
6.155	6.107	6.187	6.368	6.129	6.177	6.113	6.197	6.098	6.118	6.116	6.16	6.045	6.188	6.083				
6.155	6.107	6.187	6.368	6.129	6.177	6.113	6.197	6.098	6.118	6.116	6.16	6.045	6.188	6.083				
12.31	12.214	12.374	12.736	12.258	12.354	12.226	12.394	12.196	12.236	12.232	12.32	12.09	12.376	12.166				
3.41	3.038	3.122	3.278	3.221	2.569	3.114	2.415	3.076	2.482	3.096	2.664	3.032	3.212	3.12				
0.473	0.748	0.796	0.574	0.72	0.496	0.783	0.499	0.706	0.587	0.67	0.568	0.889	0.627	0.761				
0.095	0.121	0.113	0.131	0.106	0.081	0.121	0.092	0.106	0.084	0.099	0.092	0.111	0.104	0.126				
0.713	0.819	0.824	0.824	0.711	1.484	0.787	1.677	0.855	1.536	0.796	1.336	0.756	0.826	0.744				
1.763	1.682	1.698	1.644	1.681	1.743	1.67	1.731	1.692	1.691	1.707	1.726	1.716	1.712	1.774				
0.237	0.318	0.302	0.35	0.31	0.257	0.323	0.269	0.301	0.3	0.293	0.274	0.284	0.288	0.226				
0.354	0.361	0.364	0.349	0.356	0.329	0.347	0.327	0.331	0.327	0.362	0.313	0.367	0.342	0.35				
0.155	0.177	0.174	0.175	0.153	0.326	0.168	0.364	0.185	0.333	0.175	0.292	0.161	0.178	0.161				

	3	4	5	6	7	Mafic CC15 - 1	2	3	4	Core	Rim	5	6	Core	Rim	7	8	Core	Rim	9	Core	10
2.95	2.98	3.05	3.18	3.06	2.84	3.09	2.83	2.88	2.92	2.86	2.88	2.94	3	3.07								
3.8	3.46	3.42	3.57	4.08	3.43	3.67	3.78	8.75	3.9	9.14	3.11	8.52	3.24	8.64								
9.82	9.62	10.1	9.9	10.08	10.74	10.15	10.33	10.11	10.61	10.26	10.55	10.44	10.71	10.68								
38.65	38.45	38.43	38.36	38.49	38.21	39.27	39.01	40.31	38.17	40.4	38.48	40.25	38.15	40.62								
1.81	1.8	1.75	1.74	1.74	1.74	1.74	1.76	1.6	1.76	1.58	1.66	1.55	1.82	1.64								
10.36	10.15	10.31	10.12	10.33	10.26	10.29	10.4	10.87	10.3	10.95	10.36	10.99	10.31	11.05								
2.17	1.97	2.12	2.05	2.21	1.99	2.32	1.99	2.43	2.18	2.38	2.08	2.23	1.92	2.35								
0.69	0.82	0.73	0.86	0.68	0.63	0.74	0.79	0.47	0.69	0.42	0.74	0.5	0.75	0.36								
23.288	23.365	23.378	22.46	22.427	24.183	23.977	24.09	17.406	22.776	16.846	24.956	17.608	23.031	17.154								
5.414	5.585	5.781	6.279	5.961	2.953	3.159	3.79	2.538	4.327	2.505	3.428	2.369	4.767	2.874								
1.87	1.87	1.87	1.87	1.88	1.88	1.88	1.88	1.95	1.88	1.96	1.87	1.95	1.88	1.95								
100.822	100.07	100.939	100.389	100.938	98.856	100.286	100.65	99.314	99.513	99.301	100.114	99.347	99.578	100.388								
6.136	6.163	6.104	6.116	6.088	6.169	6.237	6.187	6.244	6.11	6.239	6.159	6.236	6.121	6.216								
6.136	6.163	6.104	6.116	6.088	6.169	6.237	6.187	6.244	6.11	6.239	6.159	6.236	6.121	6.216								
12.272	12.326	12.208	12.232	12.176	12.338	12.474	12.374	12.488	12.22	12.478	12.318	12.472	12.242	12.432								
3.092	3.131	3.107	2.995	2.968	3.266	3.186	3.194	2.254	3.05	2.175	3.341	2.282	3.092	2.195								
0.647	0.675	0.689	0.753	0.708	0.358	0.376	0.453	0.296	0.52	0.291	0.413	0.276	0.574	0.331								
0.093	0.111	0.098	0.116	0.091	0.086	0.1	0.103	0.055	0.094	0.046	0.1	0.066	0.102	0.047								
0.899	0.827	0.81	0.848	0.962	0.826	0.869	0.894	2.021	0.931	2.104	0.742	1.968	0.775	1.971								
1.762	1.743	1.754	1.729	1.751	1.775	1.751	1.767	1.804	1.766	1.812	1.777	1.824	1.773	1.812								
0.238	0.257	0.246	0.271	0.249	0.225	0.249	0.23	0.189	0.234	0.179	0.223	0.176	0.227	0.188								
0.367	0.368	0.355	0.354	0.351	0.358	0.353	0.356	0.316	0.359	0.311	0.339	0.306	0.373	0.32								
0.194	0.179	0.176	0.184	0.208	0.185	0.197	0.197	0.441	0.207	0.461	0.165	0.435	0.174	0.438								

Rim	Normal						Core	Rim	Pegmatite					
	CC15 - 1								CC16 - 1					
11	2	3	4	5	6	7	8	2	3	4	5	6		
2.88	2.97	2.88	2.86	2.76	2.96	2.85	3	2.77	3.09	3.15	3.27	3.11	3.01	3.19
3.9	3.05	3.34	2.88	1.71	4.01	3.05	8.35	4.32	2.65	2.6	2.54	2.57	2.56	2.6
10.47	10.38	10.37	10.02	9.8	9.79	10.27	10.16	10.16	9.33	9.64	9.69	10.06	9.73	9.68
38.46	38.41	38.78	38.7	37.64	38.81	38.59	40.22	38.61	38.89	37.95	38.49	38.3	38.16	38.57
1.71	1.74	1.73	1.71	1.78	1.67	1.76	1.61	1.67	1.7	1.69	1.79	1.76	1.72	1.68
10.21	10.5	10.5	10.2	10.12	10.35	10.46	10.84	10.29	10.09	9.65	9.77	9.9	9.95	9.93
2.04	1.98	2.19	2.29	3.7	1.7	2.02	2.44	2.12	1.91	1.88	2.02	2.07	2.06	2.03
0.75	0.83	0.8	0.8	0.83	0.69	0.78	0.53	0.83	0.98	0.86	0.88	0.69	0.77	0.78
23.345	23.885	24.523	25.683	28.029	22.874	24.744	17.754	22.951	25.055	24.363	24.258	25.113	25.198	24.846
3.74	4.795	3.541	2.686	1.502	4.207	4.218	3.185	3.644	5.663	6.065	6.448	5.475	5.059	5.817
1.88	1.87	1.87	1.87	1.85	1.88	1.87	1.94	1.89	1.86	1.86	1.86	1.86	1.86	1.86
99.385	100.41	100.524	99.699	99.721	98.941	100.612	100.029	99.255	101.218	99.708	101.016	100.908	100.077	100.983
6.164	6.134	6.173	6.232	6.131	6.244	6.158	6.21	6.184	6.204	6.144	6.147	6.124	6.157	6.161
6.164	6.134	6.173	6.232	6.131	6.244	6.158	6.21	6.184	6.204	6.144	6.147	6.124	6.157	6.161
12.328	12.268	12.346	12.464	12.262	12.488	12.316	12.42	12.368	12.408	12.288	12.294	12.248	12.314	12.322
3.13	3.189	3.264	3.461	3.818	3.078	3.301	2.293	3.072	3.343	3.297	3.24	3.356	3.401	3.32
0.45	0.578	0.425	0.324	0.184	0.51	0.508	0.37	0.441	0.68	0.74	0.775	0.661	0.614	0.698
0.101	0.112	0.108	0.109	0.115	0.094	0.105	0.069	0.098	0.132	0.118	0.119	0.093	0.105	0.106
0.932	0.726	0.793	0.691	0.415	0.962	0.726	1.922	1.031	0.63	0.627	0.605	0.613	0.616	0.619
1.753	1.797	1.791	1.76	1.766	1.784	1.788	1.793	1.766	1.725	1.674	1.672	1.696	1.72	1.699
0.246	0.203	0.209	0.24	0.234	0.216	0.212	0.207	0.219	0.275	0.326	0.328	0.304	0.28	0.301
0.35	0.354	0.351	0.351	0.37	0.343	0.358	0.317	0.341	0.346	0.349	0.365	0.359	0.354	0.342
0.206	0.161	0.177	0.155	0.095	0.211	0.159	0.42	0.227	0.136	0.135	0.132	0.132	0.132	0.133

Mafic							Mafic								
CC16-1							CC17A-1								
7	8	2	3	4	5	6	7	2	3	4	5	6			
3.1	3.08	2.95	3.01	2.84	2.61	3.21	2.9	3.13	3.01	3.25	3.22	3.16	3.05	3.13	3.27
2.53	2.68	2.77	2.63	2.61	2.58	2.49	2.68	2.69	2.51	2.25	2.47	2.47	2.4	2.36	3.08
9.3	10.08	9.43	9.59	9.62	9.81	9.71	9.73	9.86	9.73	9.43	9.77	9.77	9.53	9.45	9.9
38.71	38.13	38.71	38.17	38.2	38.18	37.93	38.74	38.27	38.5	38.15	38.06	38.06	38.08	37.9	38.62
1.78	1.7	1.6	1.8	1.68	1.75	1.61	1.69	1.77	1.73	1.79	1.8	1.8	1.79	1.67	1.75
9.74	10.12	10.03	9.68	9.64	9.69	10.04	9.87	10.04	9.82	9.69	9.8	9.8	9.67	10.01	9.99
2.04	2.12	2.17	2.17	1.96	2.19	1.94	2.07	2.07	2.14	1.86	2.11	2.11	1.9	2.04	1.96
0.77	0.91	0.87	0.79	0.81	0.89	0.85	0.84	0.84	0.94	0.92	0.92	0.92	0.85	0.92	1.01
25.366	24.336	25.638	25.076	25.067	24.293	25.243	25.369	24.893	24.535	24.298	24.315	24.315	24.95	24.427	23.193
4.627	5.817	3.959	4.349	4.916	5.142	4.453	4.213	5.586	5.585	6.293	6.629	6.629	5.679	6.872	6.565
1.86	1.86	1.86	1.86	1.86	1.86	1.86	1.86	1.86	1.86	1.86	1.85	1.85	1.85	1.85	1.87
99.823	100.833	99.987	99.125	99.203	99.595	99.026	100.192	100.889	100.6	99.761	100.884	100.884	99.749	100.629	101.208
6.253	6.096	6.236	6.206	6.205	6.17	6.182	6.224	6.124	6.168	6.181	6.098	6.129	6.172	6.101	6.129
6.253	6.096	6.236	6.206	6.205	6.17	6.182	6.224	6.124	6.168	6.181	6.098	6.129	6.172	6.101	6.129
12.506	12.192	12.472	12.412	12.41	12.34	12.364	12.448	12.248	12.336	12.362	12.196	12.344	12.344	12.202	12.258
3.425	3.253	3.453	3.408	3.407	3.282	3.442	3.41	3.333	3.287	3.293	3.256	3.384	3.384	3.29	3.079
0.564	0.701	0.481	0.534	0.599	0.626	0.545	0.508	0.671	0.674	0.766	0.801	0.691	0.691	0.831	0.783
0.105	0.123	0.11	0.109	0.076	0.122	0.117	0.114	0.114	0.128	0.126	0.125	0.117	0.117	0.125	0.136
0.609	0.639	0.665	0.637	0.632	0.622	0.605	0.642	0.642	0.599	0.543	0.59	0.58	0.58	0.566	0.729
1.686	1.733	1.731	1.686	1.678	1.678	1.753	1.699	1.721	1.686	1.682	1.682	1.679	1.679	1.727	1.699
0.314	0.267	0.26	0.314	0.286	0.322	0.247	0.301	0.279	0.314	0.318	0.318	0.301	0.321	0.273	0.301
0.367	0.347	0.329	0.373	0.348	0.361	0.335	0.346	0.361	0.354	0.37	0.368	0.368	0.37	0.343	0.354
0.137	0.139	0.144	0.14	0.136	0.137	0.131	0.141	0.138	0.132	0.118	0.127	0.127	0.125	0.121	0.158

Pegmatite										Mafic									
CC17A-1										CC17B-1									
7	8	2	3	4	5	6	7	8		2	3	4	5	2	3	4	5		
3.38	3.23	3.27	2.74	2.95	2.97	3.35	2.93	2.78	2.99	3.14	3.06	3.05	2.96	3.14	3.06	3.05	2.96		
2.47	3.42	2.44	2.51	2.48	2.06	2.37	2.69	2.67	3.35	3.49	3.87	2.78	2.53	3.49	3.87	2.78	2.53		
8.79	9.52	8.49	10.38	9.8	10.1	8.44	10.46	10.38	9.77	9.72	9.51	9.8	9.69	9.72	9.51	9.8	9.69		
38.88	38.94	39.03	37.16	37.87	37.57	39.53	38.63	37.59	38.55	38.94	39.11	38.77	37.94	38.94	39.11	38.77	37.94		
1.8	1.73	1.75	1.74	1.78	1.63	1.73	1.77	1.7	1.63	1.62	1.7	1.66	1.75	1.62	1.7	1.66	1.75		
9.68	10.02	9.53	10.33	10.25	9.91	9.53	10.35	10.37	9.93	9.91	10.08	9.83	9.76	9.91	10.08	9.83	9.76		
1.87	2.06	1.88	1.91	1.97	1.86	1.37	2.02	1.92	1.71	2.28	2.38	2.1	1.97	2.28	2.38	2.1	1.97		
0.97	0.9	0.87	0.81	0.74	0.97	1.03	0.79	0.74	0.87	0.81	0.74	0.85	0.75	0.81	0.74	0.85	0.75		
24.132	23.336	25.209	24.277	24.446	25.157	25.076	24.8	24.42	24.814	25.21	24.28	24.137	25.021	24.28	24.137	25.212	25.021		
6.789	5.539	5.536	5.293	5.883	5.849	6.284	5.846	5.402	5.253	5.54	5.29	3.693	4.599	5.29	3.693	4.599	4.678		
1.86	1.87	1.86	1.86	1.86	1.85	1.85	1.86	1.86	1.86	1.86	1.86	1.88	1.86	1.86	1.88	1.86	1.86		
100.621	100.565	99.865	99.01	100.029	99.926	100.56	100.426	100.512	100.007	99.87	100.16	100.511	98.909	99.01	100.16	100.511	98.909		
6.242	6.202	6.317	6.058	6.116	6.091	6.355	6.209	6.072	6.065	6.317	6.238	6.223	6.238	6.058	6.255	6.223	6.238		
6.242	6.202	6.317	6.058	6.116	6.091	6.355	6.209	6.072	6.065	6.317	6.238	6.223	6.238	6.058	6.255	6.223	6.238		
12.484	12.404	12.634	12.116	12.232	12.182	12.71	12.418	12.144	12.13	12.634	12.51	12.446	12.476	12.116	12.51	12.446	12.476		
3.238	3.108	3.41	3.31	3.302	3.411	3.373	3.334	3.273	3.348	3.41	3.221	3.266	3.221	3.31	3.265	3.266	3.221		
0.822	0.665	0.676	0.649	0.714	0.714	0.759	0.707	0.651	0.638	0.676	0.482	0.479	0.442	0.649	0.482	0.479	0.442		
0.132	0.121	0.119	0.112	0.101	0.13	0.14	0.124	0.107	0.1	0.119	0.106	0.096	0.1	0.112	0.106	0.096	0.1		
0.591	0.812	0.589	0.61	0.597	0.498	0.568	0.518	0.643	0.642	0.589	0.81	0.831	0.92	0.61	0.81	0.831	0.92		
1.665	1.71	1.653	1.804	1.774	1.721	1.642	1.645	1.777	1.793	1.653	1.804	1.697	1.723	1.653	1.804	1.697	1.723		
0.335	0.29	0.347	0.196	0.226	0.275	0.358	0.355	0.223	0.206	0.347	0.196	0.303	0.277	0.347	0.196	0.303	0.277		
0.369	0.352	0.361	0.362	0.367	0.337	0.355	0.363	0.348	0.336	0.361	0.362	0.337	0.346	0.361	0.362	0.337	0.346		
0.127	0.176	0.126	0.134	0.13	0.107	0.121	0.114	0.14	0.139	0.178	0.182	0.201	0.133	0.182	0.201	0.144	0.133		





DN3-1	Core						Rim	DN4-1	DN3-1					
	2	3	4	5	6	7			8	2	3	4	5	6
3.43	3.52	3.38	3.73	3.29	3.39	3.2	3.14	3.71	3.63	3.57	3.63	3.8	3.94	
2.94	2.56	2.87	3.06	3.72	2.61	6.1	2.55	3.6	3.2	3.36	2.98	2.55	2.77	
8.02	9.13	9.96	8.16	10.07	9.62	10.14	10.14	9.33	10.2	10.05	8.88	8.94	8.28	
40.28	38.94	38.85	40.1	39.29	38.42	39.92	38.38	39.21	38.63	38.64	39.11	39.16	39.77	
1.75	1.77	1.75	1.72	1.68	1.64	1.69	1.74	1.68	1.63	1.73	1.79	1.77	1.69	
8.95	8.99	9.2	8.86	9.61	9.34	10.1	9.86	8.81	9.06	8.98	8.76	8.81	8.66	
1.65	1.62	1.78	1.6	1.67	1.96	1.83	1.78	1.87	2.14	2.08	2	2.05	1.78	
1	0.93	0.84	0.94	0.79	0.89	0.55	0.82	0.77	0.76	0.97	0.95	1	1.08	
24.988	24.184	23.936	24.316	23.138	24.425	20.203	24.731	22.559	23.301	22.73	23.791	23.784	23.574	
6.137	6.93	6.24	6.339	5.993	5.718	5.131	6.156	5.135	5.455	5.734	5.922	7.197	7.175	
1.86	1.86	1.87	1.87	1.88	1.86	1.91	1.86	1.89	1.88	1.88	1.87	1.86	1.86	
101.005	100.434	100.676	100.695	101.131	99.873	100.774	101.157	98.564	99.886	99.724	99.683	100.921	100.579	
6.42	6.25	6.193	6.401	6.199	6.194	6.213	6.121	6.328	6.177	6.186	6.299	6.249	6.357	
6.42	6.25	6.193	6.401	6.199	6.194	6.213	6.121	6.328	6.177	6.186	6.299	6.249	6.357	
12.84	12.5	12.386	12.802	12.398	12.388	12.426	12.242	12.656	12.354	12.372	12.598	12.498	12.714	
3.332	3.245	3.192	3.246	3.052	3.293	2.629	3.299	3.047	3.118	3.042	3.203	3.175	3.15	
0.735	0.839	0.747	0.761	0.713	0.694	0.602	0.738	0.622	0.655	0.691	0.719	0.864	0.864	
0.11	0.126	0.101	0.127	0.092	0.122	0.066	0.111	0.105	0.103	0.132	0.13	0.135	0.146	
0.699	0.613	0.682	0.728	0.875	0.627	1.415	0.606	0.866	0.763	0.802	0.715	0.607	0.66	
1.528	1.546	1.571	1.515	1.624	1.613	1.684	1.685	1.523	1.552	1.54	1.512	1.506	1.483	
0.447	0.454	0.416	0.485	0.362	0.387	0.309	0.315	0.477	0.448	0.46	0.488	0.494	0.517	
0.356	0.362	0.356	0.35	0.338	0.337	0.336	0.354	0.346	0.333	0.353	0.368	0.36	0.345	
0.147	0.13	0.147	0.154	0.189	0.136	0.304	0.129	0.191	0.167	0.176	0.155	0.131	0.141	

	7	8	DNS-1	2	3	4	5	6	Core	Rim	Core	8	9	Rim	DNG-1	2	3	4
3.93	4.11	3.75	4.07	3.79	3.73	3.48	3.71	3.67	3.48	3.89	2.74	3.03	2.93	3.04				
2.56	3.24	2.19	2.78	2.96	2.45	2.92	7.55	3.62	6.85	3.94	4.07	1.89	3.57	2.62				
9.48	7.17	10.02	7.75	9.93	8.98	9.14	10.14	9.36	10.1	8.79	10.65	10.41	10.65	9.47				
39.25	41.47	38.3	40.5	38.37	38.66	38.6	40	39.45	39.53	39.48	38.59	37.8	38.73	39.83				
1.72	1.68	1.77	1.79	1.77	1.75	1.89	1.67	1.75	1.72	1.93	1.71	1.99	1.68	1.72				
8.53	8.06	8.94	8.37	9.06	8.69	8.99	9.79	8.9	9.86	8.79	10.64	9.53	10.19	9.91				
1.93	1.96	1.76	1.67	2.08	1.86	2.03	2.32	1.97	2.52	1.43	2.13	1.14	2.09	1.62				
0.96	1.08	0.96	1	0.9	1.05	0.97	0.71	0.93	0.73	0.99	0.69	0.83	0.71	0.78				
24.019	24.788	23.241	23.905	22.006	23.836	23.514	16.443	22.749	17.929	20.363	23.725	24.636	24.136	26.444				
6.425	5.247	8.112	7.062	7.851	7.428	6.697	6.387	6.68	5.425	8.976	2.962	7.017	3.727	3.085				
1.87	1.87	1.86	1.87	1.87	1.86	1.93	1.88	1.88	1.92	1.88	1.88	1.85	1.88	1.87				
100.674	100.675	100.903	100.767	100.587	100.294	100.091	100.65	100.959	100.064	100.459	99.787	100.123	100.293	100.389				
6.261	6.593	6.118	6.459	6.112	6.222	6.207	6.158	6.242	6.156	6.265	6.155	6.115	6.161	6.377				
6.261	6.593	6.118	6.459	6.112	6.222	6.207	6.158	6.242	6.156	6.265	6.155	6.115	6.161	6.377				
12.522	13.186	12.236	12.918	12.224	12.444	12.414	12.316	12.484	12.312	12.53	12.31	12.23	12.322	12.754				
3.204	3.294	3.104	3.188	2.93	3.208	3.162	2.116	3.011	2.335	2.701	3.163	3.331	3.213	3.543				
0.771	0.63	0.976	0.848	0.943	0.9	0.81	0.741	0.795	0.636	1.073	0.357	0.856	0.445	0.37				
0.13	0.137	0.13	0.135	0.121	0.143	0.132	0.093	0.119	0.096	0.133	0.093	0.114	0.087	0.103				
0.609	0.768	0.522	0.661	0.703	0.588	0.7	1.733	0.854	1.59	0.932	0.968	0.456	0.847	0.625				
1.458	1.373	1.53	1.43	1.546	1.499	1.549	1.615	1.509	1.645	1.494	1.818	1.652	1.737	1.7				
0.542	0.618	0.47	0.57	0.454	0.501	0.451	0.385	0.486	0.355	0.506	0.182	0.348	0.255	0.298				
0.35	0.341	0.361	0.364	0.36	0.359	0.388	0.328	0.353	0.342	0.391	0.348	0.411	0.341	0.351				
0.133	0.164	0.113	0.14	0.154	0.125	0.149	0.378	0.184	0.348	0.198	0.215	0.097	0.187	0.138				

5	2.99	2.92	2.89	3.1	3	2.94	2.8	2.94	2.8	2.94	3	3.14	3.01	3.06	3.08	3.03	2.94
	2.99	2.42	3.19	3.26	2.02	2.85	2.04	1.94	1.94	2.56	2.37	4.37	4.8	4.51	3.48	5.89	
	10.8	10.64	10.63	10.31	10.02	10.66	9.99	10.15	8.82	9.68	10.59	10.14	9.68	9.66	10.49		
	38.7	38.41	38.52	37.49	37.48	38.01	37.37	37.42	39.03	38.26	38.82	39.52	38.97	38.99	39.33		
	1.68	1.73	1.66	1.64	1.76	1.69	1.65	1.68	1.71	1.65	1.69	1.66	1.88	1.88	1.64		
	10.03	10.02	10.1	10.09	9.77	10.34	9.94	10.02	9.82	9.9	10.51	10.57	10.34	10.1	10.41		
	2.03	1.89	1.99	2.21	1.75	2.1	1.82	1.81	1.57	1.64	2.24	2.07	1.92	1.35	1.72		
	0.82	0.86	0.84	0.83	0.95	0.86	0.98	0.88	0.98	0.98	0.98	0.69	0.73	0.84	0.94		
	24.873	25.543	24.607	22.704	24.886	24.11	25.305	25.135	25.586	24.397	22.673	22.136	21.932	22.934	20.295		
	3.486	3.798	2.837	5.919	6.195	4.99	4.963	5.085	4.861	6.36	4.342	4.005	5.533	6.174	4.718		
	1.87	1.86	1.88	1.87	1.85	1.87	1.85	1.85	1.86	1.86	1.89	1.89	1.88	1.87	1.91		
	100.269	100.091	99.144	99.423	99.681	100.49	98.748	98.88	99.767	100.297	100.785	100.611	100.345	100.408	100.043		
	6.174	6.172	6.206	6.045	6.096	6.077	6.13	6.124	6.32	6.163	6.118	6.215	6.178	6.22	6.174		
	6.174	6.172	6.206	6.045	6.096	6.077	6.13	6.124	6.32	6.163	6.118	6.215	6.178	6.22	6.174		
	12.348	12.344	12.412	12.09	12.192	12.154	12.26	12.248	12.64	12.326	12.236	12.43	12.356	12.44	12.348		
	3.317	3.433	3.314	3.06	3.387	3.222	3.469	3.44	3.465	3.286	2.987	2.912	2.907	3.061	2.666		
	0.42	0.459	0.345	0.72	0.756	0.602	0.615	0.626	0.592	0.771	0.516	0.473	0.661	0.74	0.556		
	0.103	0.112	0.109	0.113	0.131	0.132	0.132	0.122	0.131	0.134	0.092	0.097	0.113	0.127	0.082		
	0.711	0.58	0.766	0.784	0.49	0.679	0.499	0.473	0.618	0.569	1.027	1.125	1.066	0.828	1.378		
	1.715	1.725	1.743	1.743	1.702	1.771	1.747	1.757	1.704	1.709	1.775	1.781	1.756	1.726	1.751		
	0.277	0.27	0.251	0.257	0.298	0.229	0.249	0.243	0.293	0.291	0.225	0.219	0.244	0.274	0.237		
	0.342	0.355	0.341	0.337	0.365	0.359	0.354	0.344	0.347	0.351	0.332	0.339	0.336	0.383	0.328		
	0.16	0.131	0.173	0.172	0.106	0.151	0.11	0.104	0.133	0.123	0.227	0.25	0.23	0.179	0.3		



	3	4	5	6	7	DN11-1	2	3	4	5	6	Low	High	Core	Rim	Core	Rim
3.2	3.35	2.84	3.01	2.83	2.95	2.95	2.95	3.03	2.96	2.87	2.96	2.96	2.9	2.89	2.83	3.04	3.15
3.04	3.9	4.04	3.75	5.04	2.59	3.32	3.13	2.53	3.89	5.31	4.27	6.3	1.82	6.13	2.42	2.42	2.42
9.55	9.77	10.46	9.34	10.11	9.88	9.75	9.67	10.22	10.32	9.99	10.11	9.73	9.93	9.93	9.93	10.18	10.18
38.82	39.22	38.62	38.79	38.25	37.42	37.71	38.05	37.24	38.01	38.26	37.88	38.71	36.68	38.73	37.5	37.5	37.5
1.74	1.59	1.66	1.68	1.67	1.65	1.75	1.72	1.65	1.74	1.67	1.74	1.62	1.83	1.69	1.82	1.82	1.82
10.32	10.21	10.45	10.16	10.43	10.05	9.9	10.11	10.1	10.39	10.39	10.39	10.5	10.5	10.76	10.15	10.61	10
2.12	2.24	2.31	1.78	2.01	2.37	2.48	2.32	2.23	2.37	2.26	2.26	2.5	2.5	2.44	2.63	2.63	2.2
0.93	0.73	0.85	0.8	0.68	0.88	0.8	0.85	0.85	0.79	0.65	0.64	0.36	0.84	0.62	0.62	0.82	0.82
23.604	22.896	23.379	23.206	21.343	24.422	23.785	23.744	24.182	22.81	20.511	21.993	19.812	24.321	19.388	23.549	23.549	23.549
5.642	5.028	4.513	4.695	4.687	4.566	4.628	5.252	5.388	4.334	5.278	5.042	4.288	6.589	4.57	6.625	6.625	6.625
1.87	1.88	1.88	1.88	1.89	1.86	1.87	1.87	1.87	1.88	1.9	1.88	1.91	1.85	1.91	1.91	1.86	1.86
100.836	100.814	101.002	99.091	98.94	98.638	98.943	99.746	99.21	99.404	99.179	99.455	98.82	98.75	99.248	100.124	100.124	100.124
6.183	6.198	6.1	6.256	6.126	6.115	6.12	6.132	6.055	6.101	6.102	6.069	6.15	6.035	6.127	6.044	6.044	6.044
6.183	6.198	6.1	6.256	6.126	6.115	6.12	6.132	6.055	6.101	6.102	6.069	6.15	6.035	6.127	6.044	6.044	6.044
12.366	12.396	12.2	12.512	12.252	12.23	12.24	12.264	12.11	12.202	12.204	12.138	12.3	12.07	12.254	12.088	12.088	12.088
3.145	3.025	3.088	3.132	2.859	3.337	3.227	3.199	3.287	3.063	2.737	2.948	2.632	3.345	2.566	3.173	3.173	3.173
0.675	0.599	0.537	0.568	0.564	0.563	0.567	0.638	0.66	0.522	0.632	0.607	0.513	0.818	0.543	0.804	0.804	0.804
0.125	0.098	0.102	0.109	0.092	0.122	0.11	0.116	0.117	0.107	0.088	0.087	0.048	0.117	0.083	0.112	0.112	0.112
0.722	0.919	0.951	0.902	1.203	0.631	0.803	0.752	0.613	0.931	1.262	1.02	1.492	0.446	1.446	0.581	0.581	0.581
1.761	1.729	1.769	1.756	1.79	1.76	1.772	1.746	1.76	1.787	1.775	1.802	1.832	1.789	1.798	1.727	1.727	1.727
0.239	0.271	0.219	0.244	0.21	0.24	0.278	0.254	0.24	0.213	0.225	0.198	0.168	0.211	0.202	0.273	0.273	0.273
0.354	0.321	0.335	0.346	0.341	0.344	0.362	0.354	0.342	0.356	0.34	0.356	0.328	0.384	0.341	0.374	0.374	0.374
0.158	0.202	0.207	0.195	0.26	0.139	1.74	0.163	1.34	0.206	0.361	0.222	0.322	0.096	0.317	0.127	0.127	0.127

## Representative analyses of mica from nepheline syenites, Center II, Coldwell Complex

Sample	CC1B - 1	2	3	4	5	6	CC2 - 1	2	3	4	5	6	7	CC3 - 1	2
Na2O	—	—	—	—	—	—	—	—	—	—	—	—	—	—	—
MgO	5.55	5.48	5.56	5.76	5.94	5.89	5.07	4.55	5.71	5.07	5	4.72	4.96	5.1	4.11
Al2O3	12.14	12.03	12.76	12.31	12.27	12.35	12.5	12.12	12.89	13.09	12.04	12.83	13.27	12.26	12.48
SiO2	34.35	33.94	33.88	33.93	34.49	33.9	33.87	33.53	33.03	33.08	33.16	32.15	34.02	34.78	33.57
K2O	9.45	9.71	9.65	9.68	9.66	9.7	7.9	9.58	6.58	8.6	7.97	8.05	7.31	9.39	9.22
CaO	—	—	—	—	—	—	0.58	—	0.66	—	—	0.62	—	—	—
TiO2	2.03	2.07	2.39	2.34	2.36	2.09	2.11	2.11	2	1.78	2.16	2.2	2.04	1.73	2.88
MnO	0.57	0.68	0.58	0.48	0.65	0.7	0.55	0.59	0.8	0.8	0.56	0.71	0.64	0.76	0.57
FeO	32.39	31.42	31.32	31.46	31.27	30.67	31.94	33.9	33.15	33.77	32.44	33.39	33.66	32.04	32.16
Total	96.47	95.33	96.15	95.96	96.64	95.3	94.52	96.37	94.83	96.18	93.33	94.66	95.91	96.05	94.98
Cation Assignment - Based on 22 Oxygens															
Si	5.595	5.596	5.5	5.546	5.583	5.568	5.59	5.53	5.44	5.43	5.57	5.37	5.53	5.67	5.56
Ti	0.249	0.257	0.292	0.288	0.287	0.258	0.26	0.26	0.25	0.22	0.27	0.28	0.25	0.21	0.36
Al	2.331	2.335	2.44	2.37	2.34	2.389	2.43	2.36	2.5	2.53	2.38	2.53	2.54	2.36	2.43
Fe	4.411	4.331	4.251	4.299	4.232	4.211	4.4	4.68	4.56	4.64	4.56	4.67	4.58	4.37	4.45
Mn	0.079	0.095	0.16	0.066	0.089	0.0974	0.08	0.08	0.11	0.11	0.08	0.1	0.09	0.11	0.08
Mg	1.347	1.346	1.346	1.403	1.433	1.442	1.25	1.12	1.4	1.24	1.25	1.18	1.2	1.24	1.01
Ca	—	—	—	—	—	—	0.1	—	0.12	—	—	0.11	—	—	—
Na	—	—	—	—	—	—	—	—	—	—	—	—	—	—	—
K	1.963	2.042	1.997	2.019	1.994	2.03	1.66	2.02	1.38	1.8	1.71	1.72	1.52	1.95	1.95
Total	10.38	10.406	10.486	10.445	10.375	10.4274	15.77	16.04	15.76	15.98	15.82	15.95	15.71	15.91	15.84
Mg#	0.234	0.237	0.24	0.246	0.253	0.255	0.221	0.193	0.235	0.211	0.215	0.202	0.208	0.221	0.185

		CC5-1						CC6-1						
3	4	1	2	3	4	5	6	7	1	2	3	4	5	6
3.92	3.81	9.09	8.74	7.54	7.71	6.56	7.6	8.5	6	6.06	4.91	5.26	4.64	4.11
12.59	12.95	10.8	10.79	10.93	10.82	13.48	10.84	10.66	12.25	12.15	13.93	13.53	12.26	13.24
33.8	32.4	37.84	37.68	36.12	35.57	35.04	36.72	37.2	35	35.74	34.62	32.58	33.92	34.01
9.18	8.39	9.65	9.7	9.77	9.41	9.71	9.85	9.48	8.69	8.94	8.4	7.05	8.85	9.46
—	—	—	—	—	—	—	—	—	—	—	—	—	—	—
2.91	2.34	2.54	2.56	2.21	2.37	2.22	2.41	2.48	3.11	3	1.65	1.35	2.05	2.11
0.63	0.72	1.68	1.8	2.4	2.33	1.76	2.05	2.23	0.58	0.72	0.77	0.51	0.65	0.65
32.57	33.24	24.95	24.63	26.92	26.8	25.83	27.08	25.48	29.69	29.84	31.3	33.91	31.69	32.52
95.61	93.84	96.56	95.9	95.88	95.02	94.59	96.55	96.02	95.32	96.46	95.59	94.19	94.05	96.1

5.56	5.46	5.922	5.938	5.805	5.767	5.566	5.867	5.885	5.657	5.707	5.607	5.431	5.644	5.462
0.36	0.3	0.299	0.303	0.268	0.289	0.27	0.29	0.296	0.378	0.361	0.201	0.09	0.257	0.255
2.44	2.57	1.991	2.003	2.069	2.067	2.561	1.978	1.997	2.332	2.287	2.658	2.657	2.404	2.504
4.48	4.68	3.265	3.245	3.617	3.634	3.487	3.62	3.376	4.011	3.984	4.238	4.726	4.411	4.77
0.09	0.1	0.223	0.24	0.326	0.32	0.241	0.278	0.299	0.079	0.097	0.106	0.191	0.092	0.088
0.96	0.96	2.121	2.054	1.805	1.861	1.581	1.815	2.007	1.446	1.443	1.187	1.307	1.151	0.983
—	—	—	—	—	—	—	—	—	—	—	—	—	—	—
1.93	1.8	1.925	1.95	2.008	1.946	1.998	2.016	1.92	1.792	1.82	1.734	1.498	1.878	1.937
15.82	15.86	9.824	9.795	10.093	10.117	10.138	9.997	9.895	10.038	9.992	10.124	10.469	10.193	10.537
0.176	0.17	0.394	0.388	0.333	0.339	0.312	0.334	0.373	0.265	0.266	0.219	0.217	0.207	0.171

7	8	CC7-1	2	3	4	5	6	CC8-1	2	3	CC9-1	2	3	CC10-1
4.39	3.81	4.48	5.1	4.59	5.25	6.51	5.16	3.92	4.03	4.26	5.33	4.93	4.78	5.03
12.36	13.42	13.13	12.63	12.62	12.53	12.59	12.61	13.69	17.6	12.76	12.67	11.72	12.77	14.17
33.97	33.51	33.1	33.83	34.09	33.66	34.76	34.42	32.41	30.52	33.19	31.93	33.28	33.19	32.57
9.44	9.59	8.04	8.28	9.52	8.8	9.5	9.47	7.85	6.67	8.08	6.36	7.89	8.44	8.44
—	—	—	—	—	—	—	—	—	—	—	—	—	—	—
2.28	2.17	1.66	2	2.16	1.9	1.29	2.4	2.39	0.62	2.8	1.88	1.24	2.21	2.27
0.74	0.61	0.62	0.66	0.59	0.68	0.74	0.7	0.84	0.94	0.73	0.79	0.79	0.73	0.68
31.91	30.8	33.87	32.31	32.5	31.83	30.38	31.3	33.91	33.03	34.55	34.86	34.66	34.3	30.98
95.1	93.91	94.9	94.82	96.07	94.64	95.77	96.07	95	93.4	96.37	93.83	94.52	96.43	94.15

---

5.662	5.583	5.494	5.576	5.583	5.57	5.644	5.6	5.38	5.1	5.44	5.36	5.58	5.44	5.39
0.283	0.272	0.208	0.248	0.266	0.236	0.158	0.293	0.3	0.08	0.34	0.24	0.16	0.27	0.28
2.407	2.634	2.568	2.454	2.436	2.443	2.409	2.418	2.68	3.46	2.47	2.51	2.32	2.47	2.76
4.441	4.29	4.7	4.454	4.45	4.404	4.124	4.257	4.71	4.61	4.74	4.9	4.86	4.71	4.29
0.103	0.086	0.087	0.092	0.082	0.095	0.101	0.097	0.12	0.13	0.1	0.11	0.11	0.1	0.1
1.082	0.946	1.109	1.254	1.121	1.295	1.575	1.251	0.97	1	1.04	1.34	1.23	1.17	1.24
—	—	—	—	—	—	—	—	—	—	—	—	—	—	—
1.99	2.038	1.701	1.741	1.99	1.857	1.966	1.964	1.66	1.42	1.69	1.36	1.69	1.77	1.78
10.306	10.266	10.373	10.243	10.345	10.33	10.333	10.28	15.81	15.81	15.82	15.82	15.95	15.93	15.84
0.196	0.181	0.191	0.22	0.201	0.227	0.276	0.227	0.171	0.178	0.18	0.215	0.202	0.199	0.224

2	CC11-1				2	3	4	CC12-1				2	3	4	CC13-1				2	3	CC14-1				CC15-1																																																																																																																													
	2	3	4	5				2	3	4	5				2	3	4	5			2	3	4	5	2	3	4	5	2	3	4	5																																																																																																																						
5.23	3.72	4.6	3.15	3.56	3.85	4.52	4.62	4.53	5.89	4.68	5.31	5.11	4.58	2.17	13.15	11.53	11.08	12.35	11.47	12.52	12.33	12.41	12.33	12.52	12.21	12.02	14.19	11.86	14.44	33.6	34.09	33.56	33.05	33	34.17	34.07	34.85	33.72	34.3	34.16	34.8	32.14	34.56	32.53	9.24	8.99	8.19	9.08	9.09	9.23	9.1	9.3	8.95	8.19	8.84	9.12	7.69	7.69	9.11	—	—	—	—	—	—	—	—	—	—	—	—	—	—	—	—	—	2.17	3.09	2.14	3.71	3.31	4.2	3.67	2.97	2.87	2.57	3.58	2.69	1.33	2.31	2.34	0.69	0.67	0.67	0.69	0.71	0.72	0.53	0.65	0.55	0.73	0.72	0.68	0.62	0.73	0.66	32.01	32.54	34.47	34.28	33.59	32.07	31.98	31.55	31.76	31.7	31.95	31.3	32.3	32.41	33.75	96.1	94.63	94.05	96.31	94.73	96.75	96.2	96.36	94.71	95.9	96.13	95.92	93.39	94.13	95.01														
5.48	5.67	5.64	5.46	5.54	5.53	5.54	5.64	5.58	5.56	5.56	5.66	5.38	5.72	5.42	0.27	0.39	0.27	0.46	0.42	0.51	0.45	0.36	0.36	0.31	0.44	0.33	0.17	0.29	0.29	2.53	2.26	2.2	2.4	2.27	2.39	2.37	2.37	2.4	2.39	2.34	2.3	2.8	2.31	2.84	4.37	4.53	4.85	4.73	4.71	4.34	4.35	4.27	4.39	4.3	4.35	4.25	4.52	4.48	4.71	0.1	0.09	0.1	0.1	0.1	0.1	0.07	0.09	0.08	0.1	0.1	0.09	0.09	0.1	0.09	1.27	0.92	1.15	0.77	0.89	0.93	1.1	1.12	1.12	1.42	1.13	1.29	1.28	1.13	0.54	—	—	—	—	—	—	—	—	—	—	—	—	—	—	—	—	1.92	1.91	1.76	1.91	1.95	1.91	1.89	1.92	1.89	1.69	1.84	1.89	1.64	1.62	1.94	15.95	15.77	15.87	15.84	15.88	15.71	15.77	15.77	15.81	15.78	15.75	15.81	15.87	15.65	15.83	0.225	0.169	0.192	0.14	0.159	0.176	0.202	0.208	0.203	0.248	0.206	0.233	0.221	0.201	0.103

3	CC16-1			CC17A-1			CC17B-1			DN1-1			DN2-1			DN3-1																																																																																																																																					
	1	2	3	1	2	3	1	2	3	1	2	3	1	2	3	1	2																																																																																																																																				
4.83	3.56	3.69	3.46	3.52	2.44	3.32	3.81	2.74	3.09	3.05	3.66	4.47	3.35	3.88	12.92	12.19	11.93	12.19	13.06	12.72	11.29	11.87	14.52	11.06	11.27	10.25	12.62	11.2	11.69	33.3	33.35	33.82	32.03	30.55	33.89	33.85	33.57	33.91	33.59	33.84	34.03	32.14	34.16	34.43	8.74	9.07	9	7.51	5.5	8.74	8.64	9.1	9.41	8.96	8.95	8.7	5.28	8.82	9.09	—	—	—	—	—	—	—	—	—	—	—	—	—	—	—	—	2.75	3.67	3.57	2.72	2.43	2.99	2.47	2.46	1.63	3.02	3.01	3.02	2.26	2.56	3.23	0.48	0.75	0.72	0.98	1.12	0.73	0.82	0.82	0.77	0.92	1.01	0.89	0.89	0.92	0.68	30.21	33.75	33.61	35.77	37.34	32.6	34.21	33.76	33.38	35.04	34.86	33.98	35.98	33.14	32.92	93.24	96.33	96.36	94.66	93.52	94.11	94.6	95.39	96.36	95.66	95.98	94.53	93.64	94.16	95.92														
5.55	5.49	5.55	5.4	5.22	5.62	5.68	5.58	5.54	5.62	5.62	5.72	5.4	5.73	5.65	0.34	0.45	0.44	0.34	0.31	0.37	0.31	0.31	0.2	0.38	0.38	0.38	0.32	0.4	2.54	2.36	2.31	2.42	2.63	2.49	2.23	2.33	2.8	2.17	2.21	2.03	2.5	2.22	2.26	4.21	4.64	4.61	5.05	5.33	4.52	4.8	4.7	4.56	4.9	4.84	4.78	5.06	4.65	4.52	0.07	0.1	0.1	0.14	0.16	0.1	0.12	0.12	0.11	0.13	0.14	0.13	0.13	0.13	0.09	1.2	0.87	0.9	0.87	0.9	0.6	0.83	0.95	0.67	0.77	0.76	0.92	1.12	0.84	0.95	—	—	—	—	—	—	—	—	—	—	—	—	—	—	—	—	1.86	1.9	1.88	1.62	1.2	1.85	1.85	1.93	1.96	1.91	1.9	1.87	1.13	1.89	1.9	15.77	15.83	15.8	15.85	15.75	15.56	15.82	15.91	15.84	10.26	10.23	15.83	15.63	15.78	15.77	0.222	0.158	0.163	0.147	0.144	0.117	0.147	0.168	0.128	0.136	0.136	0.161	0.181	0.153	0.174

	2	3	4	DN4-1	2	3	4	5	6	DN5-1	2	3	4	DN6-1	2
3,67	—	3,79	3,29	0,31	6,05	4,23	5,79	0,38	4,14	0,3	5,84	—	3,91	0,42	—
12,3	12,65	13,66	11,06	11,72	11,21	11,78	11,37	12,13	11,03	11,99	11,54	14,02	14,76	15,32	2,94
34,23	34,28	34,61	35,34	35,86	34,69	35,93	33,34	34,39	34,28	35,08	35,73	34,31	33,82	33,3	33,3
8,8	9,12	9,23	8,49	9,46	9,02	9,38	8,33	9,2	8,86	9,07	9,52	9,07	8,96	8,67	8,67
—	—	—	—	—	—	—	—	—	—	—	—	—	—	—	—
2,9	2,91	1,8	2,89	3	2,71	2,88	3,42	2,51	3,46	2,33	2,76	1,76	1,77	1,41	1,41
0,73	0,73	0,86	0,74	0,75	0,85	0,89	0,84	0,86	0,82	0,76	0,69	0,79	0,8	0,85	0,85
32,67	31,48	33,22	28,4	29,36	32,33	30,25	31,58	33,04	32,62	30,19	29,74	30,51	32,39	31,99	31,99
95,3	94,95	96,65	93,25	96,2	95,04	96,9	93,19	96,27	94,6	95,27	96,19	94,37	95,9	94,48	94,48

---

	2	3	4	5,82	5,75	5,73	5,74	5,62	5,63	5,69	5,71	5,75	5,64	5,52	5,5
5,64	5,64	5,63	0,36	0,36	0,34	0,35	0,43	0,31	0,43	0,29	0,33	0,33	0,22	0,22	0,18
0,36	0,36	0,22	2,15	2,22	2,19	2,22	2,26	2,34	2,16	2,3	2,19	2,19	2,72	2,84	2,98
2,39	2,45	2,62	3,91	3,94	4,47	4,04	4,45	4,52	4,53	4,11	4	4,19	4,42	4,42	4,42
4,5	4,33	4,52	0,1	0,1	0,12	0,12	0,12	0,12	0,12	0,1	0,09	0,11	0,11	0,11	0,12
0,1	0,1	0,12	1,48	1,45	1,04	1,38	0,99	1,01	0,87	1,42	1,49	0,96	0,73	0,72	0,72
0,9	0,93	0,8	—	—	—	—	—	—	—	—	—	—	—	—	—
—	—	—	0,1	—	—	—	0,11	—	0,1	—	—	—	—	—	—
—	—	—	1,91	1,93	1,9	1,91	1,79	1,92	1,87	1,88	1,95	1,9	1,87	1,83	1,83
1,85	1,91	1,91	1,78	10	10,06	10,02	15,77	10,22	15,68	15,8	15,8	15,8	15,74	15,84	15,75
15,73	15,73	15,8	15,7	10	10,06	10,02	15,77	10,22	15,68	15,8	15,8	15,8	15,74	15,84	15,75
0,167	0,177	0,15	0,275	0,269	0,189	0,255	0,182	0,183	0,161	0,257	0,271	0,186	0,142	0,14	0,14

3	4	DN7-1	2	3	4	DN8-1	2	3	4	DN9-1	2	3	DN10-1	2	3	4
3.95	3.22	3.62	0.51	5.07	4.6	0.48	4.72	5.22	5.39	5.21	5.65	4.71	5.31	4.95	4.71	5.29
11.69	12.03	12.02	12.16	12.36	13.72	11.79	12.99	13.38	13.19	12.2	12.49	13.64	11.8	11.55	12.29	12.21
33.87	33.94	35.05	33.29	33.27	30.6	34.77	32.51	32.7	36.71	34.54	34.91	34.79	34.83	34.36	33.16	34.14
9.02	8.65	8.16	5.06	6.22	5.05	8.11	9.3	7.88	8.65	9.17	9.2	9.13	9.22	9.22	8.28	9.09
—	—	—	0.65	0.65	—	—	—	—	—	—	—	—	—	—	—	—
2.94	2.9	3.24	2.95	3.83	2.69	3	1.71	2.23	1.48	2.69	2.66	2.54	2.36	2.57	2.04	3.04
0.68	0.76	0.79	0.66	0.74	0.78	0.58	0.57	0.67	0.68	0.77	0.68	0.68	0.82	0.7	0.77	0.81
32.54	34.87	33.4	32.83	33.83	35.15	30.46	31.18	32.41	29.25	30.95	30.85	30.96	31.84	32.39	32.23	30.83
94.69	96.38	96.29	94.2	95.97	92.57	94.51	92.98	94.48	95.97	95.53	96.42	96.46	96.19	95.74	93.47	95.41
5.63	5.59	5.69	5.46	5.41	5.19	5.69	5.5	5.41	5.85	5.64	5.62	5.59	5.67	5.64	5.57	5.58
0.37	0.36	0.4	0.36	0.47	0.34	0.37	0.22	0.28	0.18	0.33	0.32	0.31	0.29	0.32	0.26	0.37
2.29	2.33	2.3	2.35	2.37	2.74	2.27	2.59	2.61	2.47	2.35	2.37	2.58	2.26	2.24	2.43	2.35
4.53	4.8	4.54	4.51	4.6	4.99	4.17	4.41	4.49	3.89	4.22	4.16	4.16	4.33	4.45	4.53	4.21
0.1	0.11	0.11	0.09	0.1	0.11	0.08	0.08	0.09	0.09	0.11	0.09	0.09	0.11	0.1	0.11	0.11
0.98	0.79	0.88	1.49	1.23	1.16	1.3	1.19	1.29	1.28	1.27	1.36	1.13	1.29	1.21	1.18	1.29
—	—	—	0.11	0.11	—	—	—	—	—	—	—	—	—	—	—	—
—	—	—	0.16	—	—	0.15	—	—	0.19	—	—	—	—	—	—	—
1.91	1.82	1.69	1.06	1.29	1.09	1.69	2.01	1.66	1.76	1.91	1.89	1.87	1.91	1.93	1.77	1.89
15.81	15.79	15.61	15.61	15.58	15.64	15.72	15.99	15.84	15.71	15.82	15.81	15.74	15.87	15.89	15.84	15.82
0.178	0.141	0.162	0.248	0.211	0.189	0.238	0.213	0.223	0.248	0.231	0.246	0.214	0.23	0.214	0.207	0.235

## Representative analyses of plagioclase from nepheline syenites, Center II, Coldwell Complex

Rock Type	Layered							Layered						
Sample	CC1A-1	2	3	4	5	6	7	CC1B-1	2	3	4	5	6	7
Na2O	11.49	11.12	11.62	11.48	11.43	11.89	11.37	11.36	11.32	11.5	11.48	11.59	11.51	11.54
Al2O3	19.13	19.68	19.66	19.71	19.78	20.63	19.6	20.01	19.83	19.65	19.79	20.01	19.85	20.01
SiO2	67.39	67.74	67.32	67.53	67.48	67.13	67.19	67.06	67.18	67.33	67.19	67.58	68.11	68.28
K2O	—	0.17	0.23	0.47	0.23	—	—	0.23	0.39	0.67	0.2	0.28	—	—
CaO	—	0.23	0.23	0.24	0.53	—	0.22	0.31	0.3	0.25	0.47	0.25	0.27	—
Total	98.02	98.93	99.06	99.43	99.45	99.65	98.38	98.97	99.01	99.4	99.14	99.72	99.75	99.83
Cation Assignment - Based on 8 Oxygens														
Si	3	2.99	2.97	2.97	2.97	2.95	2.98	2.96	2.97	2.97	2.97	2.97	2.98	2.98
Al	1	1.02	1.02	1.02	1.03	1.02	1.02	1.04	1.03	1.02	1.03	1.04	1.02	1.03
Ca	—	0.01	0.01	0.01	0.03	—	0.01	0.01	0.01	0.01	0.02	0.01	0.01	—
Na	0.99	0.95	1	0.98	0.98	1.01	0.98	0.97	0.97	0.98	0.98	0.99	0.98	0.98
K	—	0.01	0.01	0.03	0.01	—	—	0.01	0.02	0.04	0.01	0.02	—	—
Total	4.99	4.98	5.02	5.02	5.01	4.98	5	5.01	5.01	5.03	5.01	5.02	5	4.99
An%	0	1.03	0.98	0.98	2.94	0	1.01	1.01	1	0.97	1.98	0.98	1.01	0

Layered			Massive						Pegmatite					
CC2 - 1	2	3	4	5	6	CC3 - 1	2	3	4	5	6	CC4 - 1	2	3
11.22	11.41	11.57	11.22	10.84	11.27	11.75	11.67	11.41	11.63	11.79	11.7	11.49	11.36	11.47
19.65	19.74	19.85	19.8	19.74	19.5	19.93	19.95	19.72	19.98	19.92	19.74	19.35	19.6	19.32
67.67	68.19	68.58	67.78	67.96	67.66	67.99	67.64	67.62	68.05	68.27	68.39	68.57	69.11	67.82
0.18	0.37	—	0.19	0.16	0.19	0.25	0.18	0.28	0.26	0.15	0.24	0.25	0.24	0.2
0.27	0.17	—	0.34	0.25	0.26	—	—	0.19	—	—	—	—	—	—
98.99	99.89	100	99.32	98.94	98.88	99.91	99.44	99.22	99.92	100.13	100.07	99.66	100.31	98.81
2.98	2.98	2.99	2.98	2.99	2.99	2.98	2.97	2.98	2.98	2.98	2.99	3	3	3
1.02	1.02	1.02	1.03	1.02	1.02	1.03	1.03	1.02	1.03	1.02	1.02	1	1	1.01
0.01	0.01	—	0.02	0.01	0.01	—	—	0.01	—	—	—	—	—	—
0.96	0.97	0.98	0.96	0.93	0.96	1	0.99	0.97	0.99	1	0.99	0.98	0.96	0.98
0.01	0.02	—	0.01	0.01	0.01	0.01	0.01	0.02	0.01	0.01	0.01	0.01	0.01	0.01
4.99	5	4.99	4.99	4.96	4.99	5.02	5.01	5	5	5.01	5.01	4.99	4.98	5
1.01	1	0	2.02	1.05	1.02	0	0	1	0	0	0	0	0	0

Massive						Layered						Hybrid			
	4	5	CC6-1	2	3	4	5	6	CC7-1	2	3	4	5	6	CC8-1
11.3	11.65	11.54	11.35	11.48	11.59	11.75	11.68	11.12	11.21	11.31	11.51	11.27	11.86	11.47	
19.18	19.11	19.76	19.9	19.5	19.63	19.75	19.78	20.03	19.88	20.17	19.82	19.74	19.61	19.76	
67.8	68.26	67.84	67.84	68.38	68.58	68.47	68.29	68.18	67.76	68	67.53	68.59	69.16	67.05	
0.17	0.25	—	0.24	0.23	—	—	—	—	0.38	0.19	0.18	—	100.63	0.16	
—	—	—	0.32	0.17	—	0.23	0.3	0.35	0.27	0.4	0.24	—	—	0.38	
98.45	99.27	99.15	99.64	99.77	99.8	100.21	100.06	99.67	99.5	100.07	99.28	99.61	—	98.81	

3	3	2.99	2.98	2.99	3	2.99	2.98	2.98	2.98	2.97	2.97	3	3	2.97
1	0.99	1.02	1.03	1.01	1.01	1.02	1.02	1.03	1.03	1.04	1.03	1.02	1	1.03
—	—	—	0.01	0.01	—	0.01	0.01	0.02	0.01	0.02	0.01	—	—	0.02
0.97	0.99	0.98	0.97	0.97	0.98	0.99	0.99	0.94	0.96	0.96	0.98	0.96	1	0.98
0.01	0.01	—	0.01	0.01	—	—	—	—	0.02	0.01	0.01	—	—	0.01
4.99	5	4.99	5	5	4.99	5	5	4.97	5	5	5.01	4.97	5	5.01
0	0	0	1.01	1.01	0	1	1	2.08	1.01	2.02	1	0	0	2.02

					Hybrid					Layered					Hybrid						
					CG9-1					CC10-1					CC11-1						
2	3	4	5		2	3	4	5		2	3	4	5		2	3	4	5			
11.24	11.5	11.39	11.48	11.72	11.63	11.38	10.83	11.06	11.23	10.96	10.89	10.92	10.92	11.13							
19.88	19.87	19.69	19.97	19.42	19.71	19.36	19.36	19.59	19.93	19.76	19.53	19.39	19.43	19							
67.3	68.03	67.5	68.23	68.32	67.74	67.65	68.09	67.64	66.84	66.76	66.96	66.92	67.55	67.33							
0.18	0.17	0.14	0.19	0.16	0.12	0.19	0.21	0.22	0.2	0.15	0.14	0.15	0.37	0.25							
0.55	0.26	0.3	0.36	—	0.23	0.18	0.25	0.29	0.48	0.54	0.47	0.25	0.2	—							
99.15	99.82	99.03	100.23	99.62	99.43	98.76	98.73	98.79	98.69	98.18	97.98	97.63	98.46	97.71							
<hr/>																					
2.97	2.98	2.98	2.98	3	2.98	2.99	3	2.99	2.96	2.97	2.98	2.99	2.99	3.01							
1.03	1.03	1.02	1.03	1	1.02	1.01	1.01	1.02	1.04	1.04	1.03	1.02	1.01	1							
0.03	0.01	0.01	0.02	—	0.01	0.01	0.01	0.01	0.02	0.03	0.02	0.01	0.01	—							
0.96	0.98	0.97	0.97	1	0.99	0.98	0.93	0.95	0.97	0.95	0.94	0.95	0.94	0.96							
0.01	0.01	0.01	0.01	0.01	0.01	0.01	0.01	0.01	0.01	0.01	0.01	0.01	0.01	0.01							
5	5	5	5	5	5.01	5	4.96	4.98	5	4.99	4.98	4.98	4.98	4.98							
3	1	1.01	2	0	0.99	1	1.05	1.03	2	3.03	2.06	1.03	1.03	0							

					Massive					Massive				
2	3	4	5	6	CCI2 - 1	2	3	4	5	CCI3 - 1	2	3	4	5
11.23	11.39	11.82	10.99	11.27	11.43	11.19	11.29	11.51	10.62	11.4	11.43	11.41	11.45	10.88
19.23	19.13	19.64	19.32	19.65	19.86	19.31	19.62	19.31	19.41	19.67	19.93	19.68	19.59	19.82
67.43	67.63	70.04	67.49	67.76	68.76	68.25	68.16	68.6	68.12	67.81	67.8	68.09	67.98	67.34
0.17	0.13	—	0.17	—	0.23	—	0.26	0.15	0.19	0.18	0.95	0.15	—	0.16
0.14	—	—	—	—	0.31	—	0.3	—	0.38	0.29	—	—	0.15	0.24
98.19	98.27	101.51	97.97	98.68	100.59	98.74	99.62	99.56	98.72	99.35	100.11	99.34	99.17	98.44
<hr/>														
3	3	3.01	3	3	2.99	3.01	2.99	3.01	3	2.98	2.97	2.99	2.99	3.01
1.01	1	0.99	1.01	1.01	1.02	1	1.01	1	1.01	1.02	1.03	1.02	1.02	1.01
0.01	—	—	—	—	0.01	—	0.01	—	0.02	0.01	—	—	0.01	0.01
0.97	0.98	0.98	0.95	0.95	0.96	0.96	0.96	0.98	0.91	0.97	0.97	0.97	0.98	0.93
0.01	0.01	—	0.01	0.01	0.01	—	0.01	0.01	0.01	0.01	0.05	0.01	—	0.01
4.99	4.99	4.99	4.97	4.97	4.99	4.97	4.99	4.99	4.95	5	5.03	4.99	4.99	4.96
1.01	0	0	0	0	1.02	0	1.02	0	2.13	1.01	0	0	1.01	1.05

Layered	Mottled - Mafic syenite										Normal syenite																			
	2	3	4	5	CC15 - 1	2	3	4	5	6	7	8	9	10	2	3	4	5	6	7	8	9	10							
CC14 - 1	11.26	11.08	11.45	10.95	11.68	11.5	11.43	11.58	11.45	11.71	11.15	10.94	11.08	11.44	11.13	11.26	11.08	11.45	10.95	11.68	11.5	11.43	11.58	11.45	11.71	11.15	10.94	11.08	11.44	11.13
	19.09	19.28	19.4	19.39	20.03	19.76	19.95	19.8	19.44	20.14	19.88	19.79	19.65	19.57	19.77	19.09	19.28	19.4	19.39	20.03	19.76	19.95	19.8	19.44	20.14	19.88	19.79	19.65	19.57	19.77
	67.42	67.17	67.49	66.83	68.37	67.9	67.54	68.11	67.6	68.3	67.51	67.43	66.95	67.65	67.83	67.42	67.17	67.49	66.83	68.37	67.9	67.54	68.11	67.6	68.3	67.51	67.43	66.95	67.65	67.83
	—	1.14	0.13	0.64	0.18	0.28	0.17	0.19	0.12	0.18	0.24	0.22	0.18	—	0.13	—	1.14	0.13	0.64	0.18	0.28	0.17	0.19	0.12	0.18	0.24	0.22	0.18	—	0.13
	—	0.22	—	0.44	0.32	0.21	0.38	0.27	0.27	0.32	0.38	0.42	0.44	—	0.21	—	0.22	—	0.44	0.32	0.21	0.38	0.27	0.27	0.32	0.38	0.42	0.44	—	0.21
	97.77	98.89	98.48	98.26	100.57	99.66	99.46	99.95	98.88	100.66	99.16	98.81	98.29	98.67	99.07	97.77	98.89	98.48	98.26	100.57	99.66	99.46	99.95	98.88	100.66	99.16	98.81	98.29	98.67	99.07
	3	2.98	2.99	2.98	2.97	2.98	2.97	2.98	2.99	2.97	2.98	2.98	2.98	2.99	2.99	3	2.98	2.99	2.98	2.97	2.98	2.97	2.98	2.99	2.97	2.98	2.98	2.98	2.99	2.99
	1	1.01	1.01	1.02	1.03	1.02	1.03	1.02	1.01	1.03	1.03	1.03	1.03	1.02	1.03	1	1.01	1.01	1.02	1.03	1.02	1.03	1.02	1.01	1.03	1.03	1.03	1.02	1.03	1.03
	—	0.01	0.01	0.02	0.01	0.01	0.02	0.01	0.01	0.02	0.02	0.02	0.02	—	0.01	—	0.01	0.01	0.02	0.01	0.01	0.02	0.01	0.01	0.02	0.02	0.02	—	0.01	0.01
	0.97	0.95	0.98	0.95	0.98	0.98	0.97	0.98	0.98	0.99	0.95	0.94	0.95	0.98	0.95	0.97	0.95	0.98	0.95	0.98	0.98	0.97	0.98	0.98	0.99	0.95	0.94	0.95	0.98	0.95
	—	0.06	—	0.04	0.01	0.02	0.01	0.01	0.01	0.01	0.01	0.01	0.01	—	0.01	—	0.06	—	0.04	0.01	0.02	0.01	0.01	0.01	0.01	0.01	0.01	—	0.01	0.01
	4.98	5.02	5	5	5.01	5.01	5.01	5.01	5	5.01	4.99	4.98	4.99	4.99	4.98	4.98	5.02	5	5	5.01	5.01	5.01	5.01	5	5.01	4.99	4.98	4.99	4.99	4.98
	0	0.98	1.01	1.98	1	0.99	2	1	1	1.96	2.04	2.06	2.04	0	1.03	0	0.98	1.01	1.98	1	0.99	2	1	1	1.96	2.04	2.06	2.04	0	1.03

Mottled - Mafic syenite			Pegmatite						Mottled - Mafic syenite						Pegmatite					
CC16A-1			CC17A-1						CC17A-1						Pegmatite					
2	3	4	5	6	7	8	9	2	3	4	5	6	2	3	4	5	6			
11.14	11.37	11.23	11.17	10.97	11.43	11.36	11.36	11.37	11.44	11.21	11.48	11.59	11.61	10.84						
19.46	19.35	19.41	19.39	19.49	19.69	19.69	19.52	19.86	19.8	19.43	19.36	19.39	19.31	19.03						
67.26	68.67	67.92	67.93	67.51	69.39	69.2	67.77	67.97	68.28	67.04	67.66	67.61	67.38	67.49						
—	—	0.23	0.12	0.17	0.15	0.12	0.17	0.15	0.17	0.14	0.14	0.14	0.19	0.22						
0.22	—	0.23	0.23	0.5	—	—	0.17	0.2	—	0.2	—	0.21	—	—						
98.08	99.38	99.02	98.85	98.64	100.68	100.36	98.99	99.55	99.69	98.02	98.65	98.94	98.49	97.57						
<hr/>																				
2.99	3.01	3	3	2.99	3	3	2.99	2.98	2.99	2.99	2.99	2.99	2.99	3.01						
1.02	1	1.01	1.01	1.02	1	1.01	1.02	1.03	1.02	1.02	1.01	1.01	1.01	1						
0.01	—	0.01	0.01	0.02	—	—	0.01	0.01	—	0.01	—	0.01	—	—						
0.96	0.97	0.96	0.96	0.94	0.96	0.96	0.97	0.97	0.97	0.97	0.99	0.99	0.99	0.94						
—	—	0.01	0.01	0.01	0.01	0.01	0.01	0.01	0.01	0.01	0.01	0.01	0.01	0.01						
4.98	4.97	4.99	4.98	4.98	4.98	4.97	4.99	4.99	4.99	4.99	5	5.01	5.01	4.96						
1.03	0	1.02	1.02	2.06	0	0	1.01	1.01	0	1.01	0	0.99	0	0						

Mottled - Mafic syenite										Pegmatite										Layered										
7	8	9	CG17B - 1		2	3	4	5	6	7	8	9	10	DN1 - 1	2															
11.32	11.56	11.09	11.41	11.17	11.31	11.3	11.4	11.15	11.23	11.34	11.1	11.34	11.37	11.41	19.33	19.75	18.88	19.15	19.35	19.49	19.38	19.57	19.03	19.33	19.29	19.21	19.24	19.66	19.5	
67.71	68.53	67.28	68.03	67.84	68.11	67.63	67.86	67.65	68.04	67.75	67.6	67.44	68.35	69.18	0.14	—	—	0.15	0.14	0.2	0.13	0.2	0.22	0.29	0.13	0.16	0.18	0.15	0.19	0.18
—	—	0.2	—	0.16	—	0.18	0.18	—	0.19	0.33	0.32	0.15	—	0.18	98.5	99.85	97.45	98.74	98.66	99.11	98.62	99.21	98.04	99.08	98.84	98.38	98.35	99.53	100.46	
3	2.99	3.01	3.01	3	3	2.99	2.99	3.01	3	2.99	3	2.99	3	2.99	3	2.99	2.99	2.99	1.02	1.02	3									
1	1.02	1	1	1.01	1.01	1.01	1.02	1	1	1	1	1	1	1.01	1	1.01	1.01	1.02	—	—	0.01									
—	—	0.01	—	0.01	—	0.01	0.01	—	0.01	0.02	0.01	0.01	0.01	0.01	0.01	0.01	0.01	0.01	0.01	0.01	0.01									
0.97	0.98	0.96	0.98	0.96	0.97	0.97	0.97	0.96	0.96	0.97	0.95	0.98	0.97	0.96	0.97	0.97	0.97	0.97	0.96	0.96	0.96									
0.01	—	—	0.01	0.01	0.01	0.01	0.01	0.01	0.02	0.01	0.01	0.01	0.01	0.01	0.01	0.01	0.01	0.01	0.01	0.01	0.01									
4.99	4.99	4.97	4.99	4.98	4.99	4.99	5	4.98	4.99	4.99	4.98	4.99	4.98	4.98	4.99	4.99	4.98	4.98	4.98	4.98	—									
0	0	1.03	0	1.02	0	1.01	1.01	0	1.01	2	1.03	1	0	1.02	0	0	1.03	0	1.02	0	1.03	1	0	1.02						

Layered					Hybrid					Hybrid				
3	4	5	DN2 - 1	2	3	4	5	DN3 - 1	2	3	4	5	DN4 - 1	2
11.25	11.54	11.72	11.54	11.25	10.94	11.43	11.57	10.88	11.1	11.3	12.18	11.42	11.35	11.53
19.89	19.64	19.82	19.55	19.79	19.66	19.78	19.83	19.81	19.73	19.73	21.08	20	19.65	19.64
68.34	68.98	69.5	68.9	68.11	67.52	68.55	68.64	68.39	68.41	68.46	66.75	69.16	68.79	68.81
0.22	0.26	—	—	0.24	0.16	0.22	0.17	1.1	0.48	0.15	—	0.44	0.15	—
0.36	0.15	—	—	0.2	0.45	0.19	0.2	—	0.33	0.21	0.36	—	—	—
100.06	100.56	101.03	99.99	99.6	98.73	100.17	100.41	100.18	100.04	99.85	100.37	101.01	99.95	99.97
2.98	3	3	3	2.99	2.98	2.99	2.99	2.99	2.99	2.99	2.92	2.99	3	3
1.02	1.01	1.01	1	1.02	1.02	1.02	1.02	1.02	1.02	1.02	1.09	1.02	1.01	1.01
0.02	0.01	—	—	0.01	0.02	0.01	0.01	—	0.02	0.01	0.02	—	—	—
0.95	0.97	0.98	0.98	0.96	0.94	0.97	0.98	0.92	0.94	0.96	1.03	0.96	0.96	0.97
0.01	0.01	—	—	0.01	0.01	0.01	0.01	0.06	0.03	0.01	—	0.02	0.01	—
4.99	4.99	4.99	4.98	4.98	4.98	4.99	4.99	4.99	4.99	4.98	5.05	4.99	4.98	4.98
2.04	1.01	0	0	1.02	2.06	1.01	1	0	2.02	1.02	1.9	0	0	0

		Hybrid					Pegmatite					Pegmatite						
		DNS-1					DNS-1					DNS-1						
		3	4	5	2	3	4	5	2	3	4	5	2	3	4	5	2	3
11.42	11.71	11.39	11.61	10.96	10.96	10.84	11.34	10.86	10.94	11.01	11.17	10.78	11.36	11.18				
19.8	19.79	19.7	20.11	19.81	19.73	19.9	19.72	19.82	19.56	19.67	19.45	18.77	19.4	19.45				
68.83	68.73	68.38	68.71	69.08	68.47	68.81	67.43	68.66	69.05	69.41	68.76	68.12	67.29	67.34				
0.18	—	0.35	0.18	0.17	0.14	—	0.18	0.16	0.19	—	0.2	0.18	0.14	—				
—	0.19	—	—	—	0.17	—	0.13	0.24	0.17	0.18	0.19	—	0.19	0.21				
100.22	100.43	99.82	100.62	100.02	99.47	99.56	98.81	99.75	99.9	100.28	99.77	97.85	98.39	98.18				
		Hybrid					Pegmatite					Pegmatite						
		DNS-1					DNS-1					DNS-1						
		3	4	5	2	3	4	5	2	3	4	5	2	3	4	5	2	3
3	2.99	2.99	2.98	3.01	3	3	2.98	3	3.01	3.01	3	3.03	2.99	2.99				
1.02	1.01	1.02	1.03	1.02	1.02	1.02	1.03	0.02	1	1.01	1.01	1	0.98	1.02				
—	0.01	—	—	—	0.01	—	0.01	0.01	0.01	0.01	0.01	—	0.01	0.01				
0.96	0.99	0.97	0.98	0.92	0.93	0.92	0.97	0.92	0.92	0.93	0.95	0.93	0.98	0.96				
0.01	—	0.02	0.01	0.01	0.01	—	0.01	0.01	0.01	—	0.01	0.01	0.01	—				
4.98	5	4.99	5	4.95	4.96	4.94	5	4.96	4.96	4.95	4.97	4.95	5	4.98				
0	1	0	0	0	1.05	0	1.01	1.06	1.06	1.06	1.03	0	1	1.02				

Layered					Layered					Massive				
		DN8 - 1	2	3	4	5	DN9 - 1	2	3	4	DN10 - 1	2	3	4
4	5	11.53	11.45	11.54	11.1	11.14	10.98	10.55	10.87	11.01	11.46	11.42	10.81	11.36
11.62	11.56	11.53	11.45	11.54	11.1	11.14	10.98	10.55	10.87	11.01	11.46	11.42	10.81	11.36
19.37	19.71	19.42	19.71	19.43	19.2	19.34	19.72	18.99	19.6	19.8	19.6	19.63	19.42	19.17
68.76	68.51	67.61	67.77	67.64	66.58	66.14	68.04	68.04	68.58	68.11	67.49	67.7	68.2	67.08
0.13	0.2	—	—	0.17	0.14	0.16	0.16	0.21	0.19	0.17	0.24	0.61	—	0.14
—	0.19	0.19	0.21	0.21	0.28	0.34	0.32	0.28	—	0.38	0.26	0.29	0.21	0.17
99.88	100.17	98.74	99.14	98.98	97.31	97.12	99.22	98.06	99.24	99.47	99.05	99.64	98.64	97.92
<hr/>														
3	2.99	2.99	2.98	2.99	2.99	2.98	2.99	3.02	3.01	2.99	2.98	2.98	3.01	2.99
1	1.01	1.01	1.02	1.01	1.02	1.03	1.02	0.99	1.01	1.02	1.02	1.02	1.01	1.01
—	0.01	0.01	0.01	0.01	0.01	0.02	0.01	0.01	—	0.02	0.01	0.01	0.01	0.01
0.98	0.98	0.99	0.98	0.99	0.97	0.97	0.94	0.91	0.92	0.94	0.98	0.97	0.92	0.98
0.01	0.01	—	—	0.01	0.01	0.01	0.01	0.01	0.01	0.01	0.01	0.03	—	0.01
4.99	5	5	4.99	5.01	4.99	5	4.97	4.94	4.95	4.97	5.01	5.02	4.95	5
0	1	1	1.01	0.99	1.01	2	1.04	1.06	0	2.06	1	0.99	1.08	1

Hybrid					
5	DN11 - 1	2	3	4	5
11	11.33	11.34	11.54	11.27	11.44
19.68	19.78	19.59	19.89	19.49	19.26
68.82	67.42	67.63	68.58	67.92	67.28
0.19	0.24	0.25	0.18	0.16	—
—	0.58	0.38	0.36	0.41	—
99.69	99.35	99.19	100.55	99.25	97.97
<hr/>					
3	2.98	2.98	2.98	2.99	3
1.01	1.02	1.02	1.02	1.01	1.01
—	0.01	0.02	0.02	0.02	—
0.93	0.99	0.97	0.97	0.96	0.99
0.01	0.01	0.01	0.01	0.01	—
4.96	5.01	5	5	4.99	4.99
0	0.99	2	2	2.02	0

## Representative analyses of K-feldspar from nepheline syenites, Center II, Coldwell Complex

Rock Type	Layered							Layered						
	CCIA - 1	2	3	4	5	6	7	CC18 - 1	2	3	5	6	7	
Sample	CCIA - 1	2	3	4	5	6	7	CC18 - 1	2	3	5	6	7	
Na2O	1.06	1.12	0.52	0.96	0.73	0.43	0.51	1.14	1.23	1.2	0.52	0.98	0.86	
Al2O3	18.75	18.32	18.44	18.77	18.53	18.37	19.21	18.59	18.73	18.67	18.93	18.87	18.57	
SiO2	63.74	63.16	63.54	63.53	63.07	63.5	63.69	63.85	63.5	63.83	63.69	64.06	63.82	
K2O	16.14	15.93	17.27	16.44	16.7	17.25	16.92	15.94	16.06	16.18	17.19	15.97	16.61	
Total	99.7	98.54	99.77	99.7	99.04	99.55	100.33	99.52	99.52	99.88	100.34	99.89	99.86	
Cation Assignment - Based on 8 Oxygens														
Si	2.97	2.97	2.97	2.96	2.96	2.97	2.95	2.97	2.96	2.97	2.96	2.97	2.97	
Al	1.03	1.02	1.02	1.03	1.03	1.01	1.05	1.02	1.03	1.02	1.04	1.03	1.02	
Na	0.1	0.1	0.05	0.09	0.07	0.04	0.05	0.1	0.11	0.11	0.05	0.09	0.08	
K	0.96	0.96	1.03	0.98	1	1.03	1	0.95	0.96	0.96	1.02	0.94	0.99	
Total	5.05	5.05	5.06	5.06	5.06	5.06	5.05	5.04	5.06	5.06	5.06	5.03	5.05	
Or%	90.57	90.57	95.37	91.59	93.46	96.26	95.24	90.48	89.72	89.72	95.33	91.26	92.52	



	Massive						Layered						Hybrid	
	4	5	CC6-1	2	3	4	5	6	CC7-1	2	3	4		5
0.31	0.47	0.76	0.39	0.78	—	—	0.41	1.1	0.93	1.04	0.52	0.48	0.43	0.89
17.96	18.2	18.6	18.5	18.4	18.6	18.41	18.32	18.65	18.62	18.45	18.67	18.34	18.55	18.49
63.97	63.93	64.25	64.39	64.46	64.5	64.47	63.96	64.73	64.75	63.76	64.32	64.14	63.99	64.06
16.38	16.94	16.5	16.77	16.41	17.1	16.32	16.79	15.8	16.17	15.82	16.88	16.92	16.58	16.01
98.62	99.54	100.11	100.05	100.05	100.2	99.2	99.49	100.28	100.47	99.07	100.38	99.88	99.55	99.45
3	2.99	2.98	2.99	2.99	2.99	3	2.99	2.98	2.98	2.98	2.98	2.98	2.98	2.98
0.99	1	1.02	1.01	1	1.02	1.01	1.01	1.01	1.01	1.02	1.02	1.01	1.02	1.01
0.03	0.04	0.07	0.04	0.07	—	—	0.04	0.1	0.08	0.09	0.05	0.04	0.04	0.08
0.98	1.01	0.98	0.99	0.97	1.01	0.97	1	0.93	0.95	0.94	1	1	0.98	0.95
5.01	5.04	5.04	5.02	5.03	5.01	4.98	5.03	5.02	5.03	5.03	5.04	5.04	5.02	5.03
97.03	96.19	93.33	96.12	93.27	100	100	96.15	90.29	92.23	91.26	95.24	96.15	96.08	92.23

Hybrid										Layered					Hybrid				
CC9 - 1					CC10 - 1					CC11 - 1									
2	3	4	5	2	3	4	5	2	3	4	5	2	3	4	5				
0.97	0.9	0.54	0.52	1.1	1	1.31	0.89	0.84	0.72	1.37	0.71	1.23	0.43	1.01					
18.26	18.27	18.59	18.29	18.59	18.33	18.79	18.49	18.25	18.73	18.7	18.49	18.01	18.15	18.07					
64.22	64.33	64.44	64.15	64.36	64.06	63.82	64.77	64.28	63.9	64.4	64	64.92	63.45	63.92					
15.74	16.12	16.53	16.69	15.01	15.22	15.34	15.79	15.51	16.12	15.25	15.98	15.02	16.17	15.35					
99.19	99.62	100.1	99.65	99.05	98.61	99.25	99.94	98.87	99.47	99.73	99.19	99.19	98.21	98.35					
<hr/>																			
2.99	2.99	2.98	2.99	2.99	2.99	2.97	2.99	3	2.97	2.98	2.98	3.01	2.99	3					
1	1	1.01	1	1.02	1.01	1.03	1.01	1	1.03	1.02	1.02	0.98	1.01	1					
0.09	0.08	0.05	0.05	0.1	0.09	0.12	0.08	0.08	0.07	0.12	0.06	0.11	0.04	0.09					
0.94	0.96	0.98	0.99	0.89	0.91	0.91	0.93	0.92	0.96	0.9	0.95	0.89	0.97	0.92					
5.02	5.03	5.02	5.03	5	5	5.03	5.01	5	5.02	5.02	5.02	5	5.01	5.01					
91.26	92.31	95.15	95.19	89.9	91	88.35	92.08	92	93.2	88.24	94.06	89	96.04	91.09					

Massive										Massive									
2	3	4	5	6	CC12-1	2	3	4	5	CC13-1	2	3	4	5	2	3	4	5	
0.69	0.89	0.96	0.59	0.76	1.13	0.38	1.08	0.69	0.49	0.72	1.23	1.09	0.51	0.34					
18.17	18.26	18.21	18.31	18.18	18.76	18.08	18.57	18.51	18.16	18.53	18.56	18.55	18.69	18.3					
63.64	63.66	63.96	64.33	64.88	64.62	64.52	64.7	64.86	65.11	64.67	64.92	63.93	64.6	64.87					
15.83	15.49	15.78	15.56	15.58	15.33	16.42	15.37	16.42	16.32	15.88	15.55	15.54	16.48	16.52					
98.34	98.29	98.91	98.8	99.41	99.83	99.39	99.73	100.48	100.09	99.81	100.27	99.1	100.28	100.04					
2.99	2.99	2.99	3	3.01	2.98	3	2.99	2.99	3.01	2.99	2.99	2.98	2.98	3					
1.01	1.01	1	1.01	0.99	1.02	0.99	1.01	1.01	0.99	1.01	1.01	1.02	1.02	1					
0.06	0.08	0.09	0.05	0.07	0.1	0.03	0.1	0.06	0.04	0.06	0.11	0.1	0.05	0.03					
0.95	0.93	0.94	0.93	0.92	0.9	0.97	0.91	0.97	0.96	0.94	0.91	0.92	0.97	0.97					
5.01	5.01	5.02	4.99	4.99	5.01	5	5.01	5.02	5	5	5.02	5.02	5.02	5					
94.06	92.08	91.26	94.9	92.93	90	97	90.1	94.17	96	94	89.22	90.2	95.1	97					

Layered	Mottled - Malfic syenite										Mott			
	CC14 - 1					CC15 - 1								
	2	3	4	5	2	3	4	5	6	7	8	9	10	
0.9	0.89	1.05	0.99	0.39	1.24	1.33	0.97	0.44	0.94	0.88	0.97	1.12	1.19	1.28
18.52	18.41	18.53	18.66	18.4	18.79	18.61	18.56	18.46	18.52	18.43	18.66	18.79	18.84	18.66
63.83	63.51	63.87	64.56	64.04	64.15	64.31	64.41	64.38	64.6	64.92	64.01	64.09	63.99	64.56
15.85	15.96	15.8	15.98	16.62	15.17	15.05	15.62	16.33	15.52	15.35	15.28	15.22	14.97	14.93
99.1	98.76	99.25	100.2	99.44	99.34	99.3	99.56	99.61	99.58	99.57	98.92	99.21	98.99	99.43
2.98	2.98	2.98	2.98	2.99	2.98	2.98	2.99	2.99	2.99	3	2.98	2.98	2.98	2.99
1.02	1.02	1.02	1.02	1.01	1.03	1.02	1.01	1.01	1.01	1	1.02	1.03	1.03	1.02
0.08	0.08	0.09	0.09	0.03	0.11	0.12	0.09	0.04	0.08	0.08	0.09	0.1	0.11	0.12
0.94	0.95	0.94	0.94	0.99	0.9	0.89	0.92	0.97	0.92	0.91	0.91	0.9	0.89	0.88
5.02	5.03	5.03	5.03	5.02	5.01	5.01	5.01	5.01	5	4.99	5	5.01	5	5
92.16	92.23	91.26	91.26	97.06	89.11	88.11	91.09	96.04	92	91.92	91	90	89	88

led - Mafic syenite		Pegmatite										Mottled - Mafic syenite				
CC16 - 1	2	3	4	5	6	7	8	9	10	CC17A - 1	2	3	4	5		
0.97	1.31	0.82	1	1.02	0.58	0.93	0.77	0.9	0.85	1.27	0.67	0.71	1.03	0.83		
18.53	18.43	18.32	18.36	18.59	18.33	18.5	18.6	18.61	18.61	18.23	18.32	18.44	18.62	18.46		
64.69	64.52	64.5	65.04	64.64	63.94	64.57	65.18	65.24	63.91	63.71	65.03	64.6	63.89	64.41		
15.78	15.08	15.91	15.61	15.83	16.22	15.76	15.74	15.9	15.59	15.28	16.64	16.31	15.76	15.87		
99.98	99.36	99.54	100	100.09	99.06	99.77	100.29	100.65	98.97	98.5	100.66	100.06	99.3	99.57		
2.99	2.99	2.99	3	2.99	2.99	2.99	3	2.99	2.98	2.99	2.99	2.99	2.98	2.99		
1.01	1.01	1	1	1.01	1.01	1.01	1.01	1.01	1.02	1.01	0.99	1.01	1.01	1.01		
0.09	0.12	0.07	0.09	0.09	0.05	0.08	0.07	0.08	0.08	0.12	0.06	0.06	0.07	0.07		
0.93	0.89	0.94	0.92	0.93	0.97	0.93	0.92	0.93	0.93	0.91	0.98	0.96	0.94	0.94		
5.01	5.01	5.01	5.01	5.02	5.02	5.01	5	5.01	5.01	5.02	5.03	5.02	5.01	5.01		
91.18	88.12	93.07	91.09	91.18	95.1	92.08	92.93	92.08	92.07	88.35	94.23	94.12	93.07	93.07		

	Mottled - Malfic-syenite														
	Pegmatite					Pegmatite									
	6	7	8	9	10	CC17B-1	2	3	4	5	6	7	8	9	10
0.41	0.39	0.36	0.54	0.44	1.02	0.94	0.46	0.99	1.05	0.32	0.96	0.46	0.39	0.79	
18.16	18.22	18.04	18.21	17.88	18.31	18.32	18.24	18.37	18.19	18.24	18.28	18.26	18.12	18.5	
62.88	63.89	63.54	64.29	63.16	64.34	63.8	63.6	64.59	63.76	63.91	64.12	64.62	64.44	63.86	
16.15	16.08	16.38	16.33	16.04	15.48	15.51	16.31	15.34	15.32	16.44	15.45	16.49	16.43	15.86	
97.6	98.58	98.32	99.37	97.52	99.15	98.57	98.61	99.3	98.32	98.91	98.81	99.82	99.38	99.01	
2.98	3	2.99	3	3	2.99	2.99	2.99	3	2.99	2.99	2.99	3	3	2.98	
1.02	1.01	1	1	1	1.01	1.01	1.01	1	1.01	1.01	1.01	1	0.99	1.02	
0.04	0.04	0.03	0.05	0.04	0.09	0.08	0.04	0.09	0.1	0.03	0.09	0.04	0.04	0.07	
0.98	0.96	0.98	0.97	0.97	0.92	0.93	0.98	0.91	0.92	0.98	0.92	0.98	0.98	0.94	
5.02	5	5.01	5.01	5.01	5.01	5.01	5.02	5	5.01	5.01	5.01	5.01	5.01	5.02	
96.08	96	97.03	95.1	96.04	91.09	92.08	96.07	91	90.2	97.03	91.09	96.08	96.08	93.07	

Layered					Layered					Hybrid				
DNI - 1	2	3	4	5	DN2 - 1	2	3	4	5	DN3 - 1	2	3	4	DN4 - 1
1	1.28	0.89	1.08	1.05	0.86	0.66	0.46	0.84	0.78	0.78	1.08	0.88	0.76	0.84
18.48	18.63	18.6	18.48	18.49	18.18	18.6	18.49	18.55	18.44	18.44	18.17	18.65	18.64	18.68
64.92	64.49	64.78	64.87	65.33	63.99	64.2	63.87	65.13	64.63	65.09	64.32	65.06	64.53	64.26
15.61	15.37	15.71	15.75	15.81	15.92	16.46	16.89	16.45	16.5	15.91	15.57	15.65	16.04	15.6
100.01	99.76	99.98	100.17	100.68	98.95	99.92	99.72	100.97	100.36	100.24	99.14	100.24	99.97	99.38
2.99	2.98	2.99	2.99	3	2.99	2.98	2.98	2.99	2.99	3	3	2.99	2.98	2.98
1	1.02	1.01	1	1	1	1.02	1.01	1	1	1	1	1.01	1.02	1.02
0.09	0.11	0.08	0.1	0.09	0.08	0.06	0.03	0.07	0.07	0.07	0.1	0.08	0.07	0.08
0.92	0.91	0.93	0.93	0.92	0.95	0.97	1	0.96	0.97	0.93	0.93	0.92	0.95	0.92
5.01	5.02	5.01	5.02	5.01	5.02	5.03	5.02	5.03	5.03	5	5.02	5	5.01	5
91.09	89.22	92.08	90.29	91.09	92.23	94.17	97.09	93.2	93.27	93	90.29	92	93.14	92

Hybrid										Pegmatite										
DNS - 1					2					DN6 - 1					DN7 - 1					
2	3	4	5		2	3	4	5		2	3	4	5		2	3	4	5		
1.06	0.87	0.56	0.87	1.03	1.43	0.61	0.8	0.84	0.46	0.31	0.32	0.86	0.95	0.27						
18.56	18.64	18.68	18.68	18.7	18.68	18.53	18.64	18.57	18.33	18	18.58	18.33	18.54	17.99						
65.17	64.76	64.55	64.67	65.12	65.19	65.6	65.12	64.57	65.29	64.23	65.23	65.23	64.95	63.35						
15.36	15.45	15.83	15.56	15.26	14.8	15.6	16.03	15.84	15.97	16.23	16.42	15.4	15.8	15.98						
100.16	99.71	99.62	99.78	100.11	100.1	100.34	100.59	99.82	100.04	98.77	100.55	99.82	100.24	97.59						
<hr/>																				
3					2.99					3.01					3					
1.01	1.01	1.02	1.02	1.01	1.01	1	1.01	1.01	1	0.99	1.01	1	1.01	1	0.99	1.01	1	1.01	1	3
0.09	0.08	0.05	0.08	0.09	0.13	0.05	0.07	0.08	0.04	0.03	0.03	0.08	0.08	0.03	0.03	0.03	0.08	0.08	0.03	0.03
0.9	0.91	0.93	0.92	0.89	0.87	0.91	0.94	0.94	0.94	0.97	0.96	0.91	0.93	0.97	0.96	0.96	0.91	0.93	0.97	0.97
5	5	4.99	5	4.99	5	4.98	5.01	5.01	4.98	5	4.99	4.99	5.01	4.99	4.99	4.99	4.99	5.01	4.99	4.99
90.91	91.92	94.9	92	90.82	87	94.79	93.06	92.16	95.92	97	96.97	91.92	92.08	97						

Layered										Layered					Massive	
2	3	4	5	DN8 - 1	2	3	4	5	DN9 - 1	2	3	4	DN10 - 1	2		
0.5	0.46	0.4	0.41	0.45	0.99	0.57	0.74	0.76	0.71	1	0.43	0.37	0.4	0.21		
18.05	18.31	17.95	18.65	18.19	18.62	18.06	18.13	18.05	18.54	18.35	18.53	18.65	18.47	18.37		
63.45	63.69	64.02	64.81	64.14	64.6	63.24	64.04	63.43	65.2	64.74	65.54	65.01	65.56	63.45		
16.05	16.26	16.17	16.7	16.31	15.54	16.06	15.29	15.6	15.75	15	16.38	16.3	16.31	16.5		
98.05	98.72	98.54	100.56	99.1	99.75	97.94	98.21	97.83	100.2	99.08	100.87	100.33	100.73	98.53		
<hr/>																
2.99	2.99	3	2.99	3	2.99	2.99	3	2.99	3	3	3	2.99	3	2.98		
1	1.01	0.99	1.01	1	1.01	1.01	1	1	1.01	1	1	1.01	1	1.02		
0.05	0.04	0.04	0.04	0.04	0.09	0.05	0.07	0.07	0.06	0.09	0.04	0.03	0.04	0.02		
0.97	0.97	0.97	0.98	0.97	0.92	0.97	0.91	0.94	0.92	0.89	0.96	0.96	0.95	0.99		
5.01	5.01	5	5.02	5.01	5.01	5.02	4.99	5.01	4.99	4.98	5	5	4.99	5.01		
95.1	96.04	96.04	96.08	96.04	91.09	95.1	92.86	93.07	93.88	90.82	96	96.97	95.96	98.02		

Hybrid									
3	4	5	DN11 - 1	2	3	4	5		
0.92	0.24	0.49	0.53	1.25	1.06	0.95	1		
18.73	17.88	18.64	18.06	18.57	18.47	18.35	18.67		
64.97	64.63	65.08	63.36	64.43	64.31	64.06	64.9		
15.63	15.98	16.49	16.3	15.37	15.55	15.64	15.7		
100.25	98.72	100.7	98.25	99.62	99.38	99	100.26		
2.99	3.02	2.99	2.99	2.98	2.99	2.99	2.99		
1.02	0.98	1.01	1	1.01	1.01	1.01	1.01		
0.08	0.02	0.04	0.05	0.11	0.1	0.09	0.09		
0.92	0.95	0.97	0.98	0.91	0.92	0.93	0.92		
5	4.98	5.01	5.02	5.02	5.02	5.01	5.01		
92	97.94	96.04	95.15	89.22	90.2	91.18	91.09		

## Representative analyses of apatite from nepheline syenites, Center II, Coldwell Complex

Rock Type	Layered							Layered									
Zone	Core							Rim									
Sample	CC1A - 1	2	3	4	5	5	5	6	6	7	7	7	7	7	CC1B - 1	2	3
SiO2	3.13	3.29	1.6	4.2	1.27	4.48	1.38	3.03	1.17	2.93	4.23	2.62	3.65	3.67			
P2O5	36.64	36.94	39.56	35.48	40.84	34.85	40.65	37.74	40.79	38.13	35.26	37.86	36.31	36.57			
CaO	49.73	49.38	52.77	47.75	53.54	46.97	52.9	50.23	53.69	50.31	48.18	50.59	48.82	49.26			
Y2O3	0.98	0.63	—	0.9	—	0.76	—	—	—	—	0.91	—	0.8	0.75			
La2O3	2.18	2.47	0.98	2.96	1	3.39	1.19	2.16	0.56	2.02	3.09	2	2.98	2.61			
Ce2O3	3.75	4.54	2.26	6.33	1.53	6.52	1.87	4.46	1.34	3.69	5.5	4.03	5.03	4.76			
Pr2O3	—	—	—	0.63	—	—	—	—	—	0.47	—	—	—	—			
Nd2O3	1.12	1.19	0.59	1.54	—	1.67	0.71	1.08	—	1.36	1.59	0.95	1.69	1.6			
F	2.62	2.37	3.03	2.31	2.92	2.69	3.57	2.4	3.19	2.19	2.45	2.65	1.82	2.27			
Total	100.14	100.86	100.79	102.11	101.1	101.33	102.27	101.1	100.73	101.1	101.2	100.76	101.11	101.49			
O=F	1.1	1	1.28	0.97	1.23	1.13	1.5	1.01	1.34	0.92	1.03	1.12	0.77	0.96			
Total	99.04	99.86	99.51	101.14	99.87	100.2	100.77	100.09	99.39	100.18	100.17	99.64	100.34	100.53			
REEZ03	7.05	8.2	3.83	11.46	2.53	11.58	3.77	7.7	1.9	7.54	10.18	6.98	9.7	8.97			

Cation Assignment - Based on 26 (O, F, OH, Cl)																	
	P	Si	Ca	Y	La	Ce	Pr	Nd	F	Cation Total							
	5.38	5.41	5.61	5.24	5.73	5.17	5.63	5.48	5.71	5.54	5.22	5.48	5.39	5.36			
	0.54	0.57	0.27	0.73	0.21	0.78	0.23	0.52	0.19	0.5	0.74	0.45	0.64	0.64			
	9.24	9.15	9.47	8.93	9.5	8.81	9.28	9.23	9.51	9.25	9.02	9.27	9.18	9.14			
	0.09	0.06	—	0.08	—	0.07	—	—	—	—	0.08	—	0.07	0.07			
	0.14	0.16	0.06	0.19	0.06	0.22	0.07	0.14	0.03	0.13	0.2	0.13	0.19	0.17			
	0.24	0.29	0.14	0.4	0.09	0.42	0.11	0.28	0.08	0.23	0.35	0.25	0.32	0.3			
	—	—	—	0.04	—	—	0.04	—	0.03	0.03	—	—	—	—			
	0.07	0.07	0.04	0.1	—	0.1	0.04	0.07	—	0.08	0.1	0.24	0.11	0.1			
	1.43	1.29	1.61	1.27	1.53	1.49	1.85	1.3	1.67	1.19	1.36	1.43	1.01	1.24			
	15.69	15.7	15.59	15.72	15.59	15.57	15.36	15.71	15.52	15.76	15.71	15.66	15.91	15.77			

Core	Rim	Low	High	Core	Rim	Core	Inner Mid	Outer Mid	Rim	Layered				
										CC2-1	2	3	Core	Rim
4	4	5	5	6	6	7	7	7	7	—	—	—	—	—
1.28	3.09	2.82	3.93	0.68	3.9	1.3	2.85	4.39	6.34	1.31	3.37	2.73	1.65	2.87
40.81	37.81	38.11	35.34	42.12	35.97	40.96	37.57	34.83	31.31	40.22	36.75	37.54	40.09	37.91
53.91	49.82	50.46	47.14	54.13	48.23	53.77	50.17	47.51	43.76	53.36	48.85	49.99	52.83	50.29
—	0.7	—	0.95	—	0.84	0.75	0.91	0.79	0.99	—	0.69	0.89	—	0.98
0.81	2.21	2.21	3.12	0.68	2.67	0.84	2.01	3.66	5.29	1.18	2.59	2	1.02	1.87
1.61	4.32	4.25	5.62	0.78	5.4	1.54	3.81	6.51	9.53	1.87	5.17	4.46	2.07	3.83
—	—	—	0.47	—	0.52	—	—	—	—	—	0.64	—	0.49	—
—	1.38	1.05	1.98	0.67	1.57	0.69	1.19	1.54	2.19	0.78	1.62	1.63	0.76	0.92
2.36	1.78	2.54	2.7	3.49	3.06	2.69	3.25	2.56	1.77	3.41	2.37	2.56	3.04	3.24
100.78	101.16	101.44	101.24	102.54	102.15	102.54	101.75	101.79	101.27	102.17	102.04	101.91	101.95	101.9
0.99	0.75	1.07	1.14	1.47	1.29	1.13	1.37	1.08	0.75	1.44	1	1.08	1.28	1.36
99.79	100.41	100.37	100.1	101.07	100.86	101.41	100.38	100.71	100.52	100.73	101.04	100.83	100.67	100.54
2.42	7.91	7.51	11.19	2.13	10.16	3.07	7.01	11.71	17.01	3.83	10.02	8.09	4.34	6.62
5.78	5.54	5.5	5.24	5.77	5.23	5.72	5.38	5.16	4.86	5.61	5.38	5.43	5.63	5.4
0.21	0.54	0.48	0.69	0.11	0.67	0.21	0.48	0.77	1.16	0.22	0.58	0.47	0.27	0.48
9.66	9.23	9.22	8.84	9.38	8.87	9.5	9.09	8.91	8.59	9.41	9.05	9.15	9.39	9.07
—	0.06	—	0.09	—	0.08	0.07	0.08	0.07	0.1	—	0.06	0.08	—	0.09
0.05	0.14	0.14	0.2	0.04	0.17	0.05	0.13	0.24	0.36	0.07	0.16	0.13	0.06	0.12
0.1	0.27	0.27	0.36	0.05	0.34	0.09	0.24	0.42	0.64	0.11	0.33	0.28	0.13	0.24
—	—	—	0.03	—	0.03	—	—	—	—	—	0.04	—	0.03	—
—	0.09	0.06	0.12	0.04	0.1	0.04	0.07	0.1	0.14	0.05	0.1	0.1	0.04	0.06
1.25	0.97	1.37	1.49	1.79	1.66	1.4	1.74	1.42	1.03	1.77	1.29	1.38	1.6	1.72
15.8	15.87	15.66	15.57	15.39	15.48	15.68	15.46	15.66	15.85	15.47	15.71	15.64	15.56	15.45

Core	Massive																	
	Rim	Core	Mid	Rim	Core	Mid	Rim	Core	Rim	CC3-1	2	3	Core	Rim				
5	5	6	6	6	7	7	7	7	8	8	8	8	—	—	—	—	—	—
1.5	2.65	0.85	2.41	4.04	2.12	3.54	2.64	3.13	1.78	2.32	3.01	3.33	0.81	3.23				
40.35	38.52	41.8	38.3	35.46	39.16	35.86	38.03	38.13	40.51	38.75	37.96	37.72	41.44	37.44				
52.61	50.55	54.07	50.59	47.84	51.06	48.45	49.86	50.01	52.67	51.12	49.63	49.86	53.41	49.6				
—	—	—	0.69	0.95	—	0.91	—	0.79	—	—	0.71	—	—	0.81				
1.12	2.2	0.76	2.07	3	1.97	3.16	2.04	2.21	1.47	1.87	1.86	2.3	0.55	2.55				
2.16	3.38	1.17	3.37	5.52	3.25	5.23	4.11	3.72	2.31	3.18	4.07	4.24	1.04	4.33				
—	—	—	—	—	—	—	0.82	—	—	—	—	—	—	—				
0.48	1.34	—	1.08	2.09	1.29	1.07	1.65	1.2	0.68	1.03	1.35	1.3	0.41	1.15				
2.99	2.53	3.53	2.64	2.65	3.08	1.89	3.52	2.49	3.35	2.74	3.17	2.56	3.31	2.56				
101.21	101.18	102.27	101.13	101.65	101.93	100.09	102.67	101.69	102.77	101.01	101.86	101.31	100.97	101.68				
1.26	1.07	1.49	1.11	1.12	1.3	0.8	1.48	1.05	1.41	1.15	1.33	1.08	1.39	1.08				
99.95	100.11	100.78	100.02	100.53	100.63	99.29	101.19	100.64	101.36	99.86	100.53	100.23	99.58	100.6				
3.76	6.92	1.93	6.52	10.61	6.51	9.46	8.62	7.13	4.46	6.08	7.28	7.84	2	8.03				

5.68	5.55	5.73	5.53	5.21	5.56	5.38	5.4	5.62	5.49	5.56	5.41	5.45	5.77	5.42				
0.25	0.45	0.14	0.41	0.7	0.35	0.63	0.44	0.29	0.53	0.39	0.51	0.57	0.13	0.55				
9.38	9.22	9.38	9.24	8.9	9.17	9.2	8.96	9.24	9.11	9.28	8.95	9.12	9.41	9.09				
—	—	—	0.06	0.09	—	0.09	—	—	0.07	—	0.06	—	—	0.07				
0.07	0.14	0.05	0.13	0.19	0.12	0.21	0.13	0.09	0.14	0.12	0.12	0.14	0.03	0.16				
0.13	0.21	0.07	0.21	0.35	0.2	0.34	0.25	0.14	0.23	0.2	0.25	0.26	0.06	0.27				
—	—	—	—	—	—	—	0.05	—	—	—	—	—	—	—				
0.03	0.08	—	0.07	0.13	0.08	0.07	0.1	0.04	0.07	0.06	0.08	0.08	0.02	0.07				
1.57	1.36	1.81	1.42	1.46	1.63	1.06	1.87	1.73	1.34	1.47	1.69	1.38	1.72	1.39				
15.54	15.65	15.39	15.64	15.62	15.48	15.9	15.33	15.42	15.64	15.61	15.38	15.63	15.43	15.64				

Core	Rim	Core	Inner zone	Outer zone	Rim	Pegmatite						Pegmatite			Massive		
						CC4-1	2	3	4	CC5-1	2	CC6-1	2	3			
4.99	2.59	0.79	2.08	3.52	4.7	0.96	41.68	41.16	41.26	42.12	41.64	39.81	2.48	2.41	2.19		
33.85	38.42	40.89	38.78	36.15	33.55	41.68	41.16	41.26	42.12	41.64	39.81	38.87	39.95	39.62			
46.07	50.83	54	51.57	48.39	46.03	54.44	54.65	52.87	54.7	54.17	51.58	51.44	51.49	51.81			
—	—	—	0.83	0.72	0.87	—	—	—	—	—	—	—	—	—			
3.83	2	0.42	1.5	2.68	3.84	1.35	1.23	2.02	0.98	—	0.98	1.83	1.49	1.53			
7.58	3.6	0.78	2.79	5.47	7.41	1.14	1.11	2.13	0.6	—	2.07	3.2	2.99	3.25			
0.86	—	—	—	0.53	0.61	—	—	—	—	—	0.7	—	0.54	—			
2.62	0.93	0.56	1.19	1.39	2.12	—	—	—	—	—	0.8	0.83	0.8	0.9			
2.55	2.48	3.56	2.53	2.53	2.37	4.09	3.61	4	4.21	3.76	2.94	2.14	3.03	3.13			
102.36	100.86	101	101.26	101.38	101.56	103.66	101.77	103.14	102.61	99.57	99.12	100.79	102.7	102.43			
1.07	1.04	1.5	1.07	1.07	1	1.72	1.52	1.68	1.77	1.58	1.24	0.9	1.28	1.32			
101.29	99.82	99.5	100.19	100.31	100.56	101.94	100.25	101.46	100.84	97.99	97.88	99.89	101.42	101.11			
14.89	6.53	1.76	5.48	10.07	13.98	2.49	2.34	4.15	1.58	0	3.75	5.86	5.82	5.68			
5.06	5.55	5.69	5.57	5.32	5.06	5.64	5.72	5.65	5.73	5.8	5.7	5.62	5.59	5.56			
0.88	0.44	0.13	0.35	0.61	0.84	0.15	0.15	0.14	0.14	0.18	0.18	0.42	0.4	0.36			
8.72	9.29	9.51	9.38	9.02	8.79	9.32	9.61	9.17	9.41	9.55	9.35	9.41	9.12	9.21			
—	—	—	0.07	0.07	0.08	—	—	—	—	—	—	—	—	—			
0.25	0.13	0.03	0.09	0.17	0.25	0.08	0.07	0.12	0.06	—	0.06	0.12	0.09	0.09			
0.49	0.22	0.05	0.17	0.35	0.48	0.07	0.07	0.13	0.04	—	0.13	0.2	0.18	0.2			
0.06	—	—	—	0.03	0.04	—	—	—	—	—	—	—	0.03	—			
0.17	0.06	0.03	0.07	0.09	0.13	—	—	—	—	—	0.04	0.05	0.05	0.05			
1.43	1.34	1.85	1.36	1.39	1.34	2.07	1.87	2.05	2.14	1.96	1.57	1.16	1.58	1.64			
15.62	15.69	15.43	15.72	15.66	15.69	15.25	15.47	15.21	15.23	15.35	15.5	15.81	15.46	15.48			

High	Low	Layered								Hybrid				
		4	5	5	6	6	CC7-1	2	3	4	4	2	3	4
3.63	2.38	3.95	2.01	4.76	2.8	3.51	3.91	4.56	5.43	0.99	3.75	3.17	2.64	2.59
36.9	39.52	36.36	39.7	35.63	38.02	36.79	36.79	35.42	33.75	42.18	35.7	37.13	37.31	37.76
49.44	52.81	48.49	52.45	47.83	50.64	49.83	49.06	48.49	45.91	54.72	49.1	50.27	50.72	50.35
0.87	0.79	—	—	0.74	0.67	0.88	—	—	—	—	—	—	0.79	0.87
2.63	1	2.89	1.33	3.06	2.03	2.6	3.03	3.03	4	0.49	3.07	2.2	2.08	2.15
4.97	2.86	5.38	2.63	5.63	3.32	4.85	5.48	5.55	8.08	1.29	5.49	4.47	3.79	3.81
—	—	—	—	0.54	—	—	—	—	1	—	—	0.64	—	—
1.77	0.87	1.26	0.69	1.66	1.03	1.59	1.45	2.14	2.27	—	1.34	1.32	1.38	1.08
2.01	2.58	2.09	2.79	2.05	2.2	2.67	2.46	1.7	2.23	3.04	2.6	2.74	1.87	2.9
102.22	102.82	100.49	101.62	101.89	100.7	102.72	102.2	100.89	102.67	102.71	101.05	101.95	100.57	101.51
0.85	1.09	0.88	1.17	0.86	0.93	1.12	1.04	0.72	0.94	1.28	1.09	1.15	0.79	1.22
101.37	101.73	99.61	100.45	101.03	99.77	101.6	101.16	100.17	101.73	101.43	99.96	100.8	99.78	100.29
9.37	4.73	9.53	4.65	10.89	6.38	9.04	9.96	10.72	15.35	1.78	9.9	8.63	7.25	7.04
5.4	5.56	5.37	5.61	5.26	5.53	5.31	5.34	5.29	5.06	5.79	5.26	5.37	5.51	5.44
0.63	0.4	0.69	0.34	0.83	0.48	0.6	0.67	0.8	0.96	0.16	0.65	0.54	0.46	0.44
9.15	9.41	9.07	9.39	8.93	9.32	9.11	9.02	9.17	8.7	9.5	9.16	9.2	9.48	9.18
0.08	0.07	—	—	0.07	0.06	0.08	—	—	—	—	—	—	0.07	0.08
0.17	0.06	0.19	0.08	0.2	0.13	0.16	0.19	0.2	0.26	0.03	0.2	0.14	0.13	0.13
0.31	0.17	0.34	0.16	0.36	0.21	0.3	0.34	0.36	0.52	0.08	0.35	0.28	0.24	0.24
—	—	—	—	0.03	—	—	—	—	0.06	—	—	—	—	—
0.11	0.05	0.08	0.04	0.1	0.06	0.1	0.09	0.13	0.14	—	0.08	0.08	0.09	0.07
1.1	1.36	1.15	1.48	1.13	1.2	1.44	1.35	0.95	1.25	1.56	1.43	1.48	1.03	1.56
15.85	15.72	15.76	15.62	15.78	15.8	15.66	15.65	15.96	15.71	15.55	15.71	15.65	15.98	15.58



												Hybrid																		
	Core			Rim			Core			Rim			CC11A-1		Core		Rim		Core											
	3	4	4	5	5	6	6	7	7	7	7	7	2	3	3	3	3	4												
—	—	—	—	—	—	—	—	—	—	—	—	—	—	—	—	—	—	—												
4.13	1.36	3.38	0.81	2.87	0.64	3.53	0.71	2.31	3.17	4.38	3.8	3.21	5.25	2.58	34.34	40.1	36.44	41.91	37.64	41.56	36.65	41.13	38.03	36.25	34.05	35.84	36.15	31.93	37.25	
47.28	53.42	49.1	54.53	50.37	54.17	48.89	54.09	50.95	49.52	46.73	48.09	49.31	45.69	50.14	1.09	—	—	—	—	—	—	—	—	—	—	—	—	—	—	—
2.9	0.77	2.6	0.43	2.27	0.75	2.55	0.55	2.04	2.63	3.57	2.45	2.42	3.71	1.93	5.98	2.03	5.22	1.09	4.54	1.15	4.89	0.94	3.54	5.15	6.57	5.59	4.38	7.68	3.7	
—	—	—	—	0.69	—	—	—	—	—	—	—	—	—	—	—	—	—	—	—	—	—	—	—	—	—	—	—	—	—	
1.78	—	1.56	—	1.39	—	1.47	—	1.08	1.4	1.97	1.89	1.34	2.57	1.33	2.4	3.28	2.61	2.75	2.79	3.04	2.55	3.34	2.67	2.12	2.79	2.82	2.81	2.35	3.4	
99.89	100.95	100.9	101.53	102.56	101.31	101.43	100.76	101.49	101.25	100.06	102.12	100.37	101.39	101.07	99.89	99.57	99.8	100.37	101.39	100.03	100.36	99.35	100.37	100.36	98.89	100.93	99.19	100.4	99.64	
1.01	1.38	1.1	1.16	1.17	1.28	1.07	1.41	1.12	0.89	1.17	1.19	1.18	0.99	1.43	98.88	99.57	99.8	100.37	101.39	100.37	100.36	99.35	100.37	100.36	98.89	100.93	99.19	100.4	99.64	
10.66	2.8	9.38	1.52	8.89	1.9	8.91	1.49	6.66	9.18	12.11	10.62	8.14	15	6.96	—	—	—	—	—	—	—	—	—	—	—	—	—	—	—	
5.18	5.63	5.35	5.83	5.41	5.79	5.35	5.74	5.49	5.37	5.12	5.24	5.31	4.89	5.36	0.74	0.23	0.59	0.13	0.49	0.11	0.61	0.12	0.39	0.55	0.78	0.66	0.56	0.95	0.44	
9.03	9.49	9.13	9.6	9.17	9.56	9.04	9.55	9.31	9.28	8.89	8.9	9.18	8.86	9.14	0.1	—	—	—	—	—	—	—	—	—	—	—	—	—	—	—
0.19	0.05	0.17	0.03	0.14	0.05	0.16	0.03	0.13	0.17	0.23	0.16	0.16	0.25	0.12	39	0.12	0.33	0.07	0.28	0.07	0.31	0.06	0.22	0.33	0.43	0.35	0.28	0.51	0.23	
—	—	—	—	0.04	—	—	—	—	—	—	—	—	—	—	0.11	—	—	—	—	—	—	—	—	—	—	—	—	—	—	
1.35	1.72	1.43	1.43	1.5	1.58	1.39	1.74	1.44	1.18	1.57	1.54	1.54	1.35	1.83	15.74	15.52	15.66	15.65	15.62	15.57	15.65	15.49	15.69	15.88	15.58	15.56	15.63	15.81	15.44	

												Massive											
Rim	Core	Rim	Core	Rim	Core	Rim	Core	Mid	Rim	CC12-1	2	3	4	5	High	Low							
4	2	5	6	5	6	6	7	7	7	—	—	—	—	—	—	—							
4.61	39.28	3.07	3.65	36.94	34.87	4.76	1.83	2.64	4.61	2.16	7.5	2.81	2.42	2.82	2.61	2.11							
32.86	51.75	49.05	47.96	46.31	34.41	39.09	37.87	33.82	38.76	29.13	38.24	38.15	37.88	37.3	39.13								
46.45	—	—	0.77	—	—	51.72	50.31	46.7	50.64	42.01	50.46	50.91	50.44	50.44	49.69	51.52							
0.87	—	—	—	—	—	—	—	0.82	0.79	1.22	—	—	—	—	0.82	—							
3.25	1.42	1.91	2.89	3.37	2.89	1.48	1.99	3.48	1.56	5.59	1.66	1.16	1.74	1.74	1.35	1.35							
6.47	2.5	4.34	5.73	6.77	6.77	2.65	3.9	6.82	3.32	10.34	3.43	2.81	3.57	3.57	3.74	2.53							
0.68	—	0.67	—	1.09	—	—	—	—	—	—	—	—	—	—	—	—							
2.04	0.79	1.39	1.6	2.2	2.2	0.99	1.09	1.6	1.1	2.79	1.36	1.35	1.01	1.42	1.03	1.03							
2.38	3.32	3.43	2.49	2.66	3.83	3.08	2.42	2.57	2.24	3.52	4.38	2.45	4.23	3.76	—	—							
99.61	101.06	100.81	99.96	101.56	101.59	100.87	100.27	100.9	100.82	101.47	101.17	99.91	101.54	101.42	101.42	101.42							
1	1.4	1.44	1.05	1.12	1.61	1.3	1.02	1.08	0.94	1.48	1.84	1.84	1.84	1.78	1.58	1.58							
98.61	99.66	99.37	98.91	100.44	99.98	99.57	99.25	99.82	99.88	99.99	99.33	98.88	99.76	99.84	99.84	99.84							
12.44	4.71	8.31	10.22	13.43	5.12	6.98	11.9	5.98	18.72	6.45	5.32	6.32	6.9	4.91	—	—							
<hr/>																							
5.04	5.55	5.34	5.24	5.13	5.49	5.45	5.11	5.59	4.58	5.42	5.35	5.52	5.29	5.49	—	—							
0.84	0.33	0.52	0.65	0.84	0.3	0.45	0.82	0.37	1.39	0.47	0.4	0.49	0.44	0.35	—	—							
9.01	9.26	8.97	9.12	8.73	9.19	9.17	8.93	9.24	8.36	9.05	9.04	9.3	8.92	9.15	—	—							
0.08	—	—	0.07	—	—	—	0.08	0.07	0.12	—	—	—	—	—	0.07	—							
0.22	0.09	0.12	0.19	0.22	0.09	0.12	0.23	0.1	0.38	0.1	0.07	0.07	0.11	0.11	0.08	0.08							
0.43	0.15	0.27	0.37	0.44	0.16	0.24	0.45	0.21	0.7	0.21	0.17	0.22	0.22	0.23	0.15	0.15							
0.05	—	0.04	—	0.07	—	—	—	—	—	—	—	—	—	—	—	—							
0.13	0.05	0.08	0.1	0.14	0.06	0.07	0.1	0.07	0.19	0.08	0.08	0.08	0.06	0.08	0.06	0.06							
1.36	1.75	1.85	1.4	1.48	2.01	1.66	1.36	1.38	1.31	1.86	2.3	1.33	2.24	1.97	—	—							
15.79	15.44	15.36	15.73	15.56	15.3	15.5	15.72	15.64	15.73	15.34	15.11	15.7	15.14	15.29	—	—							

Core	Massive										Layered					
	Rim	CC13B-1	2	3	4	Core	Rim	Core	Rim	Core	Rim	Core	Rim	CC14-1	2	3
0.94	2.69	2.54	2.58	2.56	2.51	1.13	2.77	2	2.63	2.02	2.76	0.9	3	3.28		
41.51	37.57	38.32	38.04	37.95	38.31	40.71	38.39	39.36	37.86	39.45	38.29	41.46	37.42	37.38		
54.23	50.68	50.52	50.95	51.08	51.08	53.55	50.75	52.51	50.55	52.29	50.46	54.14	49.78	49.81		
—	—	—	—	—	—	—	—	—	1	—	—	—	0.76	—		
0.57	2.2	1.63	1.96	1.61	1.76	0.53	2.12	1.2	1.9	1.41	1.79	0.87	2.21	2.73		
1.31	3.5	3.28	3.61	3.11	3.35	1.29	3.55	2.33	3.48	2.9	3.78	1.59	4.69	4.88		
—	—	—	—	—	—	—	—	—	—	—	—	—	0.71	—		
—	1.02	1.31	1.19	1.1	1	0.44	1.57	0.91	1.32	—	1.43	—	—	1.46	1.33	
3.62	3.19	2.95	2.87	2.78	3.45	3.23	2.93	3.12	2.91	3.72	2.11	3.41	2.38	2.03		
102.17	100.87	100.56	101.2	100.19	101.47	100.88	102.1	101.44	101.65	101.8	100.63	102.37	102.4	101.43		
1.52	1.34	1.24	1.21	1.17	1.45	1.36	1.23	1.31	1.23	1.57	0.89	1.44	1	0.85		
100.65	99.53	99.32	99.99	99.02	100.02	99.52	100.87	100.13	100.42	100.23	99.74	100.93	101.4	100.58		
1.88	6.72	6.22	6.76	5.82	6.11	2.26	7.24	4.44	6.7	4.31	7	2.46	9.07	7.61		
5.7	5.41	5.51	5.47	5.49	5.44	5.7	5.47	5.56	5.44	5.51	5.58	5.71	5.43	5.47		
0.15	0.46	0.43	0.44	0.44	0.42	0.19	0.47	0.33	0.45	0.33	0.47	0.15	0.51	0.57		
9.42	9.23	9.2	9.27	9.35	9.17	9.49	9.16	9.38	9.19	9.24	9.3	9.44	9.15	9.23		
—	—	—	—	—	—	—	—	—	0.09	—	—	—	0.07	—		
0.03	0.14	0.1	0.12	0.1	0.11	0.03	0.13	0.07	0.12	0.09	0.11	0.05	0.14	0.17		
0.08	0.22	0.2	0.22	0.19	0.21	0.08	0.22	0.14	22	0.18	0.24	0.09	0.29	0.31		
—	—	—	—	—	—	—	—	—	—	—	—	—	0.04	—		
—	0.06	0.08	0.21	0.07	0.06	0.03	0.09	0.05	0.08	—	0.09	—	0.09	0.08		
1.85	1.71	1.59	1.54	1.5	1.83	1.69	1.56	1.65	1.56	1.94	1.15	1.76	1.29	1.11		
15.39	15.51	15.52	15.6	15.64	15.41	15.51	15.54	15.55	15.58	15.34	15.79	15.45	15.73	15.83		



Mottled - Mafic syenite										Pegmatite									
9	10	CC16A-1	2	3	Core	Rim	Core	Rim	Core	6	7	8	Core	Rim	Core				
2.17	1.95	3.13	3.03	2.12	1.6	2.97	1.54	3.38	4.27	3.65	5.71	3	3.25	1.44					
38.91	38.87	36.84	37.3	38.99	39.85	36.91	40.11	36.53	35.13	35.63	32.32	37.67	37.58	40.64					
51	51.37	48.44	50.74	51.98	52.18	49.52	52.67	49	47.77	49.16	44.79	50.27	49.78	53.83					
0.78	0.7	0.85	—	0.91	0.87	0.84	—	0.68	0.86	0.83	1.06	0.79	1.05	—					
1.5	1.45	2.19	2.4	1.7	0.96	1.98	1.09	2.68	2.93	2.38	4.22	2.2	2.51	0.63					
2.89	2.73	4.34	4.44	3.01	1.9	3.94	2.07	4.54	5.48	4.31	8.24	4.01	4.43	1.4					
—	—	—	—	—	—	0.65	—	—	—	—	1.14	0.43	—	—					
0.98	0.86	1.23	1.32	1.08	0.52	1.23	0.7	1.59	1.57	1.24	2.49	1.22	1.67	0.53					
3.5	3.76	3.75	2.43	2.71	2.34	1.9	3.57	2.2	3.44	2.95	2.06	2.38	2.01	3.83					
101.77	101.7	100.77	101.65	102.52	100.29	99.94	101.76	100.62	101.45	100.15	102.1	101.96	102.29	102.28					
1.47	1.58	1.58	1.02	1.14	0.99	0.8	1.5	0.93	1.45	1.24	0.87	1	0.85	1.61					
100.3	100.12	99.19	100.63	101.38	99.3	99.14	100.26	99.69	100	98.91	101.23	100.96	101.44	100.67					
5.37	5.04	7.76	8.16	5.79	3.38	7.8	3.86	8.81	9.98	7.93	16.09	7.86	8.61	2.56					
5.49	5.47	5.3	5.42	5.54	5.71	5.49	5.59	5.4	5.12	5.24	4.94	5.45	5.47	5.59					
0.36	0.32	0.53	0.52	0.36	0.27	0.52	0.25	0.59	0.73	0.63	1.03	0.51	0.56	0.23					
9.1	9.15	8.82	9.33	9.34	9.46	9.32	9.3	9.17	8.81	9.15	8.67	9.21	9.17	9.37					
0.07	0.06	0.08	—	0.08	0.08	0.08	—	0.06	0.08	0.08	0.1	0.07	0.1	—					
0.09	0.09	0.14	0.15	0.11	0.06	0.13	0.07	0.17	0.19	0.15	0.28	0.14	0.16	0.04					
0.18	0.17	0.27	0.28	0.18	0.12	0.25	0.12	0.29	0.35	0.27	0.54	0.25	0.28	0.08					
0.01	—	—	—	—	—	0.04	—	—	—	—	0.07	0.03	—	—					
0.06	0.05	0.07	0.08	0.07	0.03	0.08	0.04	0.1	0.1	0.08	0.16	0.07	0.1	0.03					
1.85	1.98	2.01	1.32	1.44	1.25	1.05	1.86	1.21	1.87	1.62	1.18	1.29	1.09	1.97					
15.36	15.31	15.22	15.78	15.68	15.81	15.91	15.38	15.78	15.36	15.6	15.8	15.74	15.83	15.34					

Mottled - Mafic syenite						Pegmatite						Mottled - Mafic syenite					
Rim	CC17A-1	2	3	4	5	Core	Rim	CC17B-1	2	3	High	Core	Mid	Rim			
4.11	2.86	5.77	3.12	5.74	3.59	5.11	4.18	4.31	1.23	1.81	3.82	2.31	3.17	3.57			
35.85	37.45	32.43	37.52	31.1	36.42	32.93	35.18	34.88	40.17	39.2	35.08	38.47	36.24	35.61			
48.74	50.12	45.23	50.41	43.66	48.58	45.87	47.55	47.36	52.23	51.49	47.2	50.79	48.4	47.27			
1.03	0.68	1.13	0.61	1.06	0.93	1.05	0.97	0.84	—	0.81	0.83	0.66	0.83	0.83			
3.06	1.91	4.06	2.37	4.58	2.43	3.53	2.6	3.46	0.89	1.29	3	1.7	2.44	2.83			
5.27	4.44	7.89	4.38	8.61	5.14	7.15	5.38	6.01	1.74	2.43	5.76	3.56	4.66	5.4			
—	0.63	0.7	—	0.5	0.63	0.51	0.73	—	—	—	0.64	0.55	0.63	0.59			
1.3	1.45	2.24	1.27	2.52	1.58	2.45	1.61	1.83	0.67	0.82	1.64	1.14	1.47	1.36			
2.94	3.36	2.16	2.54	2.27	4.01	2.21	4	2.67	3.59	3.6	2.84	2.97	2.47	2.76			
102.31	102.91	101.62	102.22	100.04	103.32	100.81	102.2	101.36	100.51	101.45	100.81	102.15	100.3	100.21			
1.24	1.41	0.91	1.07	0.96	1.69	0.93	1.68	1.12	1.51	1.52	1.2	1.25	1.04	1.16			
101.07	101.5	100.71	101.15	99.08	101.63	99.88	100.52	100.24	99	99.93	99.61	100.9	99.26	99.05			
9.63	8.43	14.89	8.02	16.21	9.78	13.74	10.32	11.3	3.3	4.54	11.04	6.95	9.2	10.18			
5.2	5.34	4.94	5.41	4.85	5.17	5.02	5.07	5.17	5.65	5.52	5.21	5.49	5.38	5.29			
0.7	0.48	1.04	0.53	1.06	0.6	0.92	0.71	0.75	0.2	0.3	0.67	0.39	0.56	0.63			
8.95	9.04	8.72	9.2	8.63	8.73	8.85	8.67	8.88	9.29	9.18	8.88	9.17	9.09	8.89			
0.09	0.06	0.11	0.06	0.1	0.08	0.1	0.09	0.08	—	0.07	0.08	0.06	0.08	0.08			
0.19	0.12	0.27	0.15	0.31	0.15	0.23	0.16	0.22	0.05	0.08	0.19	0.11	0.16	0.18			
0.33	0.27	0.52	0.27	0.58	0.32	0.47	0.34	0.39	0.11	0.15	0.37	0.22	0.3	0.35			
—	0.04	0.05	—	0.03	0.04	0.03	0.05	—	—	—	0.04	0.03	0.04	0.04			
0.08	0.09	0.14	0.08	0.17	0.09	0.16	0.1	0.11	0.04	0.05	0.1	0.07	0.09	0.09			
1.59	1.79	1.23	1.37	1.32	2.13	1.26	2.15	1.48	1.88	1.9	1.57	1.59	1.37	1.53			
15.55	15.43	15.78	15.7	15.74	15.18	15.79	15.17	15.61	15.34	15.35	15.54	15.54	15.68	15.54			

Pegmatite	Core										Layered					Low	High	Core			
	5	6	7	8	Rim	8	9	Rim	9	10	Core	Rim	10	DNI-1	1				2	3	4
—	—	—	—	—	Core	Rim	Core	Rim	Core	Rim	Core	Rim	Core	Rim	Core	Rim	Core	Rim	Core	Rim	Core
3.76	3.41	6.64	6.37	4.78	4.76	5.1	5.72	5.4	4.89	5.23	5.32	5.05	4.99	5.11	4.97	5.86	0.84	—	—	—	—
35.4	35.81	30.72	30.6	34.78	1.17	0.83	0.21	0.53	1.06	0.72	0.57	0.77	0.88	0.8	1.05	0.14	—	—	—	—	—
48.26	49.03	42.9	43.08	46.38	8.44	8.61	9.53	9.18	8.53	8.91	9.34	8.9	8.88	8.75	8.6	9.52	—	—	—	—	—
1.03	0.88	1.07	1.1	1.13	0.09	0.1	0.06	0.08	0.12	0.08	0.08	0.1	0.1	—	—	—	—	—	—	—	—
2.74	2.42	4.66	4.39	3.21	0.3	0.21	0.06	0.14	0.28	0.2	0.17	0.2	0.29	0.18	0.26	0.06	—	—	—	—	—
5.02	4.86	8.92	8.54	6.01	0.58	0.38	0.11	0.26	0.53	0.35	0.27	0.41	0.49	0.37	0.53	0.08	—	—	—	—	—
—	0.52	0.8	0.59	0.47	0.04	0.03	—	—	0.06	—	—	0.05	—	0.04	0.06	—	—	—	—	—	—
1.29	1.39	2.82	2.88	1.61	0.19	0.1	—	0.08	0.19	0.1	0.09	0.11	0.13	0.12	0.14	—	—	—	—	—	—
3.1	2.97	2.24	2.49	2.95	1.45	1.62	1.42	1.43	1.36	1.49	1.31	1.65	1.3	1.81	1.37	1.67	—	—	—	—	—
100.6	101.28	100.77	100.05	101.49	101.25	101.25	100.9	102.2	100.42	100.37	101.34	102.09	102.24	101.06	101.75	—	—	—	—	—	—
1.31	1.25	0.94	1.05	1.24	1.14	1.11	1.11	1	1.13	1	1.25	0.97	1.4	1.02	1.36	—	—	—	—	—	—
99.29	100.03	99.83	99	100.25	100.11	99.79	101.2	99.29	99.37	100.09	101.12	100.84	100.04	100.39	—	—	—	—	—	—	—
9.05	9.19	17.2	16.4	11.3	2.72	7.59	16.17	10.13	8.27	11.9	13.94	11.37	15.32	2.22	—	—	—	—	—	—	—
5.2	5.25	4.77	4.76	5.1	5.72	5.4	4.89	5.23	5.32	5.05	4.99	5.11	4.97	5.73	—	—	—	—	—	—	—
0.65	0.59	1.3	1.17	0.83	0.21	0.53	1.06	0.72	0.57	0.77	0.88	0.8	1.05	0.14	—	—	—	—	—	—	—
8.98	9.09	8.44	8.49	8.61	9.53	9.18	8.53	8.91	9.34	8.9	8.88	8.75	8.6	9.52	—	—	—	—	—	—	—
0.09	0.08	0.1	0.11	0.1	0.06	0.08	0.12	0.08	0.1	0.08	0.1	0.1	—	—	—	—	—	—	—	—	—
18	0.15	0.32	0.3	0.21	0.06	0.14	0.28	0.2	0.17	0.2	0.17	0.2	0.29	0.18	0.26	0.06	—	—	—	—	—
0.32	0.31	0.6	0.58	0.38	0.11	0.26	0.53	0.35	0.27	0.41	0.49	0.37	0.53	0.08	—	—	—	—	—	—	—
—	0.03	0.05	0.04	0.03	—	—	0.06	—	—	—	—	0.05	—	0.04	0.06	—	—	—	—	—	—
0.08	0.09	0.18	0.19	0.1	—	0.08	0.19	0.1	0.09	0.11	0.13	0.12	0.14	—	—	—	—	—	—	—	—
1.7	1.62	1.3	1.45	1.62	1.42	1.43	1.36	1.49	1.31	1.65	1.3	1.81	1.37	1.67	—	—	—	—	—	—	—
15.5	15.59	15.69	15.63	15.45	15.68	15.67	15.66	15.59	15.84	15.58	15.8	15.37	15.63	15.52	—	—	—	—	—	—	—

	Layered					Core					Hybrid						
	Rim	DN2-1	2	3	4	Rim	5	6	Rim	6	Rim	6	DN3-1	2	3	4	Low
3.7	3.55	4.03	4.34	4.12	1.27	3.66	7.21	4.45	4.45	5.91	4.78	5.42	3.66	4.07	6.24		
35.48	36.53	35.4	35.96	34.91	40.99	36.22	29.71	34.72	32.09	34.55	33.02	35.94	35.26	31.62			
48.42	49.64	48.54	48.82	47.81	54.04	49.21	42.84	48.33	44.67	47.43	45.33	48.81	48.04	44.76			
0.88	—	0.88	—	—	—	—	—	—	—	—	—	—	0.83	1.19			
2.71	2.6	2.67	2.95	3.25	0.98	2.9	5.23	3.37	4.59	3.51	4.37	0.8	2.91	4.44			
4.69	5.04	5.56	5.74	6.39	1.64	5.12	10.37	6.09	8.8	6.39	7.78	3.12	5.62	8.55			
—	0.73	—	—	0.87	—	—	0.94	—	1	—	0.6	5.62	—	—			
1.55	1.57	1.62	1.56	1.74	—	1.7	3.14	1.76	2.51	1.96	2.13	1.37	1.91	2.49			
2.76	2.6	2.4	2.61	2.41	3.6	2.67	2.72	1.77	2.18	2.02	2.51	2.69	2.43	2.32			
100.19	102.26	101.09	101.99	101.67	102.52	101.48	102.17	101.96	101.74	100.64	101.16	102.02	101.07	101.61			
1.16	1.09	1.01	1.1	1.01	1.52	1.12	1.15	0.75	0.92	0.85	1.06	1.13	1.02	0.98			
99.03	101.17	100.08	100.89	100.66	101	100.36	101.02	101.21	100.82	99.79	100.1	100.89	100.05	100.63			
8.95	9.94	9.85	10.25	12.25	2.62	9.72	19.68	11.22	16.9	11.86	14.88	10.91	10.44	15.48			

5.25	5.32	5.24	5.24	5.18	5.64	5.3	4.59	5.08	4.91	5.19	5	5.26	5.23	4.83			
0.65	0.61	0.7	0.75	0.72	0.21	0.63	1.31	0.77	1.07	0.85	0.97	0.63	0.71	1.13			
9.07	9.14	9.1	9.01	8.98	9.41	9.11	8.37	8.94	8.66	9.03	8.68	9.04	9.02	8.65			
0.08	—	0.08	—	0.07	—	—	—	—	—	—	—	0.07	0.08	0.11			
0.17	0.17	0.17	0.19	0.21	0.06	0.18	0.35	0.21	0.31	0.23	0.29	0.2	0.19	0.3			
0.3	0.32	0.36	0.36	0.41	0.1	0.32	0.69	0.39	0.58	42	0.51	0.36	0.36	0.56			
—	0.05	—	—	0.06	—	—	0.06	—	0.07	—	0.04	—	—	—			
0.1	0.1	0.1	0.1	0.11	—	0.1	0.2	0.11	0.16	0.12	0.14	0.08	0.12	0.16			
1.53	1.41	1.33	1.42	1.34	1.85	1.46	1.57	1.77	1.24	1.13	1.42	1.47	1.35	1.32			
15.62	15.69	15.75	15.65	15.74	15.41	15.66	15.58	15.5	15.76	15.84	15.63	15.65	15.72	15.74			

				Hybrid										
Low	High	Core	Rim	Core	Rim	DNA-1	2	3	4	5	Core	Rim	DNS-1	2
4.37	7.1	3.83	6.46	0.99	3.46	2.38	1.77	2.45	2.14	2.41	1.2	2.32	4.21	2.33
35.25	30.4	36	31.77	41.71	36.52	37.74	39.3	38.67	39.04	38.61	40.34	38.75	34.13	38.2
48.24	42.84	48.85	44.81	54.9	49.42	49.78	52.4	51.34	51.67	52.12	53.01	50.94	47.89	51.37
—	—	—	—	—	—	0.76	0.82	—	0.82	—	—	—	0.91	0.67
3.63	5.39	2.72	4.62	0.61	2.93	1.41	1.21	1.91	1.33	1.46	0.71	1.5	3.24	1.59
5.88	10.11	5.67	8.8	1.33	5.43	3.51	1.95	3.57	2.75	3.25	1.42	2.91	6.34	3.02
—	1.04	0.82	0.88	—	1.2	0.51	—	—	—	0.52	—	—	0.92	—
1.95	3.25	1.55	2.8	—	—	1.2	0.89	1.18	0.8	1.44	0.65	1.02	1.86	0.84
2.05	2.05	2.64	2.2	3.14	2.61	3.45	2.96	3.21	3.03	2.65	3.39	3.78	2.66	2.24
101.37	102.17	102.08	102.33	102.69	101.57	100.74	101.29	102.35	101.59	102.45	100.73	101.23	102.16	100.26
0.86	0.86	1.11	0.93	1.32	1.1	1.45	1.25	1.35	1.28	1.12	1.43	1.59	1.12	0.94
100.51	101.31	100.97	101.4	101.37	100.47	99.29	100.04	101	100.31	101.33	99.3	99.64	101.14	99.32
11.46	19.79	10.76	17.1	1.94	9.56	6.63	4.05	6.66	4.88	6.67	2.78	5.43	12.36	5.45
<hr/>														
5.25	4.72	5.27	4.84	5.73	5.34	5.43	5.58	5.47	5.54	5.5	5.66	5.46	5.08	5.56
0.77	1.3	0.66	1.16	0.16	0.6	0.4	0.3	0.41	0.36	0.41	0.2	0.39	0.74	0.4
9.09	8.42	9.05	8.64	9.55	9.14	9.06	9.41	9.19	9.27	9.4	9.42	9.09	9.02	9.47
—	—	—	—	—	—	0.07	0.07	—	0.07	—	—	—	0.09	0.06
0.24	0.36	0.17	0.31	0.04	0.19	0.09	0.07	0.12	0.08	0.09	0.04	0.09	0.21	0.1
0.38	0.68	0.36	0.58	0.08	0.34	0.22	0.12	0.22	0.17	0.2	0.09	0.18	0.41	0.19
—	0.07	0.05	0.06	—	—	0.03	—	—	—	0.03	—	—	0.06	—
0.12	0.21	0.1	0.18	—	0.07	0.07	0.05	0.07	0.05	0.09	0.04	0.06	0.12	0.05
1.14	1.19	1.44	1.25	1.61	1.42	1.85	1.57	1.7	1.61	1.41	1.78	1.99	1.48	1.22
15.85	15.77	15.65	15.77	15.57	15.67	15.37	15.61	15.48	15.54	15.72	15.45	15.26	15.72	15.84

Pegmatite														
Low			High			Core			Rim					
3	4	5	5	5	DN6-1	2	3	4	5	6	6			
Pegmatite														
Core			Rim			Pegmatite			Core					
3	4	5	5	5	DN7-1	2	3	2	3	3	3			
3.66	2.56	3.14	3.65	3.26	2.39	2.69	0.64	4.49	3.08	0.98	5.58	3.14	2.23	3.07
35.67	36.73	36.11	35.32	36.23	37.88	37.51	40.31	34.18	36.63	40.14	32.43	36.21	37.69	37.01
48.8	50.11	49.57	48.49	48.88	50.41	50.18	52.4	46.3	49.55	52.46	45.23	48.75	50.57	49.47
0.72	0.86	0.76	—	0.9	0.71	0.83	1.45	0.7	0.83	—	—	1.04	0.79	—
2.84	2.24	2.43	3.28	2.17	1.67	2.04	0.62	3.6	2.11	0.76	4.36	2.66	1.75	2.48
5.15	3.95	4.56	5.73	4.55	3.02	3.66	0.89	6.7	4.2	1.84	7.94	4.28	3.17	4.44
—	—	—	—	—	—	—	—	—	—	—	—	—	—	0.63
1.79	1.24	1.49	1.55	1.53	0.96	0.99	0.76	1.74	1.11	0.7	2.04	1.3	1.03	1.55
2.8	2.83	3.15	2.67	3.2	3.16	2.75	2.94	2.55	3.1	3.32	2.51	2.76	3.13	2.64
101.51	100.52	101.28	100.69	100.71	100.2	100.64	100.02	100.32	100.61	100.19	100.09	100.14	100.36	101.29
1.18	1.19	1.33	1.12	1.35	1.33	1.16	1.24	1.07	1.31	1.4	1.06	1.16	1.32	1.11
100.33	99.33	99.95	99.57	99.36	98.87	99.48	98.78	99.25	99.3	98.79	99.03	98.98	99.04	100.18
9.78	7.43	8.48	10.56	8.25	5.65	6.69	2.27	12.04	7.42	2.6	14.34	8.24	5.95	9.1
Pegmatite														
5.23	5.38	5.25	5.24	5.28	5.46	5.45	5.74	5.14	5.33	5.68	4.95	5.34	5.45	5.4
0.63	0.44	0.54	0.64	0.56	0.41	0.46	0.11	0.8	0.53	0.16	1.01	0.55	0.38	0.53
9.05	9.29	9.13	9.11	9.02	9.2	9.22	9.45	8.81	9.12	9.4	8.75	9.1	9.26	9.14
0.07	0.08	0.07	—	0.08	0.06	0.08	0.13	0.07	0.08	—	—	0.1	0.07	—
0.18	0.14	0.15	0.21	0.14	0.1	0.13	0.04	0.24	0.13	0.05	0.29	0.17	0.11	0.16
0.33	0.25	0.29	0.37	0.29	0.19	0.23	0.05	0.44	0.26	0.11	0.52	0.27	0.2	0.28
0.03	—	—	—	—	—	—	—	—	—	—	—	—	—	0.04
0.11	0.08	0.09	0.1	0.09	0.06	0.06	0.05	0.11	0.07	0.04	0.13	0.08	0.06	0.1
1.54	1.55	1.71	1.48	1.74	1.7	1.49	1.57	1.43	1.68	1.76	1.43	1.52	1.69	1.44
15.63	15.66	15.55	15.67	15.47	15.49	15.63	15.57	15.6	15.52	15.45	15.65	15.61	15.53	15.64

Core	Layered						Core	Layered						Core	
	Rim	DN8-1	2	3	4	5		Rim	High	Low	DN9-1	2	3		4
4	4	DN8-1	2	3	4	5	4	5	5	DN9-1	2	3	4	5	6
3.8	5.35	3.59	3.35	3.31	1.2	3.74	3.59	2.52	5.56	3.78	1.14	4.35	7.33	2.82	
35.32	32.24	36.46	37.2	36.42	40.2	35.61	34.95	38.6	32.78	35.57	40.87	34.33	28.08	36.94	
48.07	45.01	48.7	50.21	49.41	52.81	48.91	48.1	52.38	45.08	48.53	53.56	46.98	40.61	49.52	
—	1.14	0.97	—	1	—	—	0.83	—	0.92	0.88	—	1.15	1.02	0.99	
3.15	4.2	2.75	2.29	2.23	1.16	3.31	3.11	1.84	4.04	2.73	0.75	3.2	5.78	1.51	
5.69	8.02	4.9	4.54	4.59	1.86	5.74	5.2	3.54	7.68	4.76	1.57	5.51	10.2	3.95	
—	0.86	—	—	0.69	—	—	—	—	0.83	—	—	—	0.71	0.59	
1.62	2.33	1.43	1.46	1.34	0.57	1.77	1.68	1.05	2.25	1.66	—	1.74	3.1	1.94	
2.24	1.91	2.44	2.6	2.69	3.25	2.46	2.37	2.9	2.19	3.2	3.33	2.44	2.42	3.16	
99.9	101.07	101.23	101.64	101.67	101.05	101.55	99.83	102.83	101.34	101.11	101.21	99.7	99.27	101.42	
0.94	0.8	1.03	1.09	1.13	1.37	1.04	1	1.22	0.92	1.35	1.4	1.03	1.02	1.33	
99.05	100.27	100.2	100.55	100.54	99.68	100.51	98.83	101.61	100.42	99.76	99.81	98.67	98.25	100.09	
10.46	15.51	9.08	8.29	8.85	3.59	10.82	9.99	6.43	14.9	9.15	2.32	10.45	19.79	7.99	
5.3	4.98	5.35	5.39	5.32	5.66	5.26	5.26	5.46	4.99	5.2	5.7	5.17	4.51	5.35	
0.67	0.98	0.62	0.57	0.57	0.2	0.64	0.64	0.42	1	0.65	0.19	0.77	1.39	0.48	
9.13	8.8	9.05	9.2	9.13	9.41	9.16	9.14	9.38	8.68	8.97	9.45	8.96	8.26	9.07	
—	0.11	0.09	—	0.09	—	0.08	—	—	0.09	0.08	—	0.11	0.1	0.09	
0.21	0.28	0.18	0.14	0.14	0.07	0.2	0.2	0.11	0.27	0.17	0.05	0.21	0.4	0.1	
0.37	0.56	0.31	0.28	0.29	0.11	0.34	0.34	0.22	0.51	0.3	0.09	0.36	0.71	0.25	
—	0.06	—	—	0.04	—	—	—	—	0.05	—	—	—	0.05	0.04	
0.1	0.15	0.09	0.09	0.08	0.03	0.11	0.11	0.06	0.14	0.1	—	0.11	0.21	0.12	
1.26	1.1	1.34	1.4	1.47	1.71	1.36	1.33	1.53	1.25	3.2	1.73	1.38	1.45	1.71	
15.78	15.89	15.68	15.68	15.66	15.49	15.75	15.78	15.65	15.74	15.48	15.47	15.7	15.64	15.49	

Mid	Rim	Core	Outer Core	Inner Rim	Rim	Massive										Hybrid			
						DN10 - 1	2	3	4	5	Core	Rim	DN11 - 1	Core					
1.42	2.86	3.54	2.52	1.29	4.73	4.94	2.84	3.92	3.03	3.48	1.5	3.23	2.66	2.8					
39.97	36.52	36.42	37.62	39.54	34.25	33.53	35.98	34.91	37.45	35.74	39.9	36.33	37.36	37.09					
52.2	49.39	48.73	50.44	52.47	47.04	45.9	46.07	48.15	50.13	48.73	52.79	49.39	50.64	49.05					
—	0.77	—	0.88	—	0.98	1.21	—	—	—	0.94	0.79	1.03	0.89	0.68					
0.87	2.15	1.99	1.58	0.64	3.42	3.74	2.39	3.25	2.15	2.25	1.26	2.47	2.36	2.24					
1.54	4.07	4.23	2.97	1.71	5.72	7.12	7.28	5.64	3.81	4.56	2.41	4.57	4.03	4.03					
—	—	—	—	—	—	0.8	0.99	—	—	0.58	—	—	0.47	0.47					
0.53	0.95	2	0.97	—	1.84	2.06	3.2	1.5	1.45	1.54	—	1.31	1.42	1.71					
3.75	2.8	2.99	2.64	3.61	2.38	2.29	2.86	2.34	2.71	2.43	2.64	2.77	2.25	2.88					
100.29	99.5	99.9	99.62	99.26	100.36	101.58	101.1	99.71	100.77	100.25	101.29	101.1	102.07	100.94					
1.58	1.18	1.26	1.11	1.52	1	0.96	1.2	0.99	1.14	1.02	1.11	1.17	0.95	1.21					
98.71	98.32	98.64	98.51	97.74	99.36	100.62	99.9	98.72	99.63	99.23	100.18	99.93	101.12	99.73					
2.94	7.17	8.22	5.52	2.35	10.98	13.72	13.86	10.39	7.41	8.93	3.67	8.35	8.28	8.45					
5.61	5.38	5.33	5.49	5.61	5.14	5.06	5.36	5.25	5.43	5.31	5.67	5.32	5.45	5.41					
0.24	0.5	0.61	0.44	0.22	0.84	0.88	0.5	0.7	0.52	0.61	0.25	0.56	0.46	0.48					
9.27	9.21	9.03	9.32	9.42	8.93	8.77	8.68	9.16	9.2	9.16	9.49	9.15	9.34	9.05					
—	0.07	—	0.08	—	0.09	0.11	—	—	—	0.09	0.07	0.1	0.08	0.06					
0.05	0.14	0.13	0.1	0.04	0.22	0.25	0.16	0.21	0.14	0.15	0.08	0.16	0.15	0.14					
0.09	0.26	0.27	0.19	0.1	0.37	0.47	0.47	0.37	0.24	0.29	0.15	0.29	0.25	0.25					
—	—	—	—	—	—	0.05	0.06	—	—	0.04	—	—	0.03	0.03					
0.03	0.06	0.12	0.06	—	0.12	0.13	0.2	0.1	0.09	0.1	—	0.08	0.09	0.11					
1.96	1.54	1.64	1.44	1.91	1.33	1.29	1.59	1.32	1.48	1.35	1.4	1.51	1.23	1.57					
15.3	15.62	15.49	15.67	5.39	15.72	15.73	15.43	15.78	15.62	15.75	15.7	15.64	15.85	15.54					

Rim	Core	Rim	Core	Rim	Core	Rim	Core	Rim	Core	Rim	Low	High
2	3	3	4	4	5	5	6	6	7	7		
4.2	2.46	4.2	0.98	4.31	3.78	2.08	2.76	4.31	1.14	3.8		
33.98	37.34	34.99	41.27	34.53	35.3	38.93	37.65	34.21	41	35.3		
46.51	50.18	47.18	53.84	47.44	48.15	51.95	50.49	47.22	53.93	47.89		
1.13	0.87	1.18	0.52	1.1	0.82	0.72	0.83	0.94	—	0.86		
3.36	1.85	3.29	0.58	3.15	2.94	1.57	2.15	3.05	0.83	2.88		
6.51	3.87	5.54	1.23	5.97	5.56	3.04	3.85	6.36	1.32	5.7		
0.88	0.58	0.47	—	0.62	—	—	—	0.49	—	0.47		
2.25	1.38	1.92	0.44	2.17	1.7	1.21	1.13	1.9	—	1.89		
2.49	3.03	2.62	3.59	2.39	1.96	1.6	3.13	2.97	3.54	2.29		
101.31	101.56	101.39	101.56	101.69	100.2	102.52	101.99	101.45	101.75	101.1		
1.05	1.28	1.1	1.51	1.01	0.83	0.67	1.32	1.25	1.49	0.96		
100.26	100.28	100.29	100.05	100.68	99.37	101.85	100.67	100.2	100.36	100.14		
13	7.68	11.22	2.25	11.91	10.2	5.82	7.13	11.8	2.15	10.94		
5.12	5.4	5.19	5.68	5.15	5.31	5.51	5.39	5.08	5.67	5.27		
0.75	0.42	0.74	0.16	0.76	0.67	0.35	0.47	0.76	0.19	0.67		
8.87	9.19	8.86	9.37	8.96	9.17	9.3	9.15	8.87	9.44	9.04		
0.11	0.08	0.11	0.05	0.1	0.08	0.06	0.07	0.09	—	0.08		
0.22	0.12	0.21	0.03	0.2	0.19	0.1	0.13	0.2	0.05	0.19		
0.42	0.24	0.36	0.07	0.39	0.36	0.19	0.24	0.41	0.08	0.37		
0.06	0.04	0.03	—	0.04	—	—	—	0.03	—	0.03		
0.14	0.08	0.12	0.03	0.14	0.11	0.07	0.07	0.12	—	0.12		
1.4	1.64	1.45	1.85	1.33	1.1	1.6	1.67	1.65	1.83	1.28		
15.69	15.56	15.61	15.39	15.74	15.89	15.58	15.52	15.55	15.42	15.76		



	Layered		Massive		Hybrid					
	CC2 - 1	CC3 - 1	2	3	4	5	6	CC11 - 1	2	
3	6.83	6.44	6.51	6.61	6.81	6.61	6.48	7.17	7.25	6.91
4	—	—	—	0.28	30.23	0.28	—	—	0.25	—
30.6	31	30.81	30.46	30.65	29.98	30.43	30.57	30.55	30.24	30.77
30.1	30.49	31.9	31.46	31.44	1.24	30.72	31.62	29.86	29.74	30.48
1.1	1.07	1.36	0.92	0.76	0.5	1.53	0.94	0.85	1.05	1.08
0.41	0.46	—	—	0.49	1.2	0.51	0.67	0.48	0.38	0.5
1.03	0.93	—	—	1.57	—	1.31	1.82	1	1.83	1.85
14.01	13.75	13.83	14.36	14.14	13.49	13.63	13.48	14.83	14.01	14.36
10.96	10.64	8.86	9.81	9.71	12.19	9.82	9.71	11.75	12.31	11.81
4.21	4.32	4.72	5.05	4.53	3.89	4.49	4.27	3.38	3.34	3.54
99.04	99.5	97.92	98.58	100.2	99.54	99.32	99.55	99.86	100.4	101.3
1.77	1.82	1.99	2.13	1.91	1.64	1.89	1.8	1.42	1.41	1.49
97.27	97.68	95.93	96.45	98.29	97.9	97.43	97.75	98.44	98.99	99.81
7.75	7.8	8.04	7.91	7.67	7.68	7.66	7.73	7.8	7.72	7.69
0.21	0.2	0.27	0.19	0.14	0.24	0.29	0.18	0.16	0.23	0.23
0.22	0.2	—	—	—	—	0.28	0.38	0.21	0.2	0.2
0.09	0.1	—	—	0.1	0.11	0.11	0.14	0.1	0.09	0.12
—	—	—	—	0.11	—	0.1	—	—	0.11	—
1.73	1.69	1.75	1.82	1.73	1.67	1.67	1.66	1.85	1.69	1.73
1.25	1.21	1.04	1.15	1.1	1.4	1.12	1.11	1.36	1.37	1.34
11.25	11.2	11.1	11.07	10.85	11.1	11.23	11.2	11.48	11.41	11.31
8.17	8.22	8.92	8.75	8.43	8.16	8.28	8.56	8.17	8.11	8.15
3.26	3.33	3.26	3.27	3.21	3.35	3.23	3.17	3.55	3.34	3.29
11.43	11.55	12.18	12.02	11.64	11.51	11.51	11.73	11.72	11.45	11.44
3.37	3.43	2.73	2.9	3.59	3.13	3.58	3.42	2.73	3.11	3.22

## Representative Analyses of Britholite

Rock Type	Layered	Layered		Hybrid		Hybrid		Hybrid		Hybrid		Hybrid		
Sample	DN1-1	2	DN2-1	2	3	4	DN3-1	2	3	4	5	6	DN4-1	2
SiO2	16.18	20.57	16.06	16.35	17.59	18.03	17.73	17.5	17.79	17.34	17.35	18.85	20.16	18.86
P2O5	7.89	—	7.35	9.1	8.69	7.57	7.52	8.49	6.52	7.55	8.45	2.51	2.4	3.57
CaO	19.74	11.24	18.4	21.49	21.61	20.94	20.11	21.52	19.6	19.69	20.99	14.59	15.57	15.22
Y2O3	0.87	—	1.59	1.26	—	—	1.55	1.51	1.63	1.37	1.34	1.61	1.98	1.18
La2O3	13.24	18.92	13.2	14.3	14.82	15.21	15.24	14.51	14.56	15.19	14.58	15.83	13.85	15.77
Ce2O3	24.64	35.06	25.16	25.41	25.66	26.26	26.07	24.32	25.23	26.62	25.95	30.77	27.93	29.62
Pr2O3	2.53	2.76	2.6	2	1.8	2.02	—	1.61	2.03	1.88	1.48	2.84	2.11	2.63
Nd2O3	6.05	8.45	6.63	6.03	6.27	6.18	6.41	6.21	6.48	6.1	5.6	8.23	7.46	7.64
Sm2O3	1.12	—	1.23	—	—	—	—	—	0.85	—	—	—	—	—
Gd2O3	0.86	—	—	—	—	—	—	—	—	—	—	—	—	—
ThO2	6.51	1.84	5.89	4.53	4.73	5.09	5.06	4.93	4.6	4.53	4.76	5.18	8.78	5.47
UO3	—	—	—	—	—	—	—	—	—	—	—	—	—	—
F	—	—	1.31	—	—	—	1.12	1.22	—	—	—	—	0.83	—
Cl	—	0.24	—	0.17	0.3	0.24	0.16	—	—	0.15	—	—	—	—
Total	99.63	99.6	99.62	100.65	101.48	101.53	100.97	101.84	99.31	100.41	100.51	100.41	101.07	99.97
O-F, Cl	—	0.1	0.55	0.07	0.13	0.1	0.54	0.51	—	0.06	—	—	0.35	—
Total	99.63	99.5	99.07	100.58	101.35	101.43	100.43	101.33	99.31	100.35	100.51	100.41	100.72	99.97
REEZ03	48.44	65.19	48.82	47.74	48.55	49.67	47.72	46.65	49.15	49.79	47.61	57.67	51.35	55.66

Cation Assignment - Based on 36 Oxygens														
P	2.35	—	2.18	2.65	2.5	2.21	2.15	2.38	1.97	2.24	2.47	0.81	0.74	1.14
Si	5.69	8.25	5.62	5.63	5.97	6.21	6	5.78	6.36	6.09	5.98	7.23	7.38	7.11
Ca	7.44	4.82	6.9	7.93	7.86	7.73	7.29	7.62	7.51	7.41	7.75	5.99	6.1	6.15
Y	0.28	—	0.3	0.23	—	—	0.28	0.27	0.31	0.26	0.25	0.33	0.39	0.24
La	1.72	2.8	1.7	1.82	1.86	1.93	1.9	1.77	1.92	1.97	1.85	2.24	1.87	2.19
Ce	3.18	5.15	3.22	3.2	3.19	3.31	3.23	2.94	3.3	3.42	3.27	4.32	3.74	4.09
Pr	0.32	0.4	0.33	0.25	0.22	0.25	—	0.19	0.26	0.24	0.19	0.4	0.28	0.36
Nd	0.76	1.21	0.83	0.74	0.76	0.76	0.77	0.73	0.83	0.77	0.69	1.13	0.97	1.03
Sm	0.14	—	0.15	—	—	—	—	—	0.1	—	—	—	—	—
Gd	0.1	—	—	—	—	—	—	—	—	—	—	—	—	—
Th	0.78	0.17	0.47	0.35	0.37	0.4	0.39	0.37	0.37	0.36	0.37	0.45	0.73	0.47
U	—	—	—	—	—	—	—	—	—	—	—	—	—	—
F	—	—	1.45	—	—	—	1.19	1.27	—	—	—	—	—	—
Cl	—	0.12	—	0.1	0.17	0.14	0.09	—	—	0.15	—	—	—	—
Cation Total	22.76	22.8	21.68	22.81	22.73	22.81	22.01	22.06	22.94	22.77	22.82	22.9	22.2	22.76

	DNS			Layered					Layered					Massive	
	1	2	3	1	2	3	4	5	1	2	3	4	5	1	2
19	17.67	19.49	19.91	19.39	18.3	18.34	16.08	16.96	17.16	18.9	17.43	18.8	21.8	20.37	
6.47	5.54	0.77	5.06	2.7	6.81	6.51	8.29	9.8	9.13	7.1	8.7	1.32	—	2.26	
18.91	17.22	7.64	18.96	14.07	19.65	19.2	20.83	21.46	20.95	20.59	21.37	11.01	12.01	12.9	
1.68	1.67	1.93	1.52	1.46	1.87	2.01	1.72	1.63	1.92	1.8	1.62	—	—	2.31	
14.81	14.72	16.27	14.37	14.49	13.93	15.25	13.49	12.18	13.21	13.97	13.75	15.24	18.67	12.81	
26.4	27	38.27	24.83	27.92	25.82	26.81	24.66	22.4	24.04	24.69	23.99	38.57	33.08	30.24	
2.24	2.01	3.46	2.55	2.94	2.11	1.42	2.22	1.94	1.79	1.75	1.92	3.65	2.81	3.36	
6.44	6.94	11.75	6.34	7.49	6.41	6.63	6.39	5.78	6.48	6.41	5.7	10.62	8.62	11.06	
—	—	—	0.84	1.2	—	—	—	0.8	0.72	—	—	—	—	1.09	
—	—	—	1.15	—	—	—	—	1.09	—	—	—	—	—	1.16	
4.93	4.55	—	5.47	6.25	4.83	4.71	5.03	4.68	4.86	5.64	5.47	1.4	—	0.78	
—	0.69	—	—	—	—	—	—	—	—	—	—	—	—	—	
0.52	—	—	—	—	—	—	—	—	—	—	—	—	—	—	
101.4	98.01	99.58	101	97.91	99.73	100.89	98.7	98.72	100.27	100.85	99.94	100.61	98.83	98.34	
0.22	—	—	—	—	—	—	—	—	—	—	—	—	—	—	
101.18	98.01	99.58	101	97.91	99.73	100.89	98.7	98.72	100.27	100.85	99.94	100.61	98.83	98.34	
49.89	50.67	69.75	50.08	54.04	48.27	50.11	46.76	44.19	46.24	46.82	45.36	68.08	65.02	60.5	
1.89	1.74	0.27	1.51	0.88	2.03	1.94	2.49	2.83	2.65	2.07	2.53	0.45	—	0.73	
6.54	6.55	7.92	7.03	7.49	6.44	6.45	5.71	5.78	5.87	6.51	5.98	7.51	8.52	7.76	
6.98	6.84	3.33	7.17	5.83	7.41	7.24	7.93	7.84	7.68	7.59	7.86	4.71	5.03	5.26	
0.31	0.33	0.42	0.29	0.3	0.35	0.38	0.33	0.3	0.35	0.33	0.3	—	—	0.47	
1.88	2.01	2.44	1.87	2.06	1.81	1.98	1.77	1.53	1.67	1.77	1.74	2.24	2.69	1.8	
3.33	3.66	5.7	3.21	3.95	3.33	3.46	3.21	2.8	3.01	3.11	3.02	5.64	4.74	4.22	
0.28	0.27	0.51	0.33	0.41	0.27	0.18	0.29	0.24	0.22	0.22	0.24	0.53	0.4	0.47	
0.79	0.92	1.71	0.8	1.03	0.81	0.83	0.81	0.7	0.79	0.79	0.7	1.51	1.2	1.5	
—	—	—	0.1	0.16	—	—	—	0.09	0.08	—	—	—	0.15	0.14	
—	—	—	0.14	—	—	—	—	0.12	—	—	—	—	0.09	0.15	
0.39	0.38	—	0.44	0.55	0.39	0.38	0.41	0.36	0.38	0.44	0.43	0.13	—	0.07	
—	0.05	—	—	—	—	—	—	—	—	—	—	—	—	—	
0.56	—	—	—	—	—	—	—	—	—	—	—	—	—	—	
22.38	22.76	22.29	22.89	22.67	22.84	22.84	22.94	22.61	22.71	22.83	22.8	22.73	22.84	22.66	

	Layered			Layered			Massive			Pegmatite						Massive	
	CC1B - 1	2	CC2 - 1	CC3 - 1	2	3	4	5	6	CC5 - 1	2	3	CC6 - 1	2			
3	18.21	22.07	18.29	15.1	17.04	15.21	17.62	18.31	18.58	16.18	24.32	18.78	19.07	17.3	19.87		
7.15	2.28	6.92	6.15	9.71	10.08	7.51	5.49	4.34	11.28	—	3.87	3.35	6.19	3.5			
20.04	12.59	18.22	10.53	21.9	18.86	20.63	17.35	14.22	23.56	9.19	12.85	12.8	13.77	13.48			
1.49	1.72	1.94	1.89	1.99	1.68	1.95	1.62	1.87	1.72	—	1.23	1.35	1.93	1.57			
13.89	19.66	14.45	14.05	14.29	14.68	13.26	13.97	14.73	12.78	23.49	16.47	15.32	14.6	16.33			
25.13	31.92	26.38	30.02	24.54	26.62	24.08	25.67	27.67	24.14	33.12	31.32	30.48	27.74	31.42			
2.31	2.16	1.94	3.12	—	2.18	1.85	2.41	2.53	1.99	2.78	2.55	3.47	2.68	2.77			
6.41	6.64	6.53	8.8	5.85	7.1	6.51	7.24	7.94	6.19	7.43	8.07	8.67	7.98	8.15			
—	—	—	1.79	—	—	—	0.99	—	—	—	0.85	—	0.64	—			
—	—	—	1.23	—	—	—	0.83	—	—	—	—	—	0.99	—			
5.69	—	5.68	2.33	4.48	4.7	5.34	5.6	5.66	3.94	—	4.5	3.91	4.4	3.17			
—	—	—	—	—	—	—	0.85	0.92	—	—	—	—	0.77	—			
—	—	—	—	—	1.11	—	—	—	—	—	—	—	—	—			
100.34	99.04	100.34	95	99.79	102.24	98.77	100.34	98.46	101.79	100.33	100.48	99.95	99.76	100.27			
—	—	—	—	—	0.47	—	—	—	—	—	—	—	0.32	—			
100.34	99.04	100.34	95	99.79	101.77	98.77	100.34	98.46	101.79	100.33	100.48	99.95	99.44	100.27			
47.74	60.38	49.3	59.01	44.68	50.58	45.7	51.11	52.87	45.1	66.82	59.26	59.47	54.63	58.67			
2.12	0.71	2.06	2.1	2.78	2.88	2.24	1.69	1.38	3.14	—	1.24	1.08	1.91	1.11			
6.37	8.03	6.46	6.09	5.77	5.14	6.2	6.65	6.97	5.33	9.2	7.11	7.28	6.3	7.42			
7.5	4.9	6.9	4.56	7.95	6.8	7.78	6.74	5.71	8.31	3.72	5.22	5.23	5.37	5.39			
0.28	0.33	0.36	0.4	0.36	0.3	0.36	0.32	0.37	0.3	—	0.25	0.27	0.37	0.31			
1.79	2.64	1.88	2.09	1.78	1.83	1.72	1.87	2.04	1.55	3.28	2.3	2.16	1.96	2.25			
3.22	4.25	3.41	4.43	3.05	3.28	3.1	3.41	3.8	2.91	4.59	4.35	4.26	3.7	4.29			
0.29	0.29	0.25	0.46	—	0.26	0.24	0.32	0.35	0.24	0.38	0.35	0.48	0.36	0.38			
0.8	0.86	0.82	1.27	0.71	0.86	0.82	0.94	1.06	0.73	1	1.09	1.18	1.04	1.09			
—	—	—	0.25	—	—	—	0.12	—	—	—	0.11	0.2	0.08	—			
—	—	—	0.17	—	—	—	0.1	—	—	—	—	—	0.12	—			
0.45	—	0.46	0.21	0.35	0.36	0.43	0.46	0.48	0.29	—	0.39	0.34	0.36	0.27			
—	—	—	—	—	—	—	0.07	0.07	—	—	—	—	0.06	—			
—	—	—	—	—	1.19	—	—	—	—	—	—	—	0.89	—			
22.82	22.15	22.6	22.03	22.75	22.9	22.89	22.69	22.23	22.8	22.17	22.41	22.48	21.64	22.5			





Massive				
4	CC13 - 1	2	3	4
—	—	—	—	0.39
—	—	—	—	0.31
2.03	1.94	1.89	1.07	2.83
29.01	30.34	30.14	29.77	29.7
26.71	27.93	27.89	27.44	26.99
31.86	34.83	35.26	33.65	34.32
1.76	2.87	2.7	2.24	3.81
2.75	—	—	3.18	—
2.6	1.32	1.34	2.28	0.83
—	1.14	—	—	—
96.72	100.38	99.23	99.63	99.17
—	0.48	—	—	—
96.72	99.9	99.23	99.63	99.17
<hr/>				
4	3.94	4.01	4	3.96
3.3	3.4	3.53	3.4	3.44
0.33	0.47	0.3	0.17	0.45
0.2	0.31	0.3	0.25	0.43
—	—	—	—	0.06
3.94	3.89	3.98	3.95	3.86
—	—	—	—	0.1
0.18	—	—	0.21	—
0.16	0.08	0.08	0.14	0.05
—	0.47	—	—	—
12.11	11.92	12.19	12.11	12.35



3	Hybrid		Massive		Massive		Massive		Massive	
	CC9-1	CC12-1	2	CC13-1 High	1 Low	2	3	1 Low	2	3
—	—	—	—	—	—	—	—	—	—	—
7.18	5.55	0.77	—	0.48	0.58	0.92	—	—	—	—
5.81	15.54	3.91	2.81	3.83	4.25	5.3	2.92	—	—	—
15.57	6.55	5.26	9.37	8.56	9	9.98	15.66	—	—	—
2.23	2.07	9.12	6.8	4.29	7.95	9.93	8.39	—	—	—
—	—	5.91	1.84	3.76	3.9	2.33	1.39	—	—	—
2.3	5.41	1.66	—	—	—	—	—	—	—	—
32.2	59.08	42.22	52.69	52.1	48.06	46.28	63.23	—	—	—
6.55	0.63	5.23	3.41	4.71	6.75	6.06	1.65	—	—	—
20.31	0.62	15.64	11.71	15.65	13.25	13.56	3.55	—	—	—
2.14	—	1.54	1.3	1.93	1.5	1.69	—	—	—	—
4.16	—	5.34	3.91	4.07	3.4	1.97	1.25	—	—	—
—	—	—	—	—	—	—	—	—	—	—
—	—	—	0.6	—	—	—	—	—	—	—
98.44	95.45	96.59	94.44	99.38	98.65	98.02	98.03	—	—	—
98.44	95.45	96.59	94.44	99.38	98.65	98.02	98.03	—	—	—
33.16	1.25	27.75	20.33	26.36	24.9	23.28	6.45	—	—	—
0.41	0.3	0.24	0.17	0.23	0.25	0.31	0.16	—	—	—
0.67	0.26	0.42	0.31	0.19	0.35	0.43	0.34	—	—	—
—	—	—	—	0.03	0.04	0.06	—	—	—	—
0.11	0.09	0.31	0.09	0.19	0.19	0.11	0.07	—	—	—
—	—	—	—	—	—	—	—	—	—	—
0.36	0.89	0.35	0.61	0.55	0.57	0.62	0.9	—	—	—
—	—	—	—	—	—	—	—	—	—	—
—	—	0.09	—	—	—	—	—	—	—	—
0.06	0.14	—	—	—	—	—	—	—	—	—
0.84	1.43	1.18	1.45	1.4	1.27	1.21	1.54	—	—	—
0.14	0.01	0.12	0.08	0.1	0.15	0.13	0.03	—	—	—
0.43	0.01	0.35	0.26	0.34	0.28	0.29	0.07	—	—	—
0.05	—	0.04	0.03	0.04	0.03	0.04	—	—	—	—
0.09	—	0.12	0.09	0.09	0.07	0.04	0.02	—	—	—
—	—	—	—	—	—	—	—	—	—	—
—	—	—	—	—	—	—	—	—	—	—
—	—	—	0.01	—	—	—	—	—	—	—
—	—	—	—	—	—	—	—	—	—	—
3.16	3.13	3.22	3.1	3.16	3.2	3.24	3.13	—	—	—

## Representative Analyses of Fergusonite

Rock Type Sample	Layered		Pegmatite			
	DN1 - 1	2	DN6 - 1	2	3	4
CaO	0.71	0.96	0.33	0.34	—	0.3
Y <sub>2</sub> O <sub>3</sub>	32.66	32.49	31.79	30.64	31.27	30.49
Nb <sub>2</sub> O <sub>5</sub>	50.16	51.49	48.05	47.59	47.66	47.58
Ce <sub>2</sub> O <sub>3</sub>	1.57	0.91	1.22	1.33	1.36	1.65
Nd <sub>2</sub> O <sub>3</sub>	2.04	1.62	2.08	2.18	2.15	1.92
Sm <sub>2</sub> O <sub>3</sub>	—	—	1.09	—	1.1	1.51
Eu <sub>2</sub> O <sub>3</sub>	—	—	1.08	0.99	0.95	0.99
Gd <sub>2</sub> O <sub>3</sub>	1.35	—	2.95	1.41	2.87	3.33
Dy <sub>2</sub> O <sub>3</sub>	2.51	3.71	3.93	3.77	4.76	4.62
Ho <sub>2</sub> O <sub>3</sub>	—	—	—	—	0.98	0.71
Er <sub>2</sub> O <sub>3</sub>	3.77	3.43	2.62	4.03	3.37	3.07
Tm <sub>2</sub> O <sub>3</sub>	—	—	—	—	0.85	—
Yb <sub>2</sub> O <sub>3</sub>	4.85	5.06	2.37	4.48	2.05	2.39
Ta <sub>2</sub> O <sub>5</sub>	—	—	2.14	2.65	—	2.05
Total	99.62	99.67	99.64	99.51	99.37	100.61
LREE <sub>2</sub> O <sub>3</sub>	4.96	2.53	8.42	5.91	8.43	9.4
HREE <sub>2</sub> O <sub>3</sub>	11.13	12.2	8.92	12.28	12.01	10.79
REE <sub>2</sub> O <sub>3</sub>	16.09	14.73	17.34	18.19	20.44	20.19
Cation Assignment - Based on 4 Oxygens						
Ca	0.03	0.05	0.02	0.01	—	0.01
Y	0.76	0.75	0.75	0.73	0.75	0.72
Nb	0.99	1.01	0.96	0.97	0.97	0.96
Ta	—	—	0.03	0.03	—	0.03
Ce	0.02	0.01	0.02	0.02	0.02	0.03
Nd	0.03	0.02	0.03	0.03	0.03	0.03
Sm	—	—	0.02	—	0.02	0.02
Eu	—	—	0.02	0.01	0.01	0.01
Gd	0.02	—	0.04	0.02	0.04	0.05
Dy	0.04	0.05	0.06	0.05	0.07	0.07
Ho	—	—	—	—	0.01	0.01
Er	0.05	0.05	0.04	0.06	0.05	0.04
Tm	—	—	—	—	0.01	—
Yb	0.06	0.07	0.03	0.06	0.03	0.03
Total	2	2.01	2.01	1.99	2.01	2.01

## Representative Analyses of Allanite

Rock Type	Layered			Layered	Hybrid
Sample	CC7 - 1	2	3	CC10 - 1	CC12 - 1
Al <sub>2</sub> O <sub>3</sub>	11.82	12.03	15.31	12.59	11.28
SiO <sub>2</sub>	31.31	32.16	33.29	30.55	30.23
CaO	13.14	12.92	13.65	11.64	8.42
TiO <sub>2</sub>	1.76	0.94	0.55	1.57	—
FeO	13.67	13.52	11.3	12.34	18.15
La <sub>2</sub> O <sub>3</sub>	8.2	8.42	6.69	7.19	5.74
Ce <sub>2</sub> O <sub>3</sub>	15.64	15.82	12.12	15.02	15.48
Pr <sub>2</sub> O <sub>3</sub>	1.59	2.09	0.8	1.98	2.38
Nd <sub>2</sub> O <sub>3</sub>	3.1	3.06	2.96	3.42	5.35
Sm <sub>2</sub> O <sub>3</sub>	—	—	—	—	0.88
ThO <sub>2</sub>	—	—	0.91	—	—
Cl	0.64	0.34	—	—	—
Total	100.86	101.29	97.58	96.29	97.9
O = F, Cl	0.27	0.14	—	—	—
Total	100.59	101.15	97.58	96.29	97.9
REE <sub>2</sub> O <sub>3</sub>	28.53	29.39	22.57	27.61	29.83
Cation Assignment - Based on 13 (O, OH, Cl)					
Si	3.17	3.25	3.3	3.21	3.25
Ti	0.14	0.07	0.04	0.12	—
Al	1.41	1.43	1.79	1.56	1.43
Fe	1.16	1.14	0.94	1.08	1.63
Ca	1.43	1.4	1.45	1.31	0.97
La	0.31	0.32	0.25	0.28	0.61
Ce	0.58	0.59	0.44	0.58	0.09
Pr	0.06	0.08	0.03	0.08	0.21
Nd	0.11	0.11	0.11	0.13	0.03
Sm	—	—	—	—	0.23
Th	—	—	0.02	—	—
Cl	0.11	0.06	—	—	—
Cation Total	8.37	8.39	8.37	8.35	8.45

### **Appendix III**

#### Cathodoluminescence Results

Spectra were acquired from petrographic slides. When possible, spectra were collected 3 separate times.

Spectra were obtained using both the 5 X objective (FOV = 2 mm) and the 10X objective (FOV = 1 mm) when possible.

Spectral analysis: background integration time = 10 seconds; analytical integration time = 10 sec; discussed with Ocean Optics technician and they felt that a 10 second integration time is optimal and reduces noise.

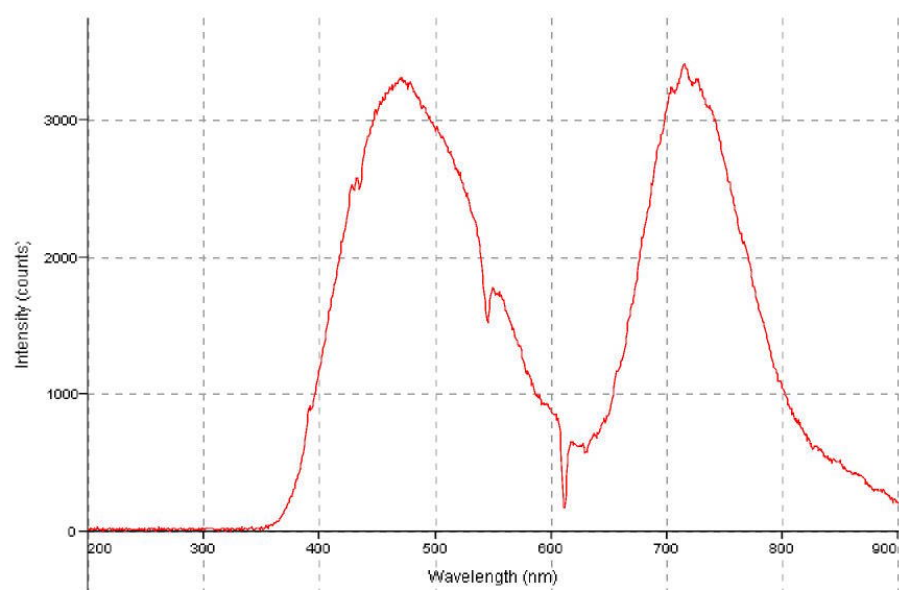
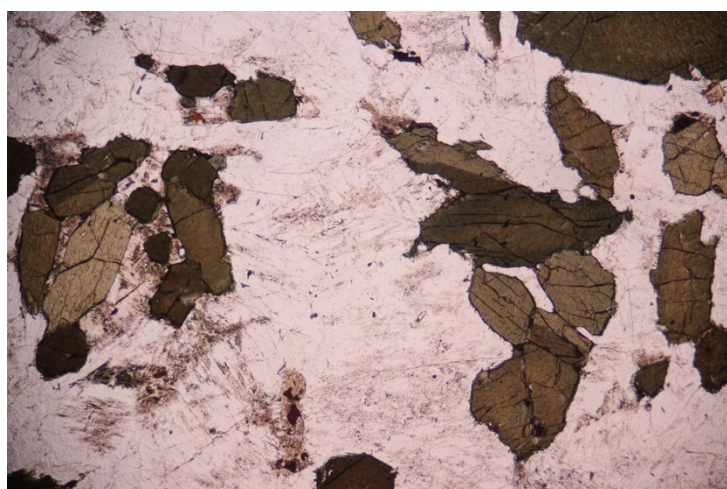
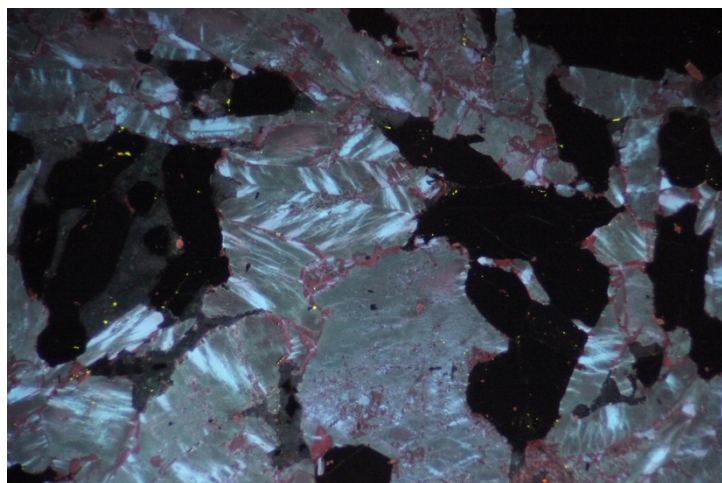
Background integration (10 seconds) was subtracted from each analysis.

CL operating conditions: 1.50-1.68 milliamperes; 4.2-5.1 kilovolts; 66.5 - 70.5 mTorr.

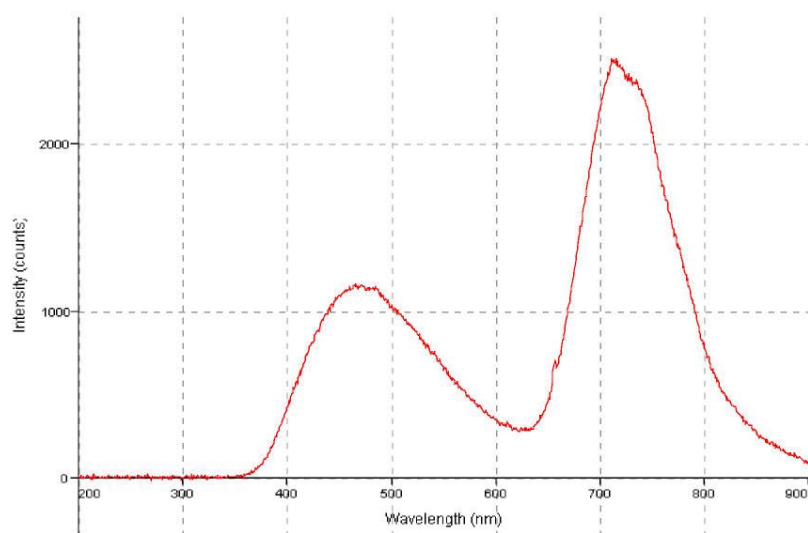
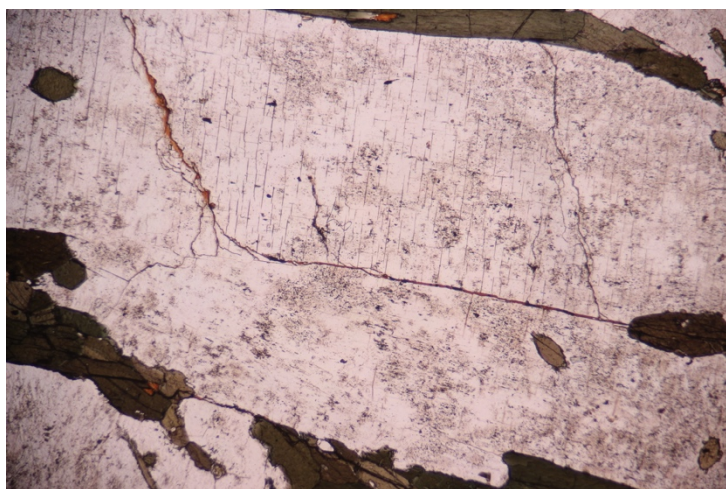
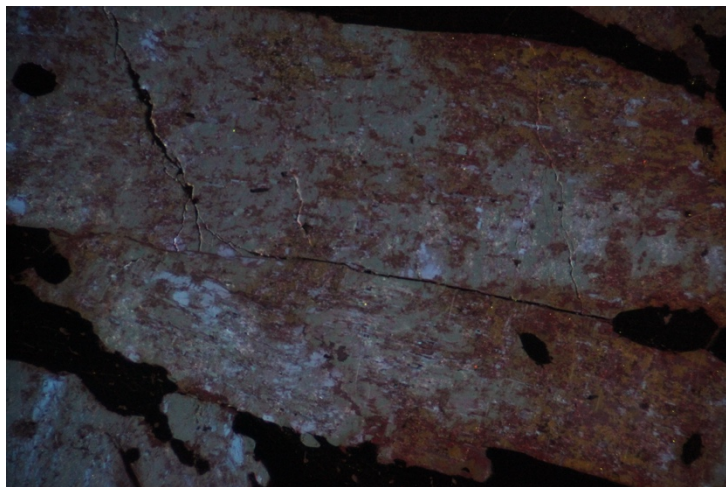
Photomicrographs were taken in cathodoluminescent (CL) conditions. Photomicrographs were taken when possible using both the 5 and 10X objective (FOV = 2 and 1 mm respectively) for all samples.

All CL spectral plots relate to the full field of view.

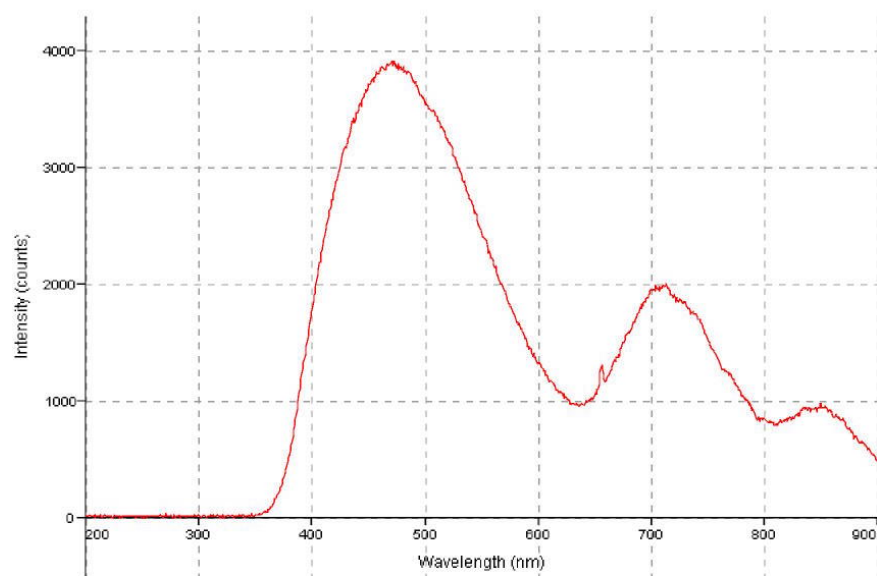
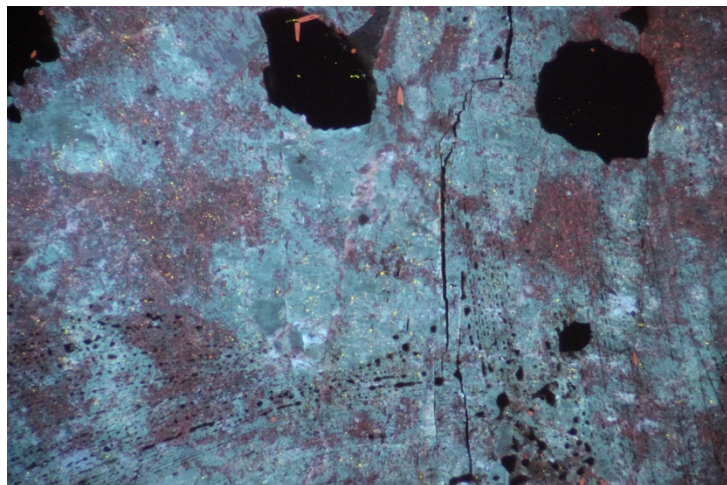
CC1A (5x objective; CLimage, PPL image, spectra)



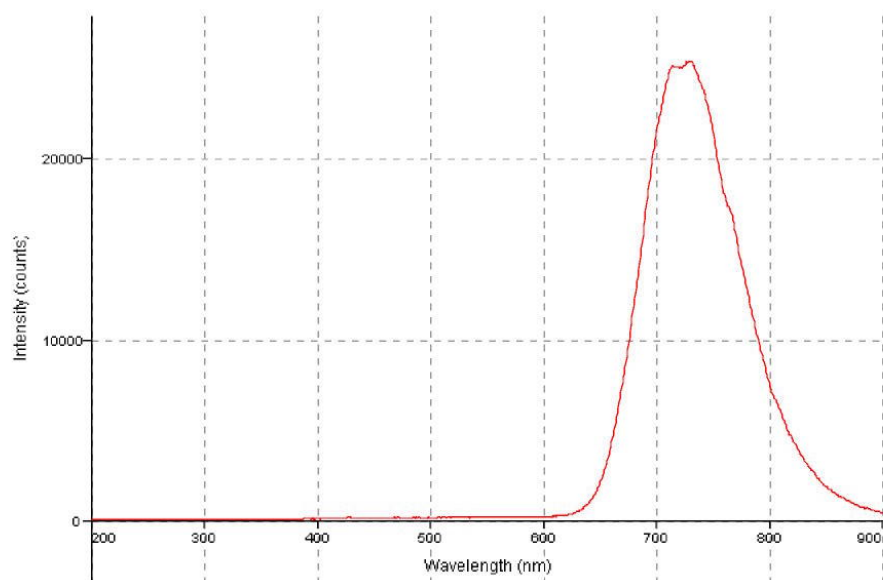
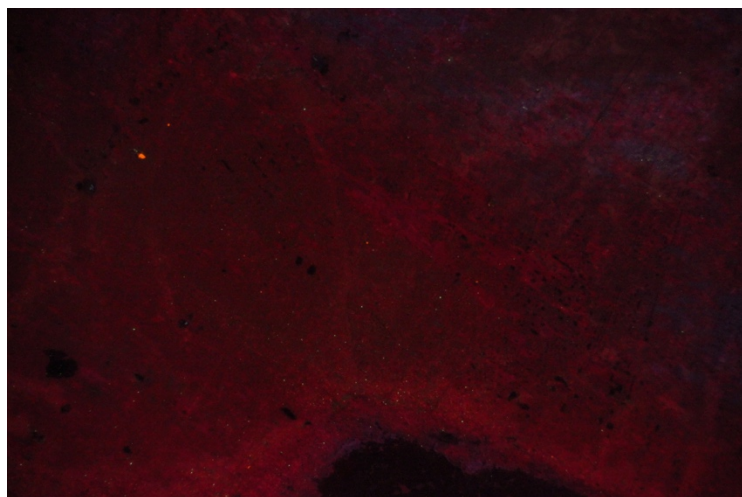
CC2 (5x objective; CLimage, PPL image, spectra)



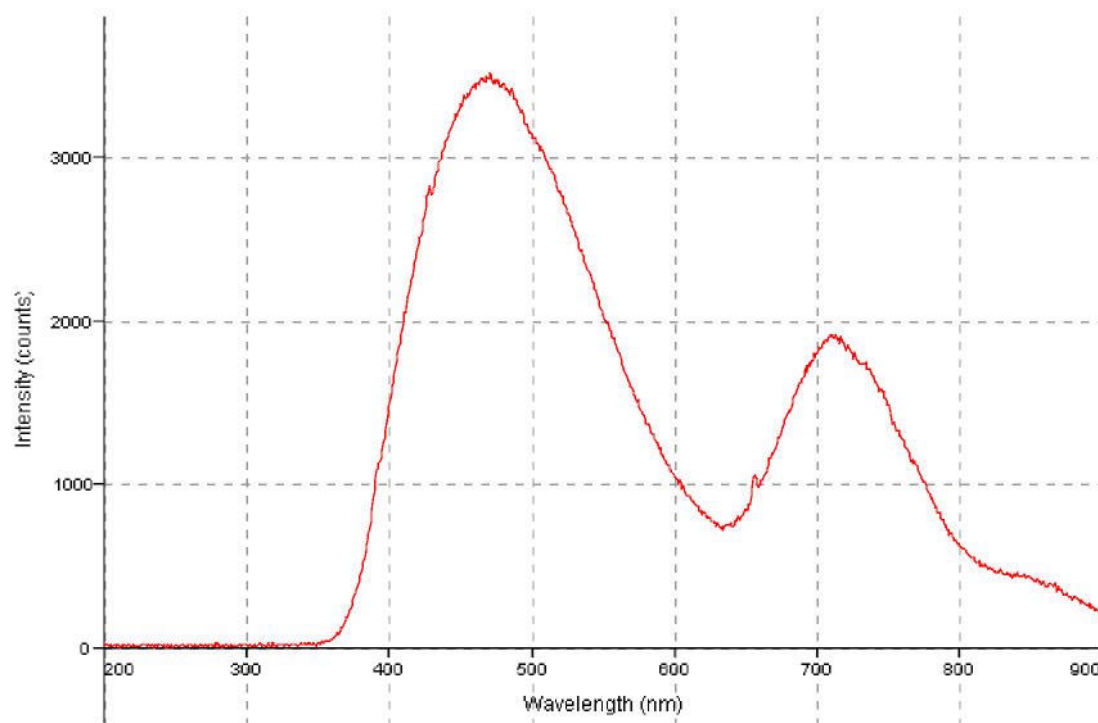
CC3 (10x objective; CLimage, PPL image, spectra)



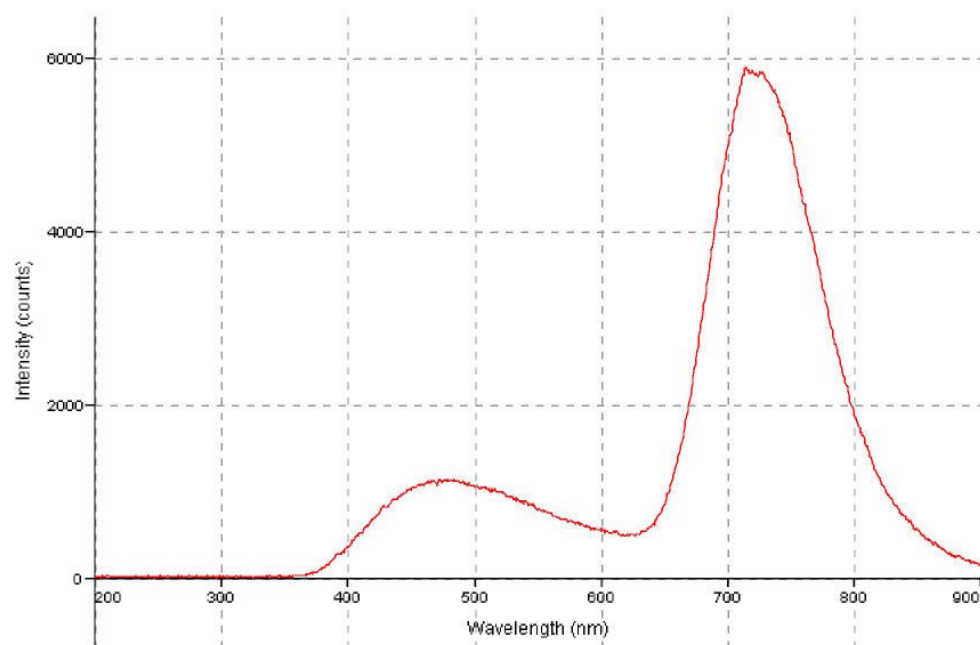
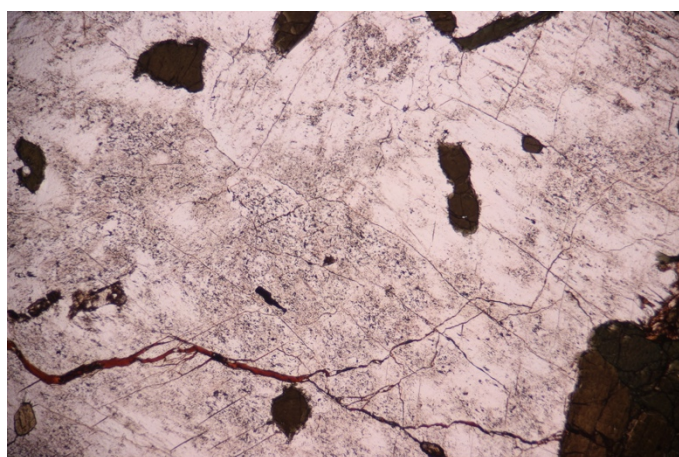
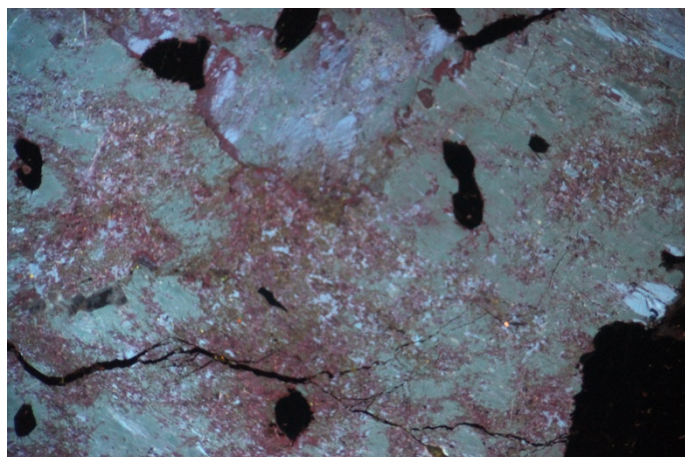
CC4 (5x objective; CLImage, PPL image, spectra)



## CC6 (5x objective; spectra)



CC7 (5x objective; CLImage, PPL image, spectra)



CC8 (5x objective; CLimage, PPL image, spectra)

